Three-dimensional linear elastic fracture mechanics: from theory to practice

Veronique Lazarus

Habilitation à Diriger des Recherches de l'Université Pierre et Marie Curie (UPMC Univ Paris 6)

Spécialité : **Sciences Pour l'Ingénieur**

présentée par

Véronique LAZARUS
Laboratoire Fluides, Automatique et Systèmes Thermiques
(FAST, UMR 7608: UPMC Univ Paris 6, Univ Paris-Sud, CNRS)
Bat 502, Campus Univ, F-91405, Orsay, France.

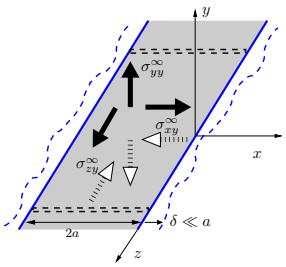

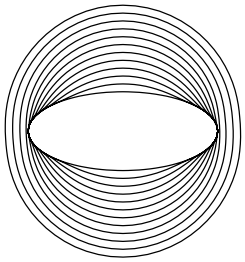
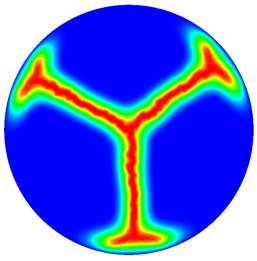

Mécanique linéaire élastique de la rupture tridimensionnelle: de la théorie à la pratique

Three-dimensional linear elastic fracture mechanics: from theory to practice

Soutenance effectuée le 6 juillet 2010
devant le jury composé de Mesdames et Messieurs :

BOUCHAUD Elisabeth	Rapporteur
RICE James R.	Rapporteur
VANEL Loïc	Rapporteur
LEBLOND Jean-Baptiste	Président
ADDA-BEDIA Mokhtar	Examinateur
MARIGO Jean-Jacques	Examinateur
ROUX Stéphane	Examinateur
SCHMITTBUHL Jean	Examinateur

Front page figures from the left to the right:

- A tunnel-crack under tensile and shear remote loading, slightly perturbed in its plane. It is the simpliest model allowing to introduce a finite length and still to obtain analytical results about crack front deformation (ch. 2, p. 76, p. 92).
- PlaneCracks numerical simulations: Successive front positions of an initial elliptical crack when it propagates under remote tensile loading (§2.4.2, p. 111). Extension to the interaction between several cracks is in progress (PhD of L. Legrand).
- Directional drying 2D simulations (C. Maurini, IJLRDA) using the regularized minimization approach of Bourdin et al. (2008).
- Twisting of a crack loaded in fatigue by mixed mode 1+2+3. The material is PMMA. In memory of F. Buchholz of Paderborn University (Germany) that performed those experiments in Paderborn University (Germany). The twisting rate can be predicted by supposing that the whole front twists around the direction of propagation to annihilate mode III (p. 64).
- Star shaped cracks obtained during directional drying of colloidal suspension in a circular capillary tube. Experiments realized by my colleague G. Gauthier. Facture mechanics energy minimisation principle allows to retrieve the experimental shapes (§3.2, p. 181, p. 186).
- Septaria crack into concretions formed within mudstones. Their origin is still badly explained, they may be shrinkage cracks? Rock and picture from J. Gargani, B. Saint-Bezar, P. Vergely of the lab "Interactions et Dynamique des Environnements de Surface", Orsay. Application of fracture mechanics energy minimisation principle is planed in collaboration with them (p. 47).
- Basalt columns of the Giant Causeway, Ireland. Those intriguing regular patterns are formed by directional cooling of a lava layer. Courtesy of my colleague Anne Davaille. Application of fracture mechanics energy minimisation principle on polygonal patterns is planed in collaboration with her (p. 47, p. 181).
- Hierarchical shrinkage crack pattern in thin layer of colloidal suspension solidified by drying. Experiments of my colleague L. Pauchard (§3.3, p. 194). We are working on crack morphology and on the mechanical characterization of the solidified suspension (PhD of M. Chekchaki).

Contents

Introduction **3**

1 Curriculum vitae **5**
Résumé . . . 5
Activités d'enseignement . . . 9
Encadrement d'étudiants/*Postgraduate students* . . . 11

2 Perturbation approaches of a planar crack in linear elastic fracture mechanics: a review **13**
2.1 Overview of the traditional LEFM approach . . . 14
2.1.1 Definition of the SIFs . . . 14
2.1.2 Crack advance versus loading criterions . . . 15
2.1.3 Crack propagation direction criterions . . . 16
2.1.4 Crack perturbation approaches . . . 16
2.2 In-plane crack front perturbation approaches for an arbitrary planar crack . . . 17
2.2.1 Definitions and elementary properties of weight functions . . . 17
2.2.2 First order variation of the stress intensity factors . . . 18
2.2.3 First order variation of the fundamental kernel . . . 19
2.2.4 Some expressions of the fundamental kernel **W** . . . 20
2.2.4.1 Circular cracks . . . 20
2.2.4.2 Half-plane crack . . . 21
2.2.4.3 Tunnel-cracks . . . 21
2.3 Particular model case of tensile straight crack fronts . . . 22
2.3.1 Unperturbed geometries and loading . . . 22
2.3.2 Fourier transform of the first order variation of the SIF . . . 23
2.4 Crack propagation in an homogeneous media . . . 24
2.4.1 Crack front shape linear bifurcation and stability analysis . . . 24
2.4.1.1 Bifurcation . . . 24
2.4.1.2 Stability . . . 26
2.4.2 Largescale propagation simulations . . . 27
2.5 Crack trapping by tougher obstacles . . . 29
2.6 Crack propagation in a disordered media . . . 31
2.6.1 Brittle fracture: case $K(x,z) = K_c(x,z)$ . . . 31
2.6.1.1 Fourier transforms of the crack front fluctuations versus toughness fluctuations . . . 32
2.6.1.2 Power spectrum of the crack front fluctuations versus toughness fluctuations . . . 33
2.6.2 Subcritical or fatigue propagation . . . 35
2.6.2.1 Evolution of the perturbation of the crack front . . . 35

2.6.2.2 General formula for the power spectrum of the perturbation of the crack front . . . 36
2.6.3 Synthesis of the theoretical results . . . 36
2.6.4 Comparison with the experiments . . . 37
2.7 Conclusion . . . 38

3 Research project: From the theory to the practice **41**
3.1 Deformations of a plane crack during its propagation . . . 41
3.2 Predictions of crack patterns using energy minimization . . . 43
3.3 Characterization of the consolidation of drying colloidal suspensions . . . 45
3.3.1 Estimation of the mechanical stresses by measuring the deflection of a plate and indentation techniques . . . 46
3.3.2 Estimation of some mechanical characteristics by measuring some geometrical features of the crack morphologies . . . 46
3.4 Summary . . . 47

Bibliographie/*References* **48**

4 Mes publications/*My publications* **59**
4.1 Liste . . . 59
4.2 Sélection de publications/*Selected publications* . . . 63
Lazarus, V., Buchholz, F.-G., Fulland, M., Wiebesiek, J. (2008) . . . 64
Lazarus, V., Leblond, J.-B., (2002)b. In-plane perturbation of the tunnel-crack under shear loading. I: Bifurcation and stability of the straight configuration of the front. . . . 76
Lazarus, V., Leblond, J.-B., (2002)c. In-plane perturbation of the tunnel-crack under shear loading. II: determination of the fundamental kernel. . . . 92
Lazarus, V. (2003). Brittle fracture and fatigue propagation paths of 3D plane cracks under uniform remote tensile loading. . . . 111
Favier, E., Lazarus, V., Leblond, J.-B. (2006)a. Coplanar propagation paths of 3D cracks in infinite bodies loaded in shear. . . . 135
Pindra, N., Lazarus, V., Leblond, J.-B. (2008)a. The deformation of the front of a 3d interface crack propagating quasistatically in a medium with random fracture properties. . . . 154
Gauthier, G., Lazarus, V., Pauchard, L. (2010). Shrinkage star-shaped cracks: Explaining the transition from 90 degrees to 120 degrees.L . . . 181
Lazarus, V., Gauthier, G., Pauchard, L., Maurini, C., Valdivia, C. (2009)a. Basalt columns and crack formation during directional drying of colloidal suspensions in capillary tubes. . . . 186
Chekchaki, M., Frelat, J., Lazarus, V., 2010. Analytical and 3D finite element study of the deflection of an elastic cantilever bilayer plate. . . . 194

Introduction

Après ma thèse de doctorat en Mécanique réalisée à l'université Pierre et Marie Curie (1994-1997), j'ai eu la chance d'intégrer cette même université en tant que maître de conférences dès 1998. C'est au sein de l'UFR de mécanique récemment intégré dans l'UFR d'ingénierie que j'ai depuis réalisé mes enseignements. C'est au sein du Laboratoire de Modélisation en Mécanique, intégré aujourd'hui dans l'Institut Jean Le Rond d'Alembert puis au sein du laboratoire Fluides Automatique et Systèmes Thermiques que j'ai réalisé mes travaux de recherche. Mes intérêts de recherche concernent principalement la mécanique linéaire élastique de la rupture d'un point de vue théorique avec un souci croissant pour la validation expérimentale et les interactions avec la physique ou les géosciences.
Cette habilitation à diriger les recherches se veut une synthèse de mes activités d'enseignement et de recherche. Le rapport est subdivisé de la façon suivante:

Le chapitre 1 concerne mon Curriculum Vitae. Après une vue générale de mon parcours, mes activités d'enseignement et d'encadrement y sont plus amplement décrits.

Dans le chapitre 2, j'ai choisi de développer, parmi mes activités de recherches, les résultats les plus aboutis, que j'ai obtenus en collaboration notamment avec J.B. Leblond et nos doctorants (E. Favier, N. Pindra, L. Legrand) concernant la déformation du front de fissures. Ces résultats sont présentés en anglais sous la forme d'un article de synthèse avec le souci d'être compréhensible à la fois par la communauté mécanique et physique de la rupture fragile.

Le chapitre 3 contient un aperçu des projets de recherche en cours et à venir. Cela concerne les prolongements du chapitre 2 ainsi que la prédiction des morphologies de fissures par minimisation d'énergie et enfin la caractérisation de suspensions colloïdales lors de leur séchage.

Le chapitre 4 contient une liste des mes publications ainsi qu'une sélection d'articles représentative des mes principaux domaines de recherche: les critères permettant de définir le trajet de propagation de fissures, les approches perturbatives du front de fissures (théorie, application à la détermination de la forme du front de fissures lors de la propagation dans un milieu homogène ou hétérogène), la fissuration de suspensions colloïdales consolidées par séchage.

Chapter 1

Curriculum vitae

Résumé

Etat civil et coordonnées

Lazarus Véronique. Maître de conférences à l'UPMC Université Paris 6.
Née le 23 mars 1971 à Sarreguemines (France). Nationalité française. 39 ans.
Mariée, 2 enfants (2000, 2002, 6 mois de congé parental en 2005).
Adresse personnelle: 5 rue de Lattre de Tassigny, 91400 Orsay, France.
Adresse professionnelle: Laboratoire FAST (UMR 7108), Bât. 502, Campus universitaire, 91400 Orsay, France.
Tel: +33 1 69 15 80 39. Fax : +33 1 69 15 80 60.
Email : veronique.lazarus@upmc.fr
Page web: http://www.fast.u-psud.fr/∼lazarus/

Formations

2008	Formation continue "De l'encadrement du projet doctoral à l'évolution de carrière du docteur" à l'Institut de Formation Doctorale de l'UPMC (5 journées).
1997	Doctorat de l'université Paris 6 (spécialité Mécanique). Mention Très Honorable avec Félicitations.
1994	Ingénieur de l'Ecole Nationale Supérieure de Techniques Avancées. Option Mécanique.
1994	DEA de Mécanique (Paris 6). Filière Solides. Mention Bien.
1989–91	Mathématiques supérieures, spéciales P' au lycée Kléber (Strasbourg).
1989	Baccalauréat C (Sarreguemines), mention Très Bien.

Expériences professionnelles

1998–	Maître de Conférences à l'Université Paris 6.	
	2008–	Laboratoire Fluides, Automatique et Systèmes Thermiques (FAST, UMR 7108). Equipe Milieux Poreux et Fracturés.
	1997–2008	Laboratoire de Modélisation en Mécanique (LMM) intégré depuis 2007 à l'Institut Jean Le Rond d'Alembert (IJLRDA, UMR 7190). Equipe Mécanique et Ingénierie des Solides Et des Structures.
	Fév-Jul 2008	Délégation au CNRS au laboratoire FAST.
	Fév-Jul 2007	Délégation au CNRS au laboratoire FAST.

Fév-Jul 2006	Congé pour Recherche et Conversion Thématique (CRCT) au laboratoire FAST.
1997–98	Attachée Temporaire d'Enseignement et de Recherche à l'Université Paris 6.
1995–97	Vacataire à l'Ecole Nationale Supérieure de Techniques Avancées.
1994–97	Doctorante au Laboratoire de Modélisation en Mécanique sous la direction de J.B. Leblond. "Quelques problèmes tridimensionnels de mécanique de la rupture fragile".
1994–97	Moniteur à l'Université Paris 6.
1994	Stage de fin d'études de six mois au centre d'Etudes et de Recherches des Renardières d'EDF sous la responsabilité de C. Eripret: "Interprétation à l'aide d'un calcul aux Eléments Finis, d'un essai de choc thermique sur une enceinte de réacteur nucléaire".

Thèmes de Recherche

Mécanique Linéaire Elastique de la Rupture bi- et tridimensionnelle. Approches théoriques et numériques.

Outils:	Méthodes perturbatives du front de fissures (formulation des fonctions de poids de Bueckner-Rice): calculs analytiques (petites perturbations) ou numériques (grandes perturbations). Approche énergétique à la rupture. Eléments finis bi- et tridimensionnels.
Applications:	Prédiction du chemin de propagation de fissures à partir des données mécaniques (chargement, comportement) et problème inverse dans des milieux fragiles homogènes et hétérogènes, des milieux de la matière molle consolidée (colloïdes, suspensions, peintures, gels), des milieux géologiques.

Publications et communications

21 Publications dans des revues à comité de lecture (7 J Mech Phys Solids, 4 Int J Solids Struct, 3 Cr Acad Sci II B, 2 Int J Fracture, 1 Phys Rev E, 1 EPL-Europhys Lett, 1 Langmuir, 1 J Appl Mech-T ASME, 1 Reflets de la Physique).

13 Congrès Internationaux avec actes, 3 sans actes. 1 Congrès Français avec actes.

2 projets ANR et 2 projets Triangle de la Physique acceptés.

Contribution à une exposition scientifique Grand public. "Ruptures: ça casse ou ça coule" (en cours de construction).

Encadrement de projets

Post-doc

04/2010-03/2012 S. Patinet (co-encadrement D. Vandembroucq, PMMH, ESPCI). Postdoctorant dans le cadre de l'ANR MEPHYSTAR sur la "Propagation de fissures dans des milieux hétérogènes de taille finie".

Thèses

09/2001-10/2005 E. Favier (co-direction J.B. Leblond). "Déformation du front de fissures planes au cours de leur propagation". Actuellement, maître de conférences à l'Université Paris Est, Marne-La-Vallée.

09/2005-07/2009 N. Pindra (co-direction J.B. Leblond). "Etude du désordre de la forme du front de fissure au cours de leur propagation". Actuellement, ATER à l'UPMC.

2007 C. Bousquet (encadrement du chap. Fracturation, direction S. Faure). Thèse CEA Marcoule. "Rôle des pluronics sur les propriétés rhéologiques de séchage et de fracturation des gels aspirables de décontamination ".

10/2007– M. Chekchaki (co-direction L. Pauchard). "Caractérisation mécanique du séchage de suspensions colloïdales."

09/2008– L. Legrand (co-direction J.B. Leblond). "Etude linéaire et non-linéaire de la déformation du front de fissures planes au cours de leur propagation et en particulier lors de leur coalescence".

Stages de Licence et Maîtrise

01-06/2000 W. Berger et B. Guillaume (codirection P.Y. Lagree), Projet Personnel en Laboratoire en 2ème année de l'ENSTA, "Modèle simplifié de la glotte".

04-09/2001 E. Favier. Stage du DEA de mécanique de Paris 6. "Etude de la stabilité de la forme rectiligne du front d'une fissure en forme de fente infinie - simulation de la propagation d'un front légèrement perturbé".

05-09/2002 L. Dufay et M. Guéniot (codirection A. Bioget, P.Y. Lagree). Stage de Maîtrise de Mécanique réalisé au Palais de la Découverte. "Le problème de Kepler et les forces de marées".

02/2007 E. Provost (codirection L. Pauchard, G. Gauthier). Stage L3. "Etude expérimentale et numérique des réseaux de fissures".

05-09/2007 A.C. Cochez. Stage M1. "Etude numérique de la propagation d'un réseau de fractures".

01-10/2008 C. Valdivia (codirection C. Maurini). Etudiant de master de Mechanical Engineer Universidad Tecnica Federico Santa Maria Valparaiso - Chili (Niveau français équivalent: Bac+6). SCAT Mobility Grant Report. "Numerical Simulation of the crack-pattern during the drying process using a variational approach".

05/2009 L. Swiecicki, S. Bennani, C. Gosselin. Travail d'Intiative Personnelle Encadrée, classes préparatoires aux grandes écoles. "Modélisation des craquelures de peinture par séchage de maïzena".

Enseignement

Environ 2200 heures d'enseignement principalement à l'université Paris 6.
20 % cours, 60% TD, 20% TP numériques, 20% TP expérimentaux.
20% Master, 80% Licence.

Thermomécanique des milieux continus. Niveau L3 au M2.

Mécanique des solides (Statique et dynamique, Résistance des matériaux, Elasticité, Comportement des milieux solides, Endommagement, Rupture fragile, Méthode des éléments finis). Niveau L1 au M2.

Mécanique des fluides (Statique et dynamique des fluides parfaits, Méthode des différences finies, TP expérimentaux). Niveau L1 au L3.

Thermique (Transferts de chaleur). Niveau L2.

Mathématique (Intégration, Analyse de Fourier et de Laplace, équations aux dérivées partielles). Niveau L3.

Histoire des sciences (Module de découverte). Niveau L1.

Informatique (C, Matlab). Niveau L3 et M2.

Activités administratives et collectives

2001-08	Membre de la Commission de Spécialistes, section 60, Université de Basse-Normandie, Caen.
2004-07	Membre de la Commission de Spécialistes, section 60, Université Paris 6.
2009-	Comité de sélection Univ. Paris 7 section 60/62-28.
2009-	Membre du Conseil de Laboratoire du FAST.
2009-	Membre du Conseil de l'école doctorale SMAER (ed 391), univ Paris 6.
2006-08	Organisation du groupe de travail des doctorants de l'Institut Jean le Rond d'Alembert.
1999-	Rapporteur pour les journaux J Mech Phys Solids, Int J Solids Struct, Int J Fracture, Eng Fract Mech, Proc. R. Soc. A.

Activités d'enseignement

Depuis le début de ma carrière universitaire, j'ai enseigné en tant que vacataire à l'ENSTA de 1995 à 1997 et en tant que moniteur (1994-98), ATER (1998-99) puis maître de conférences (depuis 1998) à l'UPMC. Depuis 1998, j'ai effectué un service plein soit 192 heures d'équivalent TD par an, sauf en 2000/2001 et 2002/2003 (congé de maternité), 2004/05 (congé parental), 2005/06 (CRCT), 2006/08 (délégation au CNRS), années durant lesquelles j'ai bénéficié d'une décharge d'un demi-service. Les différents modules auxquels j'ai participé sont décrits ci-dessous:

Thermomécanique des milieux continus. Niveau L3 au M2.

1. **Bases de la Mécanique des Milieux Continus (L3)**. TD du cours de F. Léné et P. Challande, et de R. Pradeilles-Duval à l'ENSTA.

   Introduction aux concepts de base (calcul tensoriel, cinématique, déformation, contraintes de Cauchy, lois de bilans) de la mécanique des milieux continus et illustration sur des exemples de comportements simples de milieux fluides (visqueux newtoniens) et solides (élastique linéaire).

2. **Thermomécanique des milieux continus (M2).** TD du cours de R. Gatignol.

   Présentation sous forme synthétique des notions de mécanique des milieux continus abordées en L3 et en M1 en y incorporant des cinématiques plus complexes (grandes déformations, milieux diphasiques, polarisés par ex.) et des généralités plus complexes sur les lois de comportement (objectivité, symétries matérielles). Illustrations de ces notions sur des exemples de comportement complexes: milieux hyper-élastiques, poroélastiques, fluides newtoniens et non-newtoniens, de Cosserat, mélanges, granulaires, par exemple.

Mécanique des solides. Niveau L2 au M2.

1. **Statique et dynamique des solides indéformables (L2).** TD des cours de Mme Metellus, M. Rigolot et M. Alliche.

   Description et modélisation des actions mécaniques pour le solide rigide : liaisons parfaites, efforts transmissibles, frottement, torseurs (cinématiques, cinétiques, dynamiques, des efforts). Principe fondamental de la statique et de la dynamique d'un système de solides indéformables.

2. **Résistance des matériaux (L2).** TD du cours de M. Billardon.

   Cours d'introduction à la résistance des matériaux. Introduction des notions de déformations, d'efforts intérieurs, de loi de comportement, de chargement limite par l'étude d'une barre élastique en équilibre.

3. **Elasticité linéaire.** TD du cours de Mme Léné (L3) et de Mme Pradeilles-Duval (ENSTA1).

   Introduction de la loi de comportement thermoélastique, en insistant sur le cas particulier des matériaux isotropes. Résolution du problème thermoélastique dans les cas particuliers où l'on peut exhiber des solutions exactes : méthode des déplacements et méthode des contraintes. Illustration par plusieurs exemples types: traction -compression, flexion plane, torsion. Introduction aux méthodes variationnelles et aux éléments finis.

4. **Comportement des milieux solides, Endommagement, Rupture fragile (M2).** Cours et TD. Responsable: M. Lemaître.

   Introduction par séance de cours/TD aux lois de comportement solide et aux notions d'analyse limite, d'endommagement et de rupture fragile.

5. **Travaux Pratiques de mécanique des solides (L3-M1).**

   Les différentes manips que j'ai eu l'occasion d'encadrer concernent la traction/compression d'une éprouvette cylindrique à l'aide d'une machine de traction, une barre en flexion, un cylindre sous pression, la mesure acoustique des constantes élastiques, la déformation d'un treillis à l'aide de jauges de déformation, la vibration de ressorts (phénomène de résonance), la visualisation des déformations par photoélasticité.

   Les notions de mesures de déplacements/déformation, de mesures d'effort par calibration, d'incertitudes de mesures y sont abordées.

   J'ai eu l'occasion d'encadrer conjointement les TD et les TP du même module. Cela fut bénéfique à la fois pour les étudiants et pour moi car les TP m'ont permis d'illustrer les TD par des exemples concrets et les échanges avec les étudiants, de mieux appréhender les difficultés qu'ils avaient en cours et en TD.

Mécanique des fluides. Niveau L2 au L3.

1. **Statique et dynamique des fluides parfaits (L2).** TD des cours de V. Nguyen, L. Gottesdiener et J.D. Polack.

   Introduction à la notion de pression, de description eulérienne/lagrangienne du mouvement. Utilisation du théorème de Bernoulli et du théorème des efforts globaux.

2. **Travaux Pratiques en Mécanique des Fluides (L3).**

   Les différentes manips que j'ai eu l'occasion d'encadrer concernent le tube de Venturi, la réaction d'un jet sur un obstacle, l'écoulement laminaire en conduite, l'écoulement turbulent en conduite, l'écoulement autour d'un cylindre, étude du comportement dynamique de fluides (newtoniens et non-newtoniens) par l'utilisation d'un rhéomètre de Couette.

   Ces TP sont l'occasion d'échanges scientifiques plus informels qu'en cours ou TD, riches d'enseignements avec les étudiants. Ils sont l'occasion d'aborder la méthode scientifique de façon plus réaliste que lors des TD.

Transferts thermiques (L2)

TD des cours de Mme Metellus.
Introduction aux transferts thermiques : généralités sur les différents modes de propagation de la chaleur (conduction, convection, rayonnement), conduction thermique en régime stationnaire, résistance thermique.

Mathématique (L3)

TD des cours de M. Larchevêque.
Théorie de l'intégration, série de Fourier, transformation de Fourier, transformation de Laplace, équations aux dérivées partielles.

Méthodologie du travail universitaire (L1)

Cette UE a pour but d'introduire les étudiants aux méthodes de travail et au monde universitaire scientifique. Elle se propose de les amener à réfléchir sur leur projet professionnel, leurs méthodes de travail et les outils extra-scientifiques nécessaires à leur bonne intégration à l'université (fonctionnement de la mémoire, travail en équipe, gestion du temps, gestion d'un projet, recherche et synthèse d'informations, prise de note, expression orale et écrite).

Ces objectifs sont abordés en laissant une relative liberté à l'enseignant, ce qui permet d'aborder l'enseignement sous un angle différent du traditionnel cours/TD et de faire des expériences pédagogiques nouvelles et enrichissantes. Les thèmes que j'ai choisis sont les suivants:

1. **Histoire des sciences**.

   Les outils méthodologiques sont introduits à travers la réalisation d'une chronologie générale de l'histoire des sciences, la présentation sous forme de poster de biographies de savants, l'étude de la Révolution scientifique et de textes originaux.

2. **Les outils de la Mécanique: de la modélisation à la conception.**

   Les outils méthodologiques sont abordés à travers (i) une introduction à la mécanique statique (notion de forces, moment de forces, pression, résistance des matériaux) et (ii) la réalisation (type bureau d'étude) et la présentation orale d'un mini-projet technologique (ex: F1, avion, sous-marin, mongolfière, "Là-Haut") .

Méthodes numériques (L3-M2)

1. **Méthodes numériques pour la mécanique (L3).**

   Encadrements de mini-projets simples de mécanique (poutre en flexion, conduction de la chaleur, écoulement dans une canalisation) réalisés en Fortran.

2. **Matlab, méthodes spectrales et des différences finies (M2).** Responsable: J. J. Marigo.

   Apprentissage de Matlab par la résolution de différents problèmes de mécanique et d'acoustique (vibration d'une corde, équation de la chaleur, équation de transport) par des méthodes spectrales ou de différences finies.

3. **Méthode des éléments finies.** Cours H. Dumontet.

   Programmation des éléments finis en Matlab. Réalisation et encadrement d'une série de TPs avec comme objectifs (i) d'apprendre à utiliser Matlab, (ii) d'aider à comprendre le cours et (iii) de savoir coder la méthode des éléments finis. Les différentes étapes de la programmation (maillage, construction des matrices de rigidité et du second membre élémentaires, assemblage des matrices globales, prise en compte des conditions limites, résolution du système linéaire, post-traitement et visualisation) sont traitées en partant d'un problème 1D avec un degré de liberté par noeud en allant progressivement vers un problème 2D à deux degrés de liberté par noeud.

Encadrement d'étudiants/*Postgraduate students*

Concernant les problèmes de déformation de front de fissures planes, j'ai coencadré avec J.B. Leblond, deux thèses: celle de Elie Favier qui est actuellement maître de conférences à l'université de Marne La Vallée et celle de Nadjime Pindra actuellement ATER à l'UPMC. J'ai également activement participé à la partie "fracture" de la thèse CEA (responsable Sylvain Faure) de Cécile Bousquet concernant les gels aspirables (procédé de décontamination nucléaire). Actuellement, je coencadre deux thèses: celle de Laurène Legrand sur la coalescence de deux fissures avec J. B. Leblond et celle de Mourad Chekchaki concernant les méthodes de caractérisation des suspensions colloïdales consolidées par séchage avec L. Pauchard. J'ai aussi le plaisir depuis peu d'encadrer avec Damien Vandembroucq (PMMH) un post-doctorant, Sylvain Patinet sur la propagation des fissures dans des interfaces patternées.

Par ailleurs, j'ai suivi il y a peu une formation sur l'encadrement des doctorants à l'Institut de Formation des Doctorants de Paris 6. Cela m'a permis de prendre conscience (i) des difficultés liées à la recherche d'emploi après la thèse, (ii) de l'importance d'anticiper leur avenir professionnel, (iii) des compétences développées pendant la thèse et qui peuvent être valorisées lors de la recherche d'emploi.

Chapter 2

Perturbation approaches of a planar crack in linear elastic fracture mechanics: a review

Among my research interests, I have chosen to present in this report the results I have obtained on the crack front shape deformations with my colleague and former PhD advisor, J.B. Leblond and our PhD students E. Favier, N. Pindra, L. Legrand. I have chosen to write it in the spirit of a review paper, with the hope to publish it and to be comprehensible by both mechanical engineering and statistical physics community to further be able to develop this topic in common (in particular, during the ANR project MEPHYSTAR). To emphasize my own contribution, the papers I took part in are in bold fonts.

Consider a crack embedded in an elastic solid that is loaded quasistatically (fig. 2.1). (i) Under which conditions of loading, (ii) in which direction and (iii) along which distance will this crack propagate? Linear Elastic Fracture Mechanics (LEFM) aims at answering these questions. It is widely applied in several fields, for instance: in engineering applications (Anderson, 1991) for obvious safety reasons; in geological applications (Aydin and Pollard, 1988; Atkinson, 1987) as earthquakes (Liu and Rice, 2005; Fisher et al., 1997; Grob et al., 2009; Bonamy, 2009), basalt columns (Goehring et al., 2009) or in the soft matter domain **(Gauthier et al., 2010)**. The principal aim of this review, in addition to a brief overview of the answers to the first two questions, is linked to the third question and concerns the crack front deformation of a three-dimensional planar crack during its propagation.

Nowadays, several different approaches are developed within LEFM. *Traditional* approach, in the continuity of the pioneer works of Griffith (1920) and Irwin (1958), is based on the local mechanical and energetic fields near the crack front and uses propagation criterions based on the Stress Intensity Factors K_1, K_2, K_3 or the elastic energy release rate $\mathcal{G}$. This approach aims at predicting the propagation conditions (loading, path) of a preexisting crack, but is unable to deal with the crack initiation problem. Recently new approaches have been developed that are able, in theory, to deal with both the crack initiation and propagation paths: the *energetic variational minimisation* approach to fracture and the *phase-field* method. The first (i) has been shown to include the traditional approach (Francfort and Marigo, 1998; Bourdin et al., 2008), (ii) has been approximated for numerical purposes by non-local damage first-gradient model (Bourdin et al., 2000) and (iii) has been applied to several brittle fracture problems as stability problems (Benallal and Marigo, 2007), the deterioration of the French Panthéon (Lancioni and Royer-Carfagni, 2009), the propagation direction in presence of mode 2 (Chambolle et al., 2009). The second, first developed for solidification front (Caginalp and Fife, 1986; Collins and Levine, 1986) was further extended to brittle fracture (Karma et al., 2001) and has shown

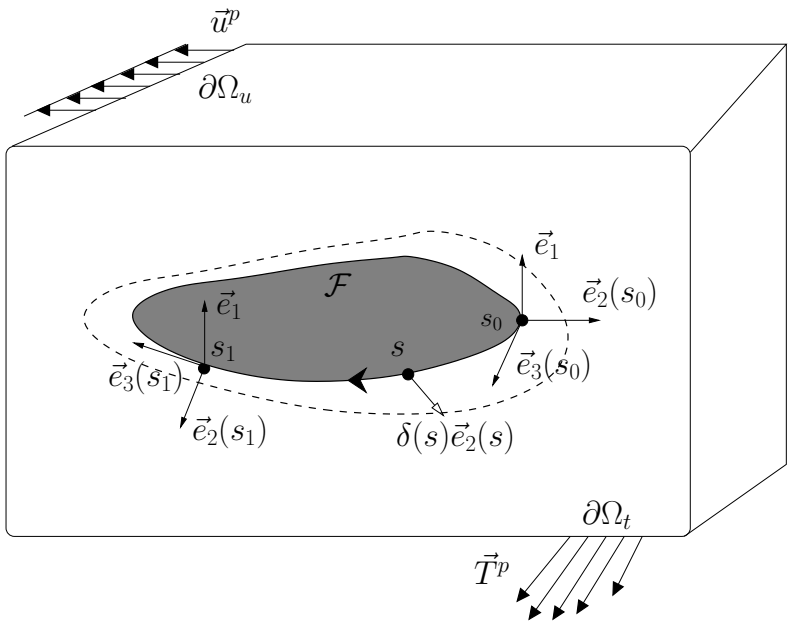

Figure 2.1: An example of three-dimensional LEFM problem: a three-dimensional planar crack (in grey) embedded in an arbitrary body loaded by external load $\vec{T}^p$, $\vec{u}^p$ on $\partial\Omega_T$, $\partial\Omega_u$. The dashed line corresponds to the position of the initial front $\mathcal{F}$ after an in-plane $\delta(s)\vec{e}_2(s)$ advance.

their efficiency to resolve problems of path determination in 2D (Henry and Levine, 2004; Hakim and Karma, 2009; Corson et al., 2009) and 3D (Pons and Karma, 2010). But the traditional approach has still its place thanks to the maturity acquired by its longer history: in particular, to deal with the crack front shape deformations an efficient perturbation method of the crack front, pioneered by Rice (1985), has been used. The method allows to update the stress intensity factors (that are prerequisite to any crack propagation prediction) for any small perturbation of the crack front without resolving the whole elasticity problem. On the one hand, the initial method of Rice (1985) has been applied to the propagation of cracks in disordered heterogeneous by the statistical physics community. On the other, it has be extended and applied to more and more complex problems by the fracture mechanics community. A review concerning the roughening of the front in disordered heterogeneous materials from a statistical physics point of view, has recently be done by Bonamy (2009). Here, the aim is to do a review of the crack front perturbation approaches from a mechanical point of view. After a brief overview of the traditional LEFM approach (section 2.1), the perturbation method is presented in the general case (section 2.2) and then for some model selected problems (section 2.3). Application to crack propagation in homogeneous media (section 2.4), crack trapping by tougher obstacles (section 2.5), propagation in disordered media (section 2.6) are then developed.

2.1 Overview of the traditional LEFM approach

2.1.1 Definition of the SIFs

Let $\mathcal{F}$ denote the crack front and s some curvilinear abscissa along it. At each point s of $\mathcal{F}$, we define a local basis of vectors $(\vec{e}_1(s), \vec{e}_2(s), \vec{e}_3(s))$ in the following way :

1. $\vec{e}_3(s)$ is tangent to $\mathcal{F}$ and oriented in the same direction as the curvilinear abscissa s;
2. $\vec{e}_2(s)$ is in the crack plane, orthogonal to $\mathcal{F}$ and oriented in the direction of propagation;

3. $\vec{e}_1(s) \equiv \vec{e}_1$ is orthogonal to the crack plane and oriented in such a way that the basis $(\vec{e}_2(s), \vec{e}_1, \vec{e}_3(s))$ is direct[1].

The SIFs $K_j(s)$, $j = 1, 2, 3$ at point s are then defined by the following formula, where Einstein's summation convention is employed :

$$\lim_{r \to 0} \sqrt{\frac{2\pi}{r}} [\![\vec{u}(s,r)]\!] \equiv 8\Lambda_{ij} K_j(s) \vec{e}_i(s). \tag{2.1}$$

In this expression $[\![\vec{u}(s,r)]\!]$ denotes the displacement discontinuity across the crack plane, oriented by the vector $\vec{e}_1$, at the distance r behind the point s of $\mathcal{F}$, in the direction of the vector $-\vec{e}_2(s)$. Also, $(\Lambda_{ij})_{1 \leq i \leq 3, 1 \leq j \leq 3} \equiv \mathbf{\Lambda}$ is the diagonal matrix defined by

$$\mathbf{\Lambda} \equiv \frac{1}{E} \begin{pmatrix} 1-\nu^2 & 0 & 0 \\ 0 & 1-\nu^2 & 0 \\ 0 & 0 & 1+\nu \end{pmatrix} \tag{2.2}$$

where E denotes Young's modulus and ν Poisson's ratio[2].

2.1.2 Crack advance versus loading criterions

A crack propagates instantaneously if the loading reaches a certain threshold (*brittle fracture*, but also continuously at a slower rate proportional to the loading (*subcritical* propagation due for instance to stress-corrosion or *fatigue* propagation due to cyclic loading). Concerning brittle fracture, Griffith (1920)'s criterion is extensively used: it states that the crack propagates if the elastic energy released by the crack propagation $\mathcal{G}$ is sufficient to counterbalance the fracture energy Γ necessary to create new surfaces.

$$\mathcal{G} < \Gamma \Rightarrow \text{ no propagation}, \tag{2.3}$$

$$\mathcal{G} = \Gamma \Rightarrow \text{possible propagation}. \tag{2.4}$$

SIFs and energy release rate $\mathcal{G}$ are linked by Irwin (1957)'s formula (Einstein summation convention is used):

$$\mathcal{G} = K_i \Lambda_{ij} K_j, \tag{2.5}$$

so that, in mode 1 ($K_2 = 0$, $K_3 = 0$), Griffith (1920)'s criterion is equivalent to Irwin (1958)'s criterion which states that the crack propagates if the Stress Intensity Factor K_1 at the crack tip exceeds the local toughness K_c:

$$K_1 < K_c \Rightarrow \text{ no propagation}, \tag{2.6}$$

$$K_1 = K_c \Rightarrow \text{possible propagation}. \tag{2.7}$$

Concerning the subcritical or fatigue propagation, Paris' law (Paris et al., 1961; Erdogan and Paris, 1963) with a threshold $\mathcal{G}_0$ or without ($\mathcal{G}_0 = 0$) is often used. It states that the crack velocity $\partial a(t)/\partial t$ goes as a power-law with the excess energy release rate $\mathcal{G}$:

$$\frac{\partial a(t)}{\partial t} = C(\mathcal{G} - \mathcal{G}_0)^\beta, \tag{2.8}$$

[1] the order of the vectors may seem a little surprising but this definition of the local basis presents the advantage that the mode 1, (resp. 2 and 3) corresponds to the displacement jump along the vector with the same numbering, that is $\vec{e}_1$ (resp. $\vec{e}_2$ and $\vec{e}_3$)

[2] A similar formula holds for an arbitrary anisotropic medium but the matrix $\mathbf{\Lambda}$ is then no longer diagonal.

and to a power of K_1 in mode 1:

$$\frac{\partial a(t)}{\partial t} = C(K_1 - K_0)^N \tag{2.9}$$

For subcritical propagation, t represents time. For fatigue, t must conventionally be re-interpreted as number of cycles and $\mathcal{G}$ as variation of the energy release rate during one cycle. An overview of the values of β or N and C for engineering materials can be found in Fleck et al. (1994). It's physical background (Vieira et al., 2008) and its validity field (Ciavarella et al., 2008) are still the subject of many research papers. Interestingly for numerical simulations, Paris' law may also be considered, in the case of very large Paris' exponent **(Lazarus, 2003)** or Paris' constant (Gao and Rice, 1989), as a kind of "viscous-plastic regularisation" of Griffith's propagation law for brittle fracture.

2.1.3 Crack propagation direction criterions

In homogeneous isotropic elastic media, except in some special conditions, it is well known that whatever the external loading, the crack front bifurcates in order to reach a situation of pure tension loading as the crack propagates (Hull, 1993). Hence, planar crack propagation is generally stable under mode 1 loading and unstable under mode 2 or 3. A literature survey of mixed mode crack growth can be found in Qian and Fatemi (1996). Under mode (1+2) conditions, the crack kinks to make mode 2 vanish. The value of the corresponding kink angle can be obtained, for instance, by the Principle of Local Symmetry (PLS) of Goldstein and Salganik (1974) or by the maximum tangential stress criterion (MTS; Erdogan and Sih 1963). The difference between these two criterions has been discussed by Amestoy and Leblond (1992). In presence of mode 3, to reach a situation of mode 1, the crack front twists around the direction of propagation. Seldom papers deals with the prediction of the propagation path in this condition. Among them, **Lazarus and Leblond (1998a)**, **Lazarus et al. (2001b)**, **Lazarus et al. (2008)** consider the particular case of 3 or 4 point bending experiments and Cooke and Pollard (1996), Lin et al. (2010), Pons and Karma (2010) the segmentation of the front.

In some particular situations, even in presence of mode 2 or 3, planar crack propagation may be stable. It is the case for instance when the crack is channelled along a planar surface of low fracture resistance, which can be the case for instance along a geological fault or in composite materials. It may also be the case in fatigue due to the presence of friction (Doquet and Bertolino, 2008).

2.1.4 Crack perturbation approaches

To predict the propagation path applying crack advance and propagation criterions described above, perturbation methods have been used. A first set of papers considers the out-of-plane perturbation of the faces of a planar crack: the first order variation of the SIF are given in Movchan et al. (1998) and applied by Obrezanova et al. (2002) to generalise the Cotterell and Rice (1980)'s stability analysis of a crack to small out-of-plane deviation of its path. A second set of papers gives the expressions of the SIFs along the front of an arbitrary kinked and curved infinitesimal extension of some arbitrary crack: Leblond (1989) and Amestoy and Leblond (1992) in 2D, and Leblond (1999) and **Leblond et al. (1999)** in 3D. These expressions have been applied for instance, to show that the PLS and the MTS yield very close but distinct kink angles (Amestoy and Leblond, 1992) or to the crack front rotation and segmentation in mixed mode 1+3 or 1+2+3 **(Lazarus and Leblond, 1998a; Lazarus et al., 2001a,b)**. A third set of papers consider the same problem then the second in the particular case of a planar crack with a coplanar extension. They are the main object of this review and are developed below.

2.2 In-plane crack front perturbation approaches for an arbitrary planar crack

Consider a plane crack of arbitrary shape embedded in some isotropic elastic medium subjected to some arbitrary loading: given forces $\vec{T}^p$ along $\partial\Omega_T$ and given displacements $\vec{u}^p$ along $\partial\Omega_u$ (Figure 2.1). The aim of this section is to give the first order variation of the stress intensity factors due to small in-plane perturbation of the crack front. Such formulae have first been derived in several particular cases notably by Rice and coworkers, and then generalised to more arbitrary problems. Here the historical chronology is not respected: first, in the present section, the most general formulae are recalled by relying on the paper of **Favier et al. (2006a)**. They are then particularised to some model problems in section 2.3.

2.2.1 Definitions and elementary properties of weight functions

Definitions Let $k_{ij}(\mathcal{F}; s'; s, r)$ denote the i-th SIF at the point s' of the crack front $\mathcal{F}$ resulting from application of a pair of opposite unit point forces equal to $\pm\vec{e}_j(s)$ on the upper $(+)$ and lower $(-)$ crack surfaces at a distance r behind the point s of the crack front the other loading being supposed to be zero ($\vec{T}^p = \vec{0}$ along $\partial\Omega_T$ and $\vec{u}^p = \vec{0}$ along $\partial\Omega_u$). These nine scalar functions are called the *crack face weight functions* (CFWFs).
The functions $k_{ij}(\mathcal{F}; s'; s, r)/\sqrt{r}$ are known to have a well-defined limit for $r \to 0$ (see for instance **Leblond et al. (1999)**). We then define the matrix $(W_{ij}(s', s))_{1\leq i\leq 3, 1\leq j\leq 3} \equiv \mathbf{W}(s', s)$ by the formula

$$W_{ij}(s', s) \equiv \pi\sqrt{\frac{\pi}{2}}\, D^2(s, s') \lim_{r\to 0} \frac{k_{ij}(\mathcal{F}; s'; s, r)}{\sqrt{r}} \tag{2.10}$$

where $D(s, s')$ denotes the cartesian distance between points s and s'. The functions $W_{ij}(s', s)$ in fact depend on the crack front shape, just like the CFWFs, but the argument $\mathcal{F}$ is omitted here for conciseness. They will be called the *fundamental kernels* (FKs) or more shortly the *kernels*.
Although the SIFs depends on the loading intensity and position, the CFWFs, hence the FKs depend on it only through the definitions of $\partial\Omega_T$ and $\partial\Omega_u$.

Properties The CFWFs are positively homogeneous of degree $-3/2$; that is, if all distances are multiplied by some positive factor λ, the CFWFs are multiplied by $\lambda^{-3/2}$. The definition (2.10) of the functions $W_{ij}(s', s)$ then implies that they are positively homogeneous of degree 0:

$$\mathbf{W}(\lambda s', \lambda s) = \mathbf{W}(s', s) \quad \forall\lambda > 0 \tag{2.11}$$

Since tensile and shear problems are uncoupled for a planar crack in an infinite body, whatever the shape of the crack front, the components k_{12}, k_{13}, k_{21} and k_{31} of the CFWFs are zero, so that by equation (2.10),

$$W_{12}(s', s) \equiv W_{13}(s', s) \equiv W_{21}(s', s) \equiv W_{31}(s', s) \equiv 0. \tag{2.12}$$

Considering two problems, one with point forces equal to $\pm\vec{e}_i$ exerted on the crack faces at (s, r) and one with point forces equal to $\pm\vec{e}_j$ exerted on the crack faces at (s', r'), applying Betti's theorem, and using equations (2.1) and (2.10), one sees that the kernels obey the following "symmetry" property :

$$\Lambda_{im} W_{mj}(s, s') = \Lambda_{jm} W_{mi}(s', s). \tag{2.13}$$

Finally, **Leblond et al. (1999)** have shown that the limit of $\mathbf{W}(s, s')$ when $s' \to s$ is universal, i.e. that it does not depend on the geometry. It is linked to the behaviour of the weight-functions when

the point of application of the loading tends toward the point of observation of the SIF which is a local property independent of the far geometry. The values of this limit are:

$$\begin{cases} \lim_{s'\to s} W_{11}(s,s') = 1 \\ \lim_{s'\to s} W_{22}(s,s') = \dfrac{2-3\nu}{2-\nu} \\ \lim_{s'\to s} W_{33}(s,s') = \dfrac{2+\nu}{2-\nu} \\ \lim_{s'\to s} W_{23}(s,s') = 0 \end{cases} \tag{2.14}$$

2.2.2 First order variation of the stress intensity factors

Let us now assume that the crack advances, under constant loading, by a small distance $\delta(s)$ within its plane in the direction perpendicular to its front (fig. 2.1). It has been shown in **Favier et al. (2006a)** that, for any loading, if $\delta(s_0) = 0$,

$$\delta\mathbf{K}(s_0) = \mathbf{N}\cdot\mathbf{K}(s_0)\delta'(s_0) + \frac{1}{2\pi}\ \mathrm{PV}\int_{\mathcal{F}} \frac{\mathbf{W}(s_0,s)}{D^2(s_0,s)}\cdot\mathbf{K}(s)\delta(s)\mathrm{d}s. \tag{2.15}$$

The condition $\delta(s_0) = 0$ ensures the existence of the Principal Value integral $\mathrm{PV}\int$. The quantities $\mathbf{K}(s) \equiv (K_i(s))_{1\le i\le 3}$ and $\delta\mathbf{K}(s) \equiv (\delta K_i(s))_{1\le i\le 3}$ here are the column vectors of initial SIFs and variations of these SIFs, and $\mathbf{N} \equiv (N_{ij})_{1\le i\le 3, 1\le j\le 3}$ is the matrix defined by

$$\mathbf{N} \equiv \frac{2}{2-\nu}\begin{pmatrix} 0 & 0 & 0 \\ 0 & 0 & -1 \\ 0 & 1-\nu & 0 \end{pmatrix}. \tag{2.16}$$

Equation (2.15) is identical to **Leblond et al. (1999)**'s general equation (30) (with the notation $\dfrac{1}{2\pi}\dfrac{\mathbf{W}(s_0,s)}{D^2(s_0,s_1)}$ instead of $\mathbf{Z}(s_0,s)$), in the special case of a planar crack with coplanar extension (and zero crack advance at the point s_0). It shall be noticed that the variation of the SIFs at a particular point s_0 depends in an non-local manner on the crack perturbation along all the front. It is due to long-range elastic interactions.
The restriction $\delta(s_0) = 0$ will now be removed by two methods:

1. Using a trick of Rice (1989), that consists of decomposing an arbitrary motion of the crack front defined by the normal advance $\delta(s)$ into two steps :

   (a) A translatory motion of displacement vector $\delta(s_0)\vec{e}_2(s_0)$. This motion brings the point s_0 to its correct final position while leaving the crack front shape unchanged. The corresponding normal advance $\delta_*(s)$ is given, to first order in $\delta(s)$, by

   $$\delta_*(s) = \delta(s_0)\ \vec{e}_2(s_0)\cdot\vec{e}_2(s). \tag{2.17}$$

   The associated variation of $\mathbf{K}(s)$ will be denoted $\delta_*\mathbf{K}(s)$.

   (b) A motion with normal advance given by $\delta(s)-\delta_*(s)$. This advance is zero at point s_0 so that the corresponding variation of $\mathbf{K}(s_0)$ is given by equation (2.15), with $\delta'(s_0)-\delta'_*(s_0) = \delta'(s_0)$ since $\delta'_*(s_0) = 0$ by equation (2.17).

Adding up the contributions from these two motions, one gets the final expression of the variation of the SIFs under constant loading in the general case:

$$\begin{aligned}\delta\mathbf{K}(s_0) &= \delta_*\mathbf{K}(s_0) + \mathbf{N}\cdot\mathbf{K}(\mathbf{s_0})\delta'(s_0) \\ &\quad + \frac{1}{2\pi}\ \mathrm{PV}\int_{\mathcal{F}} \frac{\mathbf{W}(s_0,s)}{D^2(s_0,s)}\cdot\mathbf{K}(s)\left[\delta(s)-\delta_*(s)\right]\mathrm{d}s.\end{aligned} \tag{2.18}$$

This expression allows to update the SIFs knowing the initial SIFs, FK and the displacement provided that the quantity $\delta_*\mathbf{K}$ can be calculated. The unknown quantity $\delta_*\mathbf{K}(s_0)$ is equal to zero if the translatory motion $\delta(s_0)\vec{e}_2(s_0)$ leaves the problem unchanged. It is for instance the case if the crack front is far from any boundary so that the media can be assumed to be infinite submitted to remote stress loading. Then, the first order formula simply becomes:

$$\delta\mathbf{K}(s_0) = \mathbf{N}\cdot\mathbf{K}(\mathbf{s_0})\delta'(s_0) + \frac{1}{2\pi}\ \mathrm{PV}\int_{\mathcal{F}} \frac{\mathbf{W}(s_0,s)}{D^2(s_0,s)}\cdot\mathbf{K}(s)\left[\delta(s)-\delta(s_0)\ \vec{e}_2(s_0)\cdot\vec{e}_2(s)\right]\mathrm{d}s. \tag{2.19}$$

2. Another possibility is to proceed as **Leblond et al. (1999)** and to decompose the normal advance $\delta(s)$ into a uniform advance $\delta(s_0)$ (denote $[\delta\mathbf{K}(s_0)]_{\delta(s)\equiv\delta(s_0)}$ the corresponding first order variation of the SIFs) and the advance $\delta(s)-\delta(s_0)$ for which the equation (2.15) can be used. The final expression then reads:

$$\delta\mathbf{K}(s_0) = [\delta\mathbf{K}(s_0)]_{\delta(s)\equiv\delta(s_0)} + \mathbf{N}\cdot\mathbf{K}(\mathbf{s_0})\delta'(s_0) + \frac{1}{2\pi}\ \mathrm{PV}\int_{\mathcal{F}} \frac{\mathbf{W}(s_0,s)}{D^2(s_0,s)}\cdot\mathbf{K}(s)\left[\delta(s)-\delta(s_0)\right]\mathrm{d}s. \tag{2.20}$$

This expression is useful if one can calculate $[\delta\mathbf{K}(s_0)]_{\delta(s)\equiv\delta(s_0)}$. It is the case for instance if the uniform advance $\delta(s)\equiv\delta(s_0)$ doesn't change the geometry of the problem as for a circular, straight half-plane or tunnel crack.

Formula (2.15) and its corollaries (2.18), (2.19), (2.20) have been derived for homogeneous isotropic elastic solids. For cracks at the interface between two elastic solids, such a formula exists in the sole case of a half-plane crack: the first order variation of the SIFs can be found in **Lazarus and Leblond (1998b), c** and using an other formalism (Wiener-Hopf analysis) in Bercial-Velez et al. (2005), the connection between the two methods having been done by Piccolroaz et al. (2007).

2.2.3 First order variation of the fundamental kernel

To derive higher order variation of the SIFs, the first order variation of the fundamental kernel is necessary. It has been shown by Rice (1989) in mode 1 and **Favier et al. (2006a)** in modes 2+3 that:

$$\begin{aligned}\delta\mathbf{W}(s_0,s_1) &= \mathbf{N}\cdot\mathbf{W}(s_0,s_1)\delta'(s_0) - \mathbf{W}(s_0,s_1)\cdot\mathbf{N}\,\delta'(s_1) \\ &\quad + \frac{D^2(s_0,s_1)}{2\pi}\ \mathrm{PV}\int_{\mathcal{F}} \frac{\mathbf{W}(s_0,s)\cdot\mathbf{W}(s,s_1)}{D^2(s_0,s)D^2(s_1,s)}\delta(s)\mathrm{d}s,\end{aligned} \tag{2.21}$$

if $\delta(s_0)=\delta(s_1)=0$. In order to get rid of these conditions, one must imagine a motion $\delta_{**}(s)$ such as $\delta_{**}(s_0)=\delta(s_0)$ and $\delta_{**}(s_1)=\delta(s_1)$. Denote $\delta_{**}\mathbf{W}(s_0,s_1)$ the corresponding variation of the kernel. Equation (2.21) then becomes:

$$\begin{aligned}\delta\mathbf{W}(s_0,s_1) &= \delta_{**}\mathbf{W}(s_0,s_1) + \mathbf{N}\cdot\mathbf{W}(\mathbf{s_0},\mathbf{s_1})\left[\delta'(s_0)-\delta'_{**}(s_0)\right] - \mathbf{W}(s_0,s_1)\cdot\mathbf{N}\left[\delta'(s_1)-\delta'_{**}(s_1)\right] \\ &\quad + \frac{D^2(s_0,s_1)}{2\pi}\ \mathrm{PV}\int_{\mathcal{F}} \frac{\mathbf{W}(s_0,s)\cdot\mathbf{W}(s,s_1)}{D^2(s_0,s)D^2(s_1,s)}[\delta(s)-\delta_{**}(s)]\mathrm{d}s.\end{aligned} \tag{2.22}$$

A difficulty is to be able to define $\delta_{**}(s)$ such as $\delta_{**}W(s_0,s_1)$ can be calculated. This problem has not been solved at present in the general case. In the particular case of an infinite body subjected to uniform remote loading, one can always find a combination of a translatory motion, a rotation and a homothetical transformation bringing two distinct points s_0, s_1 from any initial positions to any final positions (This is obvious using a complex variable formalism and noting that such transformations are of the form $f(z)=az+b$ where a and b are arbitrary complex parameters). Such a combination leaves the kernels unaffected so that $\delta_{**}W(s_0,s_1)=0$. Equation (2.22) then yields:

$$\begin{aligned}\delta\mathbf{W}(s_0,s_1) &= \mathbf{N}\cdot\mathbf{W}(\mathbf{s_0},\mathbf{s_1})\left[\delta'(s_0)-\delta'_{**}(s_0)\right]\\ &\quad -\mathbf{W}(s_0,s_1)\cdot\mathbf{N}\left[\delta'(s_1)-\delta'_{**}(s_1)\right]\\ &\quad +\frac{D^2(s_0,s_1)}{2\pi}\,\mathrm{PV}\int_{\mathcal{F}}\frac{\mathbf{W}(s_0,s)\cdot\mathbf{W}(s,s_1)}{D^2(s_0,s)D^2(s_1,s)}[\delta(s)-\delta_{**}(s)]\mathrm{d}s.\end{aligned} \tag{2.23}$$

Note that quantities $\delta'_{**}(s_0)$ and $\delta'_{**}(s_1)$ here are nonzero, unlike quantity $\delta'_{*}(s_0)$ in equation (2.18).

2.2.4 Some expressions of the fundamental kernel W

To initiate the perturbation approach, the FKs must be known for the unperturbed configurations. It is the case for some seldom geometries that are depicted in figures 2.2, 2.3, 2.4. In those figures, the crack front are coloured in blue and the faces in grey.

2.2.4.1 Circular cracks

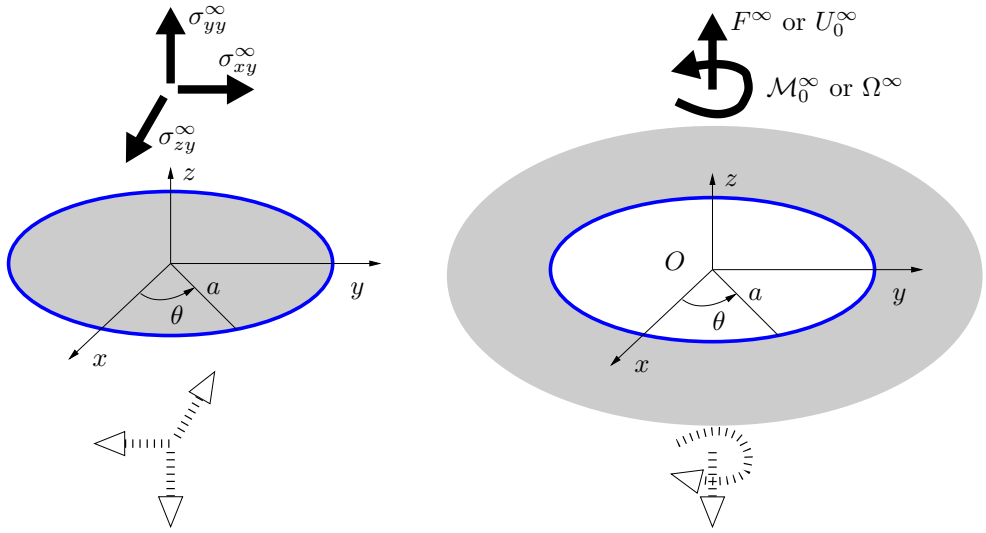

(a) An *internal circular* crack in an infinite media loaded by remote tensile and shear stresses

(b) An *external circular* crack in an infinite media loaded by remote (i) tensile net centred force or displacement and (ii) momentum or rotation

Figure 2.2: Several problems involving a circular crack.

Two cases are considered, an internal and an external crack:

- For the internal circular crack such as $\partial\Omega_u=\varnothing$, for instance loaded by remote stresses (fig. 2.2(a)), the value of the non-zero components of the kernel $\mathbf{W}$ are (Kassir and Sih, 1975; Tada

et al., 1973; Bueckner, 1987; Gao and Rice, 1987b; Gao, 1988):

$$\left\{\begin{array}{l} W_{11}(\theta_0,\theta_1) = 1 \\ W_{22}(\theta_0,\theta_1) = \dfrac{2\,\cos(\theta_0-\theta_1)-3\nu}{2-\nu} \\ W_{33}(\theta_0,\theta_1) = \dfrac{2(1-\nu)\,\cos(\theta_0-\theta_1)+3\nu}{2-\nu} \\ W_{23}(\theta_0,\theta_1) = \dfrac{1}{1-\nu}W_{32}(\theta_1,\theta_0) = \dfrac{2\,\sin(\theta_0-\theta_1)}{2-\nu}. \end{array}\right. \tag{2.24}$$

- For the external circular crack (fig. 2.2(b)), only the value in mode 1 is known (Stallybrass, 1981; Gao and Rice, 1987a; Rice, 1989) for several cases of remote boundary conditions:
  - when remote points are clamped (given $U_0^\infty = 0$, $\Omega^\infty = 0$):
  $$W_{11}(\theta_0,\theta_1) = 1 \tag{2.25}$$
  - when remote points can not rotate but can move in the $\vec{e}_1$ direction (given $F^\infty = 0$, $\Omega^\infty = 0$):
  $$W_{11}(\theta_0,\theta_1) = 1 + 4\sin^2\left(\frac{\theta_0-\theta_1}{2}\right) \tag{2.26}$$
  - when remote points can not move in the $\vec{e}_1$ direction, but can rotate (given $U_0^\infty = 0$, $\mathcal{M}_0^\infty = 0$):
  $$W_{11}(\theta_0,\theta_1) = 1 + 24\sin^2\left(\frac{\theta_0-\theta_1}{2}\right)\cos(\theta_0-\theta_1) \tag{2.27}$$
  - when remote points are constrained against any motion (given $F^\infty = 0$, $\mathcal{M}_0^\infty = 0$):
  $$W_{11}(\theta_0,\theta_1) = 1 + 4\sin^2\left(\frac{\theta_0-\theta_1}{2}\right)[1+6\cos(\theta_0-\theta_1)] \tag{2.28}$$

2.2.4.2 Half-plane crack

In the case of a half-plane crack with $\partial\Omega_u = \varnothing$, loaded for instance by remote stresses (fig. 2.3(a)) or line (fig. 2.3(b)) or surface traction (fig. 2.3(c)), the kernel is (Meade and Keer, 1984; Bueckner, 1987; Rice, 1985; Gao and Rice, 1986):

$$\left\{\begin{array}{l} W_{11}(z_1,z_0) = 1 \\ W_{22}(z_1,z_0) = \dfrac{2-3\nu}{2-\nu} \\ W_{33}(z_1,z_0) = \dfrac{2+\nu}{2-\nu} \\ W_{23}(z_1,z_0) = 0 \end{array}\right. \tag{2.29}$$

2.2.4.3 Tunnel-cracks

The model of half-plane crack is widely used due to its simplicity, but it lacks a lengthscale. To introduce a lengthscale, Leblond and coauthors have studied several cases involving a tunnel-crack (fig. 2.4) with $\partial\Omega_u = \varnothing$: Leblond et al. (1996) for the tensile tunnel-crack, **Lazarus and Leblond (2002c)** for the shear tunnel-crack (fig. 2.4(a)), **Pindra et al. (In prep)** for two coplanar tensile tunnel-cracks (fig. 2.4(b)), Legrand and Leblond (In prep.) for an external tunnel-crack (fig. 2.4(c))[3].

[3]External cracks give rise to traditional ambiguities on the external load, since they cannot withstand uniform tractions exerted at infinity. Here the situation considered unambiguously consists of two tunnel-cracks (fig. 2.4(b)) in the limiting case where $b \gg a$.

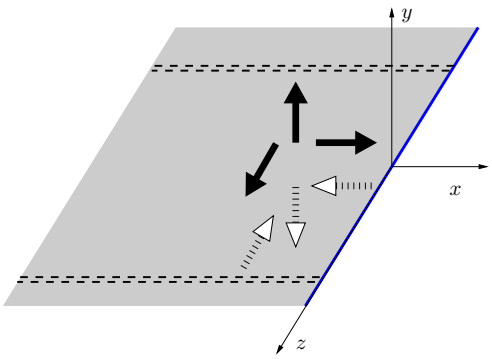

(a) A *half-plane* crack in an infinite media loaded by remote tensile and shear stresses

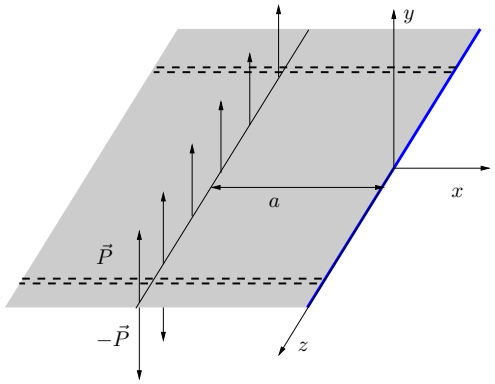

(b) A *half-plane* crack with uniform line tractions

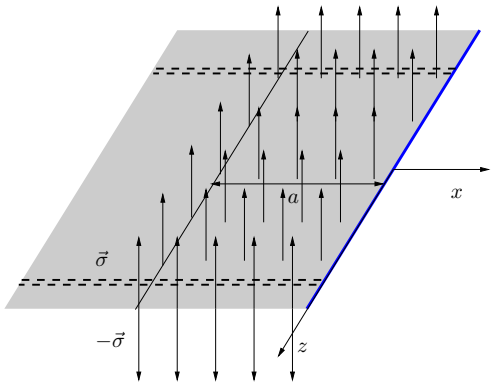

(c) A *half-plane* crack with uniform surface tractions

Figure 2.3: Several problems involving a half-plane crack

2.3 Particular model case of tensile straight crack fronts

The aim here is to introduce formulas that are useful further on for the study of some crack propagation problems involving an initially straight crack front (for sections 2.4.1 and 2.6 in particular).

2.3.1 Unperturbed geometries and loading

For simplicity, only mode 1 is considered and K_1 is re-noted K. To study the propagation of a straight crack front, the most natural and simple model is the half-plane crack loaded by remote stresses (fig. 2.3(a)). Even if a certain number of results can be obtained with this model, it lacks crucially a lengthscale. To fill this gap, this simple model has progressively be enriched. Here, the following models are considered more specifically:

1. a half-plane crack loaded by remote stresses (fig. 2.3(a)), then $K(s) = K$ is a constant due to the lack of any lengthscale in this problem;

2. a half-plane crack with uniform line tractions P at a distance a of the front (fig. 2.3(b)), then $K(z) = \sqrt{\frac{2}{\pi}} P a^{-1/2}$;

3. a half-plane crack with uniform surface tractions σ in a band of width a (fig. 2.3(c)), then

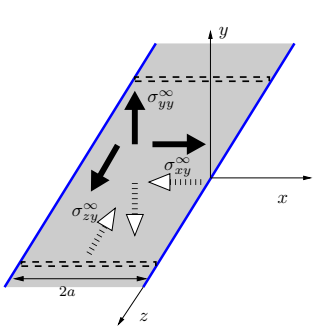

(a) A *tunnel-crack* in an infinite media loaded by remote tensile and shear stresses

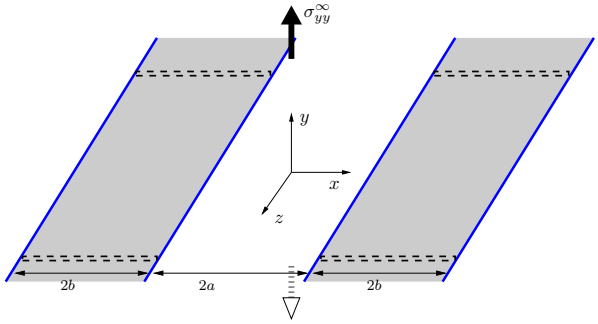

(b) Two *tunnel-cracks*, in an infinite media loaded by remote tensile stresses

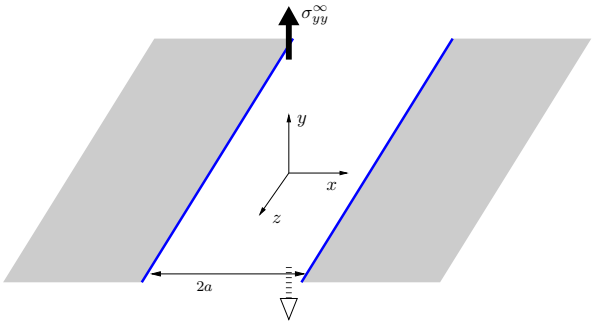

(c) An *external tunnel-crack*, in an infinite media loaded by remote tensile stresses

Figure 2.4: Several problems involving a tunnel-crack.

$$K(z) = 2\sqrt{\tfrac{2}{\pi}}\sigma\, a^{1/2};$$

4. a tunnel-crack loaded by remote stresses (fig. 2.4(a)) then $K(z) = \sigma\sqrt{\pi}a^{1/2}$;

All these problems can be included in the more general framework for which the initial SIF can be written under the form:

$$K(a) = ka^\alpha \tag{2.30}$$

where k depends on the loading level but is independent of a. The value of α are 0 in the case 1, $-1/2$ in case 2, $1/2$ in cases 3 and 4. The sign of α is of uppermost importance in the sequel. If $\alpha < 0$ the propagation is stable under constant loading and if $\alpha > 0$ unstable[4].

2.3.2 Fourier transform of the first order variation of the SIF

Define the Fourier Transform $\widehat{\phi}(k)$ of some arbitrary function $\phi(z)$ by

$$\widehat{\phi}(k) \equiv \int_{-\infty}^{+\infty} \phi(z)e^{ikz}\mathrm{d}z \quad \Leftrightarrow \quad \phi(z) \equiv \frac{1}{2\pi}\int_{-\infty}^{+\infty} \widehat{\phi}(k)e^{-ikz}\mathrm{d}k. \tag{2.31}$$

[4]This terminology makes an implicit reference to Irwin's propagation law (2.7) for which crack propagation occurs when the SIF reaches some critical value. For such a law and under constant loading, after the onset of crack propagation, the velocity of the crack goes immediately down to zero if the SIF decreases with distance, but continuously increases in the opposite case; hence the expressions "stable propagation", "unstable propagation".

Using this definition and equation (2.20) applied to the geometries listed in section 2.3.1, Fourier components $\delta\widehat{K}(k)$ of the first order variation of the mode 1 SIF $\delta K(z)$ can be written under the following form:

$$\frac{\delta\widehat{K}(k,a)}{K(a)} = \left[\frac{\frac{\mathrm{d}K(a)}{\mathrm{d}a}}{K(a)} - a^{-1}F(p)\right]\widehat{\delta}(k) = (\alpha - F(p))\,\frac{\widehat{\delta}(k)}{a} \tag{2.32}$$

Here, k is the wavenumber and $p = ka$ the dimensionless one. In the case of the tunnel-crack geometry, we have supposed that the perturbations are the same for all the fronts for simplicity, so that if we denote $\delta_n(z)$ the perturbation of $\mathcal{F}_n$, it exists a function $\delta(z)$ such as $\delta_n(z) = \delta(z)$ whatever $n = 1, N$. $F(p)$ can be derived from the expressions of the fundamental kernels listed in section 2.2.4. For instance, for the half-plane crack it reads:

$$F(p) = \frac{p}{2} \tag{2.33}$$

and for all the geometries of §2.3.1, it can be verified that (i) $F(0) = 0$ and (ii) $F(p)$ increases monotonically to finally behaves as $p/2$ for $p \to \infty$. This last behaviour is closely linked to the universal behaviour of $W_{11}(s, s')$ for $s' \to s$ (eq. 2.14).
The general formulas for the tunnel-crack, without the symmetry hypothesis $\delta_n = \delta$ of the crack advance, can be found in Favier et al. (2006b). A formula similar to (2.32) can be find in Gao and Rice (1987b) (resp. Gao and Rice (1987a)) for an internal (resp. external) circular crack, in **Pindra et al. (In prep)** for two tunnel-cracks and in Legrand and Leblond (2010) for an external tunnel-crack. For shear loading, see Gao and Rice (1986) for the half-plane crack, **Pindra et al. (2008a)** for the interfacial half-plane crack, **Pindra et al. (2010)** for the tunnel-crack.

2.4 Crack propagation in an homogeneous media

The aim of this section is to study the crack front shape changes arising from the propagation in an homogeneous media. First the problem of crack shape bifurcation and stability (section 2.4.1) is studied analytically by linear approaches, then large scale deformations (section 2.4.2) are presented using incremental non linear numerical simulations.

2.4.1 Crack front shape linear bifurcation and stability analysis

First order perturbation approaches are extensively used in linear bifurcation and stability analysis in various problems (Drazin, 1992; Bazant and Cedolin, 2003; Nguyen, 2000). Here the problem of configurational bifurcation and stability of a straight crack front is considered.

2.4.1.1 Bifurcation

Consider one of the model problems of section 2.3 and suppose that $K(z) = K_c$ for all z. The configurational bifurcation problem aims at answering the following unicity question: can one find any configuration satisfying the condition that the SIF be equal to a constant along the crack front, other than the initial straight one?
The linear bifurcation problem amounts to search for a crack front perturbation $\delta(s) \neq 0$ such as the first order variation $\delta K(s)$ of the SIF is zero. By equation (2.32), this reads:

$$[\alpha - F(p)]\,\widehat{\delta}(k) = 0, \tag{2.34}$$

so that non-zero solution exists if $[\alpha - F(p)] = 0\ \forall p$. Since $F(p) \geq 0$, it exists only if $\alpha \geq 0$ that is if the propagation is unstable under constant loading. The bifurcation corresponds to a sinusoidal

perturbation of critical wavelength λ_c solution of (α has been introduced in 2.30):

$$\lambda_c = \lambda_c^* \, a, \text{ where } \lambda_c^* = \frac{2\pi}{F^{-1}(\alpha)} \tag{2.35}$$

For the half-plane crack, it corresponds to Rice (1985)'s result:

$$\lambda_c = \frac{\pi K(a)}{\frac{\mathrm{d}K(a)}{\mathrm{d}a}}, \tag{2.36}$$

which gives $\lambda_c = 2\pi a \sim 6.283\, a$ in the case of surface tractions (fig. 2.3(c)). For the single tunnel-crack under remote loading, $\lambda_c = 6.793\, a$ (Leblond et al., 1996) and two interacting tunnel cracks $\lambda_c = 18.426\, a$ when $a \ll (b + a)$ (fig. 2.4(b)).

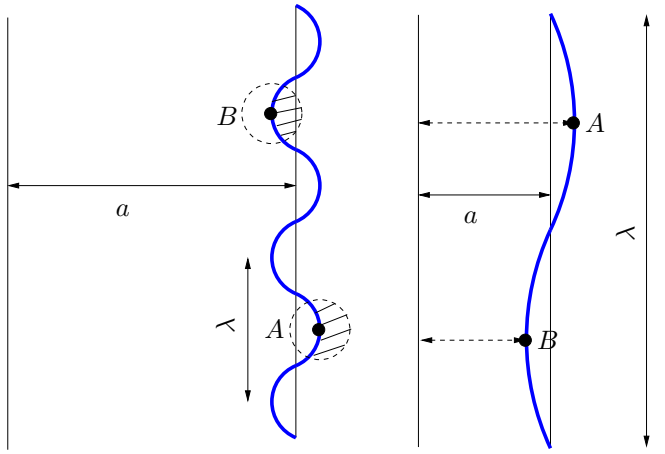

(a) Small wavelength $\lambda \ll a$ (b) Large wavelength $\lambda \gg a$

Figure 2.5: Sinusoidal perturbation of the crack front

The existence of a bifurcation if $\frac{\mathrm{d}K(a)}{\mathrm{d}a} > 0$ and the nonexistence if $\frac{\mathrm{d}K(a)}{\mathrm{d}a} < 0$ has still been noticed by Nguyen (2000) in the case of thin films. It may be rationalised as follows:

1. Consider first a perturbation of the crack fronts of small wavelength, $\lambda \ll a$ (Figure 2.5(a)). The crack advance is maximum at point A and minimum at point B. Draw small circles centred at these points. That part of the interior of the circle occupied by the unbroken ligament (hatched in Figure 2.5(a)) is larger at point A than at point B, so that the opening of the crack is more hindered near the first point than near the second. Thus the stress intensity factors $K(A)$, $K(B)$ at points A and B obey the inequality $K(A) < K(B)$.

2. Consider now a perturbation of large wavelength, $\lambda \gg a$, and again points A and B where the crack advance is respectively maximum and minimum (Figure 2.5(b)). The stress intensity factors at points A and B are almost the same as for ligaments of uniform width equal to the local width at these points (indicated by dashed double arrows in Figure 2.5(b)). It follows that $K(A) > K(B)$ if $\frac{\mathrm{d}K(a)}{\mathrm{d}a} > 0$ and that $K(A) < K(B)$ if $\frac{\mathrm{d}K(a)}{\mathrm{d}a} < 0$.

This implies:

- In the case $\frac{\mathrm{d}K(a)}{\mathrm{d}a} > 0$, the difference $K(A) - K(B)$ is negative for small λ and positive for large λ, and obviously varies continuously with this parameter. Hence some special value λ_c such that $K(A) - K(B) = 0$ must necessarily exist.

- In the case $\frac{\mathrm{d}K(a)}{\mathrm{d}a} < 0$, the difference $K(A) - K(B)$ is negative for all λ, so that no bifurcation is possible.

In the case of shear loading, the results are more complex and can be found in Gao and Rice (1987b) for the internal circular crack, in Gao and Rice (1986) for the half-plane crack and in **Lazarus and Leblond (2002b)** for the tunnel-crack. For thin films, crack front bifurcation has also be studied by Nguyen (2000); Adda-Bedia and Mahadevan (2006) and observed in experiments (Ghatak and Chaudhury, 2003).

2.4.1.2 Stability

The question here is as follows: if the crack front is slightly perturbed within the crack plane, will the perturbation increase (instability) or decay (stability) in time? Equivalently, will the crack front depart more and more from its initial configuration or tend to keep it? We restrict our attention here to the cases listed in section 2.3 for which the SIF $\mathbf{K}(z)$ in the initial configuration are uniform independent of z.

When the extrema of $\delta(z)$ and $\delta G(z)$ coincide, stability or instability prevails according to whether the maxima of $\delta G(z)$ correspond to the minima or maxima of $\delta(z)$ (Rice, 1985; Gao and Rice, 1986, 1987b; Gao, 1988; Leblond et al., 1996; Lazarus and Leblond, 1998b; Legrand and Leblond, 2010). Hence the answer to the question can simply be derived from the above bifurcation discussion: sinusoidal perturbations are stable if $\alpha - F(p) < 0$ that is for wavelength smaller than the bifurcation wavelength λ_c (eq. 2.35) and unstable for $\lambda > \lambda_c$. In the case of non-existence of a bifurcation (stable propagation $\alpha < 0$), stability is thus achieved whatever the wavelength. In the case $\alpha > 0$, the critical wavelength is proportional to a, thus continuously increases during propagation, stability ultimately prevails for all wavelengths.

But when the extrema of $\delta(z)$ and $\delta G(z)$ do not coincide, as is for instance the case of the tunnel-crack under shear loading **(Lazarus and Leblond, 2002b)**, it appears quite desirable to then discuss the stability issue in full generality, without enforcing such a coincidence **(Lazarus and Leblond, 2002a)**. It is then necessary to introduce a time dependent advance law.
Let us use here the Paris law (2.9) with $K_0 = 0$. Its leading term reads:

$$\frac{\mathrm{d}a(t)}{\mathrm{d}t} = CK^N \tag{2.37}$$

where $a(t)$ is the mean position of the crack front at instant t. Considering henceforward all perturbations as functions of the mean position a of the crack instead of time t, one gets the first order advance equation:

$$\frac{\partial \delta(k,a)}{\partial a} = N\frac{\delta K(k,a)}{K}, \tag{2.38}$$

which yields (Favier et al., 2006b) after use of FT (2.32) and integration (a_0 denotes the initial value of a):

$$\frac{\widehat{\delta}(k,a)}{\widehat{\delta}(k,a_0)} = \exp\left[N\int_{ka_0}^{ka}(\alpha - F(p))\frac{\mathrm{d}p}{p}\right] \tag{2.39}$$

or using the property $F(0) = 0$:

$$\frac{\widehat{\delta}(k,a)}{\widehat{\delta}(k,a_0)} = \left(\frac{a}{a_0}\right)^{N\alpha}\left(\frac{\psi(ka)}{\psi(ka_0)}\right)^{N\alpha}, \tag{2.40}$$

where $\psi(p)$ is defined by:

$$\psi(p) = \exp\left[-\int_0^p \frac{F(q)}{q}\mathrm{d}q\right] \tag{2.41}$$

For the half-plane crack, its value is $\psi(p) = \exp\left(-\frac{p}{2}\right)$, for the tunnel-crack it can be found in **Favier et al. (2006b)**. For the sequel, it is useful to note that whatever the geometry (half-plane or tunnel), this function $\psi(p)$ decreases from 1 to 0 when p varies from 0 to $+\infty$.
From equation (2.39), it is clear that:

- If $\frac{\mathrm{d}K(a)}{\mathrm{d}a} < 0$, then $\alpha - F(p) < 0$ so that all Fourier components of any wavelength decrease with crack growth a.
- If $\frac{\mathrm{d}K(a)}{\mathrm{d}a} > 0$, for any given k, $\left|\widehat{\delta}(k,a)\right|^2$ increases as long as a remains smaller than $\frac{2\pi}{k\lambda_c^*}$ and decreases afterwards.

For $t \to \infty$, one can show that:

$$\begin{cases} \text{For } k = 0, & \left|\dfrac{\widehat{\delta}(0,a)}{\widehat{\delta}(k,a_0)}\right|^2 = \left(\dfrac{a}{a_0}\right)^{2N\alpha} \\ \text{For } k \neq 0, & \left|\dfrac{\widehat{\delta}(k,a)}{\widehat{\delta}(k,a_0)}\right|^2 \sim \left(\dfrac{a}{a_0}\right)^{2N\alpha} \exp(-N\,|k|\,a) \to 0 \end{cases} \tag{2.42}$$

so that:

- If $\frac{\mathrm{d}K(a)}{\mathrm{d}a} < 0$, any initial perturbation disappears.
- If $\frac{\mathrm{d}K(a)}{\mathrm{d}a} > 0$, the moduli of all Fourier components ultimately decay, except for $k = 0$ which continuously increases. This phenomenon is due to the fact that for all values of λ except $+\infty$, λ always ultimately becomes smaller than $\lambda_c(a)$ since the former wavelength is fixed whereas the latter increases in proportion with a.

Thus, one can conclude that whatever the small perturbation of crack front, the initial configuration is finally retrieved[5]. In the case of stable crack propagation $\frac{\mathrm{d}K(a)}{\mathrm{d}a} < 0$, the stability prevails at all lengthscales from the beginning. In the case of unstable crack propagation $\frac{\mathrm{d}K(a)}{\mathrm{d}a} > 0$, instability first prevails for all lengthscales such as $\lambda > \lambda_c$, but since λ_c is a growing function of the crack advance a, all wavelengths finally becomes stable so that the perturbation finally disappears. This is true for all the problems listed in section 2.3 provided that the first order study stays valid. To extend them to large perturbations, higher order terms must be taken into account. This is the subject of next section.

2.4.2 Largescale propagation simulations

In the previous sections, the perturbation approach was applied to small perturbations of the crack front. Following an original idea of Rice (1989), Bower and Ortiz (1990) first extended the method to the study of arbitrary large propagation of a tensile crack leading the way to the numerical resolution of some complex three dimensional crack problems. It consists in applying numerically the perturbation approach described in section 2.2, to a succession of small perturbations arising in arbitrary large ones. The media is assumed to be infinite loaded by remote stresses so that the SIF can be updated using formula (2.19) and the FKs using formula (2.23). The crack front shape at each instant is obtained by

[5] the wavelength $k = 0$ corresponds indeed to a infinite wavelength that is an almost straight crack front.

the inversion of heavily implicit systems of equations resulting from the direct application of Irwin's criterion (2.7). The method was then extended and simplified by **Lazarus (2003)**; notably a unified Paris' type law (2.9) formulation for fatigue and brittle fracture ($N \to +\infty$) is proposed that gives the advance of the crack front in explicit form once the SIF is known. Extension to shear loading is performed in **Favier et al. (2006a)**.

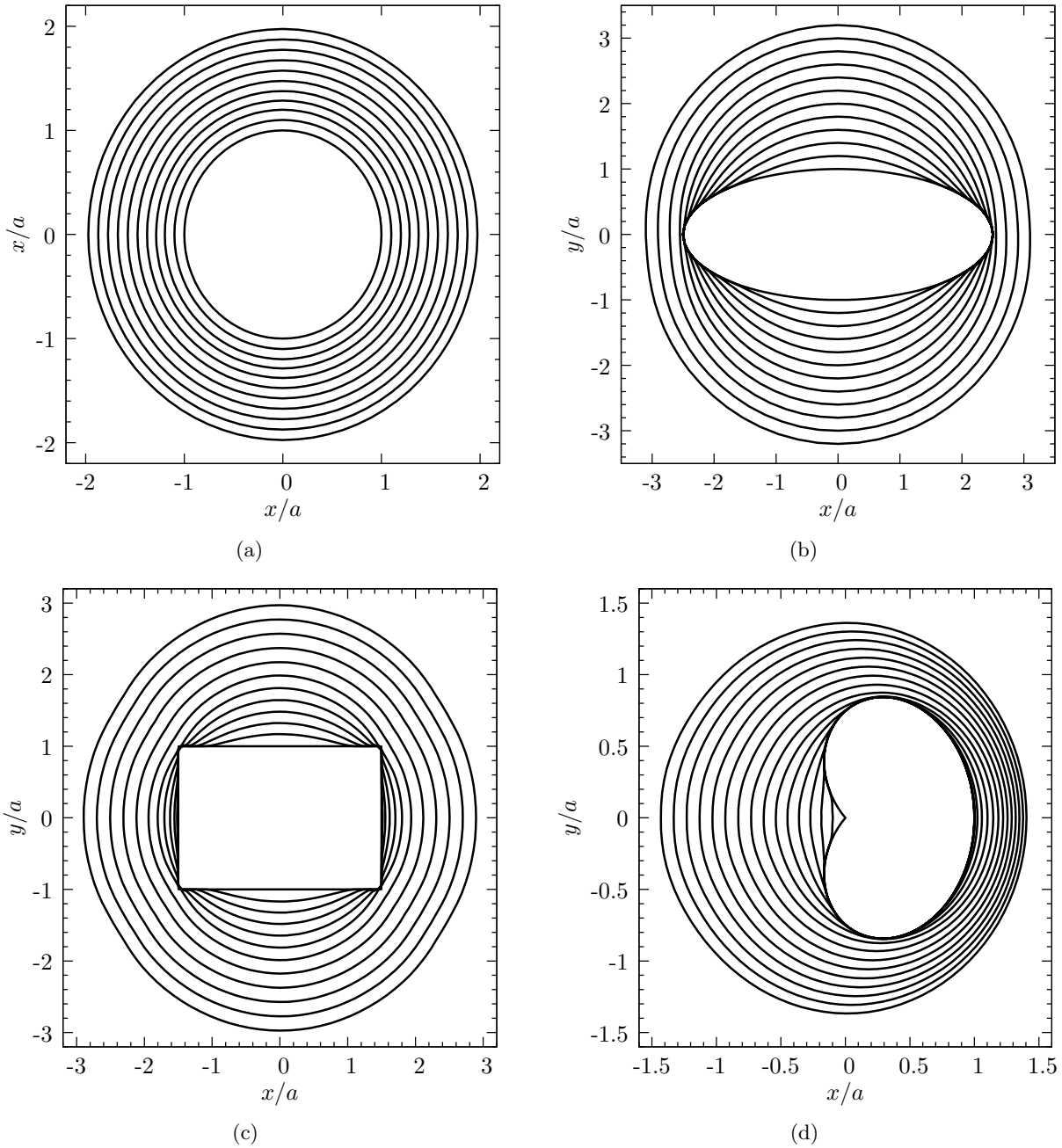

Figure 2.6: Successive crack fronts of pure tensile mode cracks in brittle fracture (eq. 2.9 with $N = 50$, $K_0 = 0$). Similar figures for fatigue can be found in Lazarus (2003) and show the same circular stationnary crack shape.

Concerning propagation in an homogeneous media, **Lazarus (2003)** studied the asymptotic behaviour of the SIF near an angular point of the front and retrieved the theoretical results of Leblond and Leguillon (1999) about the SIF singularity around a corner point of the front, the fatigue and brittle propagation paths of some special crack shapes (elliptical, rectangular, heart shaped ones) (fig. 2.6) loaded by remote tensile stresses. It appears that in all the cases studied, the crack becomes and stays circular after a certain time emphasizing that among all the configurations studied only the circular crack shape is stationnary. In the case of shear loading **(Favier et al., 2006a)**, it appears (fig. 2.8) that the stationnary shape is nearly elliptic, the ratio of the axes being well approximated by:

$$\frac{a}{b} = (1-\nu)^{\frac{\beta}{\beta+1}}, \tag{2.43}$$

β is the Paris law exponent in mixed mode loading (2.8), b corresponds to the axis in the direction of the shear loading. Whether all embedded plane cracks tend toward a configuration with uniform value of $\mathcal{G}(s)$ is a general result, has however, to my best knowledge, not been demonstrated, even if one guess that energy minimisation is the physical ground.

2.5 Crack trapping by tougher obstacles

In previous section, all the material constants (elasticity coefficients, fracture toughness) were supposed to be homogeneous throughout the media. In the sequel, the toughness becomes heterogeneous, but the elasticity coefficients are supposed to remain constant so that the perturbation approach of section 2.2 remains valid. If the toughness is heterogeneous, the crack advance changes from point to point and the crack front shape changes during propagation even if the SIFs were initially uniform. In this section, the propagation of the front through well defined tougher obstacles is studied. In section 2.6, the toughness is supposed to be disordered so that a statistical approach is necessary.
Tougher inclusions may prevent or hinder the final breaking of a solid by two mechanisms: crack bridging and crack front trapping. The mechanism of toughening referred to as bridging occurs when unbroken inclusions lag behind a main crack front hindering its opening by pinning or friction; and as trapping when the crack front is deformed when it penetrates into the tougher zone or bows out it (Lange, 1970).
Whereas some aspects of crack bridging can be studied by 2D elasticity problems (Budiansky et al., 1988), crack trapping induces crack front shape deformations that makes the elasticity problem fully 3D. To understand the mechanism, let us consider a tunnel-crack loaded by remote tensile loading σ (fig. 2.4(a)) . The SIF for the straight-crack front then reads:

$$K = \sigma\sqrt{\pi a} \tag{2.44}$$

In the absence of obstacles, the propagation is unstable under constant loading so that the breakdown of the solid occurs as soon as the threshold is reached, unless the loading is decreased to ensure that $K(s) \leq K_c$ at each instant: $\sigma = K_c/\sqrt{\pi a}$. In the presence of tougher ($K_c^p > K_c^m$, K_c^p, K_c^m being resp. the matrix and particles toughness), the crack propagation of a tunnel-crack of width $2a_0$ starts when $\sigma = \sigma_0$, where $\sigma_0 = K_c^m/\sqrt{\pi a_0}$. Then,

- either the spacing between the obstacles is large enough, so the SIF in the matrix still increases at constant loading. The final breakdown then occurs for $\sigma = \sigma_0$.
- either the spacing is small enough, so the SIF in the matrix decreases at constant loading. Then a transient period of stable propagation at constant loading exists, so that the unstable propagation loading, that is the breakdown one, is increased.

In this last case, the breakdown may appear in two different situations:

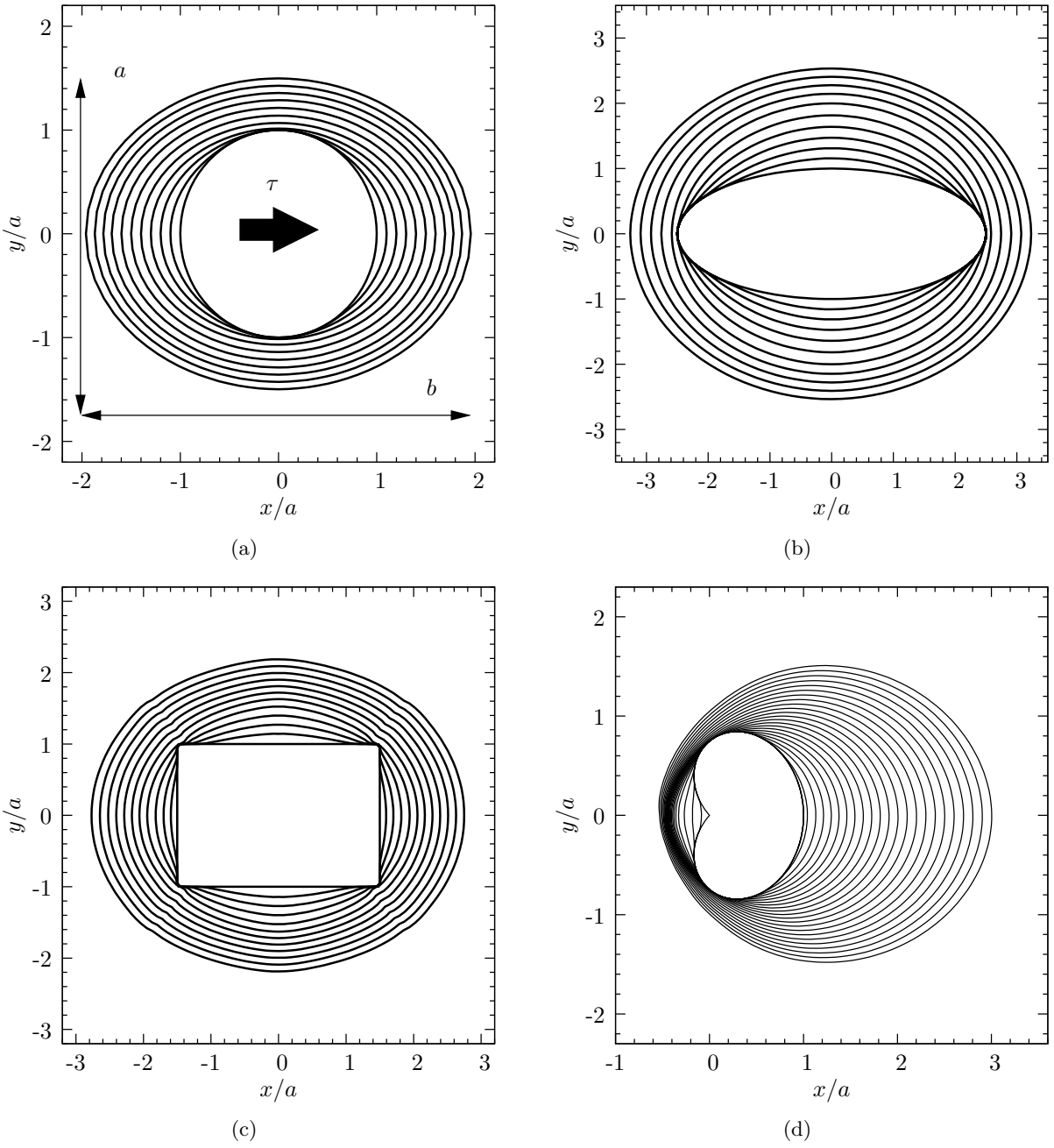

Figure 2.7: Successive crack fronts of pure shear mode cracks in brittle fracture (eq. 2.8 with $\beta = 25$, $\mathcal{G}_0 = 0$). Shear is along the $x-$axis. Similar figures for fatigue can be found in Favier et al. (2006a) and show also a quasielliptic stationnary crack shape.

1. The crack front has penetrated under a stable manner into the obstacles until reaching a configuration such as $K(s) = K_c(s)$ for all s at unstable breakdown instant. The corresponding loading level σ_c can then be determined by the following relation derived by Rice (1988); Gao and Rice (1989):

$$\frac{\sigma_c^2}{\sigma_0^2} = \frac{< K_c^2 >}{(K_c^m)^2} \tag{2.45}$$

This situation is called "regular" by Gao and Rice (1989). It appears for not too large toughness differences (to ensure not too large crack front deformations) and particles that are large enough in the direction of propagation (to have the time to reach the equilibrium position). First order simulations of this regime have been performed by Gao and Rice (1989) using the perturbation approach described in section 2.2.2. The results have been compared to simulations of the same problem performed using a Boundary Element Method showing the accuracy and the limits of the first order approach. They have also been compared to experiments by Dalmas et al. (2009): good agreement between the theoretical and experimental crack shapes have been shown. The work of Gao and Rice (1989) realized in mode 1 is extended to modes 2 and 3 in Gao et al. (1991).

2. The unstable breakdown occurs before $K(s) = K_c(s)$ is reached for all s, so that only a part of the front propagates at the breakdown instant, $K(s)$ being lower than $K_c(s)$ on the other part. In this situation, called "irregular" by Gao and Rice (1989) and "unstable" by Bower and Ortiz (1991), the value of σ_c can only be determined numerically in each particular case. It has been done by Bower and Ortiz (1990, 1991, 1993), using the incremental method described in section 2.4.2, for a half plane crack propagating through an array of particles. Their results concerning the bow out of the crack front segments beyond an unbroken particle when the toughness of the particles is high enough to prevent the penetration of the front in the particle are compared to experiments by Mower and Argon (1995) and show good agreement in general.

2.6 Crack propagation in a disordered media

In the last two decades, a number of works have been devoted to the study of the evolution in time of the shape of the front of planar cracks propagating in mode 1 in an elastic solid with randomly variable fracture toughness. These works can be roughly divided into three groups. The first group includes the works of Perrin and Rice (1994), Ramanathan and Fisher (1997) and Morrissey and Rice (1998, 2000). They were devoted to the theoretical study of some statistical features of the geometry of the front of a tensile half-plane crack propagating dynamically. The second group of papers consists of some experimental studies of the evolution in time of the deformation of the front propagating quasistatically; see e.g. Schmittbuhl and Måløy (1997), Delaplace et al. (1999), Schmittbuhl and Vilotte (1999), Schmittbuhl et al. (2003a). The third group studied statistical properties of the shape of crack fronts for a straight crack (half-plane or tunnel-crack) propagating quasistatically: on the one hand, Schmittbuhl et al. (1995a) and Katzav and Adda-Bedia (2006) focusing notably on self-affine properties of the crack front shape and on the other hand **Favier et al. (2006b)**, **Pindra et al. (2008a)**, **Pindra et al. (2010)**, Legrand and Leblond (2010) focusing essentially on the time evolution of the statistical properties (correlation functions and power spectra).
The main results of this last set of somewhat complex papers, in particular of **Favier et al. (2006b)** and **Pindra et al. (2008a)**, are recalled in this section under a new simplified form in the spirit to be comprehensible by a broader audience. The model problems listed in section 2.3 are considered, first in the case of brittle fracture (§2.6.1), than in the case of subcritical or fatigue growth (§2.6.2). In §2.6.3 a synthetic table is presented showing the main results. Comparison with experiments is done in section 2.6.4.

2.6.1 Brittle fracture: case $K(x, z) = K_c(x, z)$

Let us consider a half-plane or tunnel crack. We suppose that the SIF for the straight configuration is given by equation (2.30). The aim of this paragraph is to describe the crack front shape corresponding to $K(x, z) = K_c(x, z)$ for all points of the front when $K_c(x, z)$ is varying randomly.

2.6.1.1 Fourier transforms of the crack front fluctuations versus toughness fluctuations

If the toughness $K_c(x,z)$ is uniformly equal to a constant K_c, the crack front remains straight during propagation. Then the loading $k(t)$ corresponding to position $a(t)$ of the front at time t verifies:

$$k(t) = K_c a(t)^{-\alpha} \tag{2.46}$$

The parameter t, called "time" for convenience, appearing in this equation is not a physical time but a purely kinematical time, enabling us to locate the equilibrium position corresponding to a given loading $k(t)$. Remember that the propagation is stable (resp. unstable) if $\alpha < 0$ (resp. $\alpha > 0$), in the sense that the loading has to be increased (resp. decreased) for the crack to advance (a increases).

Now introduce some small fluctuations of the toughness :

$$K_c(z,x) = \overline{K}_c(1+\kappa(z,x)), \quad |\kappa| \ll 1 \tag{2.47}$$

It produces small fluctuations $\delta(z,a(t))$ and $\delta K(z,a(t))$ of the crack front position $a(z,t)$ and of the SIF $K(z,t)$ around its mean values $a(t)$ and $K(a(t))$ so that :

$$\left\{ \begin{array}{lcll} a(z,t) & \equiv & a(t)+\delta(z,a(t)), & |\delta(z,a(t))| \ll a(t) \\ K(z,a(t)) & \equiv & K(a(t))+\delta K(z,a(t)), & |\delta K(z,a(t))| \ll K(a(t)) \end{array} \right. \tag{2.48}$$

Expanding Irwin's criterion (2.7) to first order, identifying terms of order 0 and 1 and replacing the kinematical time t by the mean crack position a, one gets :

$$\left\{ \begin{array}{l} K(a) = \overline{K}_c \\ \\ \dfrac{\delta K(z,a)}{K(a)} = \kappa(z,a) \end{array} \right. \tag{2.49}$$

Taking the Fourier transform of the equation (2.49.2) and using equation (2.32) giving the first order variation of the SIF as a function of the crack perturbation, one gets:

$$\hat{\delta}(k,a) = \frac{a\hat{\kappa}(k,a)}{\alpha - F(ka)} \tag{2.50}$$

Unfortunately, if $\alpha > 0$, the expression (2.50) is meaningless because the FT is divergent for p such as $\alpha - F(p) = 0$. This is linked to the existence of bifurcations (see section 2.4.1). We shall therefore consider the sole case of stable 2D crack propagation ($\alpha < 0$) henceforward. Eq. (2.50) then takes the form:

$$\hat{\delta}(k,a) = -\frac{a\hat{\kappa}(k,a)}{|\alpha| + F(p)} \tag{2.51}$$

This equation allows to obtain the first order crack front fluctuations δ for any given small toughness fluctuation κ. Notice that it is entirely determined by the instantaneous distribution of the toughness. It may be used to study the shape deformations during trapping by tougher obstacles. In the sequel, however we suppose the material to be disordered so that only statistical properties of κ are known and statistical study becomes necessary.

2.6.1.2 Power spectrum of the crack front fluctuations versus toughness fluctuations

From equation (2.51), one gets for the power spectrum $\widehat{\mathcal{A}}(k,a)$ of the fluctuation $\delta(z)$ of the crack front:

$$\widehat{\mathcal{A}}(k,a) = a^2 \frac{\widehat{\mathcal{K}}(k)}{\left(|\alpha| + F(p)\right)^2} \tag{2.52}$$

where $\widehat{\mathcal{K}}(k)$ is the power spectrum associated with the toughness fluctuations κ supposed statistical homogeneous so that $\widehat{\mathcal{K}}(k)$ is independent of a. This expression is quiet general. Some properties of it, in the particular case of uncorrelated fluctuations are given in the sequel.

In the case of white noise $\widehat{\mathcal{K}}(k,a) = \widehat{\mathcal{K}}_0$, equation (2.52) gives $\frac{\widehat{\mathcal{A}}(k,a)}{\widehat{\mathcal{K}}_0 a^2}$ under an analytical form:

$$\frac{\widehat{\mathcal{A}}(k,a)}{\widehat{\mathcal{K}}_0 a^2} = \frac{1}{\left(|\alpha| + F(p)\right)^2} \tag{2.53}$$

It is plotted as a function of $p = ka$ in figure 2.8(a) for several values of α and a tunnel or a half-plane crack. In all these cases, one can notice the presence of two regimes, with a transition between them depending on the crack geometry and on the loading: one universal regime (independent of the geometry) for $p = ka \gg 1$ that is small wavelengths $\lambda \ll a$ where $\frac{\widehat{\mathcal{A}}(k,a)}{\widehat{\mathcal{K}}_0 a^2}$ decreases with ka and a second, geometry dependent one, for $p = ka \ll 1$ that is large wavelengths $\lambda \gg a$ corresponding to a saturation. The existence of this second regime is closely linked to the finite size of the system and can not be obtained by the model of a half-plane crack loaded by remote tensile stresses that, we recall, lacks any lengthscale.
One can notice that such a behaviour (see Barabási and Stanley (1995)) corresponds to a Family and Vicsek (1985) scaling defined by $\widehat{\mathcal{A}}(k,a) = a^{\frac{1+2\zeta}{\tau}} G(ka^{1/\tau})$ where $G(x)$ is constant for $x \ll 1$ and $G(x) \sim x^{-1-2\zeta}$ for $x \gg 1$. Comparison with (2.53) gives indeed:

$$G(x) = \widehat{\mathcal{K}}_0 \left(|\alpha| + F(x)\right)^{-2}, \quad \zeta = 0.5 \text{ (roughness exponent) and } \tau = 1 \text{ (dynamic exponent).} \tag{2.54}$$

To better understand the Family and Vicsek (1985) scaling, let us study the dependence over k and a of $\frac{\widehat{\mathcal{A}}(k,a)}{\widehat{\mathcal{K}}_0}$ and consider the particular case of a half-plane crack with $\alpha = -1/2$. One can notice on figure 2.8(b), that for a given value of the mean position a:

- The large wavelength components are more developed than the small ones and are constant above a certain threshold.
- When a increases, the large wavelength components increases, but the small ones are steadystate and more and more components are in this last steadystate regime.

One can notice on figure 2.8(c), that for a given value of k, that is λ:

- The components increases with a until reaching a saturation.
- The increasing regime rate is similar whatever the wavelength, but when k decreases, that is λ increases, the increasing regime lasts longer so that the final amplitude increases with wavelength.

One can also derive the asymptotic expressions of the power spectrum $\widehat{\mathcal{A}}(k,a)$:

$$\widehat{\mathcal{A}}(k) = \frac{4\widehat{\mathcal{K}}(k)}{k^2} \text{ for } k \neq 0 \quad \text{ and } \widehat{\mathcal{A}}(0) = \frac{\widehat{\mathcal{K}}(0) a^2}{\alpha^2} \text{ for } k = 0 \tag{2.55}$$

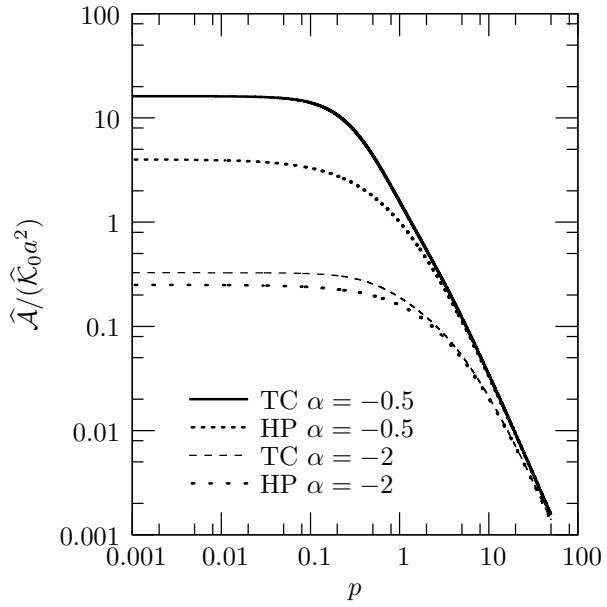

(a) Master curves for different geometries (TC=tunnel-crack, HP=half-plane crack) and values of α.

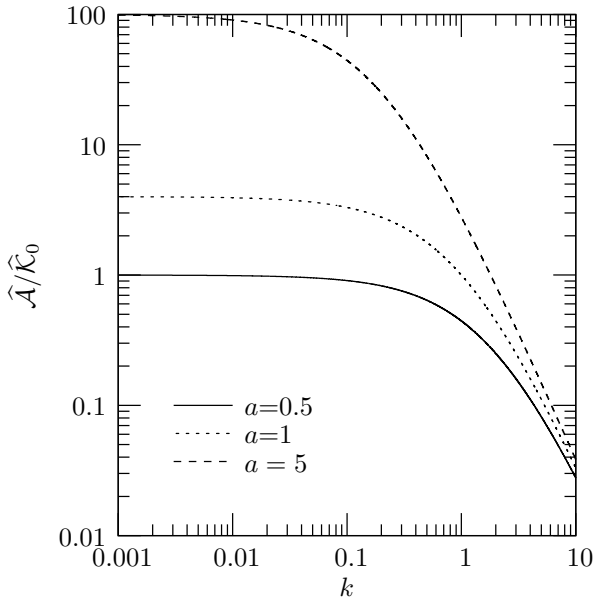

(b) Dependence toward k for several given values of a (half-plane crack with $\alpha = -1/2$).

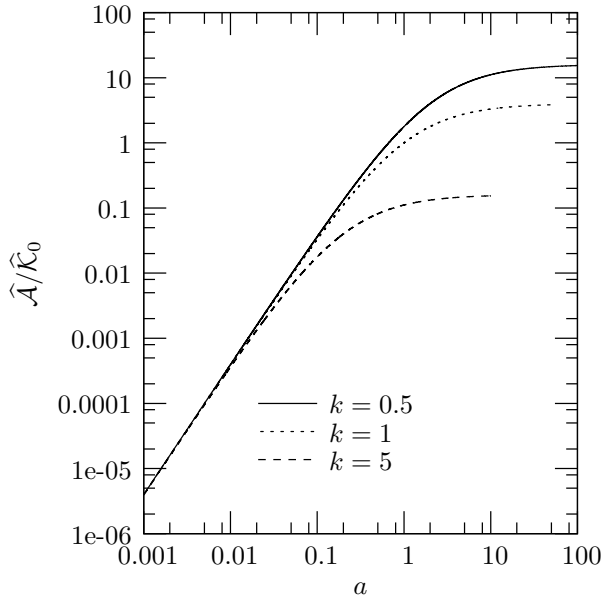

(c) Dependence toward a for several given values of k (half-plane crack with $\alpha = -1/2$).

Figure 2.8: Power spectrum of the crack front fluctuations for white noise toughness fluctuations.

One shall notice that the convergence is not uniform so that the asymptotic behaviour of the autocorrelation function can not be obtained by simply inversion of the asymptotic behaviour of its Fourier transform. For the results concerning the autocorrelation or related function as the square fluctuations, the reader is invited to reefer at **Pindra et al. (2008a)** or to the table 2.1. One shall however notice that relation (2.52) is the cornerstone for such a derivation. It shall also allow to perform numerical simulations of the evolution of the power spectrum or the functions related to the autocorrelation by

inverse Fourier Transform if the toughness fluctuation power spectrum is given. Such developments is left for further work.
Similar results for an interfacial half-plane crack have been derived by **Pindra et al. (2008a)**: the mismatch of elastic properties between the materials introduces oscillations in the longtime behaviour but no significant difference in the mean behaviour. The case of a shear tunnel-crack has been considered by **Pindra et al. (2010)**: the results are rather similar to those previously obtained for mode 1; one novelty, however, is that, the fronts no longer tend to become symmetrical in time as in mode 1 **(Favier et al., 2006b)**, so that correlations between crack front fluctuations at two points are higher for points located on the same front than for points located on distinct ones.

2.6.2 Subcritical or fatigue propagation

Let us suppose now that the crack advance is given by Paris' law (2.9) with $K_0 = 0$. The inhomogeneity of the material is modelled by assuming the Paris constant to slightly fluctuated around its mean value; the Paris exponent N being considered as uniform for simplicity:

$$C(z,x) = C(1 + \delta c(z,x)), \quad |\delta c(z,x) \ll 1| \tag{2.56}$$

It produces small fluctuations $\delta(z, a(t))$ and $\delta K(z, a(t))$ of the crack position and the SIF around its mean position a (eq. 2.48).

2.6.2.1 Evolution of the perturbation of the crack front

Expanding first the propagation law to first order in $\delta(z,t)$, $\delta K(z,t)$ and identifying terms of order 0 and 1, one gets

$$\left\{ \begin{array}{lcl} \dfrac{da}{dt}(t) & = & C\left[K(t)\right]^N \\ \dfrac{\partial \delta}{\partial t}(z,t) & = & C[K(t)]^N \left[N \dfrac{\delta K(z,a(t))}{K(t)} + \delta c(z,a(t)) \right]. \end{array} \right.$$

Eliminating dt between these expressions and considering henceforward all perturbations as functions of the mean position $a(t) \equiv a$ of the crack instead of time, one gets

$$\frac{\partial \delta}{\partial a}(z,a) = N \frac{\delta K(z,a)}{K(a)} + \delta c(z,a).$$

Upon use of the Fourier decompositions of $\delta(z,a)$, $\delta K(z,a)$, $\delta c(z,a)$ and equation (2.32), this finally yields the evolution equation of the Fourier transform $\widehat{\delta}(k,a)$ of the perturbation of the crack front:

$$\frac{\partial \widehat{\delta}}{\partial a}(k,a) = \frac{N}{a}\left[\alpha - F(ka)\right]\widehat{\delta}(k,a) + \widehat{\delta c}(k,a). \tag{2.57}$$

Assuming the crack to be initially straight and integrating the linear, inhomogeneous, first-order differential equation (2.57) by standard methods, one gets

$$\widehat{\delta}(k,a) = \int_{a_0}^{a} \left(\frac{a}{a'}\right)^{N\alpha} \left[\frac{\psi(ka)}{\psi(ka')}\right]^N \widehat{\delta c}(k,a')\,\mathrm{d}a' \tag{2.58}$$

where a_0 denotes the initial value of a and ψ the function defined by equation (2.41).
Notice that contrary to the brittle case (eq. 2.51), this equation is valid whatever the sign of α and that an effect of memory of previous configurations of the crack front is present here. This equation allows to obtain the crack front fluctuations δ for any given Paris' constant fluctuation δc. This shall be done numerically and is leaved for a further work. In the sequel, however only statistical properties of δc are known, so that statistical study becomes necessary.

2.6.2.2 General formula for the power spectrum of the perturbation of the crack front

By the expression (2.58) of $\widehat{\delta}(k,a)$, one gets for the power spectrum of the crack front fluctuations:

$$\widehat{\mathcal{A}}(k,a) = \int_{a_0}^{a}\int_{a_0}^{a} \left(\frac{a^2}{a_1 a_2}\right)^{N\alpha} \left(\frac{[\psi(ka)]^2}{\psi(ka_1)\psi(ka_2)}\right)^{N} \widehat{\mathcal{C}}(k, a_2 - a_1)\,\mathrm{d}a_1\,\mathrm{d}a_2\,, \tag{2.59}$$

where $\widehat{\mathcal{C}}(k, a_2 - a_1)$ is the power spectrum of the Paris' constant fluctuations δc.
Due to the memory effect, this equation is more complex than the equivalent (2.52) one in brittle fracture. Its properties for any value of a has not at present been studied. Its asymptotic behaviour for $a \to \infty$ has however be obtained by **Favier et al. (2006b)** and **Pindra et al. (2008a)**. For $k = 0$, one gets:

$$\widehat{\mathcal{A}}(0,a) \sim \begin{cases} \dfrac{\widetilde{\mathcal{C}}(0,0)}{2N\alpha - 1}\, a_0 \left(\dfrac{a}{a_0}\right)^{2N\alpha} & \text{if } \alpha > \dfrac{1}{2N}, \\ \dfrac{\widetilde{\mathcal{C}}(0,0)}{1 - 2N\alpha}\, a \text{ if } \alpha < \dfrac{1}{2N}, \end{cases} \tag{2.60}$$

and for $k \neq 0$:

$$\widehat{\mathcal{A}}(k,a) \sim \frac{\widetilde{\mathcal{C}}(k,0)}{N|k|} \tag{2.61}$$

where $\widetilde{\mathcal{C}}(k,k')$ is the double z,x-Fourier transform of the function $\mathcal{C}$.
One can notice, like in brittle fracture that the large wavelengths are preferentially selected by the system and that ultimately only the zero wavenumber $k = 0$ component still evolves with a, the other components being in a steadystate (independent of a) rough regime. It seems however that the first order study is not sufficient to determine the roughness exponent in this case (it gives indeed $\zeta = 0$). This is probably linked to the memory effect that delay the development of this regime. A second order study is then necessary. It has been performed by Katzav and Adda-Bedia (2006) who obtains a roughness exponent of $\zeta = 0.5$.

2.6.3 Synthesis of the theoretical results

The previous results derived for the half-plane or tunnel crack, with additional ones derived from **Favier et al. (2006b)** and **Pindra et al. (2008a)** are summarized in table 2.1. We recall that in this table $F(p)$ is the function introduces in 2.3.2. This function is such as $F(0) = 0$ and increases monotonically to finally behaves as $p/2$ for $p \to \infty$. The function ψ is defined by eq. (2.41) and decreases from 1 to 0 when p varies from 0 to $+\infty$.
One notices that in all the cases the system preferentially "selects" perturbations of the crack front with small wavenumbers k, that is, large wavelengths $\lambda = 2\pi/|k|$. Physically it is link to the process explained in §2.4.1. One can also easily discuss, using the table 2.1, the differences between brittle fracture and fatigue, the role of the loading type (sign of α) and of the crack geometry (function $F(p)$ and ψ):

- Concerning the crack advance law, one can notice by comparison of columns 3 and 4, that the relations are less complex in brittle fracture than in fatigue since their is no time dependence of the response in the first case contrary to the second. One can also notice that the disorder grows faster in brittle fracture than in fatigue, the development being slowed down by a memory effect. And finally, for $\alpha > 0$, the treatment is possible only in fatigue, since in brittle fracture the appearance of bifurcation renders the problem ill-posed.

- Thus, the dependence upon the sign of α can be considered only in fatigue. Comparison of columns 2 and 3 shows that the disorder grows faster for $\alpha > \frac{1}{2N}$ than for $\alpha < \frac{1}{2N}$. It is

Table 2.1: Main results concerning the propagation in a disordered media

	fatigue $\alpha > \frac{1}{2N}$	fatigue $\alpha < \frac{1}{2N}$	brittle $\alpha < 0$
For any a:			
$\widehat{\delta}$	$\displaystyle\int_{a_0}^{a} \left(\frac{\psi(ka)}{\psi(ka')}\right)^N \left(\frac{a}{a'}\right)^{N\alpha} \widehat{\delta c}(k,a')\mathrm{d}a'$	idem	$\displaystyle -\frac{a\widehat{\kappa}(k,a)}{\lvert\alpha\rvert + F(ka)}$
$\widehat{\mathcal{A}}$	$\displaystyle\int_{a_0}^{a}\int_{a_0}^{a} \left(\frac{a^2}{a_1 a_2}\right)^{N\alpha} \left(\frac{[\psi(ka)]^2}{\psi(ka_1)\psi(ka_2)}\right)^N \widehat{\mathcal{C}}(k, a_2 - a_1)\,\mathrm{d}a_1\,\mathrm{d}a_2$	idem	$\displaystyle a^2 \frac{\widehat{\mathcal{K}}(k)}{(\lvert\alpha\rvert + F(ka))^2}$
For $a \to \infty$:			
$\widehat{\mathcal{A}}(k,a)$	$\displaystyle\frac{\widetilde{\mathcal{C}}(k,0)}{N\lvert k\rvert}$	$\displaystyle\frac{\widetilde{\mathcal{C}}(k,0)}{N\lvert k\rvert}$	$\displaystyle\frac{4\widehat{\mathcal{K}}(k)}{k^2}$
$\widehat{\mathcal{A}}(0,a)$	$\displaystyle\frac{\widetilde{\mathcal{C}}(0,0)}{2N\alpha - 1}\, a_0 \left(\frac{a}{a_0}\right)^{2N\alpha}$	$\displaystyle\frac{\widetilde{\mathcal{C}}(0,0)}{1 - 2N\alpha}\, a$	$\displaystyle\widehat{\mathcal{K}}(0)\frac{a^2}{\alpha^2}$
$\mathcal{A}(z)$	$\displaystyle\frac{\widetilde{\mathcal{C}}(0,0)}{\pi(2N\alpha - 1)} \left(\frac{a}{a_0}\right)^{2N\alpha - 1} \int_{-\infty}^{+\infty} \psi(p)^{2N} dp$	$\displaystyle\frac{\widetilde{\mathcal{C}}(0,0)}{\pi N} \ln a$	$\displaystyle\frac{2a\widehat{\mathcal{K}}(0)}{\pi\lvert\alpha\rvert}$

obvious since instable wavelengths exists for $\alpha > 0$ and not for $\alpha < 0$. The selection of the large wavelengths remains however since the large ones grow faster than the small ones.

- Concerning the crack geometry, one can notice that the asymptotic behaviour for $a \to \infty$ is independent of F, that is the same for the half-plane and tunnel cracks. Moreover, we have seen in section 2.6.1.2, that in brittle fracture, the power spectrum satisfies a Family-Vicsek scaling in both cases and the geometry introduces a difference only for the transition toward the large wavelength saturation regime.

2.6.4 Comparison with the experiments

Due to the difficulty of observation of the crack front during the propagation, few different experiments exist at present, that allow to study the crack front deformations. Among them Daguier et al. (1995) used ink injections to follow the crack front in brittle fracture and fatigue. Schmittbuhl and Måløy (1997) studied the in-plane propagation through a transparent plexiglas block, the toughness fluctuations being obtained by sand blasting the surface of two plexiglas plates before to weld them together. This last setup has vastly been used since this pioneer work to study several properties of the crack advance: the crack front roughness (Schmittbuhl and Måløy (1997); Delaplace et al. (1999); Schmittbuhl et al. (2003a), **Pindra et al. (2009)**), the time development of the crack front fluctuations (Maloy and Schmittbuhl, 2001), the intermittent pinning/depinning dynamics (Måløy et al., 2006; Grob et al., 2009). All these papers conclude that the front roughness is self-affine with an exponent $\zeta = 0.5 - 0.6$. Interestingly, Maloy and Schmittbuhl (2001) noticed that the front fluctuations satisfies a Family-Vicsek scaling, the roughness exponents being $\zeta = 0.5 - 0.6$ and $\tau = 1.1 - 1.2$.
Two different explications of the experimental results can been given:

1. Schmittbuhl et al. (1995a); Rosso and Krauth (2002); Schmittbuhl and Vilotte (1999) have obtained numerically, using the perturbation approach for a half-plane crack of Rice (1985), the condition $K(z) \leq K_c(z)$ and quenched noise, a different value of the roughness exponent: $\zeta \sim 0.4$. The discrepancy between this value and the experiments has emulated the community: percolation damage models have been proposed (Schmittbuhl et al., 2003b; Hansen and Schmittbuhl, 2003) that yields a roughness exponent of $\zeta = 0.62 \pm 0.05$ that seems in agreement

with the experiment. Finally, recently Santucci et al. (2009) conciliate the two values obtained theoretically and numerically by more precise experimental crack front position measures: they find $\zeta = 0.57$ at small lengthscales ($<$ size of the sandblasting particles) that is in agreement with the damage percolation model and $\zeta = 0.38$ at larger lengthscales that is in agreement with the numerical perturbation approach.

2. Maloy and Schmittbuhl (2001)'s experimental result seems in agreement with the Family-Vicsek scaling (2.54) obtained by assuming $K(z) = K_c(z)$ and white noise toughness fluctuations. In this view, the exponent $\zeta = 0.38$ observed by Santucci et al. (2009) at larger lengthscales may correspond to the crossover from the rough to the saturation regimes of the Family-Vicsek scaling.

At present, none of this view seems plainly satisfactory. We hope that the present review will help to clarify the discrepancies. In this aim, we emphasize that for any comparison with experiments, attention must be paid to:

- The lengthscales involved in the experiments: brittle fracture results are valid only beyond the process zone and uncorrelated toughness fluctuations only beyond the correlation length. The influence of the plate thickness shall also be considered.

- The crack advance law: dynamic or quasistatic? Brittle or subcritical (table 2.1 shows different behaviour for each case)? If brittle, does the crack front position satisfy $K(z) = K_c(z)$ for all z or does it exist some points where $K(z) < K_c(z)$ (Roux et al., 2003)? In the experiments of Maloy and Schmittbuhl (2001), the intermittent pinning/depinning dynamics militates rather for the second case.

- The first order perturbation approaches: check its validity domain in term of $|\delta| \ll a$ but also in term of $\frac{\mathrm{d}|\delta|}{\mathrm{d}z} \ll 1$.

- The toughness fluctuations nature: annealed or quenched, correlated or uncorrelated? Indeed, annealed or quenched noise may give different results (Kardar, 1998): annealed noise corresponds to the first order study of section 2.6.1, quenched noise is accessible only by numerical simulations (Schmittbuhl et al., 1995b) and introduces second order terms in the model that have not been considered at present properly. Correlated or uncorrelated noise gives different toughness fluctuation power spectrums and may influence the response (see equation 2.52 and Schmittbuhl and Vilotte (1999)).

2.7 Conclusion

Crack front small perturbation approach initiated by Rice (1985) and later extended to more complex cases has been recalled. This approach allows to update the stress intensity factors when the crack front is slightly perturbed in its plane. Applications concerning the deformation of the crack front when it propagates in an homogeneous or heterogeneous media have been considered in brittle fracture or fatigue/subcritical propagation. Only the case of one crack propagating in an infinite plane without interaction with a boundary has been considered. The stable shapes corresponding to uniform SIF have been derived: straight or circular, but also when bifurcations exists, wavy crack fronts. For a straight crack, it has been shown that perturbation of all lengthscales progressively disappears unless disordered fracture properties yields Family and Vicsek (1985) roughness of the crack front.
This approach has recently be extended to interaction between several cracks: the FK for two tunnel-cracks has been derived (**Pindra et al. (In prep)**, Legrand and Leblond (In prep.)) and the disorder during their coalescence studied (Legrand and Leblond, 2010). Interestingly, they show that, stability first prevails for all lengthscales such as $\lambda < \lambda_c$, but since λ_c is this time a decreasing function of the

crack advance, all wavelengths finally become unstable so that the perturbation does not vanish. This underlines that stability results depend on the interaction of the crack with other cracks and more generally also, with obstacles or solid boundaries. Such a conclusion has still been obtained by Gao et al. (1991) who studied the stability issue when the front approaches a stress free plate boundary: when the crack is far enough from the boundary, the critical wavelength λ_c increases with crack growth (the model of infinite solid is then valid) and when it approaches the boundary, λ_c decreases with crack growth.
Besides, comparison with experiments have to be deepened in terms of crack shape but also macroscopic loading.

Chapter 3

Research project: From the theory to the practice

Two current challenges of Linear Elastic Fracture Mechanics (LEFM) are (i) to take into account the non-linearities induced by the crack front deformations and (ii) to better understand the mechanism of fracture initiation. For these purposes, two promising tools can be used: the Rice (1985) crack front perturbation theory for predicting the crack front deformation (see chap. 2) and the energetic approach of Francfort and Marigo (1998, 2000, 2008) for determining the crack initiation and propagation path. However, these theoretical approaches have been validated mainly only qualitatively by experiments. Further effort is required to make quantitative comparisons and to render these tools useful in practice, e.g. to improve the safety predictions or to create tougher materials.
My current research is motivated by this long-term vision, and by my increasing interest in applying LEFM to physical problems. In this context, I propose to develop three specific directions. First, I plan to extend crack perturbation approach exposed in chapter 2 to more realistic geometries, and quantitatively compare its predictions for both homogeneous and heterogeneous media with 3D finite element simulations and with experiments designed for this purpose. Second, I plan to apply the energetic approach to fracture mechanics to different physical problems involving drying, impact, indentation and geological phenomena (basalt columns, polygonal patterns on Earth and on Mars, martian spiders, septarias, continental break up above mantle plumes) using the energy-minimization either directly or using a regularized form by a non-local damage model. While the first two directions are generally applicable to any brittle material, the third direction will be to apply the LEFM to the specific case of fracture in drying colloidal suspensions. A prerequisite for this, that is render difficult by the time dependence of the drying process, is the precise characterization of the mechanical properties of the consolidated suspension, which will require extension of recently developed experimental tools (indentation tests, estimation of the mechanical stresses by measuring the deflection of a plate, estimation of mechanical characteristics by measuring some geometrical features of the crack morphologies).

3.1 Deformations of a plane crack during its propagation

The propagation path of cracks are routinely predicted by the engineers using two-dimensional LEFM. However in three dimensions, the problem arises still many open questions even for coplanar propagation of plane cracks. The path depends in general on both the specimen and crack geometries (position, size, shape). Classical tools such as finite elements or its more sophisticated X-FEM extension are able to predict the path more or less accurately if the specimen and the crack size scales are all of the same order. When the scales are disparate, however, it becomes extremely difficult to reconcile the crack

microscopic and the specimen macroscopic aspects of the problem. One possibility is to simplify the structural aspects and to concentrate on the local deformation of the crack front by assuming that the medium is infinite subjected to remote loading. The crack perturbation approach initiated by Rice (1985) and reviewed in chapter 2, allows then to determine the stress intensity factors (SIF).

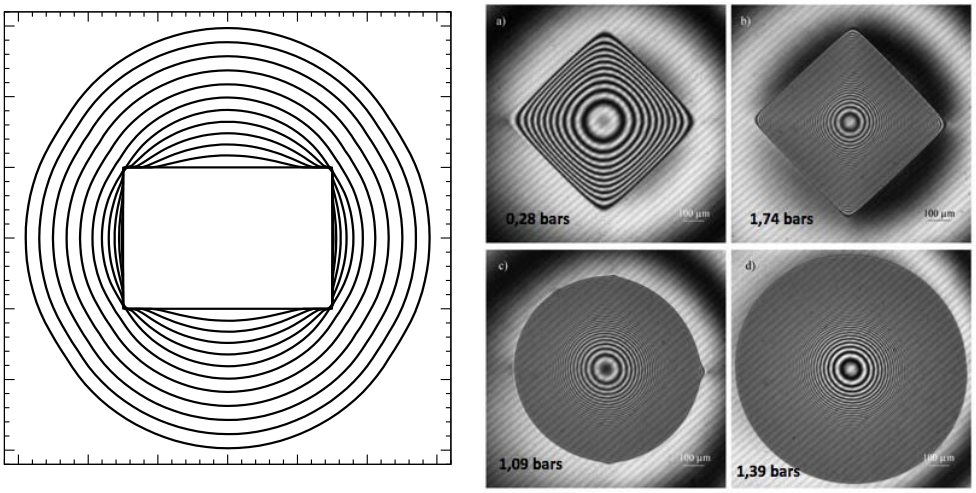

(a) PlaneCracks simulation **(Lazarus, 2003)** (b) Blister experiments (Dupeux et al., 1998)

Figure 3.1: Successive positions (top view) during the propagation of an initially rectangular crack in an homogeneous medium. The crack propagates first at the edges where the stress intensity factors are higher. The shape finally becomes and remains circular.

With the aim of obtaining quantitative predictions of both crack front shapes and macroscopic loading, the theoretical studies exposed in chapter 2 will be extended in several directions and compared to experiments designed for this purpose.

- As mentioned in section 2.2.2, the perturbation approach is only applicable in practice if the precise specimen boundary conditions can be neglected. It is therefore necessary to determine to what extent this approximation is valid in practice. 3D finite element simulations will be performed in order to determine the range of validity of the perturbation approach in term of specimen/crack size scales. The aim is to determine the precise conditions under which the specimen boundary conditions can be neglected. Later on, the possibility of reconciling the microscopic and macroscopic aspects by using the matched asymptotic expansions, will be studied.

- Recent comparisons with experiments using plates (§2.6.4) have shown the potential importance of the plate thickness on the results. Thus, the perturbation approach will be extended to some more complex and realistic geometries than those listed in section 2.2.4, namely a tunnel-crack in a finite-thickness specimen (thesis of L. Legrand, in collaboration with J.B. Leblond, IJLRDA Univ Paris 6 and M. Adda-Bedia, LPS, ENS Paris). The predictions of this more realistic model will be compared to the experiments (§2.6.4) initiated by Schmittbuhl and Måløy (1997) (collaboration J. Schmittbuhl, IPG Strasbourg).

- Using equations (2.51) and (2.58) giving the crack front shape evolution knowing the local fracture properties, simulations of the crack front shape evolution will be performed. Comparison

with the experiments of Dalmas et al. (2009) and new designed experiments of M. Adda-Bedia is planed in collaboration with the author.

- The predictions of the numerical code PlaneCracks corresponding to **(Lazarus, 2003)** (§2.4.2) concerning the propagation of circular, elliptical, rectangular and heart shape (fig. 2.6) cracks will be compared to blister-tests similar to those of Dupeux et al. (1998) (fig. 3.1(b)) in terms of shape and loading (collaboration M. Braccini, SIMAP, Univ Grenoble).

- The code PlaneCracks will be extended to two embedded crack fronts to study large crack deformation during coalescence (thesis of L. Legrand). Blister test experiments on two cracks are also envisaged (collaboration M. Braccini). For thicker specimen (for which our model is more realistic), the set up of Bunger and Detournay (2008) may be used. Contact has been established for this purpose with A. Bunger (CSIRO Petroleum Resources, Australia).

- The code PlaneCracks will also be extended to tunnel-cracks with periodic crack front shape perturbations and its predictions compared to experiments performed in the SVI laboratory of Saint-Gobain Recherche (collaboration D. Dalmas, Lab. SVI, Aubervilliers and D. Vandembroucq, Lab PMMH, ESPCI, Paris).

- The above points concern only the in-plane crack front deformations. Crack out of plane perturbations resulting from the propagation in heterogeneous media **(Ponson et al., 2007)** are difficult to tackle theoretically, and will instead be approached using model experiments. In particular, the size effects will be considered. I will take part to the design and interpretation of those experiments with D. Bonamy (Lab. SPCSI, CEA Saclay) and M. Francois and H. Auradou (FAST).

Parts of this work are supported by the ANR MEPHYSTAR ("MEchanics and STAtistical PHYsics of Rupture in heterogeneous materials", 2010-2013). The project involves the laboratories SPCSI (CEA Saclay), SVI (Saint-Gobain Recherche), PMMH (ESPCI Paris), and FAST.

3.2 Predictions of crack patterns using energy minimization

The energetic variational approach to fracture mechanics proposed by Francfort and Marigo (1998) is an extension of the Griffith postulate that a crack propagates if the elastic energy released by propagation counterbalances the energy needed to create the crack. It is based on the principle that the quasi-static crack evolution is obtained by minimizing the sum of the elastic energy of the cracked body and the crack energy. The advantage of the method over the classical Griffith approach is that it can predict, without additional ingredients, both the crack initiation and the crack propagation path. For numerical simulations, the approach can be regularized by a non-local damage model (Bourdin et al., 2008).
In the last ten years, efforts have mainly focused on theoretical and numerical developments. As a result, few of the numerical simulations presented in Bourdin et al. (2000, 2008) have yet been compared directly with experiments. Recently, in collaboration with C. Maurini (IJLRDA, Univ Paris 6) for the theory and G. Gauthier and L. Pauchard (FAST) for the experiments, the theoretical approach has been tested against experiments on fractures that form during directional drying of colloidal suspensions (fig. 3.2). The regularized form of the approach **(Lazarus et al., 2009a)** yields qualitative agreement between the experimental (fig. 3.2a) and numerical crack patterns (fig. 3.2c), while the direct approach **(Gauthier et al., 2010)** successfully predicts the number of cracks emerging from a star-shaped crack (fig. 3.2b). These first promising results will be extended in the future in several directions.

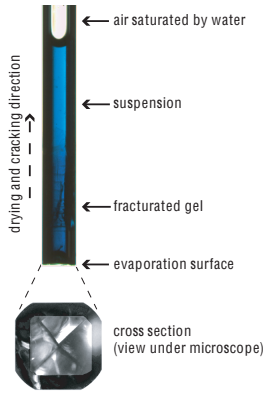

(a) Directional drying experiments

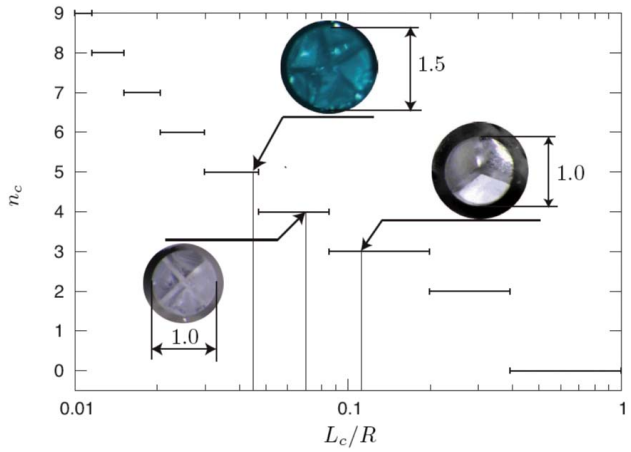

(b) Number n_c of radial cracks obtained by the energy minimization principle **(Gauthier et al., 2010)**. L_c is the Griffith length (ratio between the energy needed to create cracks and to deform the material elastically), R the tube radius.

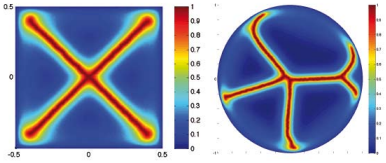

(c) Crack patterns obtained by the regularized energetic approach **(Lazarus et al., 2009a)**

Figure 3.2: Crack patterns in directional drying experiments. Capillary tubes are filled with a colloidal suspension. The open bottom boundary allows for evaporation of the solvent. Cracks appear following the compaction front (front of the bottom-up growing gel). Their cross-sectional shape depends on the tube shape and the drying rate.

(a) Port Arthur rectangular tessellated pavement, Tasmania (picture of C. Foscan)

(b) Giant's Causeway hexagonal tessellated pavement, Ireland (picture of A. Davaille)

Figure 3.3: Examples of natural polygonal patterns

- In collaboration with G. Gauthier and L. Pauchard, *further directional drying experiments are planned*. With C. Maurini and B. Bourdin (Dept of Math., Louisiana State Univ), *we will perform FE simulations of the experiments, using both the energetic and the classical Griffith approaches. Contacts has also been established with the team of H. Balke (Institut fur Festkörpermechanick, TU Dresden), which is working on similar problems (Hofmann et al., 2006).*

- Star-shaped cracks are observed in many situations, especially during the time shortly after crack initiation. Such cracks therefore provide an interesting test case for approaching the initiation problem and verifying the validity of the energetic approach. *Accordingly, we propose to extend the method used by* **Gauthier et al. (2010)** *for directional drying experiments, to crack nucleation arising during the drying of some thin films, during some indentation (Rhee et al., 2001), and impact problems (collaboration N. Vandenberghe, IRPHE, Marseille).*

- Natural polygonal pavements formed by shrinkage cracking are often hexagonal in planform (e.g., Giant's Causeway, Ireland; fig. 3.3(b); DeGraff and Aydin (1987)), but can also have square planforms in some cases (e.g., Port Arthur, Tasmania; fig. 3.3(a); Branagan and Cairns (1993)). Several aspects of their formation are still poorly understood. *Possible scenarios include creation of star-shaped cracks followed by progressive formation of the self-organized pavements, sequential formation of channelling cracks leading to craquelures followed by maturation toward a regular pavement (Goehring et al., 2010) or the formation spaced in time of two orthogonal networks of parallel cracks. We propose to simulate these scenarios by energy minimization and apply the results to polygons on Earth (with A. Davaille, FAST) and eventually on Mars. Complementary discussions have also been initiated with other geophysicists, including L. Goehring (Dept of Mat Sci and Metal, Univ Cambridge) and N. Mangold (Lab de planétologie et géodynamique de Nantes UMR 6112).*

3.3 Characterization of the consolidation of drying colloidal suspensions

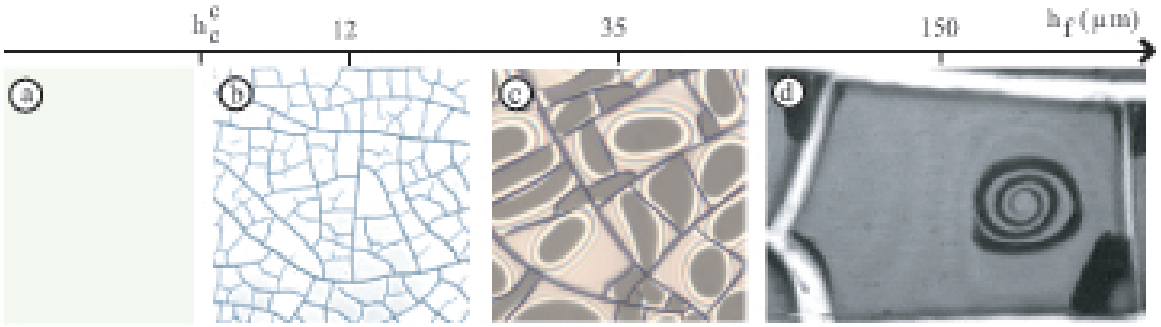

Figure 3.4: Crack patterns at the final stage of the drying process of a nanolatex suspension for different layer thicknesses h_f. Uniform layer (a), cracks in the film thickness (b), delamination (c), spiral crack (d).

During the drying of colloidal suspensions (particle size $< 1\mu$m), the initially stable solution destabilizes, and the particles agglomerate to form a solid porous material that shrinks as the liquid evaporates. When the contraction is constrained by adhesion to a wall or substrate, tensile stresses develop that can give rise to various crack patterns. Some examples are shown in fig. 3.2 for directional drying and

in fig. 3.4 for isotropic thin film drying. Various qualitative explanations for the crack morphologies have been proposed (Bohn et al., 2005), **(Gauthier et al., 2007)** but quantitative predictions of the formation dynamics, shape and sizes of the cracks are still lacking.
A prerequisite for understanding crack formation in such situations is a good characterization of the mechanical properties of the porous medium (e..g., the fracture toughness, which is required to apply LEFM). Such characterization is rendered difficult by the time-dependence of the problem and by the impossibility of using classical techniques like traction tests. As a result, only two measured values of the toughness have been published , one by Zarzycki (1988), the other by ourselves **(Gauthier et al., 2010)**, and moreover the two disagree. A further prerequisite is the determination of the mechanical stresses level. It can be measured by depositing the suspension on a cantilever plate (Tirumkudulu and Russel, 2004): during drying, contraction stresses induce a deflection of the plate, from which the magnitude of the stresses can be inferred using Stoney's formula.
During the past two years, we have made significant advances towards achieving these characterization prerequisites. We have developed and improved the cantilever plate method. We have also applied, not without difficulties, indentation techniques to consolidated drying suspensions. And, we have developed less conventional methods based on the fracture morphologies themselves. All these methods are described below.

3.3.1 Estimation of the mechanical stresses by measuring the deflection of a plate and indentation techniques

With M. Chekchaki (Ph. D. student) and L. Pauchard, we have extended and developed two techniques for characterizing partially dried colloidal suspensions: the cantilever technique of Tirumkudulu and Russel (2004), and micro-indentation testing. In the former case, the Stoney stress-deflection formula, is based on assumptions (small film/substrate thickness ratio, uniform film stress state) that are often not valid in drying experiments. To extend this relation to the conditions of our experiments **(Chekchaki et al., 2010)** we have used 3D FE simulations. Besides, we have designed, not without difficulties, an experimental procedure that gives reproducible results. We are also engaged in an ongoing effort to adapt the classical indentation test (widely used for metal and ceramic films; Oliver and Pharr (1992)) so that it can be used to characterize the film at the end of the drying process. The feasibility of these extended characterization methods has been demonstrated by the Ph. D. thesis research and further work in this direction is envisaged.

- We have used until now a traditional Vickers (sharp) indenter. We have noticed that it generates significant damage and plastic deformations. *Hence, spherical indenter will be purchased and used. We will improve the experimental procedure to allow humidity control. We will use it for different drying conditions, suspensions and layer thicknesses.*

- In addition to the indentation performed at the end of the drying process, *tests will be done during the drying process and coupled with the stress evolution measured by the cantilever technique, in order to better understand the consolidation process.*

- During the drying process, *different time scales associated with evaporation, viscosity, and porous media diffusivity may be important. An effort will be made to estimate these time scales in order to determine the dominant effect.*

3.3.2 Estimation of some mechanical characteristics by measuring some geometrical features of the crack morphologies

If one can predict, for instance using the models of section 3.2, the crack patterns as a function of the formation conditions (loading, material behaviour), inversely quantitative measurements of some

geometrical aspects of the pattern (such as crack spacing e.g.) can be used to deduce quantitative information on the consolidation (such as material toughness and the level of the loading). This idea has already been used in **Gauthier et al. (2010)** in conjunction with the LEFM approach (section 3.2) in one particular case. We propose to extend it to other systems and compare it with other methods.

- In addition to the crack spacing, *other geometrical parameters (critical thicknesses, distance between the crack tips and the solidification front, angles...) will also be used.*

- For validation purposes, *the values of the toughness obtained by this method will be compared with values obtained by indentation.*

- In conjunction with our geophysicist colleagues (section 3.2), we will apply our method to *derive qualitative and quantitative information on the conditions of formation of geological patterns on Earth and other planets, such as the cooling rate during the formation of basalt columns (with A. Davaille and L. Goehring), the pressure level responsible for martian spiders (Thomas et al., 2010) in the Kieffer (2007) model (with F. Schmidt, lab IDES, Interactions et Dynamique des Environnements de Surface, Orsay), the formation mechanism of septarias (Seilacher, 2001) (with J. Gargani, B. Saint-Bezar, P. Vergely, IDES), the 3 branches continental break up (Storey, 1995) above mantle plumes (with A. Davaille).*

- From the value of the toughness, information on the consolidation of the porous matrix can be obtained. *Porosity and Young's modulus will be measured to obtain an estimate of the effective fracture energy of the solid links between the particles. The influence on the porous solid structure of the rate and conditions (directional/isotropic) of drying will also be studied (collaboration G. Gauthier).*

- In parallel to the previous point, *"visualization" of the consolidate porous matrix is envisaged. Due to the nanometric size of the particles, this requires to use sophisticated methods. Hence, a proposal has been submitted to the ILL (Institut Laue-Langevin, Grenoble) to obtain neutron-beam time (principal proposer B. Cabanne, PMMH). Another is envisaged to the neighbouring synchrotron SOLEIL to obtain photonbeam time.*

3.4 Summary

My research interests concern two- and three-dimensional problems in Linear Elastic Fracture Mechanics. My approach is primarily theoretical and numerical, but with an increasing interest in experimental validation and physical applications since my first sojourn at the FAST laboratory in 2006. Among the tools I use are the crack front perturbation approaches (see chap. 2), finite-element simulations, and the energetic approach to fracture. I apply them, with some colleagues, to the determination of the crack initiation and propagation paths in homogeneous and heterogeneous brittle media, soft condensed matter in particular colloidal suspensions, and geological materials. The research directions I would enjoy pursuing can be summarized as follows[1]:

- Concerning the crack front deformation, the perturbation approaches will be extended to progressively more realistic geometries. Their domain of validity in terms of crack/specimen size ratios will be determined by 3D FE simulations. Their predictions will be compared with experiments with increasing emphasis on quantitative comparison. Later on, the reconciliation of the different length scales is envisaged using the matched asymptotic expansions method.

[1] the framework is slightly different than outlined above to emphasize the links between parts of sections 3.2 and 3.3.

- Concerning the crack initiation and propagation path prediction, our efforts to apply and validate the energetic approach to fracture will be continued. It will be applied to cracks resulting from shrinkage (drying, cooling), impact and indentation process. Inversely, information on the material constants and loading will be derived from the crack patterns. The inverse method will be applied to the characterization of consolidated colloidal suspensions and to several geological problems on Earth and on other planets.

- Concerning the drying of colloidal suspensions, we will continue to develop methods for characterizing the consolidated solid matrix. Additional directional and isotropic drying experiments will be performed to determine the influence of the drying conditions (rate, directional vs. film) and the characteristics of both the solvent and the particles (size, material, mono/polydispersion) on the structure of the porous medium. Visualisation using neutron or Xray beams is also envisaged.

This research project aims at making useful the Linear Elastic Fracture Mechanics in new fields related to the engineering sciences, the physicochemistry of the soft matter and the geosciences. The interdisciplinary character of my research, so as my growing interest in experimental validation of the theory, allow me to form PhD student to a vast set of competences. This may be useful for them to find a job in both academic and industrial worlds.

Bibliography

Adda-Bedia, M., Mahadevan, L., 2006. Crack-front instability in a confined elastic film. Proceedings of the royal society A-Mathematical physical and engineering sciences 462 (2075), 3233 – 3251.

Amestoy, M., Leblond, J.-B., 1992. Crack Paths in Plane Situations - II. Detailed Form of the Expansion of the Stress Intensity Factors. International Journal of Solids and Structures 29, 465–501.

Anderson, T. L., 1991. Fracture Mechanics: Fundamentals and Applications. CRC Press, Inc., Boca Raton, USA.

Atkinson, B. K., 1987. Fracture mechanics of rock. Academic Press geology series.

Aydin, A., Pollard, D. D., 1988. Progress in understanding jointing over the past century. Geological Society of America Bulletin 100, 1181–1204.

Barabási, A.-L., Stanley, H. E., 1995. Fractal concepts in surface growth.

Bazant, Z. P., Cedolin, L., 2003. Stability of Structures: Elastic, Inelastic, Fracture, and Damage Theories, new ed edition (february 14, 2003) Edition. Dover Publications.

Benallal, A., Marigo, J.-J., 2007. Bifurcation and stability issues in gradient theories with softening. Modelling and Simulation in Materials Science and Engineering 15 (doi:10.1088/0965-0393/15/1/S22), S283–S295.

Bercial-Velez, J., Antipov, Y., Movchan, A., May 2005. High-order asymptotics and perturbation problems for 3d interfacial cracks. Journal of the Mechanics and Physics of Solids 53 (5), 1128–1162.

Bohn, S., Pauchard, L., Couder, Y., 2005. Hierarchical crack pattern as formed by successive domain divisions. Physical Review E 71, 046214.

Bonamy, D., 2009. Intermittency and roughening in the failure of brittle heterogeneous materials. Journal of Physics D: Applied Physics 42 (21), 214014 (21pp).

Bourdin, B., Francfort, G., Marigo, J.-J., 2008. The variational approach to fracture. Journal of elasticity 91 (1), 5 – 148.

Bourdin, B., Francfort, G. A., Marigo, J. J., 2000. Numerical experiments in revisited brittle fracture. Journal of the Mechanics and Physics of Solids 48 (4), 797–826.

Bower, A. F., Ortiz, M., 1990. Solution of three-dimensional crack problems by a finite perturbation method. Journal of the Mechanics and Physics of Solids 38 (4), 443–480.

Bower, A. F., Ortiz, M., 1991. A three-dimensional analysis of crack trapping and bridging by tough particles. Journal of the Mechanics and Physics of Solids 39 (6), 815–858.

Bower, A. F., Ortiz, M., 1993. An analysis of crack trapping by residual stresses in brittle solids. Transactions of the ASME. Journal of Applied Mechanics 60 (1), 175–82.

Branagan, D. F., Cairns, H. C., 1993. Tessalated pavements in the sydney region, new south wales. Journal and Proceedings of the Royal Society of New South Wales 126 (1), 63–72.

Budiansky, B., Amazigo, J. C., Evans, A. G., 1988. Small-scale crack bridging and the fracture toughness of particulate-reinforced ceramics. Journal of the Mechanics and Physics of Solids 36 (2), 167 – 187.

Bueckner, H. F., 1987. Weight functions and fundamental fields for the penny-shaped and the half-plane crack in three-space. International Journal of Solids and Structures 23 (1), 57–93.

Bunger, A. P., Detournay, E., 2008. Experimental validation of the tip asymptotics for a fluid-driven crack. Journal of the Mechanics and Physics of Solids 56 (11), 3101 – 3115.

Caginalp, G., Fife, P., 1986. Phase field methods for interfacial boundaries. Physical Review B 33, 7792–7794.

Chambolle, A., Francfort, G., Marigo, J.-J., 2009. When and how do cracks propagate? Journal of the Mechanics and Physics of Solids 57 (9), 1614 – 1622.

Chekchaki, M., Frelat, J., Lazarus, V., 2010. Analytical and 3D finite element study of the deflection of an elastic cantilever bilayer plate. Transactions of the ASME. Journal of Applied Mechanics , Accepted.

Chekchaki, M., Lazarus, V., Sept. 2009. Analytical and 3d finite element study of the deflection of an elastic cantilever bilayer plate. In: et.al., J. A. (Ed.), 7th EUROMECH Solid Mechanics Conference (ESMC2009). European Mechanics Society, Lisbon, Portugal.

Chekchaki, M., Lazarus, V., Pauchard, L., In prep.a. Characterization of consolidated colloidal suspensions .

Chekchaki, M., Lazarus, V., Pauchard, L., In prep.b. Influence of the width of the plate on the beam deflection induced by the drying consolidation of colloidal suspensions .

Ciavarella, M., Paggi, M., Carpinteri, A., 2008. One, no one, and one hundred thousand crack propagation laws: A generalized barenblatt and botvina dimensional analysis approach to fatigue crack growth. Journal of the Mechanics and Physics of Solids 56 (12), 3416 – 3432.

Collins, J. B., Levine, H., 1986. Diffuse interface model of diffusion- limited cristal growth. Physical Review B 31, 6119–6122.

Cooke, M. L., Pollard, D. D., 1996. Fracture propagation paths under mixed mode loading within rectangular blocks of polymethyl methacrylate. Journal of Geophysical Research 101 (B2), 3387–3400.

Corson, F., Adda-Bedia, M., Henry, H., Katzav, E., 2009. Thermal fracture as a framework for quasi-static crack propagation thermal fracture as a framework for quasi-static crack propagation thermal fracture as a framework for quasi-static crack propagation thermal fracture as a framework for quasi-static crack propagation. International Journal of Fracture 158 (1), 1–14.

Cotterell, B., Rice, J. R., 1980. Slightly curved or kinked cracks. International Journal of Fracture 16 (2), 155–169.

Daguier, P., Bouchaud, E., Lapasset, G., 1995. Roughness of a crack front pinned by microstructural obstacles. EPL (Europhysics Letters) 31 (7), 367–372.

Dalmas, D., Barthel, E., Vandembroucq, D., 2009. Crack front pinning by design in planar heterogeneous interfaces. Journal of the Mechanics and Physics of Solids 57 (3), 446 – 457.

DeGraff, J. M., Aydin, A., 1987. Surface morphology of columnar joints and its significance to mechanics and direction of joint growth. Geological Society of America 99, 600–617.

Delaplace, A., Schmittbuhl, J., Måløy, K. J., 1999. High resolution description of a crack front in a heterogeneous plexiglas block. Physical Review E (Statistical Physics, Plasmas, Fluids, and Related Interdisciplinary Topics) 60 (2), 1337–43.

Doquet, V., Bertolino, G., MAY 2008. Local approach to fatigue cracks bifurcation. International journal of fatigue 30 (5), 942–950.

Drazin, P. G., 1992. Nonlinear systems. Press Syndicate of the University of Cambridge, Cambridge, livre de Christian Ruyer-Quil. Introduction a la theorie des bifurcations.

Dupeux, M., Bosseboeuf, A., Buttard, D., 1998. Investigation of the mechanical properties and ahdesion of PVD tungsten films on Si and silicon compounds by bulge and blister tests. In: Brown, S. B., Muhlstein, C., Krulevitch, P., Johnston, G. C., Howe, R. T., Gilbert, J. R. (Eds.), Microelectromechanical Structures for Materials Research. Vol. 518 of Mater. Res. Soc. Symp. Proc. pp. 87–92.

Erdogan, G., Paris, P., 1963. A critical analysis of crack propagation laws. ASME J. Basic Engng Trans. 85, 528–534.

Family, F., Vicsek, T., 1985. Scaling of the active zone in the eden process on percolation networks and the ballistic deposition model. Journal of Physics A: Mathematical and General 18 (2), L75.

Faure, S., Maurel, D., Cuer, F., Lazarus, V., Pauchard, L., Sept. 2009. Surfactants adsorption effects on rheological and cracking properties of self-dried decontamination gel films. In: 23rd Conference of the European Colloid and Interface Society, 3rd Workshop of COST Action D4 (ECIS 2009). Department of Chemical Engineering, Yeditepe University, Istanbul, Turkey., Antalya (Turkey).

Favier, E., Lazarus, V., Leblond, J.-B., 18-21 september 2003a. Fatigue and brittle fracture propagation paths of planar tunnel-cracks with perturbed front under uniform remote tensile loadings. In: Fatigue Crack Paths, FCP2003, Parma (Italy). ESIS, European Structural Integrity Society.

Favier, E., Lazarus, V., Leblond, J.-B., 8-11 September 2003b. Instability and disorder of the front of some tensile tunnel-crack slightly perturbed within its plane. In: Forum, M. S. (Ed.), Modern Practice in Stress and Vibration Analysis 2003 (MPSVA2003), University of Glasgow (GB). Vol. 440-441. Trans Tech Publications, Switzerland, http://www.scientific.net.

Favier, E., Lazarus, V., Leblond, J.-B., September 2004. Numerical simulation of propagation of 3d planar cracks in infinite bodies in tension or shear. In: Yao, Z. H., Yuan, M. W., Zhong, W. X. (Eds.), Computational Mechanics, Proceedings of the Sixth World Congress on Computational Mechanics in conjunction with the Second Asia-Pacific Congress on Computational Mechanics. Tsinghua University Press & Springer, Beijing, China.

Favier, E., Lazarus, V., Leblond, J.-B., Mars 2005. Disorder of the front of a tensile tunnel-crack propagating in some inhomogeneous medium. In: Carpinteri, A., Mai, Y.-W., Ritchie, R. O. (Eds.), 11th International Conference on Fracture. Turin, Italy.

Favier, E., Lazarus, V., Leblond, J.-B., 2006a. Coplanar propagation paths of 3D cracks in infinite bodies loaded in shear. International Journal of Solids and Structures 43 (7-8), 2091–2109.

Favier, E., Lazarus, V., Leblond, J.-B., 2006b. Statistics of the deformation of the front of a tunnel-crack propagating in some inhomogeneous medium. Journal of the Mechanics and Physics of Solids 54 (7), 1449–1478.

Fisher, D. S., Dahmen, K., Ramanathan, S., Ben-Zion, Y., 1997. Statistics of earthquakes in simple models of heterogeneous faults. Physical Review Letters 78 (25), 4885–8.

Fleck, N., Kang, K., Ashby, M., 1994. Overview no. 112: The cyclic properties of engineering materials. Acta Metallurgica et Materialia 42 (2), 365 – 381.

Francfort, G. A., Marigo, J. J., 1998. Revisiting brittle fracture as an energy minimization problem. Journal of the Mechanics and Physics of Solids 46, 1319–1342.

Fulland, M., Lazarus, V., 5-10 September 2004. Numerical simulations of crack front twisting under consideration of local mode II and/or global mode III effects. In: Yao, Z. H., Yuan, M. W., Zhong, W. X. (Eds.), Computational Mechanics, Proceedings CD-ROM of the Sixth World Congress on Computational Mechanics in conjunction with the Second Asia-Pacific Congress on Computational Mechanics. Vol. CD-Rom. Tsinghua University Press & Springer, Beijing, China.

Gao, H., 1988. Nearly circular shear mode cracks. International Journal of Solids and Structures 24 (2), 177–193.

Gao, H., Rice, J. R., 1986. Shear stress intensity factors for planar crack with slightly curved front. ASME Journal of Applied Mechanics 53 (4), 774–778.

Gao, H., Rice, J. R., 1987a. Nearly circular connections of elastic half spaces. ASME Journal of Applied Mechanics 54 (4), 627–634.

Gao, H., Rice, J. R., 1987b. Somewhat circular tensile cracks. International Journal of Fracture 33 (3), 155–174.

Gao, H., Rice, J. R., 1989. A first-order perturbation analysis of crack trapping by arrays of obstacles. Transactions of the ASME 56, 828–836.

Gao, H., Rice, J. R., Lee, J., 1991. Penetration of a quasi-statically slipping crack into a seismogenic zone of heterogeneous fracture resistance. Journal of Geophysical Research 96 (B13), 21535–21548.

Gauthier, G., Lazarus, V., Pauchard, L., 2007. Alternating crack propagation during directional drying. Langmuir 23 (9), 4715–4718.

Gauthier, G., Lazarus, V., Pauchard, L., 2010. Shrinkage star-shaped cracks: Explaining the transition from 90 degrees to 120 degrees. EPL 89, 26002.

Ghatak, A., Chaudhury, M. K., 2003. Adhesion-induced instability patterns in thin confined elastic film. Langmuir 19 (7), 2621–2631.

Goehring, L., Conroy, R., Akhter, A., Clegg, W. J., Routh, A. F., 2010. Evolving mud-crack patterns. Soft Matter Submitted nov 09.

Goehring, L., Mahadevan, L., Morris, S. W., 2009. Nonequilibrium scale selection mechanism for columnar jointing. Proceedings of the National Academy of Sciences 106 (2), 387–392.

Goldstein, R. V., Salganik, R. L., 1974. Brittle fracture of solids with arbitrary cracks. International Journal of Fracture 10, 507–523.

Griffith, A. A., 1920. The phenomena of rupture and flow in solids. Philosophical Transactions of the Royal Society of London 221, 163–198.

Grob, M., Schmittbuhl, J., Toussaint, R., Rivera, L., Santucci, S., Maloy, K. J., JUL 2009. Quake Catalogs from an Optical Monitoring of an Interfacial Crack Propagation. Pure and applied geophysics 166 (5-7), 777–799.

Hakim, V., Karma, A., 2009. Laws of crack motion and phase-field models of fracture. Journal of the Mechanics and Physics of Solids 57 (2), 342 – 368.

Hansen, A., Schmittbuhl, J., 2003. Origin of the universal roughness exponent of brittle fracture surfaces: stress-weighted percolation in the damage zone. Physical Review Letters 90 (4), 045504/1–4.

Henry, H., Levine, H., 2004. Dynamic instabilities of fracture under biaxial strain using a phase field model. Physical Review Letters 93 (10), 105504.

Hofmann, M., Bahr, H. A., Linse, T., Bahr, U., Balke, H., Weiss, H. F., 2006. Self-driven tunneling crack arrays-a 3d-fracture mechanics bifurcation analysis. International Journal of Fracture 141 (3-4), 345–356.

Hull, D., 1993. Tilting cracks: the evolution of fracture surface topology in brittle solids. International Journal of Fracture 62 (2), 119–138.

Irwin, G. R., 1957. Analysis of stresses and strains near the end of a crack traversing a plate. Journal of Applied Mechanics 24, 361–364.

Irwin, G. R., 1958. Fracture. Hand. der Physik. Vol. IV. Springer, Berlin.

Kardar, M., 1998. Nonequilibrium dynamics of interfaces and lines. Physics Reports-Rev. Sec. Phys. Lett. 301 (1-3), 85–112.

Karma, A., Kessler, D. A., Levine, H., 2001. Phase-field model of mode iii dynamic fracture. Physical Review Letters 87, 045501.

Kassir, M. K., Sih, G., 1975. Three Dimensional Crack Problems. Nordhoff International Publishing, Leyden, The Netherlands.

Katzav, E., Adda-Bedia, M., 2006. Roughness of tensile crack fronts in heterogenous materials. Europhysics Letters 76 (3), 450–456.

Kieffer, H. H., AUG 9 2007. Cold jets in the Martian polar caps. Journal Of Geophysical Research-Planets 112 (E8).

Lancioni, G., Royer-Carfagni, G., APR 2009. The Variational Approach to Fracture Mechanics. A Practical Application to the French Panth,on in Paris. Journal of elasticity 95 (1-2), 1–30.

Lange, F. F., 1970. The interaction of a crack front with a second-phase dispersion. Philosophical Magazine 22 (179).

Lazarus, V., 1999. Fatigue propagation path of 3D plane cracks under mode I loading. Comptes-Rendus de l'Académie des Sciences, Série IIb 327 (13), 1319–1324.

Lazarus, V., 2003. Brittle fracture and fatigue propagation paths of 3D plane cracks under uniform remote tensile loading. International Journal of Fracture 122 (1-2), 23–46.

Lazarus, V., In prep. Self-consistent measures of the toughness during the drying induced consolidation of colloidal suspensions .

Lazarus, V., Buchholz, F.-G., Fulland, M., Wiebesiek, J., 2008. Comparison of predictions by mode II or mode III criteria on crack front twisting in three or four point bending experiments. International Journal of Fracture 153, 141–151.

Lazarus, V., Buchholz, F.-G., Wiebesiek, J., September 2006. Crack front twisting in three point bending, comparison between a local and a global approach. In: 35-th Solid Mechanics Conference, SolMech2006. Institute of Fundamental Technological Research, Polish Academy of Sciences, Krakow (Poland).

Lazarus, V., Davaille, A., Gauthier, G., In prep.a. Polygonal crack patterns: from 90 to 120 degrees crack junctions .

Lazarus, V., Gauthier, G., Davaille, A., Pauchard, L., 2010. Contraction star-shaped cracks: From 90 degrees to 120 degrees crack intersections. In: Geophysical Research Abstracts. European Geosciences Union General Assembly Vienna.

Lazarus, V., Gauthier, G., Pauchard, L., Maurini, C., Valdivia, C., July 2009a. Basalt columns and crack formation during directional drying of colloidal suspensions in capillary tubes. In: 12th International Conference on Fracture (ICF12). Ottawa (Canada).

Lazarus, V., Leblond, J.-B., 1996. Theoretical study of crack front rotation and segmentation in brittle cracked solids subjected to arbitrary mixed mode (I+III or I+II+III) loadings. In: XIXth International Congress of Theoretical and Applied Mechanics, Kyoto (Japan). International Union of Theoretical and Applied Mechanics.

Lazarus, V., Leblond, J.-B., 1-5 April 1997. Three-dimensional crack-face weight functions for the semi-infinite interface crack. In: Karihaloo, B. L., Mai, Y. W., Ripley, M. I., Ritchie, R. O. (Eds.), Proceedings of ICF9, Advances in Fracture Research, Sydney (Australia). Vol. 4. Elsevier Science under the auspices of the International Congress on Fracture, Elsevier Science.

Lazarus, V., Leblond, J.-B., 1998a. Crack paths under mixed mode (I+III) or (I+II+III) loadings. Comptes Rendus de l'Académie des Sciences, Série II (Mécanique, Physique, Astronomie) 326 (3), 171–177.

Lazarus, V., Leblond, J.-B., 1998b. Three-dimensional crack-face weight functions for the semi-infinite interface crack. I. Variation of the stress intensity factors due to some small perturbation of the crack front. Journal of the Mechanics and Physics of Solids 46 (3), 489–511.

Lazarus, V., Leblond, J.-B., 1998c. Three-dimensional crack-face weight functions for the semi-infinite interface crack. II. Integrodifferential equations on the weight functions and resolution. Journal of the Mechanics and Physics of Solids 46 (3), 513–536.

Lazarus, V., Leblond, J.-B., 3-7 december 2001. The tunnel-crack with a slightly wavy front under shear loading. In: Ravi-Chandar, K., Karihaloo, B. L., Kishi, T., Ritchie, R. O., Yokobori Jr, A. T., Yokobori, T. (Eds.), Advances in Fracture Research, Proceedings of ICF10, Honolulu (Hawaii). Vol. CDRom. Elsevier Science under the auspices of the International Congress on Fracture.

Lazarus, V., Leblond, J.-B., 2002a. Crack front stability for a tunnel-crack propagating along its plane in mode 2+3. Comptes Rendus de l'Académie des Sciences Paris, Serie II (Mecanique, Physique, Astronomie) 330 (6), 437–443.

Lazarus, V., Leblond, J.-B., 2002b. In-plane perturbation of the tunnel-crack under shear loading. I: Bifurcation and stability of the straight configuration of the front. International Journal of Solids and Structures 39 (17), 4421–4436.

Lazarus, V., Leblond, J.-B., 2002c. In-plane perturbation of the tunnel-crack under shear loading. II: determination of the fundamental kernel. International Journal of Solids and Structures 39 (17), 4437–4455.

Lazarus, V., Leblond, J.-B., Legrand, L., Pindra, N., Sept. 2009b. In-plane coalescence of slit-cracks. In: et.al., J. A. (Ed.), 7th EUROMECH Solid Mechanics Conference (ESMC2009). European Mechanics Society, Lisbon, Portugal.

Lazarus, V., Leblond, J.-B., Mouchrif, S.-E., 2001a. Crack front rotation and segmentation in mixed mode I+III or I+II+III - part I: Calculation of Stress Intensity Factor. Journal of the Mechanics and Physics of Solids 49 (7), 1399–1420.

Lazarus, V., Leblond, J.-B., Mouchrif, S.-E., 2001b. Crack front rotation and segmentation in mixed mode I+III or I+II+III - part II: Comparison with experiments. Journal of the Mechanics and Physics of Solids 49 (7), 1421–1443.

Lazarus, V., Maurini, C., Gauthier, G., Pauchard, L., In prep.b. Crack patterns obtained for different cell-shapes in directional drying experiments and non-local gradient damage model simulations .

Lazarus, V., Pauchard, L., In prep.a. Critical thicknesses and Griffith's length during dessication of a colloidal film .

Lazarus, V., Pauchard, L., In prep.b. From craquelures to spiral crack patterns: influence of the thickness on the crack patterns obtained during the drying of a suspension thin layer .

Leblond, J.-B., 1989. Crack Paths in Plane Situations - I. General Form of the Expansion of the Stress Intensity Factors. International Journal of Solids and Structures 25, 1311–1325.

Leblond, J.-B., 1999. Crack paths in three-dimensional elastic solids. i: two-term expansion of the stress intensity factors–application to crack path stability in hydraulic fracturing. International Journal of Solids and Structures 36 (1), 79 – 103.

Leblond, J.-B., Lazarus, V., Mouchrif, S.-E., 1999. Crack paths in three-dimensional elastic solids. II. Three-term expansion of the stress intensity factors - Applications and perspectives. International Journal of Solids and Structures 36 (1), 105–142.

Leblond, J.-B., Leguillon, D., 1999. Asymptotic behavior of stress intensity factors near an angular point of a crack front. European Journal of Mechanics, A/Solids 18 (1), 135–145.

Leblond, J.-B., Mouchrif, S.-E., Perrin, G., 1996. The tensile tunnel-crack with a slightly wavy front. International Journal of Solids and Structures 33 (14), 1995–2022.

Legrand, L., Leblond, J. B., 2010. Evolution of the shape of the fronts of a pair of semi-infinite cracks during their coplanar coalescence. ZAMM Submitted.

Legrand, L., Leblond, J.-B., In prep. In-plane perturbation of a system of two coplanar slit-cracks - II: Case of a large distance between the outer crack fronts. International Journal of Solids and Structures .

Lin, B., Mear, M. E., Ravi-Chandar, K., 2010. Criterion for initiation of cracks under mixed-mode i+iii loading. International Journal of Fracture In press.

Liu, Y., Rice, J., AUG 16 2005. Aseismic slip transients emerge spontaneously in three-dimensional rate and state modeling of subduction earthquake sequences. Journal of geophysical research-Solid earth 110 (B8).

Maloy, K., Schmittbuhl, J., 2001. Dynamical event during slow crack propagation. Physical Review Letters 87 (10), 105502/1–4.

Måløy, K. J., Santucci, S., Schmittbuhl, J., Toussaint, R., 2006. Local waiting time fluctuations along a randomly pinned crack front. Physical Review Letters 96, 045501.

Meade, K. P., Keer, L. M., 1984. On the problem of a pair of point forces applied to the faces of a semi-infinite plane crack. Journal of Elasticity 14 (1), 3–14.

Morrissey, J., Rice, J., 1998. Crack front waves. Journal of the mechanics and physics of solids 46 (3), 467 – 487.

Movchan, A. B., Gao, H., Willis, J. R., 1998. On perturbations of plane cracks. International Journal of Solids and Structures 35 (26-27), 3419–3453.

Mower, T., Argon, A., 1995. Experimental investigations of crack trapping in brittle heterogeneous solids. Mechanics of Materials 19 (4), 343–64.

Nguyen, Q.-S., 2000. Stability and nonlinear solid mechanics. John Wiley.

Obrezanova, O., Movchan, A., Willis, J., Jan. 2002. Stability of an advancing crack to small perturbation of its path. Journal of the Mechanics and Physics of Solids 50 (1), 57–80.

Oliver, Pharr, 1992. An improved technique for determining hardness and elastic modulus using load and displacement sensing indentation experiments. Journal of Materials Research 7 (6), 1564.

Paris, P., Gomez, M., Anderson, W., 1961. A rational analytic theory of fatigue. Trends Eng. 13, 94, pioneer work on paris law. Reference finded in doi:10.1016/j.jmps.2006.01.007.

Pauchard, L., Lazarus, V., Abou, B., Sekimoto, K., Aitken, G., Lahanier, C., Mars 2007. Craquelures dans les couches picturales des peintures d'art. Reflets de la Physique, Société Française de Physique 3, 5–9, https://hal.archives-ouvertes.fr/hal-00158845.

Perrin, G., Rice, J. R., 1994. Disordering of a dynamic planar crack front in a model elastic medium of randomly variable toughness. Journal of the Mechanics and Physics of Solids 42 (6), 1047–1064.

Piccolroaz, A., Mishuris, G., Movchan, A. B., 2007. Evaluation of the Lazarus-Leblond constants in the asymptotic model of the interfacial wavy crack. Journal of the Mechanics and Physics of Solids 55 (8), 1575–1600.

Pindra, N., Lazarus, V., Leblond, J., Schmittbuhl, J., Toussaint, R., July 2009. Deformation of the crack front during propagation in some disordered medium: theoretical and experimental studies. In: 12th International Conference on Fracture (ICF12). Ottawa (Canada).

Pindra, N., Lazarus, V., Leblond, J.-B., August 2007. Désordre du front d'une fissure semi-infinie d'interface. In: de Mécanique, A. F. (Ed.), CFM07, 18e Congrès Francais de Mécanique. Grenoble.

Pindra, N., Lazarus, V., Leblond, J.-B., 2008a. The deformation of the front of a 3d interface crack propagating quasistatically in a medium with random fracture properties. Journal of the Mechanics and Physics of Solids 56 (4), 1269–1295.

Pindra, N., Lazarus, V., Leblond, J.-B., 2008b. Slight in-plane perturbation of a system of two coplanar parallel tensile slit-cracks. In: 36-th Solid Mechanics Conference, SolMech2008. Institute of Fundamental Technological Research, Polish Academy of Sciences, Gdansk (Poland).

Pindra, N., Lazarus, V., Leblond, J.-B., 2010. Geometrical disorder of the fronts of a tunnel-crack propagating in shear in some heterogeneous medium. Journal of the Mechanics and Physics of Solids 58, 281–299.

Pindra, N., Lazarus, V., Leblond, J.-B., In prep. In-plane perturbation of a system of two coplanar slit-cracks - I: Case of arbitrarily spaced crack fronts. International Journal of Solids and Structures .

Pons, A. J., Karma, A., 2010. Helical crack-front instability in mixed-mode fracture. Nature 464, 85–89.

Ponson, L., Auradou, H., Pessel, M., Lazarus, V., Hulin, J. P., 2007. Failure mechanisms and surface roughness statistics of fractured fontainebleau sandstone. Physical Review E 76 (036108).

Qian, J., Fatemi, A., 1996. Mixed mode fatigue crack growth: a literature survey. Engineering Fracture Mechanics 55 (6), 969.

Ramanathan, S., Fisher, D. S., 1997. Dynamics and instabilities of planar tensile cracks in heterogeneous media. Physical Review Letters 79 (5), 877–80.

Rhee, Y., Kim, H., Deng, Y., Lawn, B., 2001. Contact-induced damage in ceramic coatings on compliant substrates: Fracture mechanics and design. Journal of The American Ceramic Society 84 (5), 1066–1072.

Rice, J. R., 1985. First-order variation in elastic fields due to variation in location of a planar crack front. ASME Journal of Applied Mechanics 52 (3), 571–579.

Rice, J. R., 1988. Crack fronts trapped by arrays of obstacles: Solutions based on linear perturbation theory. In: Rosakis, A. J., Ravi-Chandar, K., Rajapakse, Y. (Eds.), nalytical, Numerical and Experimental Aspects of Three Dimensional Fracture Processes. Vol. 91. ASME Applied Mechanics Division, American Society of Mechanical Engineers, New York, pp. 175–184.

Rice, J. R., 1989. Weight function theory for three-dimensional elastic crack analysis. In: Wei, R. P., Gangloff, R. P. (Eds.), Fracture Mechanics : Perspectives and Directions (Twentieth Symposium). American Society for Testing and Materials STP 1020, Philadelphia, USA.

Rosso, A., Krauth, W., 2002. Roughness at the depinning threshold for a long-range elastic string. Physical review E 65 (2), 025101.

Roux, S., Vandembroucq, D., Hild, F., 2003. Effective toughness of heterogeneous brittle materials. European Journal of Mechanics - A/Solids 22 (5), 743–749.

Santucci, S., Grob, M., R.Toussaint, Schmittbuhl, J., Hansen, A., Måløy, K. J., July 2009. Crackling dynamics during the failure of heterogeneous material: Optical and acoustic tracking of slow interfacial crack growth. In: 12th International Conference on Fracture (ICF12). Ottawa (Canada).

Schmittbuhl, J., Delaplace, A., Måløy, K. J., Perfettini, H., Vilotte, J. P., 2003a. Slow crack propagation and slip correlations. Pure and applied geophysics 160 (5-6), 961–976.

Schmittbuhl, J., Hansen, A., Batrouni, G., 2003b. Roughness of interfacial crack fronts: stress-weighted percolation in the damage zone. Physical Review Letters 90 (4), 045505/1–4.

Schmittbuhl, J., Måløy, K. J., 1997. Direct observation of a self-affine crack propagation. Physical Review Letters 78 (20), 3888–91.

Schmittbuhl, J., Roux, S., Vilotte, J. P., Maloy, K.-J., 1995a. Interfacial crack pinning: effect of nonlocal interactions. Physical Review Letters 74 (10), 1787–1790.

Schmittbuhl, J., Vilotte, J.-P., 1999. Interfacial crack front wandering: influence of quenched noise correlations. Physica A 270 (1-2), 42–56.

Schmittbuhl, J., Vilotte, J.-P., Roux, S., 1995b. Reliability of self-affine measurements. Physical Review E 51 (1), 131–147.

Seilacher, A., 2001. Concretion morphologies reflecting diagenetic and epigenetic pathways. Sedimentary Geology 143 (1-2), 41–57.

Stallybrass, M., 1981. On the concentrated loading of certain elastic half-space problems and related external crack problems. A new approach. International Journal of Engineering Science 19 (8), 1123–1144.

Storey, B., 1995. The role of mantle plumes in continental break up : case histories from gondwanaland. Nature 377, 301–308.

Tada, H., Paris, P. C., Irwin, G. R., 1973. The Stress Analysis of Cracks Handbook. Del Research Corporation, Hellertown, USA.

Thomas, N., Hansen, C., Portyankina, G., Russell, P., 2010. Hirise observations of gas sublimation-driven activity in mars' southern polar regions: Ii. surficial deposits and their origins. Icarus 205 (1), 296 – 310, mRO/HiRISE Studies of Mars.

Tirumkudulu, M. S., Russel, W. B., 2004. Role of capillary stresses in film formation. Langmuir 20 (7), 2947–2961.

Vieira, A. P., Jose S. Andrade, J., Herrmann, H. J., 2008. Subcritical crack growth: The microscopic origin of paris' law. Physical Review Letters 100 (19), 195503, origine physic de la loi de Paris.

Zarzycki, J., 1988. Critical stress intensity factors of wet gels. Journal of Non-Crystalline Solids 100, 359–363.

Chapter 4

Mes publications/*My publications*

4.1 Liste

Conférences sans actes/*Conference without proceedings*

1. Lazarus, V., Leblond, J.-B., 1996. Theoretical study of crack front rotation and segmentation in brittle cracked solids subjected to arbitrary mixed mode (I+III or I+II+III) loadings. In: XIXth International Congress of Theoretical and Applied Mechanics, Kyoto (Japan). International Union of Theoretical and Applied Mechanics

2. Lazarus, V., Leblond, J.-B., Legrand, L., Pindra, N., Sept. 2009b. In-plane coalescence of slit-cracks. In: et.al., J. A. (Ed.), 7th EUROMECH Solid Mechanics Conference (ESMC2009). European Mechanics Society, Lisbon, Portugal

3. Lazarus, V., Gauthier, G., Davaille, A., Pauchard, L., 2010. Contraction star-shaped cracks: From 90 degrees to 120 degrees crack intersections. In: Geophysical Research Abstracts. European Geosciences Union General Assembly Vienna

Conférences avec actes/*Conference with proceedings*

1. Lazarus, V., Leblond, J.-B., 1-5 April 1997. Three-dimensional crack-face weight functions for the semi-infinite interface crack. In: Karihaloo, B. L., Mai, Y. W., Ripley, M. I., Ritchie, R. O. (Eds.), Proceedings of ICF9, Advances in Fracture Research, Sydney (Australia). Vol. 4. Elsevier Science under the auspices of the International Congress on Fracture, Elsevier Science

2. Lazarus, V., Leblond, J.-B., 3-7 december 2001. The tunnel-crack with a slightly wavy front under shear loading. In: Ravi-Chandar, K., Karihaloo, B. L., Kishi, T., Ritchie, R. O., Yokobori Jr, A. T., Yokobori, T. (Eds.), Advances in Fracture Research, Proceedings of ICF10, Honolulu (Hawaii). Vol. CDRom. Elsevier Science under the auspices of the International Congress on Fracture

3. Favier, E., Lazarus, V., Leblond, J.-B., 18-21 september 2003a. Fatigue and brittle fracture propagation paths of planar tunnel-cracks with perturbed front under uniform remote tensile loadings. In: Fatigue Crack Paths, FCP2003, Parma (Italy). ESIS, European Structural Integrity Society

4. Favier, E., Lazarus, V., Leblond, J.-B., 8-11 September 2003b. Instability and disorder of the front of some tensile tunnel-crack slightly perturbed within its plane. In: Forum, M. S. (Ed.), Modern Practice in Stress and Vibration Analysis 2003 (MPSVA2003), University of Glasgow (GB). Vol. 440-441. Trans Tech Publications, Switzerland, http://www.scientific.net

5. Fulland, M., Lazarus, V., 5-10 September 2004. Numerical simulations of crack front twisting under consideration of local mode II and/or global mode III effects. In: Yao, Z. H., Yuan, M. W., Zhong, W. X. (Eds.), Computational Mechanics, Proceedings CD-ROM of the Sixth World Congress on Computational Mechanics in conjunction with the Second Asia-Pacific Congress on Computational Mechanics. Vol. CD-Rom. Tsinghua University Press & Springer, Beijing, China

6. Favier, E., Lazarus, V., Leblond, J.-B., September 2004. Numerical simulation of propagation of 3d planar cracks in infinite bodies in tension or shear. In: Yao, Z. H., Yuan, M. W., Zhong, W. X. (Eds.), Computational Mechanics, Proceedings of the Sixth World Congress on Computational Mechanics in conjunction with the Second Asia-Pacific Congress on Computational Mechanics. Tsinghua University Press & Springer, Beijing, China

7. Favier, E., Lazarus, V., Leblond, J.-B., Mars 2005. Disorder of the front of a tensile tunnel-crack propagating in some inhomogeneous medium. In: Carpinteri, A., Mai, Y.-W., Ritchie, R. O. (Eds.), 11th International Conference on Fracture. Turin, Italy

8. Lazarus, V., Buchholz, F.-G., Wiebesiek, J., September 2006. Crack front twisting in three point bending, comparison between a local and a global approach. In: 35-th Solid Mechanics Conference, SolMech2006. Institute of Fundamental Technological Research, Polish Academy of Sciences, Krakow (Poland)

9. Pindra, N., Lazarus, V., Leblond, J.-B., August 2007. Désordre du front d'une fissure semi-infinie d'interface. In: de Mécanique, A. F. (Ed.), CFM07, 18e Congrès Francais de Mécanique. Grenoble

10. Pindra, N., Lazarus, V., Leblond, J.-B., 2008b. Slight in-plane perturbation of a system of two coplanar parallel tensile slit-cracks. In: 36-th Solid Mechanics Conference, SolMech2008. Institute of Fundamental Technological Research, Polish Academy of Sciences, Gdansk (Poland)

11. Chekchaki, M., Lazarus, V., Sept. 2009. Analytical and 3d finite element study of the deflection of an elastic cantilever bilayer plate. In: et.al., J. A. (Ed.), 7th EUROMECH Solid Mechanics Conference (ESMC2009). European Mechanics Society, Lisbon, Portugal

12. Faure, S., Maurel, D., Cuer, F., Lazarus, V., Pauchard, L., Sept. 2009. Surfactants adsorption effects on rheological and cracking properties of self-dried decontamination gel films. In: 23rd Conference of the European Colloid and Interface Society, 3rd Workshop of COST Action D4 (ECIS 2009). Department of Chemical Engineering, Yeditepe University, Istanbul, Turkey., Antalya (Turkey)

13. Lazarus, V., Gauthier, G., Pauchard, L., Maurini, C., Valdivia, C., July 2009a. Basalt columns and crack formation during directional drying of colloidal suspensions in capillary tubes. In: 12th International Conference on Fracture (ICF12). Ottawa (Canada)

14. Pindra, N., Lazarus, V., Leblond, J., Schmittbuhl, J., Toussaint, R., July 2009. Deformation of the crack front during propagation in some disordered medium: theoretical and experimental studies. In: 12th International Conference on Fracture (ICF12). Ottawa (Canada)

Publications dans une revue à comité de lecture/*Articles in peer-reviewed journals*

1. Lazarus, V., Leblond, J.-B., 1998a. Crack paths under mixed mode (I+III) or (I+II+III) loadings. Comptes Rendus de l'Académie des Sciences, Série II (Mécanique, Physique, Astronomie) 326 (3), 171–177

2. Lazarus, V., Leblond, J.-B., 1998b. Three-dimensional crack-face weight functions for the semi-infinite interface crack. I. Variation of the stress intensity factors due to some small perturbation of the crack front. Journal of the Mechanics and Physics of Solids 46 (3), 489–511

3. Lazarus, V., Leblond, J.-B., 1998c. Three-dimensional crack-face weight functions for the semi-infinite interface crack. II. Integrodifferential equations on the weight functions and resolution. Journal of the Mechanics and Physics of Solids 46 (3), 513–536

4. Lazarus, V., 1999. Fatigue propagation path of 3D plane cracks under mode I loading. Comptes-Rendus de l'Académie des Sciences, Série IIb 327 (13), 1319–1324

5. Leblond, J.-B., Lazarus, V., Mouchrif, S.-E., 1999. Crack paths in three-dimensional elastic solids. II. Three-term expansion of the stress intensity factors - Applications and perspectives. International Journal of Solids and Structures 36 (1), 105–142

6. Lazarus, V., Leblond, J.-B., Mouchrif, S.-E., 2001a. Crack front rotation and segmentation in mixed mode I+III or I+II+III - part I: Calculation of Stress Intensity Factor. Journal of the Mechanics and Physics of Solids 49 (7), 1399–1420

7. Lazarus, V., Leblond, J.-B., Mouchrif, S.-E., 2001b. Crack front rotation and segmentation in mixed mode I+III or I+II+III - part II: Comparison with experiments. Journal of the Mechanics and Physics of Solids 49 (7), 1421–1443

8. Lazarus, V., Leblond, J.-B., 2002a. Crack front stability for a tunnel-crack propagating along its plane in mode 2+3. Comptes Rendus de l'Académie des Sciences Paris, Serie II (Mecanique, Physique, Astronomie) 330 (6), 437–443

9. Lazarus, V., Leblond, J.-B., 2002b. In-plane perturbation of the tunnel-crack under shear loading. I: Bifurcation and stability of the straight configuration of the front. International Journal of Solids and Structures 39 (17), 4421–4436

10. Lazarus, V., Leblond, J.-B., 2002c. In-plane perturbation of the tunnel-crack under shear loading. II: determination of the fundamental kernel. International Journal of Solids and Structures 39 (17), 4437–4455

11. Lazarus, V., 2003. Brittle fracture and fatigue propagation paths of 3D plane cracks under uniform remote tensile loading. International Journal of Fracture 122 (1-2), 23–46

12. Favier, E., Lazarus, V., Leblond, J.-B., 2006a. Coplanar propagation paths of 3D cracks in infinite bodies loaded in shear. International Journal of Solids and Structures 43 (7-8), 2091–2109

13. Favier, E., Lazarus, V., Leblond, J.-B., 2006b. Statistics of the deformation of the front of a tunnel-crack propagating in some inhomogeneous medium. Journal of the Mechanics and Physics of Solids 54 (7), 1449–1478

14. Pauchard, L., Lazarus, V., Abou, B., Sekimoto, K., Aitken, G., Lahanier, C., Mars 2007. Craquelures dans les couches picturales des peintures d'art. Reflets de la Physique, Société Française de Physique 3, 5–9, https://hal.archives-ouvertes.fr/hal-00158845

15. Gauthier, G., Lazarus, V., Pauchard, L., 2007. Alternating crack propagation during directional drying. Langmuir 23 (9), 4715–4718

16. Ponson, L., Auradou, H., Pessel, M., Lazarus, V., Hulin, J. P., 2007. Failure mechanisms and surface roughness statistics of fractured fontainebleau sandstone. Physical Review E 76 (036108)

17. Pindra, N., Lazarus, V., Leblond, J.-B., 2008a. The deformation of the front of a 3d interface crack propagating quasistatically in a medium with random fracture properties. Journal of the Mechanics and Physics of Solids 56 (4), 1269–1295

18. Lazarus, V., Buchholz, F.-G., Fulland, M., Wiebesiek, J., 2008. Comparison of predictions by mode II or mode III criteria on crack front twisting in three or four point bending experiments. International Journal of Fracture 153, 141–151

19. Pindra, N., Lazarus, V., Leblond, J.-B., 2010. Geometrical disorder of the fronts of a tunnel-crack propagating in shear in some heterogeneous medium. Journal of the Mechanics and Physics of Solids 58, 281–299

20. Chekchaki, M., Frelat, J., Lazarus, V., 2010. Analytical and 3D finite element study of the deflection of an elastic cantilever bilayer plate. Transactions of the ASME. Journal of Applied Mechanics , Accepted

21. Gauthier, G., Lazarus, V., Pauchard, L., 2010. Shrinkage star-shaped cracks: Explaining the transition from 90 degrees to 120 degrees. EPL 89, 26002

In preparation:

1. Pindra, N., Lazarus, V., Leblond, J.-B., In prep. In-plane perturbation of a system of two coplanar slit-cracks - I: Case of arbitrarily spaced crack fronts. International Journal of Solids and Structures

2. Lazarus, V., Maurini, C., Gauthier, G., Pauchard, L., In prep.b. Crack patterns obtained for different cell-shapes in directional drying experiments and non-local gradient damage model simulations

3. Lazarus, V., Pauchard, L., In prep.b. From craquelures to spiral crack patterns: influence of the thickness on the crack patterns obtained during the drying of a suspension thin layer

4. Lazarus, V., Davaille, A., Gauthier, G., In prep.a. Polygonal crack patterns: from 90 to 120 degrees crack junctions

5. Lazarus, V., In prep. Self-consistent measures of the toughness during the drying induced consolidation of colloidal suspensions

6. Lazarus, V., Pauchard, L., In prep.a. Critical thicknesses and Griffith's length during dessication of a colloidal film

7. Chekchaki, M., Lazarus, V., Pauchard, L., In prep.b. Influence of the width of the plate on the beam deflection induced by the drying consolidation of colloidal suspensions

8. Chekchaki, M., Lazarus, V., Pauchard, L., In prep.a. Characterization of consolidated colloidal suspensions

Vulgarisation/*Broad audience*

Participation à l'exposition "Ruptures : ça roule ou ça casse" /*Scientific exhibition "Fractures : it flows or it breaks".*
Réalisée par Centre Sciences, CCSTi de la région Centre en partenariat avec l'Espace des sciences - CCSTi de Rennes, coordonnée par Michel Darche, Etienne Guyon et Tanguy Rouxel. En cours de réalisation (2009-2010)

Programmes de recherche/*Research programs*

2010–2013 ANR-09-SYSC-006 programme SYSCOMM. "MEcanique et PHYsique STAtistique de la Rupture dans les matériaux fragiles hétérogènes/*Mechanics and Statistical Physics of Rupture in Brittle Heterogeneous Materials*"
Coordinateur principal: D. Dalmas (LSVI). Partenaires: Laboratoire Surface du Verre et Interfaces (LSVI, Unité Mixte CNRS/Saint-Gobain - UMR 125), SPCSI, CEA Saclay - IRAMIS, Laboratoire PMMH (ESPCI, UMR 7636), FAST (UMR 7108)

2006–2009 ANR-05-JCJC-0029-01 Jeunes chercheuses et jeunes chercheurs. " De l'histoire d'un système complexe aux morphologies des déformations induites par relaxation des contraintes/*From the history of a complex system to the deformation patterns induced by stress relaxation*".
Coordinateur principal: L. Pauchard (FAST). Partenaires: FAST (UMR 7108), Matières et Systèmes Complexes (UMR 7057), LMM (UMR 7190).

2009 RTRA Triangle de la physique. Projet FracHet "Plasticity, fracture and dynamical heterogeneities in glasses". Coordinateur principal: E. Bouchaud (CEA-SPEC). Partenaires: CEA-SPEC, CEA-SPCSI, CEA-LLB et Orsay-FAST.

2007 RTRA Triangle de la physique Projet CODERUP "Rupture et Endommagement des matériaux : Comment déchiffrer les surfaces de rupture?/*Fracture and damage: how to unravel fracture surfaces?*". Coordinateur principal: H. Auraldou (FAST). Partenaires: SPCSI, CEA Saclay - IRAMIS; FAST.

4.2 Sélection de publications/*Selected publications*

The 3D LEFM problems I have considered until now, can be divided in two groups: the determination of the out-of-plane propagation of a crack loaded in shear and the determination of the crack front deformations during the coplanar propagation of plane cracks. Concerning the out of plane propagation, criterions allowing to predict the crack front twisting in presence of mode 3 have been proposed and compared to experiments. Concerning the in-plane propagation, small deformations of the crack front during its propagation have been studied analytically and large deformations numerically. Both homogeneous and heterogeneous materials have been considered. All these studies use perturbation of the crack front approaches, presented in chapter 2, initiated by Rice (1985), the development of which I took part for more complex cases. Since my arrival at the laboratory FAST, in addition to these theoretical studies, I become also interested in the fractures appearing during the drying of suspensions of colloidal particles (size of 1 nm to 1 μm). The first studies have shown the potential of these experiments to bring new insights into the energetic principles used in fracture mechanics, the physico-chemistry of the consolidation process and some geological crack patterns.
To summarize, the research fields I considered until now can be divided as follows (in this list, the papers that are included in the sequel are in bold):

1. **Crack propagation path in presence of mode 3**. Whatever the external loading, in an homogeneous solid, a crack tries to reach mode 1 (tensile) loading conditions. In mode 1+2, the crack kinks to annihilate mode 2, the angle can be obtained by 2D considerations using for instance the Principle of Local Symmetry (Goldstein and Salganik, 1974). In presence of mode 3, the crack front twists around the direction of propagation, this renders the problem 3D. During my PhD a criterion able to predict the crack rotation rate has been proposed in the particular case of 3 or 4 PB experiments and experiments have been performed in Sheffield (Lazarus and Leblond, 1998a; Lazarus et al., 2001b). The criterion uses the expression of stress intensity factors resulting from a little 3D arbitrary extension of the crack front, the development of which I took

part (Leblond et al., 1999; Lazarus et al., 2001a). Additional works done in collaboration with the University of Paderborn (Germany) have shown that 3 or 4 PB experiments yield strong coupling of the modes 2 and 3 and hence, are inadequate to clearly separate the criterions based on the presence of mode 3, and more conventional mode 2 based criterions **(Lazarus et al., 2008)**.

2. **Three-dimensional perturbation of the crack front approaches.** This approach, initiated by Rice (1985) and reviewed in chapter 2, gives the formulas to update the stress intensity factors for a small in-plane crack front increment. I participate to the derivation of those formulas in the case of an interfacial half-plane crack (Lazarus and Leblond, 1998c) and the tunnel-crack under shear loading **(Lazarus and Leblond, 2002c)**.

3. **PlaneCracks: Numerical simulations of large scale propagation of planar cracks.** Following an idea of Bower and Ortiz (1990), I developed a code, named PlaneCracks, to simulate the brittle or fatigue propagation of a plane crack of arbitrary closed crack fronts. The code was first written in mode 1 (Lazarus, 1999), **(Lazarus, 2003)** and than extended to mode 2+3 **(Favier et al., 2006a)**.

4. **Analytical studies of the crack front deformation.** Using the perturbation approach of chapter 2, we have performed the configurational bifurcation and stability analysis (see §2.4.1) for an interfacial half-plane crack (Lazarus and Leblond, 1998b) and for a tunnel-crack under shear loading (Lazarus and Leblond, 2002a), **(Lazarus and Leblond, 2002b)**. Further on, these studies have been extended to the study of the crack front deformation when it propagates in an heterogeneous media (§2.6) for a tunnel-crack under tensile (Favier et al., 2006b) and shear loading (Pindra et al., 2010), but also the interfacial half-plane crack **(Pindra et al., 2008a)**.

5. **Fracture during drying of colloidal suspensions.** Since my first sojourn at lab FAST (2006), I extended my research interests to shrinkage cracks and in particular to the fracture arising during the drying of suspensions of colloidal particles. I consider both the drying of thin films (Pauchard et al., 2007) and directional drying in capillary tubes (Gauthier et al., 2007). The application of LEFM minimisation principle to those last experiments has underlined the importance of the Griffith length **(Gauthier et al., 2010)**. Comparison of directional drying experiments with a regularized form of the energetic approach by a non-local damage model (fig. 3.2(c)) has also been performed for different cell shapes and have shown qualitative agreement **(Lazarus et al., 2009a)**. Experimental characterization techniques are also currently developed **(Chekchaki et al., 2010)**.

Int J Fract (2008) 153:141–151
DOI 10.1007/s10704-008-9307-2

ORIGINAL PAPER

Comparison of predictions by mode II or mode III criteria on crack front twisting in three or four point bending experiments

V. Lazarus · F.-G. Buchholz · M. Fulland · J. Wiebesiek

Received: 31 July 2008 / Accepted: 17 December 2008 / Published online: 20 January 2009

Abstract Whatever the external loading, a crack front in a solid tries to reach mode I loading conditions after propagation. In mode I+II, the crack kinks to annihilate mode II, kinking angle being well predicted by the principle of local symmetry (PLS) or by the maximum tangential stress criterion (MTS). In presence of mode III, the problem becomes three-dimensional and the proposed propagation criterion are not yet well proved and established. In particular in three point bending experiments (3PB) with an initially inclined crack, the crack twists around the direction of propagation to finally reach a situation of pure mode I. The aim of the paper is to compare the propagation paths predicted by two different criteria for 3PB fatigue experiments performed on PMMA. The first criterion developed by Schollmann et al. (Int J Fract 117(2):129–141, 2002), is a three-dimensional extension of the MTS criterion and predicts the local angles that annihilates mode II and III at each point of the front. The second one developed by Lazarus et al. (J Mech Phys Solids 49(7):1421–1443, 2001b), predicts an abrupt and then progressive twisting of the front to annihilate mode III. Due to presence of sign changing mode II and almost uniform mode III in the experiments, both criteria give good results. However, since mode III is predominant over mode II in the case under consideration, the global criterion gives better results. Nevertheless, the local type criterion seems to be of greater universality for practical engineering applications.

Keywords Brittle fracture · Mode II · Mode III · Maximum tangential stress criterion · 3D crack propagation path · 3D fracture criteria · LEFM

1 Introduction

In homogeneous isotropic elastic media, except in some special conditions, it is well known that whatever the external loading, the crack front bifurcates in order to reach a situation of pure mode I as the crack propagates (Hull 1993). A literature survey of mixed mode crack growth can be found in Qian and Fatemi (1996). Under mode (I+II) conditions, the crack kinks to annihilate mode II, as depicted in Fig. 5c. The value of the corresponding kink angle can be obtained, for instance, by the Principle of local Symmetry (PLS) of Goldstein and Salganik (1974) or by the maximum tangential stress criterion (MTS; Erdogan and Sih 1963). In presence of mode III, to reach a situation of mode I, the crack front twists around the direction of propagation. The

V. Lazarus (✉)
UPMC Univ Paris 6, Univ Paris-Sud, CNRS, UMR 7608, Lab FAST, Bat 502, Campus Univ, 91405 Orsay, France
e-mail: veronique.lazarus@upmc.fr

F.-G. Buchholz · M. Fulland · J. Wiebesiek
Institute of Applied Mechanics, University of Paderborn, Pohlweg 47-49, 33098 Paderborn, Germany
e-mail: fus.buchholz@t-online.de

M. Fulland
e-mail: fulland@fam.upb.de

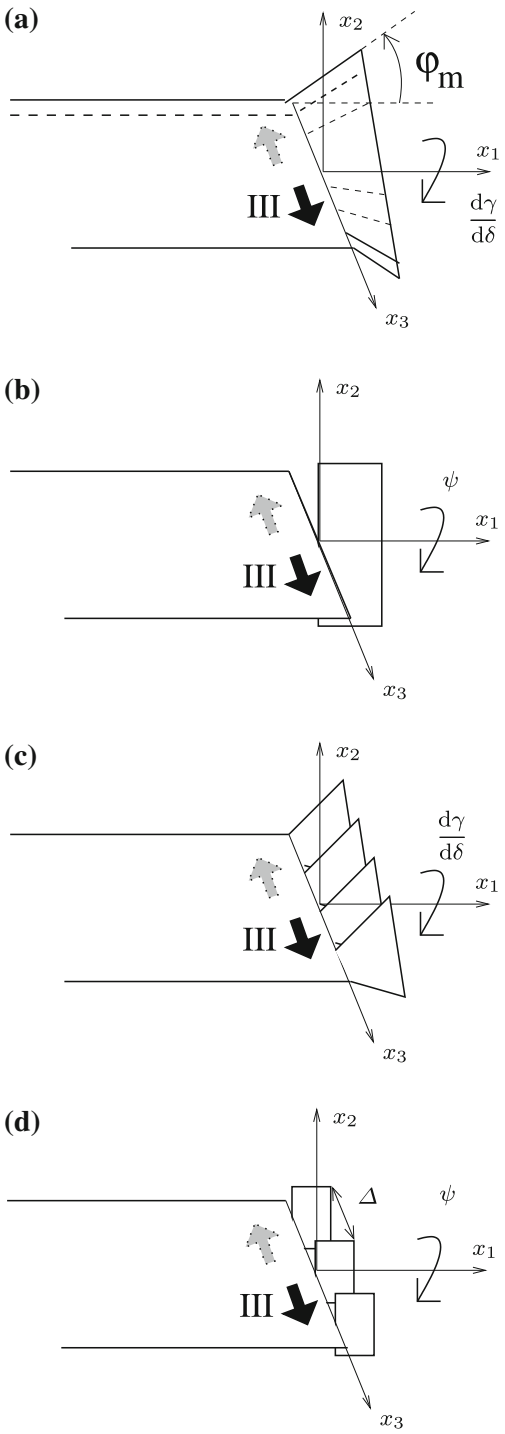

Fig. 1 Several basic propagation possibilities in presence of mode III. **a** Gradual one-piece twisting; **b** Abrupt one-piece twisting; **c** Gradual piecewise twisting; **d** Abrupt piecewise twisting

way this twisting occurs is case dependent: in some cases, it occurs gradually (Fig. 1a, c), in some other cases abruptly (Fig. 1b, d); sometimes the whole front twists in one-piece (see Fig. 1a, b) and in some other cases, the front twists piecewise leading to a factory roof pattern (see Fig. 1c, d). The conditions of transition between these several crack patterns remain an open question. For instance, gradually piecewise rotation has been observed by Sommer (1969), Hourlier and Pineau (1979); abruptly piecewise rotation by Palaniswamy and Knauss (1975). In Makabe et al. (2006), depending on the loading conditions, both progressive and abrupt rotation have been observed. Abrupt piecewise twisting at a small, *mesoscopic*, length-scale and progressive rotation of the whole crack front at a *macroscopic* length-scale, has been observed in three or four points bending (3PB or 4PB) experiments. Such experiments and observations have been made by Yates and Mohammed (1996) on steel specimens in fatigue, by Cooke and Pollard (1996), Buchholz et al. (1998, 2005) on PMMA blocks in fatigue, by Lazarus and Leblond (1998), Lazarus et al. (2001b) on PMMA specimens under monotonic increasing loading. These patterns can also be recognized on geological materials (Pollard et al. 1982; Aydin and Pollard 1988) at different length-scales.

The qualitative way of crack propagation is well explained by its tendency to reach mode I conditions (Hull 1993; Pook 1995). But it is not sufficient to predict the propagation path quantitatively and a few fracture criteria have been proposed so far. Concerning the abrupt rotation of the crack front, several criteria have been proposed. But the only paper we are aware of, that compares the results with experimental findings is Cooke and Pollard (1996), who showed that all the criteria overestimate the real value. Lazarus et al. (2001b) proposed the following fit:

$$\psi = \frac{1}{4}\arctan\frac{2K_{\mathrm{III}}}{(1-2\nu)K_{\mathrm{I}}} \tag{1}$$

by interpolation of their experimental data. In the special case of 3 or 4PB experiments, the gradually rotation of the front, has been predicted, on the one hand, by Gravouil et al. (2002) and Buchholz et al. (2004) using MTS-criteria and by Lazarus and Leblond (1998), Lazarus et al. (2001b) using a criterion predicting the twisting rate of the whole crack front. Whereas the kink angles given by MTS criteria lead to the annihilation of mode II, the twisting rate of Lazarus and Leblond (1998), Lazarus et al. (2001b) leads to the annihilation of mode III. Hence it may be surprising that both criteria manage to find the experimental propagation path. Also the aim of this paper is to discriminate these two kind of criteria by comparing the predictions of the MTS criterion (Erdogan and Sih 1963) or its

3D extension (Schollmann et al. 2002) and those of the criterion proposed by Lazarus and Leblond (1998), Lazarus et al. (2001b) to 3PB fatigue experiments performed on PMMA.

These experiments are presented in Sect. 2. Both modes II and III are present in the experiments. By symmetry, mode II Stress Intensity Factor (SIF) takes opposite signs at each side of the front, hence MTS criterion (or equivalent 3D ones, see Sect. 3.1) predicts an opposite sign of the kink angle. Mode III yields a uniform twisting of the whole front by Lazarus et al. criterion (Sect. 3.2). Hence, at least qualitatively, the same kind of twisting propagation path is expected and the quantitative comparison (Sect. 4) with the experiments shows that both criteria allow to recover quite well the experimental values. Nevertheless, two facts shall limit the extensive use of MTS criterion (or equivalent ones such as PSL or 3DMTS generalization) in presence of mode III although MTS criteria seem to be sufficient for any practical engineering purposes. The first fact is that increasing mode III over mode II rate, gives advantage to Lazarus et al. criterion toward the MTS one, and the second that MTS criterion predicts well the kink angle near the free surfaces but too low ones near the center of the front.

2 Experiments

2.1 Setup

The experiments are 3PB experiments performed on PMMA specimens containing an initial inclined slit (Fig. 2). The geometrical parameters of the 3PB-specimens are as follows: length $L = 260\,\text{mm}$, $2L_e = 240\,\text{mm}$, thickness $t = 10\,\text{mm}$, width $W = 60\,\text{mm}$, normalized crack length $a/w = 1/3$, angles of the inclined planes of the initial cracks or notches with $\gamma = 75°$, 60° and 45°. For the simulation the material parameters are given by the experi-mental specimens from PMMA with Young modulus $E = 2,800\,\text{N/mm}^2$ and Poisson ratio $\nu = 0.38$. The specimens are subject to a cyclic lateral force of $F = 2.4\,\text{kN}$ and the stress ratio of the cyclic loading is $R = 0.1$.

2.2 Propagation paths

For $\gamma = 90°$, the initial notch is located in the middle (x, z) plane of the specimen. Due to symmetry

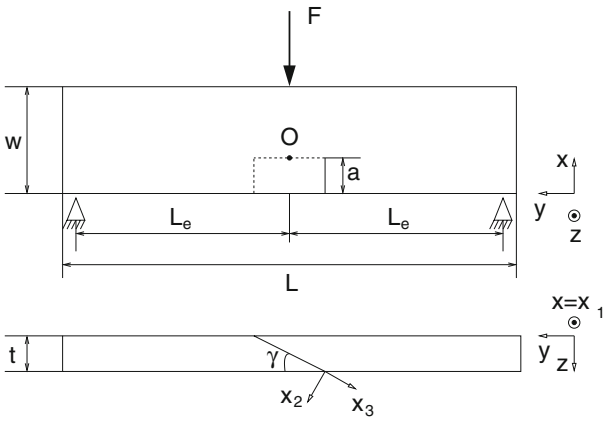

Fig. 2 3PB-specimen with an inclined initial notch

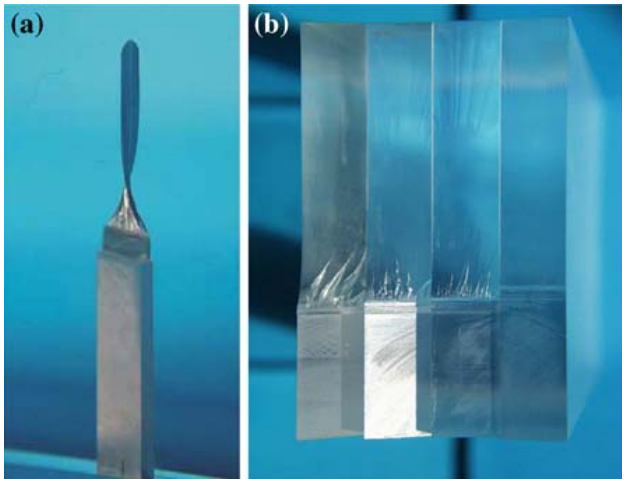

Fig. 3 Gradual one-piece crack twisting. **a** Global view for $\gamma = 45°$; **b** Final view for several angles $\gamma = 45°, 60°, 75°, 90°$

reasons, the crack is then loaded in mode I only and crack propagates straight and breaks the specimen in two equivalent pieces. For γ less than 90° the initial notch is loaded in both tension and out-of-plane shear, and the crack bifurcates during propagation. Pictures of the propagation path (Fig. 3) show that, at a *macroscopic* length-scale, the crack front gradually twists around the direction of propagation to finally reach the middle mode I plane (x, z) of the specimen. Hence, crack propagates to annihilate shear loading. One can notice in Fig. 3b, that the rotation becomes more important with decreasing value of γ. By observing the crack facies postmortem, one can also notice that the intersection between the crack surface and a plane (y, z) is always straight (one can adjust a straight ruler on this intersection). This will be of importance for the geometric description of this macroscopic crack surface.

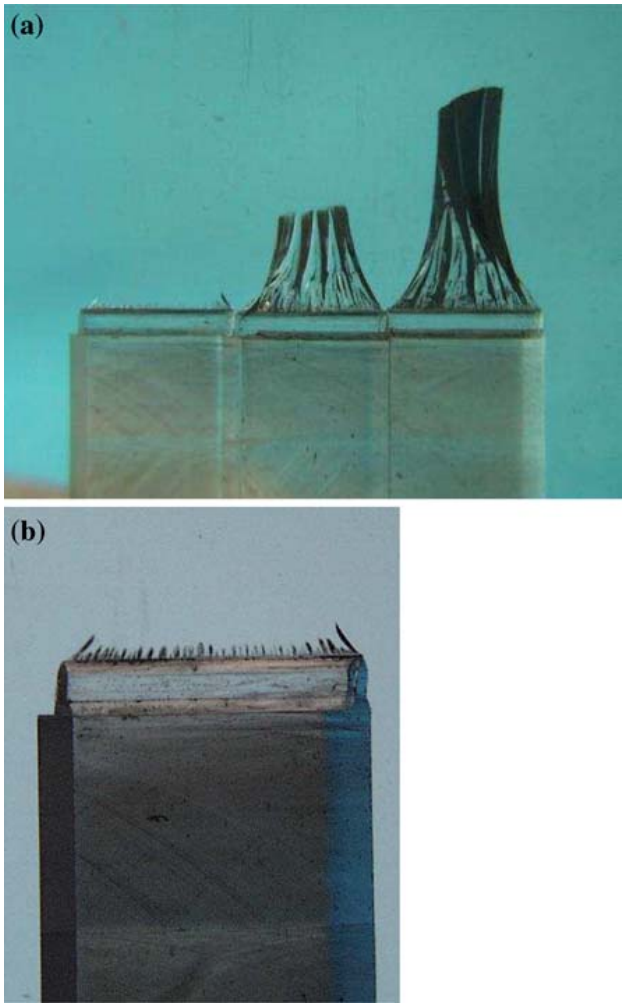

Fig. 4 Different stages of the crack propagation path. **a** Three different stages of propagation: initial facets (on the left), gradual one-piece twisting (two ones on the right) ($\gamma = 45°$); **b** Zoom on the initial facets formed by abrupt piecewise twisting

On a smaller *mesoscopic* length-scale, one can notice on the pictures of Fig. 4, some little facets looking like abrupt factory roofs or echelon cracks, the plane of each facet being obtained by abrupt rotation of angle ψ about the x-direction of propagation (Fig. 1d). Our principal aim in this paper is not to determine the angle ψ locally for positions along the crack front (although it will be needed in one of the criteria) but the geometry of the macroscopic smoothly twisting crack extension.

2.3 Quantitative description of the macroscopic crack extension

Figure 5a schematically shows the whole extension of the crack obtained experimentally, and Fig. 5b–d this same extension but restricted to a distance of propagation δ from the initial slit, δ being supposed small enough so that crack extension in each plane $x_3 = Cst.$ coincide with its tangent (Fig. 5c). Let us denote d the half-length of the initial front, $\varphi(x_3)$ the kink angle

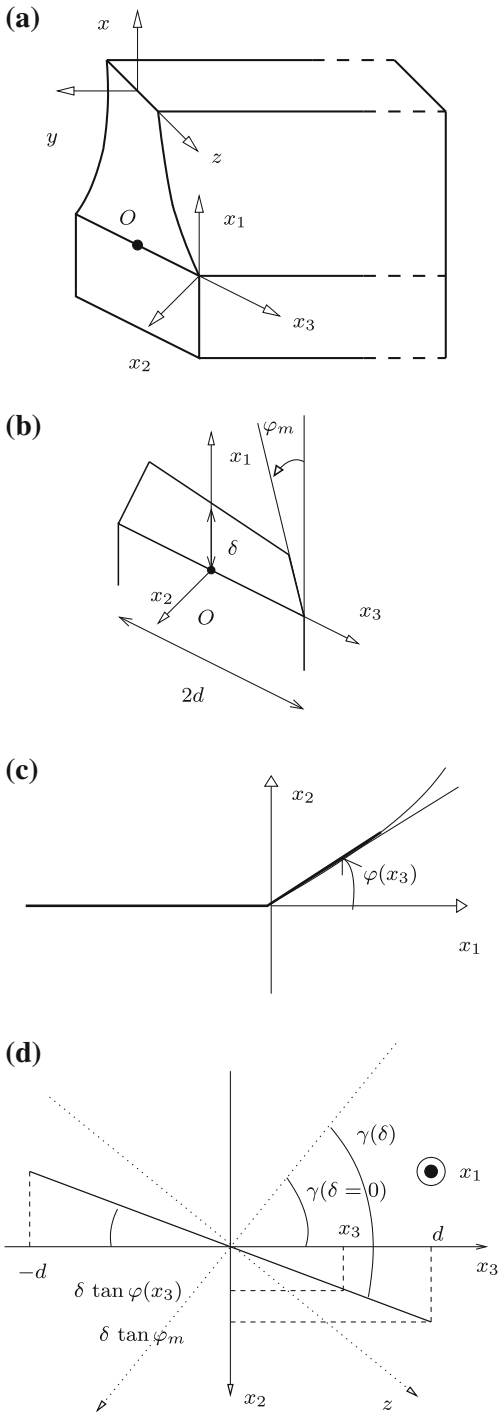

Fig. 5 Schematic view of the crack surface and local kinking. **a** Whole surface; **b** 3D view of the local kinking; **c** In a plane $x_3 = Cst.$; **d** In a plane $x_1 = \delta$

(rotation angle of the crack extension around Ox_3) at the point of coordinate x_3 of the front, φ_m the kink angle for $x_3 = d$. The intersection of the crack and a plane $x_1 = \delta$ being observed to be a straight line, one can use Thales' theorem (see Fig. 5d) to obtain:

$$\frac{\delta \tan \varphi_m}{d} = \frac{\delta \tan \varphi(x_3)}{x_3}$$

which yields:

$$\varphi(x_3) = \arctan\left(\frac{x_3}{d} \tan \varphi_m\right) \tag{2}$$

so that one can derive the kink angle all along the crack front by simply performing the measure of the kink angle φ_m at the external surface. Here care must be taken that φ_m is defined in the plane $x_3 = d$ normal to the crack front hence is different from the "kink" angle α measured on the free surface plane $z = t/2$. They are linked by:

$$\cos \varphi_m = \frac{\cos \alpha}{\sqrt{\sin^2 \gamma + \cos^2 \gamma \cos^2 \alpha}} \tag{3}$$

Since some experimenters give values of the rotation rate $\mathrm{d}\gamma/\mathrm{d}\delta$ rather than the kink angle, we give also the following relation between φ_m and $\mathrm{d}\gamma/\mathrm{d}\delta$, which can easily be derived from Fig. 5d:

$$\frac{\mathrm{d}\gamma}{\mathrm{d}\delta} = \frac{\tan \varphi_m}{d} \tag{4}$$

In the sequel we will focus our attention on the determination of the kink angle. The value of the rotation rate can then be deduced from Eq. 4.

2.4 Quantitative description of the mesoscopic facets

The initial facets have not at the moment be studied precisely and shall be the subject of a further work. For the purpose of this paper (the study of the macroscopic extension), we will use a simplified description by assuming that all the initial facets are deduced from the initial slit by rotation of a same angle ψ about the Ox_1 axis. They disappear when they merge into the global crack surface which gradually rotates about the same axis with the rotation rate $\frac{\mathrm{d}\gamma}{\mathrm{d}\delta}$. Hence, their length δ_c is linked to the rotation rate by the following formula:

$$\frac{\mathrm{d}\gamma}{\mathrm{d}\delta}\delta_c = \psi \tag{5}$$

3 Propagation criteria

For the determination of the kink angle, two types of criteria are proposed in the sequel. The first type predicts independently the kink angle at each point x_3 of the crack front by using the values of the SIFs at the same point x_3, hence will be called *local type* criteria in the sequel. These criteria are the PLS (Goldstein and Salganik 1974), the MTS (Erdogan and Sih 1963) and its 3D extension (Schollmann et al. 2002). The second type of criteria supposes that the kink angle is of the form of Eq. 2 and predicts the maximum kink angle φ_m or equivalently the rotation rate $\mathrm{d}\gamma/\mathrm{d}\delta$ considering the mean value of the SIFs along the whole crack front. They will be called *global type* criteria in the sequel. These criteria consist in maximizing the mean value of K_I (mode I SIF) or the mean value of $\mathcal{G}$ (total energy release rate). All these criteria are described in the following sections.

3.1 Local type criteria

Consider a point of the crack front and denote K_I, K_II, K_III the SIFs at this point. After propagation the crack has kinked by an angle φ. We will consider three criteria giving this kink angle versus the initial SIFs (before propagation): the Principle of Local Symmetry (PLS), The Maximum Tangential Stress criterion (MTS), and a 3D extension of the MTS (3DMTS).[1]

The Principle of Local Symmetry states that after propagation the mode II SIF shall become zero. This yields:

$$K_\mathrm{I} F_{\mathrm{II,I}}(\varphi) + K_\mathrm{II} F_{\mathrm{II,II}}(\varphi) = 0 \tag{6}$$

where functions $F_{i,j}$ have been derived in Amestoy and Leblond (1992).

The Maximum Tangential Stress criterion states that the crack propagates in the direction where the circumferential tensile stress $\sigma_{\theta\theta}$ is maximum. This yields:

$$K_\mathrm{I} \sin \varphi + K_\mathrm{II}(3 \cos \varphi - 1) = 0 \tag{7}$$

The 3D extension of the MTS (3DMTS) developed by Schollmann et al. (2002) states that the crack will grow radially from the crack front into the direction which is perpendicular to maximum principal stress σ_1'.

[1] Other criteria exist, see Qian and Fatemi (1996), but the aim here is not to make a systematic review of these local criteria but to compare two types (local and global) of criteria.

This direction corresponds to an abrupt twist angle ψ of the front around the direction of propagation and a kink angle φ which is linked to the SIFs by:

$$
\begin{aligned}
&6\,K_{\mathrm{I}}\,\tan\left(\frac{\varphi}{2}\right)+K_{\mathrm{II}}\left(6-12\tan^2\left(\frac{\varphi}{2}\right)\right)\\
&+\left\{24\left[K_{\mathrm{I}}-3\,K_{\mathrm{II}}\,\tan\left(\frac{\varphi}{2}\right)\right]\right.\\
&\cdot\left[K_{\mathrm{I}}\,\tan\left(\frac{\varphi}{2}\right)+K_{\mathrm{II}}\left(1-2\tan^2\left(\frac{\varphi}{2}\right)\right)\right]\\
&\left.+32\,K_{\mathrm{III}}^2\,\tan\left(\frac{\varphi}{2}\right)\cdot\left(1+\tan^2\left(\frac{\varphi}{2}\right)\right)^2\right\}\\
&\cdot\left\{\left[4\,K_{\mathrm{I}}-12\,K_{\mathrm{II}}\,\tan\left(\frac{\varphi}{2}\right)\right]^2\right.\\
&\left.+64\,K_{\mathrm{III}}^2\left(1+\tan^2\left(\frac{\varphi}{2}\right)\right)^2\right\}^{-1/2}=0
\end{aligned}
\tag{8}
$$

Since PLS and MTS criterion give nearly the same value of the kink angle,[2] we will only consider in the sequel the MTS and 3DMTS criterion.

3.2 Global type criterion of Lazarus and Leblond

Starting from the idea that the twisting of the crack front is due to the presence of mode III, a criterion linked to the disappearance of mode III has to be derived. This criterion is necessary of global type (that is involving all the points of the front) since this twisting around the direction of propagation can only be achieved if all the points twist together. Lazarus and Leblond (1998), Lazarus et al. (2001b) proposed two such criteria:

MVG: maximize the Mean Value of $\mathcal{G}(x_3,\delta)$ along the front with respect to φ_m

MVK: maximize the Mean Value of $K_I(x_3,\delta)$ along the front with respect to φ_m

where $\mathcal{G}(x_3,\delta)$ denotes the total energy release rate and $K_{\mathrm{I}}(x_3,\delta)$ the mode I SIF, both after a propagation over a distance δ and at the point of coordinate x_3 of the front. One has:

$$
\begin{aligned}
\mathcal{G}(x_3,\delta)=&\frac{1-\nu^2}{E}\left[K_{\mathrm{I}}^2+K_{\mathrm{II}}^2\right](x_3,\delta)\\
&+\frac{1+\nu}{E}K_{\mathrm{III}}^2(x_3,\delta)
\end{aligned}
\tag{9}
$$

Applying these criteria for a vanishing δ, that is, a vanishing crack extension length, one gets a zero value for φ_m.

[2] Indeed Amestoy and Leblond (1992) have shown that the difference is of order m^6 with $m=\varphi/\pi$

This implies that the criteria must be applied after a *non-zero propagation length*. On picture 4b, one observes the presence of little facets at the beginning of the propagation. During the formation of the facets, the points of the crack front propagate in an "individual" manner. Afterward, as soon as the facets have disappeared and the entire front twists as a whole, their behaviour becomes "collective". From there derives the idea *to fix δ in the criteria to the length δ_c of these little facets*.

In order to apply the criteria, let us suppose the length δ_c of the extension to be small enough for the expansion of the stress intensity factors $K_{\mathrm{I}}(x_3,\delta)$, $K_{\mathrm{II}}(x_3,\delta)$, $K_{\mathrm{III}}(x_3,\delta)$ in powers of the crack extension length δ obtained by Leblond (1989) and Lazarus et al. (2001a) to be applicable. These expressions give the SIFs after propagation $K_p(x_3,\delta)$ in function of the initial SIFs $K_p(x_3)$, $p=\mathrm{I},\mathrm{II},\mathrm{III}$. Denote k_p the mean value of these quantities:

$$
k_p=\frac{1}{2d}\int_{-d}^{d}K_p(x_3)dx_3 \tag{10}
$$

If $|k_{\mathrm{III}}/k_{\mathrm{I}}|\ll 1$ and $|k_{\mathrm{II}}/k_{\mathrm{I}}|\ll 1$, the criteria MVK and MVG then give respectively the following formulas for φ_m:

$$
\varphi_m=\frac{8\frac{\delta_c}{d}}{1+\frac{16\sqrt{2}}{3\pi}\sqrt{\frac{\delta_c}{a}}-\frac{5}{12}\frac{\delta_c}{a}+\frac{6}{\pi}\frac{2-3\nu}{2-\nu}\frac{\delta_c}{d}}\frac{k_{\mathrm{III}}}{k_{\mathrm{I}}} \tag{11}
$$

$$
\varphi_m=\frac{4\frac{\delta_c}{d}}{(2-\nu)\left(\frac{1}{3}+\frac{4}{3\pi}\sqrt{\frac{2\delta_c}{a}}-\frac{16}{3\pi^2}\frac{\delta_c}{a}+\frac{2}{\pi}\frac{2-3\nu}{2-\nu}\frac{\delta_c}{d}\right)}\times\frac{k_{\mathrm{III}}}{k_{\mathrm{I}}} \tag{12}
$$

These theoretical expressions of φ_m were obtained analytically for $|k_{\mathrm{III}}/k_{\mathrm{I}}|\ll 1$ and $|k_{\mathrm{II}}/k_{\mathrm{I}}|\ll 1$. However, φ_m can be computed numerically for arbitrary values of $K_{\mathrm{III}}/K_{\mathrm{I}}(x_3)$ and $K_{\mathrm{II}}/K_{\mathrm{I}}(x_3)$. The results show that the analytic formulae are valid even for $k_{\mathrm{III}}/k_{\mathrm{I}}$ and $k_{\mathrm{II}}/k_{\mathrm{I}}$ of order unity.

Equations 11 and 12 give φ_m in function of the given specimen geometry a,d, material ν and the loading $k_{\mathrm{III}}/k_{\mathrm{I}}$ and of the length δ_c of the facets. Hence, to apply these criterions, we have to determine theoretically the length of the facets in function of the geometry and the loading of the specimen. Yet, the length of the facets δ_c is linked to the orientation ψ of the facets and to the rotation rate $\frac{\mathrm{d}\gamma}{\mathrm{d}\delta}$ of the macroscopic extension by

Eq. 5. In this expression, ψ may be estimated through Eq. 1. After use of Eq. 4, this yields:

$$\frac{\tan\varphi_m}{d}\delta_c = \frac{1}{4}\arctan\frac{2k_{\mathrm{III}}}{(1-2\nu)k_{\mathrm{I}}} \tag{13}$$

The couple of Eqs. 11, 13 or 12, 13 forms two equations with two unknown factors φ_m and δ_c that can be solved numerically to obtain δ_c and φ_m as a function of $a, d, \nu, k_{\mathrm{III}}/k_{\mathrm{I}}$.

4 Comparison with the experiments

4.1 Determination of the SIF

The Stress Intensity Factors are computed using the program ADAPCRACK3D developed at the Institute of Applied Mechanics at University of Paderborn (Fulland et al. 2000; Schollmann et al. 2003). It is a Finite-Element based tool for simulation of crack propagation processes in three-dimensional structures. The program delegates the determination of the mechanical fields to the commercial FE-Solver ABAQUS. Using these fields, the SIFs for all three fracture modes are then determined by the module NETCRACK3D by the use of the MVCCI-method (Rybicki and Kanninen 1977; Buchholz 1984). They are given in Fig. 6 for one half of the front (the other part can be deduced from the fact that due to symmetry considerations, $K_{\mathrm{II}}/K_{\mathrm{I}}$ is an odd function of x_3 and $K_{\mathrm{III}}/K_{\mathrm{I}}$ is an even one). Results for the points located at points $x_3 = \pm d$ shall be disregarded since the classical SIFs cannot be defined at these free surface points (Bazant and Estenssoro 1979) due to the corner singularity, which differs from $-1/2$. One observes that K_{III} predominates over K_{II}, that $K_{\mathrm{III}}/K_{\mathrm{I}}$ is nearly uniform and increases while γ decreases (more inclined notch).

4.2 Comparison between MTS, 3DMTS, MVK and MVG

By measuring the "kink" angle α at the free surfaces $z = \pm t/2$, using Eq. 3 the kink angle φ_m for $x_3 = \pm d$ is obtained and using Eq. 2 their values for the interior points of the front. Figs. 7 and 8 compare the experimental kink angle along the front with the ones obtained by, on the one hand, MTS and 3DMTS criteria and on the other hand, MVK and MVG criteria (again only the values for one half of the front is plotted thanks

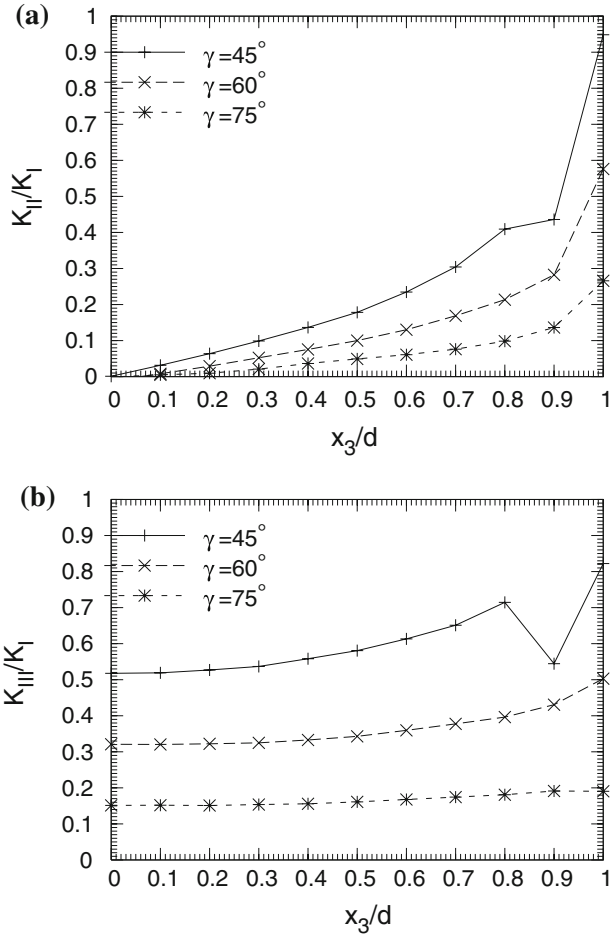

Fig. 6 Stress Intensity Factors for the initial slit. **a** K_{II}/K_I; **b** K_{III}/K_I

to symmetry and external points shall be disregarded since SIF are not defined at these points).

The following observations become apparent:

1. Despite the two concepts rely on totally different aspects of the loading situation of the crack front both predictions of the kinking angle are quite satisfactory.
2. For the MTS and 3DMTS criteria, an excellent agreement is found near the free surfaces. But the kink angles are notably underestimated in the middle of the front. This is not surprising, since the small initial facets, which could be observed in the experiments, suggest that the twisting linked to mode III, is of relevance in those cases. Due to its omission, the twisting of the whole crack front is underestimated.
3. For the MVK and MVG criteria an excellent agreement with the experiments can be found. The relative errors are less than 5% for $\gamma = 75°, 60°$ which

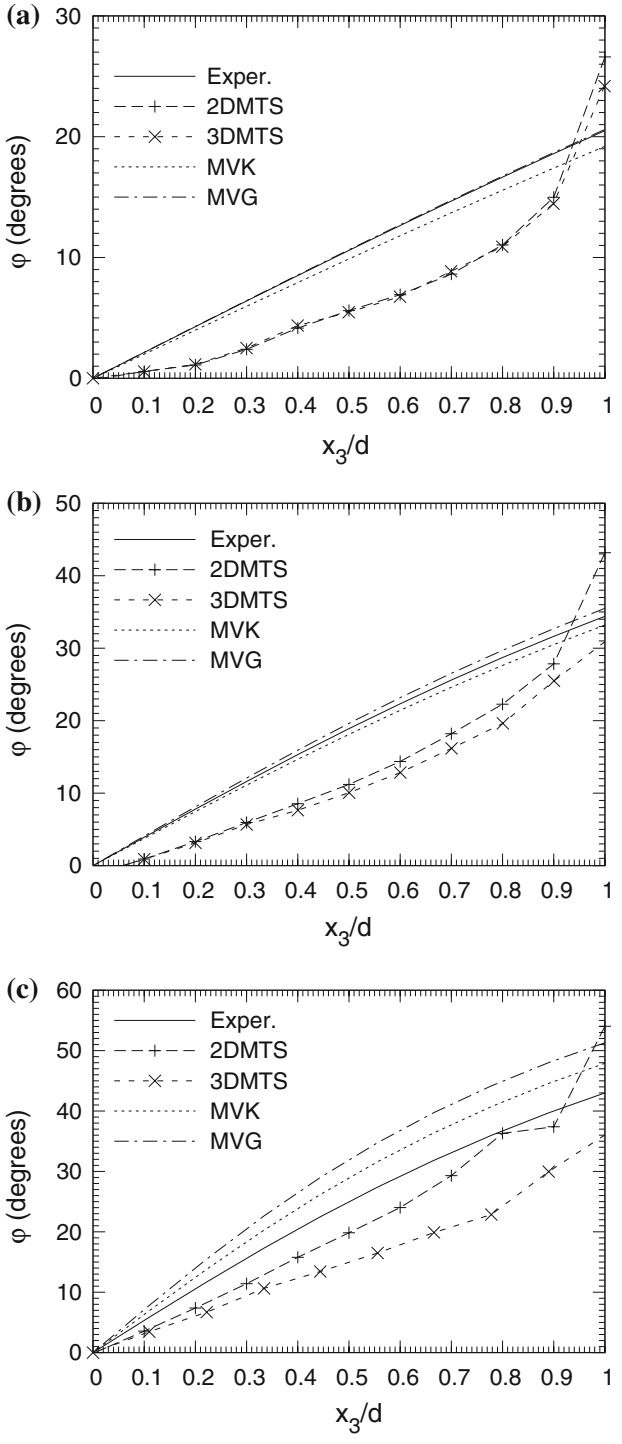

Fig. 7 Comparison of MTS, 3DMTS and MVK, MVG. **a** $\gamma = 75°$; **b** $\gamma = 60°$; **c** $\gamma = 45°$

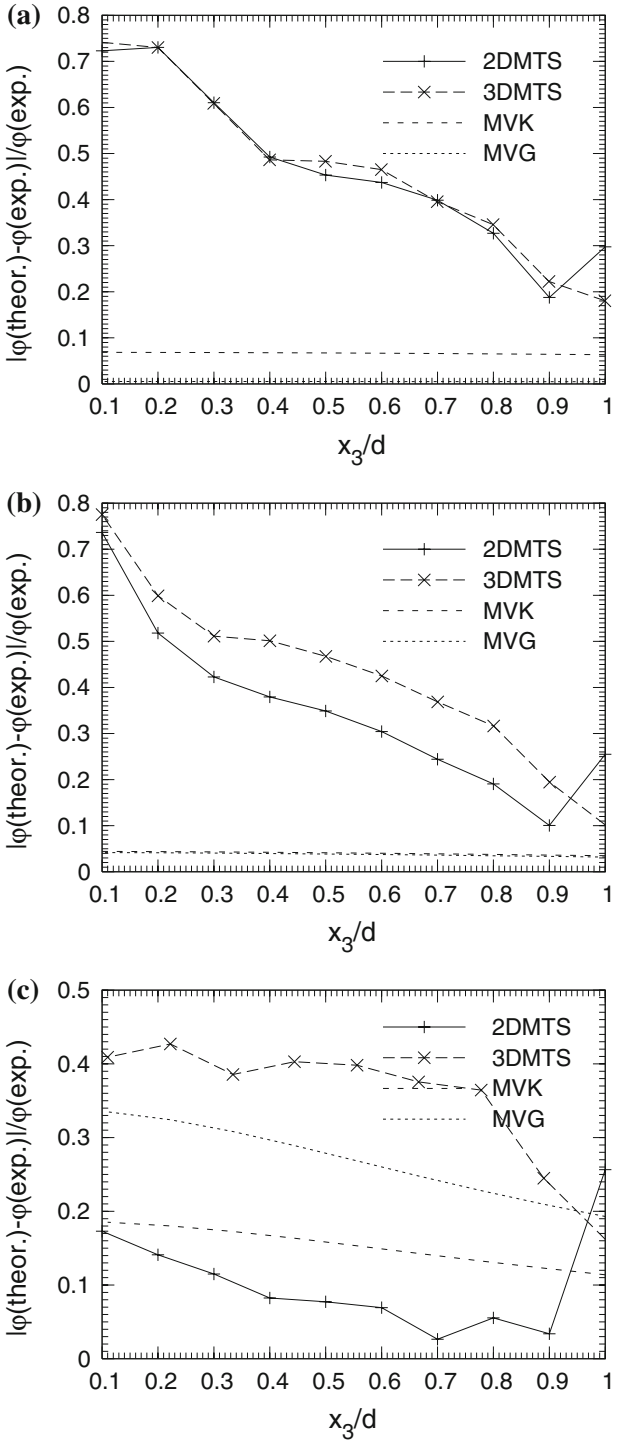

Fig. 8 Relative error. **a** $\gamma = 75°$; **b** $\gamma = 60°$; **c** $\gamma = 45°$

may be explicated by the uncertainties of measure that can be estimated to be $\sim$ 10%. For $\gamma = 45°$, the error is about 20%. The error increase may be due to the lack of taking K_{II} into account and to the use of a first order expression of φ_m with respect to K_{III}/K_I which is less valid for smaller values of γ.

4. For $\gamma = 75°$, 60° MTS and 3DMTS give very similar results, but for $\gamma = 45°$, MTS seems to be more accurate. It seems that the kink angle is better predicted by maximize the opening stress on facets containing the crack front (MTS) than on any facets in front of the tip (3DMTS). Hence even in presence

of mode III, MTS or equivalently PSL shall be used rather than 3DMTS.

5. Criteria MVK and MVG yield very similar values, hence are difficult to discriminate by the experiments. Nevertheless, a more precise estimation of the errors gives a slight advantage to MVK. It was still the case in Lazarus et al. (2001b) for similar experiments made on steel.

4.3 Propagation path by ADAPCRACK3D

Even if global type criteria give better prediction for the initial kink angle, application of the local type ones iteratively during propagation gives a crack surface very similar to the experiments (see Fig. 9 compared to 3a). This demonstrates the ability of ADAPCRACK3D to perform simulations of 3D crack propagation paths, even if the initial kink angle is slightly underestimated. The mesh and the deformation of the specimen during computation is depicted in Fig. 10.

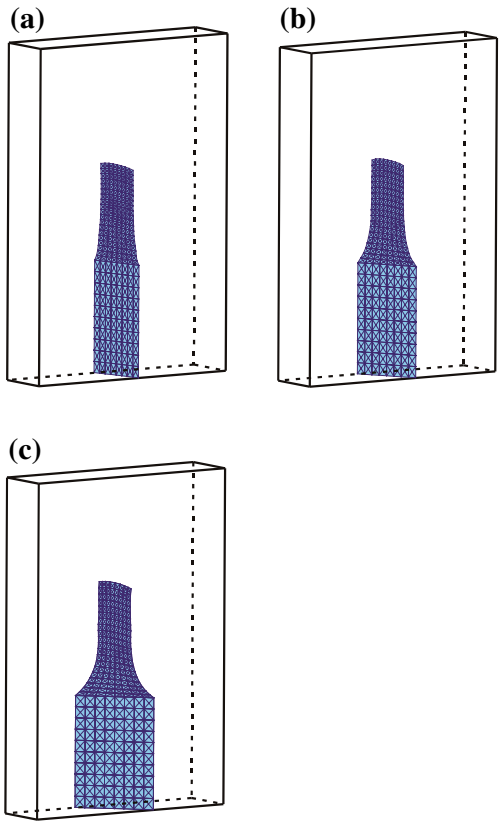

Fig. 9 Computed crack paths. **a** $\gamma = 75°$; **b** $\gamma = 60°$; **c** $\gamma = 45°$

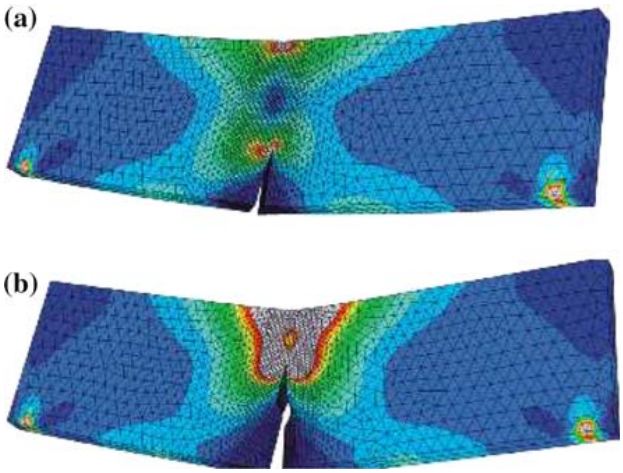

Fig. 10 Deformed FE-model of the 3PB-specimens ($\gamma = 45°$, displacement magnification factor DMF = 50). **a** With initial crack; **b** After 20 steps of simulated incremental fatigue crack growth

5 Conclusion

By comparison of the criteria with the experiments, one can notice that:

- The presence of both mode II and mode III along the crack front implies that both investigated criteria give good results concerning the development of the crack front in 3PB specimen under notable mode III influence.
- The global type criteria by Lazarus and Leblond, which was especially designed for those crack cases, predict the macroscopic deflection of the crack front by supposing that the whole front twists around the direction of propagation to annihilate mode III. Its results match the experimentally obtained crack development with excellent accuracy. But the criterion, specially designed for these experiments, seems difficult to be extended to any other configuration.
- The local type MTS criteria predict crack growth by definition of a local kinking angle that annihilate mode II. They differ more from the experimental findings than the predictions of the criterion by Lazarus and Leblond, since they disregard the local twisting ψ due to mode III. But they are of greater universality, as it is applicable to arbitrary 3D-crack problems.
- Moreover from a global point of view the smaller rotation rate resulting from the underestimation of the crack front twisting due to the disregard of the twisting angle does not notably change the overall

shape of the final crack surface. Hence MTS criterion seems sufficient for any practical engineering purposes.

It can finally be concluded, that obviously the crack front rotation, which is observed under notable mode III influence in 3PB specimens, can be described by both local and global type criteria. Hence, it is not possible to definitely conclude whether the twisting observed in 3PB or 4PB is a mode II or a mode III effect. But since the global type criterion gives better results, one shall conclude that it is rather a mode III one.

Now, a more extensive experimental study of crack propagation paths in presence of mode III shall be done. The conditions of transition between these several crack patterns (abrupt or progressive, one-piece or piecewise twisting, see Fig. 1) shall be lightened. The size effects, loading conditions on the spacing and rotation angle of the factory-roof patterns shall be studied. Extensive comparison of the twisting angle ψ of 3DMTS criterion or the empiric formula (1) with the twisting of the facets are envisaged in a near future.

References

Amestoy M, Leblond JB (1992) Crack paths in plane situations—II. Detailed form of the expansion of the stress intensity factors. Int J Solids Struct 29:465–501

Aydin A, Pollard DD (1988) Progress in understanding jointing over the past century. Geol Soc Am Bull 100:1181–1204

Bazant Z, Estenssoro L (1979) Surface singularity and crack propagation. Int J Solids Struct 15(5):405–426

Buchholz FG (1984) Improved formulae for the finite element calculation of the strain energy release rate by the modified crack closure integral method. In: Robinson J (ed) Accuracy, reliability and training in FEM technology. Robinson and Associates, Dorset pp 650–659

Buchholz FG, Wang H, Lin J, Richard HA (1998) 3d fracture analyses and experimental results on three-point bend specimens with slant cracks. In: Atluri SN, O'Donoghue PE (eds) Modeling and simulation based engineering. Proceedings of the international conference of engineering science (ICES 98), vol II, Tech Science Press: Palmdale, Atlanta, Georgia, USA, pp 1238–1243

Buchholz FG, Chergui A, Richard HA (2004) Fracture analyses and experimental results of crack growth under general mixed mode loading conditions. Eng Fract Mech 71(4–6): 455–468

Buchholz FG, Wiebesiek J, Fulland M, Richard H (2005) Comparison of computational 3d crack path simulations with experimental findings for 3pb-specimens with inclined crack planes. In: Aliabadi MH, Buchholz FG, Alfaite J (eds) Advances in fracture and damage mechanics IV. Proceedings of the 4th international conference on fracture and damage mechanics (FDM05), EC Ltd: UK, Mallorca, Spain, pp 143–148

Cooke ML, Pollard DD (1996) Fracture propagation paths under mixed mode loading within rectangular blocks of polymethyl methacrylate. J Geophys Res 101(B2):3387–3400

Erdogan G, Sih GC (1963) On the crack extension in plates under plane loading and transverse shear. ASME J Basic Eng 85:519–527

Fulland M, Schöllmann M, Richard HA (2000) Adapcrack3d-development of the program for the simulation of three-dimensional crack propagation processes. In: Atluri SN, Brust FW (eds) Advances in computational engineering & sciences. Tech Science Press, Palmdale, USA pp 948–953

Goldstein RV, Salganik RL (1974) Brittle fracture of solids with arbitrary cracks. Int J Fract 10:507–523

Gravouil A, Moes N, Belytschko T (2002) Non-planar 3d crack growth by the extended finite element and level sets. II. Level set update. Int J Numer Methods Eng 53(11):2569–2586

Hourlier F, Pineau A (1979) Fissuration par fatigue sous sollicitations polymodales (mode I ondulé + mode III permanent) d'un acier pour rotors 26 NCDV 14. Mémoires Scientifiques de la Revue de Métallurgie pp 175–185

Hull D (1993) Tilting cracks: the evolution of fracture surface topology in brittle solids. Int J Fract 62(2):119–138

Lazarus V, Leblond JB (1998) Crack paths under mixed mode (I+III) or (I+II+III) loadings. Comptes Rendus de l'Académie des Sciences, Série II (Mécanique, Physique, Astronomie) 326(3):171–177

Lazarus V, Leblond JB, Mouchrif SE (2001a) Crack front rotation and segmentation in mixed mode I+III or I+II+III—part I: calculation of stress intensity factor. J Mech Phys Solids 49(7):1399–1420

Lazarus V, Leblond JB, Mouchrif SE (2001b) Crack front rotation and segmentation in mixed mode I+III or I+II+III—part II: comparison with experiments. J Mech Phys Solids 49(7):1421–1443

Leblond JB (1989) Crack paths in plane situations—I. General form of the expansion of the stress intensity factors. Int J Solids Struct 25:1311–1325

Makabe C, Anggit M, Sueyoshi T, Yafuso T (2006) The formation mechanism of the factory-roof pattern in a torsional fatigue specimen with circumferential notch. J Test Eval 34(5):423–429

Palaniswamy K, Knauss WG (1975) Crack extension in brittle solids. Mechanics Today, Pergamon Press 4:87

Pollard DD, Segall P, Delaney PT (1982) Formation and interpretation of dilatant echelon cracks. Geol Soc Am Bull 93:1291–1303

Pook L (1995) On fatigue crack paths. Int J Fatigue 17(1):5–13

Qian J, Fatemi A (1996) Mixed mode fatigue crack growth: a literature survey. Eng Fract Mech 55(6):969

Rybicki EF, Kanninen MF (1977) A finite element calculation of stress intensity factors by a modified crack closure integral. Eng Fract Mech 9:931–938

Schollmann M, Richard H, Kullmer G, Fulland M (2002) A new criterion for the prediction of crack development in multiaxially loaded structures. Int J Fract 117(2):129–141

Schollmann M, Fulland M, Richard HA (2003) Development of a new software for adaptive crack growth simulations in 3d structures. Eng Fract Mech 70(2):249–268

Sommer E (1969) Formation of fracture 'lances' in glass. Eng Fract Mech 1:539–546

Yates JR, Mohammed RA (1996) Crack propagation under mixed mode (I + III) loading. Fatigue Fract Eng Mater Struct 19(10):1285–1290

PERGAMON

International Journal of Solids and Structures 39 (2002) 4421–4436

INTERNATIONAL JOURNAL OF SOLIDS and STRUCTURES

www.elsevier.com/locate/ijsolstr

In-plane perturbation of the tunnel-crack under shear loading I: bifurcation and stability of the straight configuration of the front

Véronique Lazarus *, Jean-Baptiste Leblond

Laboratoire de Modélisation en Mécanique, Université Pierre et Marie Curie, 8 Rue du Capitaine Scott, 75015 Paris, France

Received 31 October 2001; received in revised form 4 April 2002

Abstract

One considers a planar tunnel-crack embedded in an infinite isotropic brittle solid and loaded in mode 2 + 3 through some uniform shear remote loading. The crack front is slightly perturbed within the crack plane, from its rectilinear configuration. Part I of this work investigates the two following questions: Is there a wavy "bifurcated" configuration of the front for which the energy release rate is uniform along it? Will any given perturbation decay or grow during propagation? To address these problems, the distribution of the stress intensity factors (SIF) and the energy release rate along the perturbed front is derived using Bueckner–Rice's weight function theory. A "critical" sinusoidal bifurcated configuration of the front is found; both its wavelength and the "phase difference" between the fore and rear parts of the front depend upon the ratio of the initial (prior to perturbation of the front) mode 2 and 3 SIF. Also, it is shown that the straight configuration of the front is stable versus perturbations with wavelength smaller than the critical one but unstable versus perturbations with wavelength larger than it. This conclusion is similar to those derived by Gao and Rice and the authors for analogous problems.

Keywords: Tunnel-crack; Shear loading; Mode 2; Mode 3; Crack front; In-plane perturbation; Bifurcation; Stability; Bueckner–Rice theory; Weight functions

1. Introduction

Consider a plane crack with arbitrary contour $\mathscr{F}$, embedded in an arbitrary isotropic elastic body Ω. Let M denote the generic point of $\mathscr{F}$. If the crack advances, under constant loading, by a small distance $\delta a(M)$ within the plane in the direction perpendicular to the front $\mathscr{F}$, the variations $\delta K_m(M)$, $m = 1, 2, 3$ of the stress intensity factors (SIF) at point M are given, to first order in the perturbation, by the following formulae:

* Corresponding author.
E-mail addresses: vlazarus@ccr.jussieu.fr (V. Lazarus), leblond@lmm.jussieu.fr (J.-B. Leblond).

0020-7683/02/$ - see front matter © 2002 Elsevier Science Ltd. All rights reserved.
PII: S0020-7683(02)00349-9

$$\delta K_m(M) = [\delta K_m(M)]_{\delta a(M')\equiv\delta a(M)} + N_{mn}K_n(M)\frac{\mathrm{d}\delta a(M)}{\mathrm{d}s} + \mathrm{PV}\int_{\mathscr{F}} Z_{mn}(\Omega;M,M')K_n(M')[\delta a(M') - \delta a(M)]\,\mathrm{d}s', \tag{1}$$

where s, s' denote the curvilinear abscissae along the front of points M and M' respectively, and Einstein's implicit summation convention is employed for the index $n = 1,2,3$. In these equations, the $K_n(M)$ are the initial SIF (prior to perturbation of the crack front). The $[\delta K_m(M)]_{\delta a(M')\equiv\delta a(M)}$ are the values of the $\delta K_m(M)$ for a uniform advance equal to $\delta a(M)$ ($\delta a(M') \equiv \delta a(M), \forall M' \in \mathscr{F}$). The N_{mn} are the components of a *universal* (geometry-independent) operator. They are given by (other components being zero):

$$N_{23} = -\frac{2}{2-\nu}, \quad N_{32} = \frac{2(1-\nu)}{2-\nu}, \tag{2}$$

where ν denotes Poisson's ratio. The $Z_{mn}(\Omega;M,M')$ are the components of a *non-universal* (geometry dependent, whence the argument "Ω") operator $\mathbf{Z}$ called the *fundamental kernel* in the sequel, since it appears as the kernel of the principal value (PV) integral. Some general properties of these functions are as follows:

$$\begin{aligned} &Z_{mn}(\Omega;M,M') = Z_{nm}(\Omega;M',M),\ (m,n) = (1,1);(2,2);(3,3);(1,2),\\ &Z_{3n}(\Omega;M,M') = (1-\nu)Z_{n3}(\Omega;M',M),\ n = 1;2, \end{aligned} \tag{3}$$

$$\begin{aligned} &\lim_{M'\to M} Z_{11}(\Omega;M,M')D^2(M,M') = \frac{1}{2\pi},\\ &\lim_{M'\to M} Z_{22}(\Omega;M,M')D^2(M,M') = \frac{2-3\nu}{2\pi(2-\nu)},\\ &\lim_{M'\to M} Z_{33}(\Omega;M,M')D^2(M,M') = \frac{2+\nu}{2\pi(2-\nu)},\\ &\lim_{M'\to M} Z_{mn}(\Omega;M,M')D^2(M,M') = 0, \quad m \neq n, \end{aligned} \tag{4}$$

where $D(M,M')$ denotes the Cartesian distance between the points M and M'. Note that Eq. (4) warrant that the integral in Eq. (1) makes sense as a Cauchy principal value.

Eq. (1) was first established by Gao and Rice for various particular cases: the half-plane crack in mode 1 (Rice, 1985) and $1+2+3$ (Gao and Rice, 1986), the circular connection in mode 1 (Gao and Rice, 1987a), the penny-shaped crack in mode 1 (Gao and Rice, 1987b) and $1+2+3$ (Gao, 1988). In all these papers, the fundamental kernel did not appear in the generic name $\mathbf{Z}$ but in an explicit form depending on the configuration studied. Eq. (1) was then extended by Rice (1989) and Nazarov (1989) to arbitrary planar crack shapes in mode 1, and finally by Mouchrif (1994) and Leblond et al. (1999) to cracks of completely arbitrary, non-planar shapes including possible kink angles and arbitrary combinations of modes. In these more general cases, since the fundamental kernel depends on the geometry which was supposed to be more or less arbitrary, it appeared under a generic form; $\mathbf{Z}$ is the notation used in Leblond et al. (1999). The values of the N_{mn} given by (2) can be deduced from the works of Rice (1985), Gao and Rice (1986, 1987a,b) and Gao (1988). Finally, properties (3) and (4) were proved for arbitrary plane cracks loaded in pure mode 1 by both Rice (1989) and Nazarov (1989), and for arbitrary curved crack geometries and mixed mode conditions by Mouchrif (1994) and Leblond et al. (1999). All these works heavily relied on the use of Bueckner–Rice's weight-function theory (Bueckner, 1970; Rice, 1972; Rice, 1985).

In all the above-mentioned special cases, the problems of configurational bifurcation and stability of the crack front during in-plane propagation, under uniform remote loading, could be addressed by using the explicit expression of $\mathbf{Z}$ in Eq. (1) to calculate the energy release rate along a slightly perturbed front. The *bifurcation problem* was the following one: is there, in addition to the trivial, initial (straight or circular) configuration of the crack front, some non-trivial, wavy configuration for which the energy release rate is still uniform? The *stability problem* was as follows: if the crack front is slightly perturbed within the crack

plane, will the perturbation decay or increase as propagation proceeds? This issue could be addressed by considering that the perturbation decayed if the energy release rate was lowest at the most advanced parts of the crack front, and that it grew if the opposite held true.

For half-plane cracks and internal circular cracks under mixed mode loadings, and for circular connections under mode 1 loading, Rice (1985), Gao and Rice (1986, 1987a,b) and Gao (1988) have shown that there is a sinusoidal bifurcated configuration of "critical" wavelength λ_c, and that stability prevails for perturbations of wavelength smaller than λ_c and instability for wavelengths larger than it. An analogous result has been established for interface half-plane cracks by Lazarus and Leblond (1998). However, for half-plane cracks, as pointed out by Gao and Rice (1986) because of the lack of a characteristic lengthscale in the problem, the somewhat deceiving conclusion is only that "planar crack growth should be configurationally stable to perturbations involving wavelengths that are small compared to overall body or crack dimensions". Leblond et al. (1996) have introduced a characteristic lengthscale by studying the *tunnel-crack* under mode 1 loading. They have shown that the critical wavelength λ_c is a characteristic multiple of the crack width and that the critical bifurcated configuration is symmetric with respect to the middle axis of the crack.

The aim of Part I of this work is to consider the same bifurcation and stability problems for the tunnel-crack as Leblond et al. (1996), but for mixed mode $(2 + 3)$ shear loadings. Propagation is assumed to be coplanar; this is reasonable provided that the crack is channeled along a planar surface of low fracture resistance, which can be the case for instance for a geological fault. Also, propagation is considered to be governed by the local energy release rate, the critical value of which is assumed to be independent of mode combination. Again, this is reasonable (Rice, private communication) for coplanar propagation along a weak surface, since energy dissipation occurs through the same physical mechanisms (shear and friction) in both modes 2 and 3.

Bifurcation and stability issues of course depend on the geometry considered. Therefore some general properties of the operator $\mathbf{Z}$ for a tunnel-crack, are needed as a prerequisite. These properties are expounded in Section 2. They allow us to derive, in Section 3, an expression of the variation of the energy release rate due to a small wavy perturbation of the crack front that forms the basis of our discussion of bifurcation and stability problems. In Section 4, it is then shown that there is a critical, sinusoidal bifurcated configuration of the front. Its wavelength is a multiple of the width of the crack and depends upon the ratio of the mode 2 and 3 initial SIF (prior to perturbation of the front). Also, the bifurcated configuration is symmetric with respect to the middle axis of the crack only for initial conditions of pure mode 2 or 3; for mixed mode conditions, there is a "phase difference" between the bifurcated configurations of the fore and rear parts of the crack front. The stability issue is addressed, in Section 5, only in some simple, special cases where the extrema of the perturbation and the energy release rate coincide. It is shown that in the most interesting case, stability prevails for perturbations of wavelength smaller than the critical one.

It should be noticed that a significant part of the analysis of bifurcation and stability can be carried out using only the properties of the fundamental kernel $\mathbf{Z}$ expounded in Section 2, that is without explicitly knowing its components. However, such an explicit knowledge is of course necessary for a fully quantitative analysis. But the calculation of $\mathbf{Z}$ is long and complex; for reasons of compactness of the present paper, we shall therefore merely accept its results here and postpone its detailed presentation to Part II.

2. General properties of the fundamental kernel Z

2.1. Definitions and notations

The situation considered is depicted in Fig. 1. The crack lies on the plane $y = 0$ and the fore and rear parts of the front are parallel straight lines of equation $(x = a)$ and $(x = -a)$ respectively. The position of a point M of the front is specified through the Cartesian coordinate $z^{\pm}$, where the upper index indicates

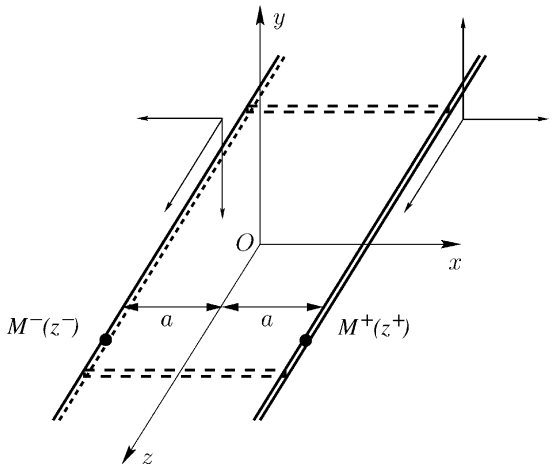

Fig. 1. Tunnel-crack of width $2a$.

whether the point considered belongs to the fore ($x = a$) or rear part ($x = -a$) of the front. The SIF at a point M of the front are defined with respect to the local set of axes (x, y, z) if M belongs to the line ($x = a$) and $(-x, -y, z)$ if it belongs to the line ($x = -a$).

The only geometric parameter in the problem is the half-width a of the crack; it follows that the influence of the argument "Ω" upon the fundamental kernel $\mathbf{Z}(\Omega; M, M')$ in fact reduces to a dependence of this operator upon a. Furthermore, the problem is invariant in the direction z of the crack front and simple dimensional considerations in Eq. (1) show that $\mathbf{Z}(\Omega; M, M') \equiv \mathbf{Z}(a; z^{\pm}, z'^{\pm})$ is positively homogeneous of degree -2 with respect to its three arguments. Combining these features with the obvious symmetry with respect to the central axis Oz, one concludes that the fundamental kernel can be written in the following form:

$$\mathbf{Z}(a; z^{+}, z'^{+}) = \mathbf{Z}(a; z^{-}, z'^{-}) \equiv \frac{\mathbf{f}((z' - z)/a)}{(z' - z)^2}, \tag{5}$$

$$\mathbf{Z}(a; z^{+}, z'^{-}) = \mathbf{Z}(a; z^{-}, z'^{+}) \equiv \frac{\mathbf{g}((z' - z)/a)}{a^2}, \tag{6}$$

where, in virtue of Eq. (4), the components of operators $\mathbf{f}$ and $\mathbf{g}$ are bounded for $z' \to z$ and verify the following properties:

$$\begin{aligned}
&\lim_{z' \to z} f_{11}((z' - z)/a) = \frac{1}{2\pi}, \\
&\lim_{z' \to z} f_{22}((z' - z)/a) = \frac{2 - 3\nu}{2\pi(2 - \nu)}, \\
&\lim_{z' \to z} f_{33}((z' - z)/a) = \frac{2 + \nu}{2\pi(2 - \nu)}, \\
&\lim_{z' \to z} f_{mn}((z' - z)/a) = 0, \quad m \neq n.
\end{aligned} \tag{7}$$

Another basic property of $\mathbf{f}$ and $\mathbf{g}$ is that:

$$f_{12} = f_{21} = f_{13} = f_{31} = g_{12} = g_{21} = g_{13} = g_{31} \equiv 0. \tag{8}$$

This is because, as is well-known, tensile and shear problems are uncoupled for a planar crack with an arbitrary contour in an infinite body; that is, if $K_2 \equiv 0$ and $K_3 \equiv 0$ (tensile problem), the variations δK_2 and δK_3 are zero when the crack propagates within its plane; and similarly if $K_1 \equiv 0$ (shear problem), $\delta K_1 \equiv 0$.

Furthermore, elementary considerations of symmetry with respect to the plane $z = 0$ show that f_{11}, f_{22}, f_{33}, g_{11}, g_{22}, g_{33} are even, and f_{23}, g_{23}, f_{32} and g_{32} are odd functions. Eqs. (3), (5) and (6) then imply that (with $u \equiv (z' - z)/a$):

$$\begin{aligned} f_{32}(u) &= (1-\nu) f_{23}(-u) = -(1-\nu) f_{23}(u), \\ g_{32}(u) &= (1-\nu) g_{23}(-u) = -(1-\nu) g_{23}(u). \end{aligned} \tag{9}$$

Therefore, the fundamental kernel $\mathbf{Z}$ is entirely determined by the eight components 11, 22, 33, 23 of the operators $\mathbf{f}$ and $\mathbf{g}$.

2.2. Expressions of the δK_m, $m = 2,3$ in terms of $\boldsymbol{f}$ and $\boldsymbol{g}$

As already mentioned, for the tunnel-crack under shear loading, $\delta K_1 \equiv 0$. Furthermore, for $m = 2$, 3, with the notations (5) and (6) and because of properties (8) and (9), the fundamental Eq. (1) reads for a point $M^+(z^+)$ belonging to the line $(x = a)$:

$$\begin{aligned} \delta K_2(z^+) = {} & [\delta K_2(z^+)]_{\delta a(z'^{\pm}) \equiv \delta a(z^+)} - \frac{2}{2-\nu} K_3(z^+) \frac{\mathrm{d}\delta a}{\mathrm{d}z}(z^+) \\ & + \mathrm{PV} \int_{-\infty}^{+\infty} \left[f_{22}\left(\frac{z'-z}{a}\right) K_2(z'^+) + f_{23}\left(\frac{z'-z}{a}\right) K_3(z'^+) \right] \frac{\delta a(z'^+) - \delta a(z^+)}{(z'-z)^2} \, \mathrm{d}z' \\ & + \int_{-\infty}^{+\infty} \left[g_{22}\left(\frac{z'-z}{a}\right) K_2(z'^-) + g_{23}\left(\frac{z'-z}{a}\right) K_3(z'^-) \right] \frac{\delta a(z'^-) - \delta a(z^+)}{a^2} \, \mathrm{d}z', \end{aligned} \tag{10}$$

$$\begin{aligned} \delta K_3(z^+) = {} & [\delta K_3(z^+)]_{\delta a(z'^{\pm}) \equiv \delta a(z^+)} + \frac{2(1-\nu)}{2-\nu} K_2(z^+) \frac{\mathrm{d}\delta a}{\mathrm{d}z}(z^+) \\ & + \mathrm{PV} \int_{-\infty}^{+\infty} \left[f_{33}\left(\frac{z'-z}{a}\right) K_3(z'^+) - (1-\nu) f_{23}\left(\frac{z'-z}{a}\right) K_2(z'^+) \right] \frac{\delta a(z'^+) - \delta a(z^+)}{(z'-z)^2} \, \mathrm{d}z' \\ & + \int_{-\infty}^{+\infty} \left[g_{33}\left(\frac{z'-z}{a}\right) K_3(z'^-) - (1-\nu) g_{23}\left(\frac{z'-z}{a}\right) K_2(z'^-) \right] \frac{\delta a(z'^-) - \delta a(z^+)}{a^2} \, \mathrm{d}z'. \end{aligned} \tag{11}$$

The values of $\delta K_2(z^-)$ and $\delta K_3(z^-)$, for a point $M^-(z^-)$ belonging to the line $(x = -a)$, are given by the same expressions with the obvious substitutions $z^+ \to z^-$, $z'^{\pm} \to z'^{\mp}$.

3. Perturbation of the tunnel-crack under uniform remote shear loading

Let the tunnel-crack be subjected to some uniform remote plane (τ_p) and antiplane (τ_a) shear loading so that Cauchy stress tensor at infinity reads $\boldsymbol{\sigma}_\infty = \tau_\mathrm{p}(\vec{e_y} \otimes \vec{e_x} + \vec{e_x} \otimes \vec{e_y}) + \tau_\mathrm{a}(\vec{e_y} \otimes \vec{e_z} + \vec{e_z} \otimes \vec{e_y})$. Then the SIF, prior to any perturbation of the front, are given by:

$$K_1(z^\pm) = 0; \quad K_2(z^\pm) = \tau_\mathrm{p}\sqrt{\pi a} \equiv K_2; \quad K_3(z^+) = \tau_\mathrm{a}\sqrt{\pi a} \equiv K_3^+; \quad K_3(z^-) = -\tau_\mathrm{a}\sqrt{\pi a} = -K_3^+ \equiv K_3^-. \tag{12}$$

The variation of the SIF will be studied for three types of perturbation of the front: translation, rotation and sinusoidal undulation (Fig. 2). The study of the translation will serve to simplify (in the case of a uniform remote loading), the expressions (10) and (11) of $\delta K_2(z^+)$ and $\delta K_3(z^+)$. The study of the rotation will allow the calculation of some integrals involving operators $\mathbf{f}$ and $\mathbf{g}$. These integrals are given here although they will be needed only in Part II, because the reasoning is similar to that for the translation. The study of the sinusoidal undulation is a necessary prerequisite for that of the bifurcation and stability problems.

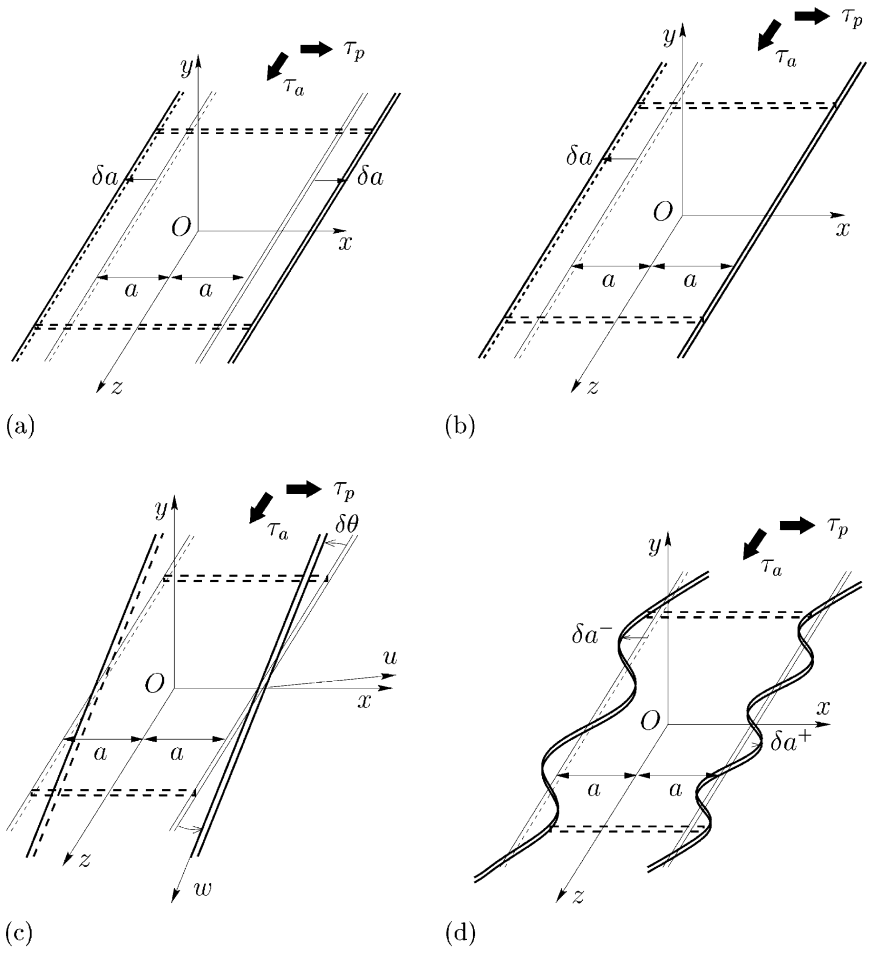

Fig. 2. In-plane perturbations of the tunnel-crack under uniform remote shear loading. (a) Translation of both parts of the front. (b) Translation of the rear part of the front. (c) Rotation about the Oy axis. (d) Wavy front.

3.1. Translation of the front

If both parts of the front move by a uniform amount δa as in Fig. 2(a), the new SIF are those of a tunnel-crack of width $2(a+\delta a)$ subjected to the remote loading $\boldsymbol{\sigma}_\infty$. Hence to first order in $\delta a/a$:

$$\begin{aligned}&[\delta K_2(z^\pm)]_{\delta a(z'^\pm)\equiv\delta a} = K_2\frac{\delta a}{2a},\\ &[\delta K_3(z^+)]_{\delta a(z'^\pm)\equiv\delta a} = K_3^+\frac{\delta a}{2a},\quad [\delta K_3(z^-)]_{\delta a(z'^\pm)\equiv\delta a} = K_3^-\frac{\delta a}{2a}.\end{aligned} \tag{13}$$

If now the sole rear part of the front moves by an amount δa as in Fig. 2(b), the new SIF are those of a tunnel-crack of width $2a+\delta a$ subjected to the remote loading $\boldsymbol{\sigma}_\infty$. Thus $\delta K_2(z^\pm) = (K_2\delta a)/(4a)$ and $\delta K_3(z^\pm) = (K_3^\pm\delta a)/(4a)$. Eqs. (10) and (11) then yield:

$$\int_{-\infty}^{+\infty} g_{22}(u)\,\mathrm{d}u = -\int_{-\infty}^{+\infty} g_{33}(u)\,\mathrm{d}u = \frac{1}{4},\quad \int_{-\infty}^{+\infty} g_{23}(u)\,\mathrm{d}u = 0. \tag{14}$$

The last relation was obvious a priori since g_{23} is odd.

By using Eqs. (13) and (14), the relations (10) and (11) can be rewritten in the following slightly simplified form (for a uniform remote loading):

$$\begin{aligned}\delta K_2(z^+) = {} & \frac{K_2}{4}\frac{\delta a(z^+)}{a} - \frac{2}{2-\nu}K_3^+\frac{\mathrm{d}\delta a}{\mathrm{d}z}(z^+) + K_2\mathrm{PV}\int_{-\infty}^{+\infty} f_{22}\left(\frac{z'-z}{a}\right)\frac{\delta a(z'^+)-\delta a(z^+)}{(z'-z)^2}\,\mathrm{d}z' \\ & + K_3^+\int_{-\infty}^{+\infty} f_{23}\left(\frac{z'-z}{a}\right)\frac{\delta a(z'^+)-\delta a(z^+)}{(z'-z)^2}\,\mathrm{d}z' + K_2\int_{-\infty}^{+\infty} g_{22}\left(\frac{z'-z}{a}\right)\frac{\delta a(z'^-)}{a^2}\,\mathrm{d}z' \\ & + K_3^-\int_{-\infty}^{+\infty} g_{23}\left(\frac{z'-z}{a}\right)\frac{\delta a(z'^-)}{a^2}\,\mathrm{d}z', \end{aligned} \tag{15}$$

$$\begin{aligned}\delta K_3(z^+) = {} & \frac{K_3^+}{4}\frac{\delta a(z^+)}{a} + \frac{2(1-\nu)}{2-\nu}K_2\frac{\mathrm{d}\delta a}{\mathrm{d}z}(z^+) + K_3^+\mathrm{PV}\int_{-\infty}^{+\infty} f_{33}\left(\frac{z'-z}{a}\right)\frac{\delta a(z'^+)-\delta a(z^+)}{(z'-z)^2}\,\mathrm{d}z' \\ & - (1-\nu)K_2\int_{-\infty}^{+\infty} f_{23}\left(\frac{z'-z}{a}\right)\frac{\delta a(z'^+)-\delta a(z^+)}{(z'-z)^2}\,\mathrm{d}z' + K_3^-\int_{-\infty}^{+\infty} g_{33}\left(\frac{z'-z}{a}\right)\frac{\delta a(z'^-)}{a^2}\,\mathrm{d}z' \\ & - (1-\nu)K_2\int_{-\infty}^{+\infty} g_{23}\left(\frac{z'-z}{a}\right)\frac{\delta a(z'^-)}{a^2}\,\mathrm{d}z', \end{aligned} \tag{16}$$

where the "PV" symbols have been canceled in the integrals involving f_{23} since this function is odd.

The expressions of $\delta K_2(z^-)$ and $\delta K_3(z^-)$ are similar with the substitutions $z^+ \to z^-$, $z'^\pm \to z'^\mp$, $K_3^\pm \to K_3^\mp$.

3.2. Rotation of the front

Let us suppose that the perturbation is a rotation of both parts of the front about $\overrightarrow{e_y}$ as in Fig. 2(c) so that $\delta a(z^+) = \delta\theta.z$ and $\delta a(z^-) = -\delta\theta.z$, $|\delta\theta| \ll 1$. Then to first order in $\delta\theta$, the new SIF are those of a tunnel-crack of width $2a$ subjected to the uniform remote loading $(\tau_\mathrm{p} - \delta\theta.\tau_\mathrm{a})(\overrightarrow{e_y}\otimes\overrightarrow{e_u} + \overrightarrow{e_u}\otimes\overrightarrow{e_y}) + (\tau_\mathrm{a} + \delta\theta.\tau_\mathrm{p})(\overrightarrow{e_y}\otimes\overrightarrow{e_w} + \overrightarrow{e_w}\otimes\overrightarrow{e_y})$ where $\overrightarrow{e_u}$ and $\overrightarrow{e_w}$ are defined in Fig. 2(c). Thus $\delta K_2(z^\pm) = -\delta\theta.K_3^+$ and $\delta K_3(z^\pm) = \pm\delta\theta.K_2$. Relations (15) and (16) then yield a system of two equations in the two unknown integrals $\int_{-\infty}^{+\infty} f_{23}(u)(\mathrm{d}u/u)$ and $\int_{-\infty}^{+\infty} u g_{23}(u)\,\mathrm{d}u$, the solution of which reads:

$$\int_{-\infty}^{+\infty} f_{23}(u)\frac{\mathrm{d}u}{u} = -\frac{\nu^2}{2(2-\nu)(1-\nu)}, \tag{17}$$

$$\int_{-\infty}^{+\infty} u g_{23}(u)\,\mathrm{d}u = \frac{\nu}{2(1-\nu)}. \tag{18}$$

3.3. Wavy perturbation of the crack front

Let us now suppose that, as in Fig. 2(d):

$$\begin{cases} \delta a(z^+) = \alpha^+\cos(k^+z + \phi^+) \\ \delta a(z^-) = \alpha^-\cos(k^-z + \phi^-) \\ \dfrac{|\alpha^+|}{a} \sim \dfrac{|\alpha^-|}{a} \ll 1. \end{cases} \tag{19}$$

Then, by substituting Eq. (19) in (15) and (16) and using the notation

$$p^{\pm} \equiv k^{\pm} a, \tag{20}$$

(p^+, p^- are "reduced", dimensionless wavevectors), one finds to first order in $(\alpha^{\pm}/a)$, after a lengthy but straightforward calculation:

$$\begin{aligned}\delta K_2(z^+) = {} & \frac{\alpha^+}{a}\cos(k^+ z + \phi^+) K_2 \bar{f}_{22}(p^+) + \frac{\alpha^+}{a}\sin(k^+ z + \phi^+) K_3^+ \mathrm{i}\bar{f}_{23}(p^+) + \frac{\alpha^-}{a}\cos(k^- z + \phi^-) K_2 \hat{g}_{22}(p^-) \\ & + \frac{\alpha^-}{a}\sin(k^- z + \phi^-) K_3^- \mathrm{i}\hat{g}_{23}(p^-),\end{aligned} \tag{21}$$

$$\begin{aligned}\delta K_3(z^+) = {} & \frac{\alpha^+}{a}\cos(k^+ z + \phi^+) K_3^+ \bar{f}_{33}(p^+) - (1-\nu)\frac{\alpha^+}{a}\sin(k^+ z + \phi^+) K_2 \mathrm{i}\bar{f}_{23}(p^+) \\ & + \frac{\alpha^-}{a}\cos(k^- z + \phi^-) K_3^- \hat{g}_{33}(p^-) - (1-\nu)\frac{\alpha^-}{a}\sin(k^- z + \phi^-) K_2 \mathrm{i}\hat{g}_{23}(p^-),\end{aligned} \tag{22}$$

the expressions of $\delta K_2(z^-)$ and $\delta K_3(z^-)$ being given by the same formulae with the obvious substitutions $\pm \leftrightarrow \mp$ for the superscripts of α, k, p, ϕ and K_3. In these expressions, the functions $\bar{f}_{mn}$ are defined as:

$$\begin{aligned}\bar{f}_{mn}(p) &= \frac{1}{4} + \mathrm{PV}\int_{-\infty}^{+\infty} f_{mn}(u)\frac{\mathrm{e}^{\mathrm{i}pu}-1}{u^2}\,\mathrm{d}u = \frac{1}{4} + 2\int_0^{+\infty} f_{mn}(u)\frac{\cos pu - 1}{u^2}\,\mathrm{d}u, \quad (m,n) = (2,2);(3,3), \\ \bar{f}_{23}(p) &= -\frac{2}{2-\nu}\mathrm{i}p + \mathrm{PV}\int_{-\infty}^{+\infty} f_{23}(u)\frac{\mathrm{e}^{\mathrm{i}pu}-1}{u^2}\,\mathrm{d}u = -\frac{2}{2-\nu}\mathrm{i}p + 2\mathrm{i}\int_0^{+\infty} f_{23}(u)\frac{\sin pu}{u^2}\,\mathrm{d}u,\end{aligned} \tag{23}$$

(where use has been made of the parity properties of the f_{mn}). Also, the functions $\hat{g}_{mn}$ are the Fourier transforms of the g_{mn} defined as:

$$\begin{aligned}&\hat{g}_{mn}(p) = \int_{-\infty}^{+\infty} g_{mn}(u)\mathrm{e}^{\mathrm{i}pu}\,\mathrm{d}u, \\ \Rightarrow &\begin{cases}\hat{g}_{mn}(p) = 2\displaystyle\int_0^{+\infty} g_{mn}(u)\cos pu\,\mathrm{d}u, \quad (m,n) = (2,2);(3,3) \\ \hat{g}_{23}(p) = 2\mathrm{i}\displaystyle\int_0^{+\infty} g_{23}(u)\sin pu\,\mathrm{d}u,\end{cases}\end{aligned} \tag{24}$$

(where use has been made of the parity properties of the g_{mn}).

Notice that $\bar{f}_{22}$, $\bar{f}_{33}$, $\hat{g}_{22}$, $\hat{g}_{33}$, $\mathrm{i}\bar{f}_{23}$, $\mathrm{i}\hat{g}_{23}$ are real so that the expressions (21) and (22) of $\delta K_2(z^+)$ and $\delta K_3(z^+)$ are real in spite of the presence of the imaginary number i.

4. Study of the bifurcation problem

Any sinusoidal perturbation of the crack front may be written, for a suitable choice of the origin, in the form (19) with $\phi^+ = 0$, $\phi^- = \phi \in [-\pi, \pi)$, and α^+, α^-, p^+, $p^- > 0$. The bifurcation problem consists in looking whether there are some constants $(\alpha^+, \alpha^-, p^+, p^-, \phi)$ for which the variation of energy release rate $\delta\mathscr{G}$ due to the perturbation (19) vanishes. (In fact, what is really to be investigated is $\delta\mathscr{G} - \delta\mathscr{G}_c$ where $\mathscr{G}_c$ denotes the critical value of $\mathscr{G}$; but this is equivalent to studying $\delta\mathscr{G}$ since $\mathscr{G}_c$ is assumed to be a constant, independent of mode combination). Such a set of variables $(\alpha^+, \alpha^-, p^+, p^-, \phi)$ will be called a *bifurcation mode*.

4.1. Expression of the variation of the energy release rate

Expanding Irwin's formula to first order in $(\alpha^{\pm}/a)$, one finds that the variation of the energy release rate due to the perturbation (19) is:

$$\delta\mathscr{G}(z^{\pm}) = 2\frac{1-\nu^2}{E}\left[K_2\delta K_2(z^{\pm}) + \frac{1}{1-\nu}K_3^{\pm}\delta K_3(z^{\pm})\right], \tag{25}$$

where E is Young's modulus and $\delta K_2(z^{\pm})$ and $\delta K_3(z^{\pm})$ are given by Eqs. (21) and (22). Hence, substituting 0 for ϕ^+ and ϕ for ϕ^- in these equations, one finds that

$$\begin{aligned}\delta\mathscr{G}(z^{+}) = 2\frac{1-\nu^2}{E}\frac{K_2^2}{a}\{&\alpha^{+}F(p^{+})\cos(k^{+}z) + \alpha^{-}[G(p^{-})\cos\phi + H(p^{-})\sin\phi]\cos(k^{-}z)\\ &+ \alpha^{-}[H(p^{-})\cos\phi - G(p^{-})\sin\phi]\sin(k^{-}z)\},\end{aligned} \tag{26}$$

$$\begin{aligned}\delta\mathscr{G}(z^{-}) = 2\frac{1-\nu^2}{E}\frac{K_2^2}{a}\{&\alpha^{-}F(p^{-})\cos(k^{-}z+\phi) + \alpha^{+}[G(p^{+})\cos\phi + H(p^{+})\sin\phi]\cos(k^{+}z+\phi)\\ &+ \alpha^{+}[-H(p^{+})\cos\phi + G(p^{+})\sin\phi]\sin(k^{+}z+\phi)\}.\end{aligned} \tag{27}$$

In these expressions $F(p) \equiv F(p, K_3^{+}/K_2)$, $G(p) \equiv G(p, K_3^{+}/K_2)$, $H(p) \equiv H(p, K_3^{+}/K_2)$ are the quantities given by:

$$\begin{aligned}F(p) &= \bar{f}_{22}(p) + \frac{1}{1-\nu}\frac{K_3^{+2}}{K_2^2}\bar{f}_{33}(p),\\ G(p) &= \hat{g}_{22}(p) - \frac{1}{1-\nu}\frac{K_3^{+2}}{K_2^2}\hat{g}_{33}(p),\\ H(p) &= -2\mathrm{i}\frac{K_3^{+}}{K_2}\hat{g}_{23}(p).\end{aligned} \tag{28}$$

It was noticed by Gao and Rice (1986), Gao (1988), Lazarus and Leblond (1998) that the extrema of the perturbation of the front and of the energy release rate coincide for a half-plane or a penny-shaped crack in an homogeneous body, and for an interface half-plane crack. One could therefore speculate that this was a "general property". However, since the terms proportional to $\sin(k^{-}z)$ and $\sin(k^{+}z+\phi)$ do not vanish in the expressions (26) and (27) of $\delta\mathscr{G}(z^{\pm})$, this property does not hold for the tunnel-crack.

4.2. Graphs of functions $\bar{f}_{22}$, $\bar{f}_{33}$, $\hat{g}_{22}$, $\hat{g}_{33}$, $\hat{g}_{23}$

Knowledge of the functions $\bar{f}_{22}, \bar{f}_{33}, \hat{g}_{22}, \hat{g}_{33}, \hat{g}_{23}$ now becomes necessary to pursue the discussion. For the sake of shortness of the present paper, the rather involved calculation of these functions is postponed to Part II and we shall only give here the results obtained, for the value $\nu = 0.3$ of Poisson's ratio, in the form of graphs. (see Figs. 3 [1] and 4.)

4.3. Case where $p^{+} \neq p^{-}$

If $p^{+} \neq p^{-}$, for $\delta\mathscr{G}(z^{\pm})$ to be zero for all z^{+} and z^{-}, the terms proportional to $\cos(k^{+}z)$, $\cos(k^{-}z)$, $\sin(k^{-}z)$ in the expression (26) of $\delta\mathscr{G}(z^{+})$, and those proportional to $\cos(k^{-}z+\phi)$, $\cos(k^{+}z+\phi)$, $\sin(k^{+}z+\phi)$ in the

[1] Since $\bar{f}_{23}$ does not appear in expressions (26) and (27) for $\delta\mathscr{G}(z^{\pm})$, this function is not given in Fig. 3.

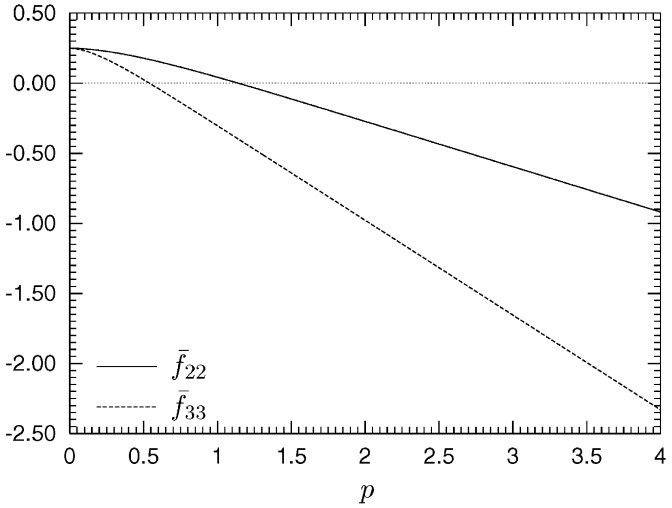

Fig. 3. Functions $\bar{f}_{mn}(p)$.

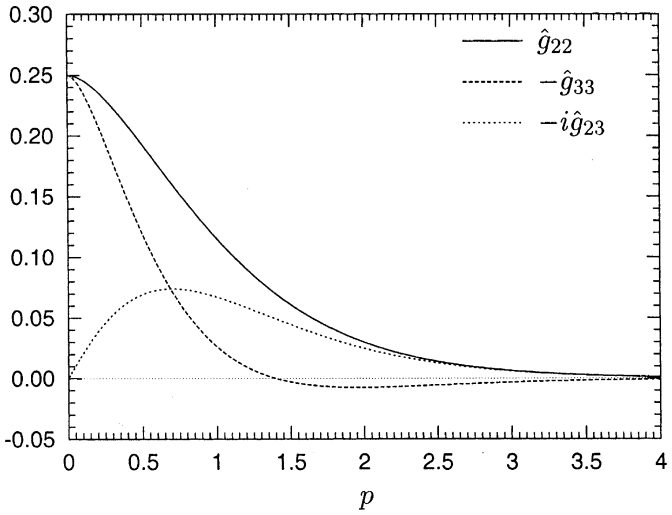

Fig. 4. Functions $\hat{g}_{mn}(p)$.

expression (27) of $\delta\mathscr{G}(z^-)$ must be individually zero. Since we are looking for non-trivial solutions, one of the coefficients α^+, α^-, say α^+, must be non-zero. The preceding conditions then implies:

$$F(p^+) = 0; \quad G(p^+)\cos\phi + H(p^+)\sin\phi = 0; \quad H(p^+)\cos\phi - G(p^+)\sin\phi = 0$$

and thus $F(p^+) = G(p^+) = H(p^+) = 0$. Now it is clear from definitions (28) and Figs. 3 and 4 that $F(p^+)$ only vanishes for some $p^+ \neq 0$ whereas $H(p^+)$ only vanishes for $p^+ = 0$. Thus these conditions cannot be satisfied for a single p^+. Hence:

There is no bifurcation mode with $p^+ \neq p^-$. (29)

4.4. Case where $p^+ = p^- \equiv p$

If $p^+ = p^- \equiv p$, for $\delta\mathscr{G}(z^\pm)$ to be zero for all z^+ and z^-, the terms proportional to $\cos(kz)$ and $\sin(kz)$ in the expression of $\delta\mathscr{G}(z^+)$, and those proportional to $\cos(kz+\phi)$ and $\sin(kz+\phi)$ in the expression of $\delta\mathscr{G}(z^-)$ must be zero. This implies that:

$$\begin{cases} \alpha^+ F(p) + \alpha^- (G(p)\cos\phi + H(p)\sin\phi) = 0 \\ \alpha^- F(p) + \alpha^+ (G(p)\cos\phi + H(p)\sin\phi) = 0 \\ H(p)\cos\phi - G(p)\sin\phi = 0. \end{cases}$$

The first two equations imply that $\alpha^+/\alpha^- = \alpha^-/\alpha^+ \Rightarrow \alpha^+ = \pm\alpha^-$. Since we have chosen α^+ and α^- to be positive:

$$\begin{cases} \alpha^+ = \alpha^- \equiv \alpha \neq 0 \\ F(p) + G(p)\cos\phi + H(p)\sin\phi = 0 \\ H(p)\cos\phi - G(p)\sin\phi = 0. \end{cases} \tag{30}$$

Using second and third equations of (30), one gets $\cos\phi = -F(p)G(p)/(G^2(p) + H^2(p))$, $\sin\phi = -F(p)H(p)/(G^2(p) + H^2(p))$. Use of the relation $\cos^2\phi + \sin^2\phi = 1$ then yields

$$\begin{cases} F(p) = \pm\sqrt{G^2(p) + H^2(p)} \\ \cos\phi = -G(p)/F(p), \quad \sin\phi = -H(p)/F(p). \end{cases} \tag{31}$$

For a given ratio K_3^+/K_2, first relation of (31) is an equation on p the solution of which represents the "critical reduced wavevector". It can be solved numerically for each value of K_3^+/K_2 using values of the functions $\bar{f}_{mn}$ and $\hat{g}_{mn}$ given in Figs. 3 and 4. The second equation of Eq. (31) then define the corresponding "critical phase difference" between the configurations of the fore and rear parts of the front.

Since $\bar{f}_{22}(0) = \bar{f}_{33}(0) = \hat{g}_{22}(0) = -\hat{g}_{33}(0) = 1/4$ and $\hat{g}_{23}(0) = 0$ (see Eqs. (14), (23) and (24)), $F(0) = G(0) = (1 + (1/(1-\nu))(K_3^{+2}/K_2^2))/4$ and $H(0) = 0$ (see Eq. (28)). Therefore, if one chooses the sign + in first equation of (31), one finds that $p = 0$, $\phi = -\pi$ is a solution. This is a trivial bifurcation mode which merely corresponds to some translation of the crack in the x-direction. One can check numerically that this is the only one for the choice of the sign + in first equation of (31).

However, if one chooses the sign −, the resolution gives another unique, non-zero solution p_c and a corresponding angle ϕ_c, which define a non-trivial bifurcation mode. Hence there is a single such mode defined by the following equations:

$$\begin{cases} F(p_c) = -\sqrt{G^2(p_c) + H^2(p_c)} \\ \cos\phi_c = -G(p_c)/F(p_c), \sin\phi_c = -H(p_c)/F(p_c). \end{cases} \tag{32}$$

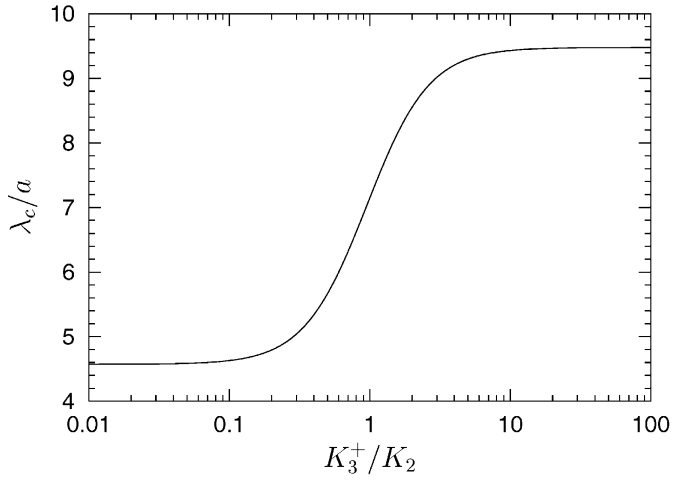

Fig. 5. Critical reduced wavelength versus the ratio of the initial SIF.

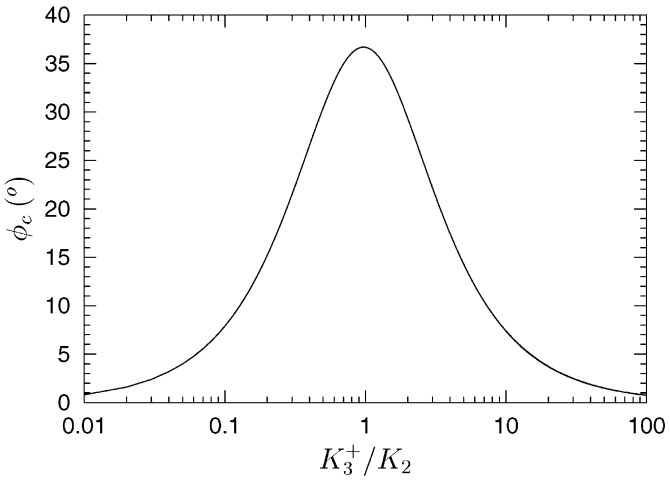

Fig. 6. Critical phase difference versus the ratio of the initial SIF.

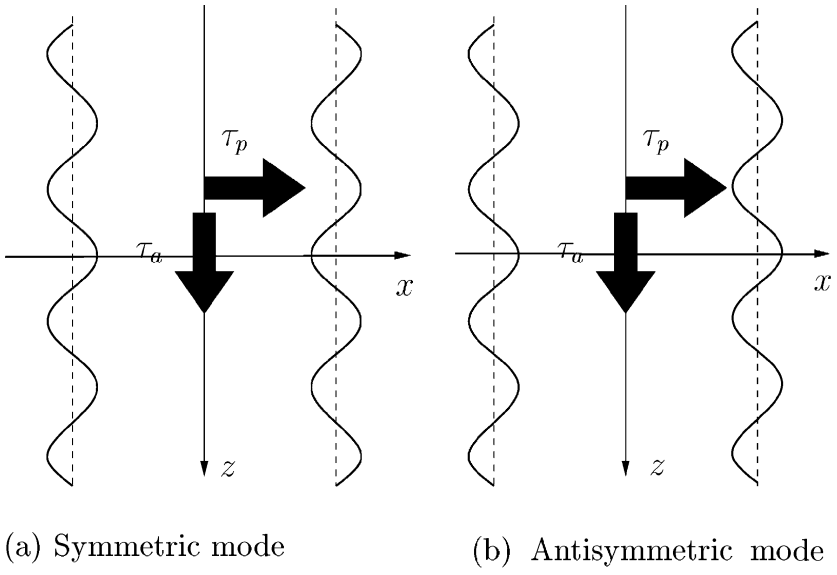

Fig. 7. Symmetric and antisymmetric modes.

Figs. 5 and 6 [2] represent the "critical reduced wavelength" $\lambda_c/a \equiv 2\pi/p_c$ and the critical phase difference ϕ_c of the bifurcated mode as functions of K_3^+/K_2, for $\nu = 0.3$. K_3^+/K_2 is assumed here to be positive; it is obvious that if it changes sign, λ_c remains unchanged and ϕ_c changes sign. One sees that the critical wavelength is larger in pure mode 3 than in pure mode 2. Also, the critical phase difference vanishes in pure mode 2 and mode 3, that is, the bifurcated configuration becomes symmetric with respect to the middle axis Oz of the crack in these cases (see Fig. 7(a)). It is recalled that the bifurcation mode was also found to be symmetric for a pure mode 1 loading (Leblond et al., 1996). Moreover $\phi_c \in (-\pi/2, \pi/2)$, hence the bifurcated mode is always closer to a symmetric configuration ($\phi = 0$, Fig. 7(a)) than to an antisymmetric one ($\phi = -\pi$, Fig. 7(b)).

[2] Note that, in spite of appearances, the curve in Fig. 6 is *not* symmetric with respect to the vertical line $K_3^+/K_2 = 1$; for instance $\phi_c \simeq 7.89^\circ$ for $K_3^+/K_2 = 0.1$ and $\phi_c \simeq 7.38^\circ$ for $K_3^+/K_2 = 10$.

5. Study of the stability problem

The question here is as follows: if the crack front is slightly perturbed within the crack plane, will the perturbation increase (*instability*) or decay (*stability*) in time? Equivalently, will the crack front depart more and more from straightness or tend to again become straight? But since not only the *amplitude* but also the *shape* of the perturbation change during propagation, the very notions of "increase" and "decay" of the perturbation are ambiguous and prone to problems of definition, so that the stability issue is complex.

In fact, we shall deal with it only in a special case for which the discussion becomes very easy and in line with previous ones of Gao and Rice cited above. This case corresponds to wavy perturbations with $p^+ = p^- \equiv p$, $\alpha^+ = \alpha^- \equiv \alpha$ and ϕ given by third equation of (30). Indeed the terms proportional to $\sin(kz)$ and $\sin(kz+\phi)$ in the expressions (26) and (27) of $\delta\mathscr{G}(z^+)$ and $\delta\mathscr{G}(z^-)$ then vanish so that the extrema of $\delta\mathscr{G}(z^+)$ coincide with those of $\delta a(z^+)$, and similarly for those of $\delta\mathscr{G}(z^-)$ and $\delta a(z^-)$. One then simply gets stability if the maxima of $\delta\mathscr{G}(z^+)$ and $\delta\mathscr{G}(z^-)$ correspond to the minima of $\delta a(z^+)$ and $\delta a(z^-)$, and instability if they correspond to the maxima of $\delta a(z^+)$ and $\delta a(z^-)$. This holds true whatever the propagation law governed by the energy release rate provided that it is independent of mode combination, and in particular for brittle fracture governed by the criterion $\mathscr{G} = \mathscr{G}_c$ if $\mathscr{G}_c$ is independent of K_3^+/K_2.

Stability then prevails if the cofactors of $\cos(kz)$ and $\cos(kz+\phi)$ in the expressions of $\delta\mathscr{G}(z^+)$ and $\delta\mathscr{G}(z^-)$ are negative [3]:

$$\text{Stability} \Longleftrightarrow S \equiv F + G\cos\phi + H\sin\phi < 0, \quad \tan\phi = H/G. \tag{33}$$

Now,

$$\begin{aligned} \tan\phi = H/G &\Rightarrow (\cos\phi, \sin\phi) = \pm(G,H)/\sqrt{G^2+H^2} \\ &\Rightarrow F + G\cos\phi + H\sin\phi = F \pm \sqrt{G^2+H^2}. \end{aligned}$$

Therefore the stability condition (33) may be written as follows:

$$\text{Stability} \Longleftrightarrow \begin{cases} S \equiv F + \sqrt{G^2+H^2} < 0 \text{ and } (\cos\phi, \sin\phi) = \dfrac{(G,H)}{\sqrt{G^2+H^2}} \\ \text{or} \\ S \equiv F - \sqrt{G^2+H^2} < 0 \text{ and } (\cos\phi, \sin\phi) = -\dfrac{(G,H)}{\sqrt{G^2+H^2}}. \end{cases} \tag{34}$$

Thus we should distinguish between the cases $(\cos\phi, \sin\phi) = (G,H)/\sqrt{G^2+H^2}$ and $(\cos\phi, \sin\phi) = -(G,H)/\sqrt{G^2+H^2}$:

- The more interesting case corresponds to $(\cos\phi, \sin\phi) = (G,H)/\sqrt{G^2+H^2}$. Then, for each ratio K_3^+/K_2, using the values of the functions $\bar{f}_{mn}$ and $\hat{g}_{mn}$ given in Figs. 3 and 4, one can check that S is positive for $p < p_c$ and negative for $p > p_c$: for instance, for $p = 0$, $F = G = (1 + (1/(1-\nu))(K_3^{+2}/K_2^2))/4 > 0$ and $H = 0$ (see above) so that $S = F + G > 0$, and for $p \to +\infty$, $F \to -\infty$, $G \to 0$, $H \to 0$, so that $S \sim F < 0$; also for $p = p_c$, $S = 0$ by first equation of (32). Hence *stability prevails for* $p > p_c$.
- In the less interesting case where $(\cos\phi, \sin\phi) = -(G,H)/\sqrt{G^2+H^2}$, S is negative for all ratios K_3^+/K_2 and values of p; for instance, for $p = 0$, $S = F - G = 0$, for $p \to +\infty$, $S \sim F < 0$, and for $p = p_c$, $S = -2\sqrt{G^2+H^2} < 0$ by first equation of (32). Thus *stability always prevails*.

[3] In these equations and the sequel, indications of dependence of functions F, G, H and S upon p are left out for the sake of simplicity.

Now consider an unstable configuration, having thus $p < p_c$ and $(\cos\phi, \sin\phi) = (G,H)/\sqrt{G^2+H^2}$. Then $\lambda/a \equiv 2\pi/p > \lambda_c/a \equiv 2\pi/p_c > 4.5$ (see Fig. 5) $\Rightarrow p < 1.4 \Rightarrow -\hat{g}_{33} > 0$ (see Fig. 4) $\Rightarrow G > 0$ (see second equation of (28) and Fig. 4) $\Rightarrow \cos\phi > 0 \Rightarrow \phi \in (-\pi/2, \pi/2)$. On the other hand, consider a (stable) configuration having also $p < p_c$ but $(\cos\phi, \sin\phi) = -(G,H)/\sqrt{G^2+H^2}$. Then, by the same reasoning, $\cos\phi < 0 \Rightarrow \phi \in [-\pi, -\pi/2] \cup (\pi/2, \pi)$. Thus, among configurations having $p < p_c$, unstable ones are characterized by the fact that they have $\phi \in (-\pi/2, \pi/2)$. Since configurations having $p > p_c$ are stable, *unstable configurations are completely characterized, among all possible ones, by the fact that they have both* $p < p_c$ *and* $\phi \in (-\pi/2, \pi/2)$; that is, their wavelength is larger than the critical one ($\lambda > \lambda_c$) and they are closer to a symmetric configuration ($\phi = 0$, Fig. 7(a)) than to an antisymmetric one ($\phi = -\pi$, Fig. 7(b)). In more discursive terms:

- If the configuration of the front is closer to a symmetric one than to an antisymmetric one, *stability prevails for wavelengths smaller than the critical value and instability for wavelengths greater than it.* This finding is similar to those of Leblond et al. (1996) in pure mode 1, Gao and Rice (1986) and Gao (1988) for half-plane and penny-shaped cracks in mode 1 and 2 + 3, and Lazarus and Leblond (1998) for interface half-plane cracks in mode 1 + 2 + 3.
- If the configuration of the front is closer to an antisymmetric one than to a symmetric one, *stability prevails for all wavelengths.*

Two final remarks are in order. First, what was considered above was (just like in previous works of Gao and Rice cited above) the question of stability versus perturbations of *fixed, prescribed* wavelength. One may also raise the question of stability versus *arbitrary* perturbations. In this respect, the straight configuration of the front is inherently unstable, since whatever the crack width, any perturbation having $p^+ = p^-$, $\alpha^+ = \alpha^-$, $(\cos\phi, \sin\phi) = (G,H)/\sqrt{G^2+H^2}$ and $\lambda > \lambda_c$ is bound to develop in time, as discussed above.

Second, in the case of pure mode 1, for the same geometrical configuration, Leblond et al. (1996) have studied the stability problem without any restrictions on $\alpha^{\pm}$ and ϕ, thus in the absence of coincidence of the extrema of $\delta a(z^{\pm})$ and $\delta\mathscr{G}(z^{\pm})$. It is probably possible to extend their approach to mixed mode 2 + 3. But the study is then much more involved, and furthermore feasible only for fatigue or subcritical propagation laws but not for brittle fracture. These were the two reasons for considering only a simple special case here, leaving the extension of Leblond et al. (1996)'s study to mode 2 + 3 for future work.

6. Conclusions and perspectives

It has been shown that the only non-trivial bifurcated mode has the same amplitude and wavelength λ_c on both parts of the front. However, for mixed mode 2 + 3 loading conditions, there is a "phase difference" ϕ_c between the configurations of the two parts of the front depending upon the ratio of the initial mode 2 and 3 SIF. In contrast, in pure mode 2 or 3, the bifurcated mode is symmetric with respect to the central axis Oz of the crack.

The stability problem of the rectilinear configuration of the crack front has been studied only for some simple, special wavy perturbations for which the extrema of the perturbation and the energy release rate coincide. It has been shown that instability prevails for wavelengths larger than the critical one λ_c if the configuration of the front is close to a symmetric one and stability in the other cases, in particular if the configuration of the front is close to an antisymmetric one.

The wavy bifurcated configuration of the front may recall, although the problem is not of same nature, the telephone cord blisters appearing in thin films, observed for instance by Gille and Rau (1984) or

Thouless (1993). But the fore and rear parts of the front of the blister are in an antisymmetric mode and cannot therefore correspond to our bifurcated mode or instability domain.

This work is liable to extensions along three lines:

(1) The first one would be to discuss stability versus wavy perturbations of fixed wavelength without any restrictive condition ensuring coincidence of their extrema and those of the energy release rate. This seems feasible through extension of the work of Leblond et al. (1996) pertaining to the same geometric configuration but pure mode 1 conditions, to general loading conditions. However, this implies dropping the brittle-type criterion $\mathscr{G} = \mathscr{G}_c$ and adopting some subcritical growth or fatigue propagation law instead.

(2) The second one would be to consider the more general stability problem against arbitrary perturbations. The purpose here would be to study the evolution of the crack front toward "smoothness", or contrarily "disorder". This could be achieved by taking the Fourier transform of the perturbation so as to reduce the problem to the study of the evolution of sinusoidal perturbations, following the line just sketched. The previous study suggests that Fourier components of wavelength longer than λ_c will grow and the other ones decrease; that is, perturbations of short wavelength will disappear and only those of long wavelength will develop. But it is difficult to say a priori if the resulting crack front will become more "smooth" or more "disordered". Clearly, these ambiguous notions need to be given an accurate mathematical definition before any discussion is possible.

(3) The third one is related to non-linear effects disregarded in the first-order perturbation analysis. More specifically, the following problem arises. The critical wavelength evidenced here is proportional to the width of the crack. Thus, let us consider a wavy perturbation of the crack front of wavelength larger than the critical one. Then the amplitude of the oscillations will grow, but the width of the crack and therefore the critical wavelength will do just the same. Therefore the wavelength of the perturbation will become smaller than the critical one, and stability again prevail, after a certain distance of propagation. But if this distance is too large, the first-order perturbation method used in this paper may become invalid and non-linear effects important. It is improbable that this topic can be addressed analytically, but it may be handled using numerical methods (see for instance, Bower and Ortiz (1990) and Lazarus (1999)).

References

Bower, A.F., Ortiz, M., 1990. Solution of three-dimensional crack problems by a finite perturbation method. Journal of the Mechanics and Physics of Solids 38 (4), 443–480.

Bueckner, H.F., 1970. A novel principle for the computation of stress intensity factors. Zeitschrift fur Angewandte Mathematik und Mechanik 50 (9), 529–546.

Gao, H., 1988. Nearly circular shear mode cracks. International Journal of Solids and Structures 24 (2), 177–193.

Gao, H., Rice, J.R., 1986. Shear stress intensity factors for planar crack with slightly curved front. ASME Journal of Applied Mechanics 53 (4), 774–778.

Gao, H., Rice, J.R., 1987a. Nearly circular connections of elastic half spaces. ASME Journal of Applied Mechanics 54 (4), 627–634.

Gao, H., Rice, J.R., 1987b. Somewhat circular tensile cracks. International Journal of Fracture 33 (3), 155–174.

Gille, G., Rau, B., 1984. Buckling instability and adhesion of carbon layers. Thin Solid Films 120 (2), 109–121.

Lazarus, V., 1999. Fatigue propagation path of 3D plane cracks under mode I loading. Comptes-Rendus de l'Académie des Sciences, Série IIb 327, 1319–1324.

Lazarus, V., Leblond, J.-B., 1998. Three-dimensional crack-face weight functions for the semi-infinite interface crack. I. Variation of the stress intensity factors due to some small perturbation of the crack front. Journal of the Mechanics and Physics of Solids 46 (3), 489–511.

Leblond, J.-B., Lazarus, V., Mouchrif, S.-E., 1999. Crack paths in three-dimensional elastic solids. II. Three-term expansion of the stress intensity factors—Applications and perspectives. International Journal of Solids and Structures 36 (1), 105–142.

Leblond, J.-B., Mouchrif, S.-E., Perrin, G., 1996. The tensile tunnel-crack with a slightly wavy front. International Journal of Solids and Structures 33 (14), 1995–2022.

Mouchrif, S.-E., 1994. Trajets de propagation de fissures en mécanique linéaire tridimensionnelle de la rupture fragile. Ph.D. thesis, Université Paris 6, France.

Nazarov, S.A., 1989. Derivation of variational inequality for shape of a small increment of an I-mode crack. Mechanics of Solids 24 (2), 145–152.

Rice, J.R., 1972. Some remarks on elastic crack-tip stress fields. International Journal of Solids and Structures 8 (6), 751–758.

Rice, J.R., 1985. First-order variation in elastic fields due to variation in location of a planar crack front. ASME Journal of Applied Mechanics 52 (3), 571–579.

Rice, J.R., 1989. Weight function theory for three-dimensional elastic crack analysis. In: Wei, R.P., Gangloff, R.P. (Eds.), Fracture Mechanics: Perspectives and Directions (Twentieth Symposium). American Society for Testing and Materials STP 1020, Philadelphia, USA.

Thouless, M.D., 1993. Combined buckling and cracking of films. Journal of the American Ceramic Society 76 (11), 2936–2938.

PERGAMON

International Journal of Solids and Structures 39 (2002) 4437–4455

INTERNATIONAL JOURNAL OF SOLIDS and STRUCTURES

www.elsevier.com/locate/ijsolstr

In-plane perturbation of the tunnel-crack under shear loading II: Determination of the fundamental kernel

Véronique Lazarus *, Jean-Baptiste Leblond

Laboratoire de Modélisation en Mécanique, Université Pierre et Marie Curie, 8 rue du Capitaine Scott, 75015 Paris, France

Received 31 October 2001; received in revised form 4 April 2002

Abstract

For any plane crack in an infinite isotropic elastic body subjected to some constant loading, Bueckner–Rice's weight function theory gives the variation of the stress intensity factors due to a small coplanar perturbation of the crack front. This variation involves the initial SIF, some geometry independent quantities and an integral extended over the front, the "fundamental kernel" of which is linked to the weight functions and thus depends on the geometry considered. The aim of this paper is to determine this fundamental kernel for the tunnel-crack. The component of this kernel linked to purely tensile loadings has been obtained by Leblond et al. [Int. J. Solids Struct. 33 (1996) 1995]; hence only shear loadings are considered here. The method consists in applying Bueckner–Rice's formula to some point-force loadings and special perturbations of the crack front which preserve the crack shape while modifying its size and orientation. This procedure yields integrodifferential equations on the components of the fundamental kernel. A Fourier transform in the direction of the crack front then yields ordinary differential equations, that are solved numerically prior to final Fourier inversion.

Keywords: Tunnel-crack; Shear loading; Mode 2; Mode 3; Crack front; In-plane perturbation; Fundamental kernel; Bueckner–Rice theory; Weight functions; Integrodifferential equations; Fourier transform

1. Introduction

Consider a plane crack embedded in an infinite isotropic elastic solid subjected to some arbitrary, constant loading. Eq. (1) of Part I gives the variation of the SIF resulting from any small, in-plane perturbation of the crack front. This equation notably involves an integral extended over the front. As will be detailed below, the "fundamental kernel" **Z** in this integral is linked to the weight functions of the crack, i.e. to the SIF induced on the crack front by unit point forces exerted on the crack lips, in the limit when the points of application of these forces get infinitely close to the crack front. Therefore, it depends upon the entire geometry of the crack. It can be deduced for instance from the works of Bueckner (1987) or Meade and Keer (1984) on weight functions for a half-plane crack, from those of Kassir and Sih (1975), Tada et al.

* Corresponding author.
E-mail addresses: vlazarus@ccr.jussieu.fr (V. Lazarus), leblond@lmm.jussieu.fr (J.-B. Leblond).

0020-7683/02/$ - see front matter
PII: S0020-7683(02)00333-5

(1973) and Stallybrass (1981) for a circular connection and from that of Bueckner (1987) for a penny-shaped crack. This has been done by Rice (1985) and Gao and Rice (1986) for a half-plane crack, by Gao and Rice (1987a) for a circular connection and by Gao and Rice (1987b) and Gao (1988) for a penny-shaped crack. The weight functions and the fundamental kernel are also known for an interface half-plane crack (Lazarus and Leblond, 1998). For the tunnel-crack, the component Z_{11} linked to *tensile* loadings has been derived by Leblond et al. (1996). The aim of Part II of this work is to derive the other components Z_{mn}, $m,n = 2,3$ linked to *shear* loadings. [1]

The method used is based on both works of Leblond et al. (1996) and Lazarus and Leblond (1998). It is of "special" rather than "general" nature in the terminology employed by Bueckner (1987). This means that it avoids the calculation of the entire solution of the elasticity problems implied, but concentrates instead on the sole feature of interest, namely the distribution of the SIF along the crack front. Considering the complexity of the equations obtained even with such a "reduction", one may reasonably conjecture that any "general" method of solution would be intractable.

The principle of our method is to apply Eq. (1) of Part I to some special loadings and perturbations of the front. The loadings considered consist of point forces applied close to the crack front, so that the SIF prior to the perturbation are just components of the fundamental kernel $\mathbf{Z}$. The perturbations envisaged consist of a small translation of the rear part of the front and a small rotation of both parts about an axis normal to the crack plane. Since the shape of the crack is preserved in these transformations, the new SIF are still connected to $\mathbf{Z}$. One thus obtains integrodifferential equations on the components of $\mathbf{Z}$ which can be solved through Fourier transform along the direction of the crack front.

The paper is organized as follows. Necessary elements from Part I are recalled in Section 2 for completeness. The integrodifferential equations on the components of $\mathbf{Z}$ are presented in Section 3. The Fourier transform of these equations in the direction of the crack front yields second order ordinary differential equations, duly completed by suitable "initial" conditions. This complete system of equations is presented in Section 4, and the necessary subsequent Fourier inversion is sketched in Section 5. As could be forecast in view of the complexity of the problem, this system does not have any simple analytical solution and must be solved numerically. The numerical procedure and results are presented in the final Section 6.

2. Preliminaries

2.1. Elements of Part I

For ease of reference, indispensable elements of Part I are briefly recalled here.

For the tunnel-crack of width $2a$, the fundamental kernel $\mathbf{Z}$, which depends a priori on three parameters, a, z, z', can be expressed in terms of two operators $\mathbf{f}$ and $\mathbf{g}$ depending only on one parameter through the following relations:

$$\mathbf{Z}(a;z^+,z'^+) = \mathbf{Z}(a;z^-,z'^-) \equiv \frac{\mathbf{f}((z'-z)/a)}{(z'-z)^2} \tag{1}$$

$$\mathbf{Z}(a;z^+,z'^-) = \mathbf{Z}(a;z^-,z'^+) \equiv \frac{\mathbf{g}((z'-z)/a)}{a^2} \tag{2}$$

Moreover, the following relations hold:

[1] As will be seen, all other remaining components are zero.

$$f_{12} = f_{21} = f_{13} = f_{31} = g_{12} = g_{21} = g_{13} = g_{31} \equiv 0 \tag{3}$$

$$f_{32} = -(1-\nu) f_{23}, \quad g_{32} = -(1-\nu) g_{23} \tag{4}$$

Hence, the determination of the fundamental kernel is reduced to that of eight scalar functions of one variable: f_{11}, f_{22}, f_{33}, f_{23}, g_{11}, g_{22}, g_{33}, g_{23}.

The functions f_{11} and g_{11} pertaining to mode 1 loadings have been calculated by Leblond et al. (1996). The aim of this work is to determine the six other functions, pertaining to shear mode $2+3$ loadings. Among them, f_{22}, f_{33}, g_{22}, g_{33} are even and f_{23}, g_{23} odd functions.

Our starting point is Eq. (1) of Part I, which takes the form (10) and (11) for δK_2 and δK_3 in the case of a tunnel-crack. In a compact form more suitable here, these equations read:

$$\begin{aligned}\delta K_m(z^+) = {} & [\delta K_m(z^+)]_{\delta a(z'^\pm)\equiv\delta a(z^+)} + N_{mn} K_n(z^+) \frac{\mathrm{d}\delta a}{\mathrm{d}z}(z^+) + \mathrm{PV}\int_{-\infty}^{+\infty} f_{mn}\left(\frac{z'-z}{a}\right) K_n(z'^+) \frac{\delta a(z'^+) - \delta a(z^+)}{(z'-z)^2}\,\mathrm{d}z' \\ & + \int_{-\infty}^{+\infty} g_{mn}\left(\frac{z'-z}{a}\right) K_n(z'^-) \frac{\delta a(z'^-) - \delta a(z^+)}{a^2}\,\mathrm{d}z', \quad m,n = 2,3\end{aligned} \tag{5}$$

where Einstein's implicit convention is used for the index n and

$$N_{23} = -\frac{2}{2-\nu}, \quad N_{32} = \frac{2(1-\nu)}{2-\nu} \tag{6}$$

ν denoting Poisson's ratio and other components of $\mathbf{N}$ being zero. The values of the $\delta K_m(z^-)$ for a point $M^-(z^-)$ belonging to the line $(x=-a)$ are given by the same expression with the obvious substitutions $z^+ \to z^-$, $z'^\pm \to z'^\mp$.

2.2. Relations between functions f_{mn}, g_{mn} and crack-face weight functions

Let $k_{mi}(a; z^\pm; x', z')$ $(m = 1,2,3,\ i = x,y,z)$ denote the mth SIF generated at the point $z^\pm$ of the front of a tunnel-crack of width $2a$ by unit point forces $\pm\vec{e}_i$ exerted on the points $(x', 0^\pm, z')$ of the crack faces. Leblond et al. (1999) have shown that the fundamental kernel $\mathbf{Z}$ is linked to these *crack-face weight functions* by the following formula:

$$Z_{mn}(a; z^\pm, z'^\pm) = \Delta_{ni}(z'^\pm) k_{mi}(a; z^\pm; z'^\pm) \tag{7}$$

where Einstein's implicit summation convention is employed for the index i. In this equation,

$$k_{mi}(a; z^\pm; z'^+) \equiv \lim_{x'\to a} \frac{k_{mi}(a; z^\pm; x', z')}{\sqrt{a-x'}}, \quad k_{mi}(a; z^\pm; z'^-) \equiv \lim_{x'\to -a} \frac{k_{mi}(a; z^\pm; x', z')}{\sqrt{a+x'}} \tag{8}$$

and the coefficients $\Delta_{ni}(z'^\pm)$ depend on the orientation of the local set of axes chosen to define the SIF (see Leblond et al., 1999). One verifies that for the choice made in Part I (set of axes (x,y,z) for the line $(x=a)$ and set of axes $(-x,-y,z)$ for the line $(x=-a)$),

$$\begin{aligned}\Delta_{1y}(z'^+) = \Delta_{2x}(z'^+) = \Delta_{3z}(z'^+) = \frac{\sqrt{2\pi}}{4}, \\ \Delta_{1y}(z'^-) = \Delta_{2x}(z'^-) = -\Delta_{3z}(z'^-) = \frac{\sqrt{2\pi}}{4},\end{aligned} \tag{9}$$

other components being zero.

Combination of Eqs. (1), (2), (7) and (9) then yields the following formulae relating the components of $\mathbf{f}$ and $\mathbf{g}$ and the crack-face weight functions:

$$\begin{aligned}
&\frac{4}{\sqrt{2\pi}} f_{11}(z/a) = z^2 k_{1y}(a; z^+; 0^+) = z^2 k_{1y}(a; z^-; 0^-) \\
&\frac{4}{\sqrt{2\pi}} f_{22}(z/a) = z^2 k_{2x}(a; z^+; 0^+) = z^2 k_{2x}(a; z^-; 0^-) \\
&\frac{4}{\sqrt{2\pi}} f_{33}(z/a) = z^2 k_{3z}(a; z^+; 0^+) = -z^2 k_{3z}(a; z^-; 0^-) \\
&\frac{4}{\sqrt{2\pi}} f_{23}(z/a) = -z^2 k_{2z}(a; z^+; 0^+) = z^2 k_{2z}(a; z^-; 0^-) = \frac{z^2}{1-\nu} k_{3x}(a; z^+; 0^+) = \frac{z^2}{1-\nu} k_{3x}(a; z^-; 0^-)
\end{aligned} \tag{10}$$

and

$$\begin{aligned}
&\frac{4}{\sqrt{2\pi}} g_{11}(z/a) = a^2 k_{1y}(a; z^+; 0^-) = a^2 k_{1y}(a; z^-; 0^+) \\
&\frac{4}{\sqrt{2\pi}} g_{22}(z/a) = a^2 k_{2x}(a; z^+; 0^-) = a^2 k_{2x}(a; z^-; 0^+) \\
&\frac{4}{\sqrt{2\pi}} g_{33}(z/a) = -a^2 k_{3z}(a; z^+; 0^-) = a^2 k_{3z}(a; z^-; 0^+) \\
&\frac{4}{\sqrt{2\pi}} g_{23}(z/a) = a^2 k_{2z}(a; z^+; 0^-) = -a^2 k_{2z}(a; z^-; 0^+) = \frac{a^2}{1-\nu} k_{3x}(a; z^+; 0^-) = \frac{a^2}{1-\nu} k_{3x}(a; z^-; 0^+)
\end{aligned} \tag{11}$$

(where parity properties of the f_{mn} and g_{mn} have been used).

3. Integrodifferential equations on the functions f_{22}, f_{33}, f_{23}, g_{22}, g_{33}, g_{23}

3.1. Overview of the method

Let us consider a tunnel-crack of width $2a$, assuming $a = 1$ without any loss of generality, subjected to a pair of unit point forces $\pm\vec{e}_i$ exerted on the crack faces. Then the SIF K_n before any perturbation of the crack front are the weight functions k_{ni}. If now the perturbation consists of a translation of one part of the front or a rotation of both parts, the crack shape is preserved so that the SIF after perturbation are also linked to the weight functions. Eq. (5) then yields equations on the weight functions. Applying the forces close to the front, one thus obtains equations on the functions $k_{mi}(a; z^{\pm}; z'^{\pm})$ defined by (8). By using relations (10) and (11) connecting the functions $k_{mi}(a; z^{\pm}; z'^{\pm})$ and the operators **f** and **g**, one finally obtains six integrodifferential equations on the six unknown functions f_{22}, f_{33}, f_{23}, g_{22}, g_{33}, g_{23}.

In practice, the point forces will be applied close to the point $(1, 0, 0)$ of the fore part of front. The index i will be taken as x or z since the choice $i = y$ would yield equations on the already known functions f_{11} and g_{11}. Two motions of the crack front will be studied:

- a translatory motion of the sole rear part of the front, the variations δK_m of the SIF being observed at the point z^+ of the fore part of the front (Fig. 1(a));
- an in-plane rotation, by an angle $\varepsilon \ll 1$, of the fore part of the front around the point $(1, 0, 0)$ and of the rear part of the front around the point $(-1, 0, z)$, the variations δK_m of the SIF being then observed at the point z^- of the rear part of the front (Fig. 1(b)).

3.2. Equations on the weight functions

Let us consider the unperturbed crack and suppose that some unit point forces $\pm\vec{e}_i$, $i = x$ or z are applied at points $(x, 0^{\pm}, 0)$ of the crack faces. Then the SIF before any perturbation of the crack front are given by:

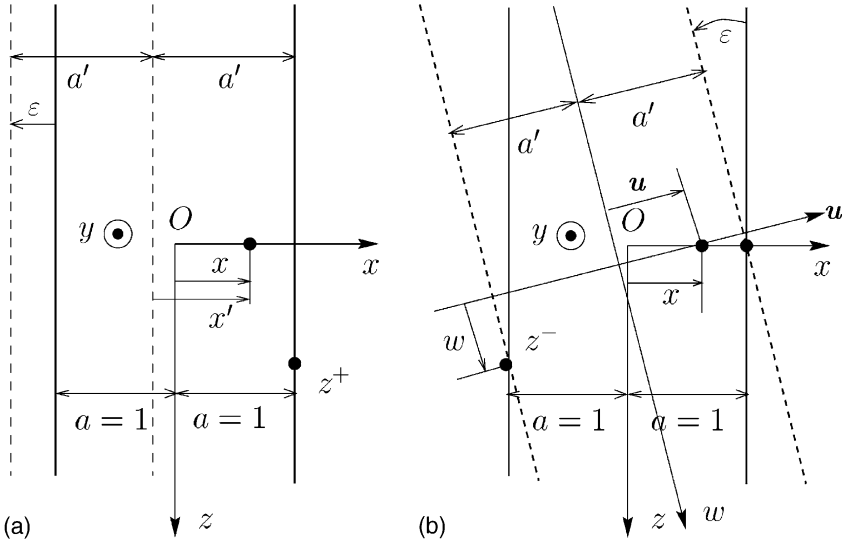

Fig. 1. Special motions of the crack front.

$$K_n(z'^{\pm}) = k_{ni}(1; z'^{\pm}; x, 0) \tag{12}$$

Let us now consider (Fig. 1(a)) a simple translatory motion of the sole rear part of the front, defined by $\delta a(z'^{+}) \equiv 0$, $\delta a(z'^{-}) \equiv \varepsilon$ where ε denotes a small parameter. Then the new SIF are those of a tunnel-crack of width $2a'$ with $a' = 1 + \varepsilon/2$, subjected to point forces exerted at the points $(x', 0^{\pm}, 0)$ with $x' = x + \varepsilon/2$ (see Fig. 1(a)). Thus

$$\delta K_m(z^+) = k_{mi}(1 + \varepsilon/2; z^+; x + \varepsilon/2, 0) - k_{mi}(1; z^+; x, 0) \tag{13}$$

so that, by Eq. (5):

$$k_{mi}(1 + \varepsilon/2; z^+; x + \varepsilon/2, 0) - k_{mi}(1; z^+; x, 0) = \varepsilon \int_{-\infty}^{+\infty} g_{mn}(z' - z) k_{ni}(1; z'^-; x, 0)\, \mathrm{d}z' \tag{14}$$

Next consider a rotation of the fore and rear parts of the front, defined by $\delta a(z'^{+}) \equiv \varepsilon z'$, $\delta a(z'^{-}) \equiv \varepsilon(z - z')$ where ε again denotes a small parameter (Fig. 1(b)). The axes adapted to the new front are (u, y, w) (see Fig. 1(b)). Since

$$\vec{e_x} = \vec{e_u} + \varepsilon \vec{e_w}, \quad \vec{e_z} = \vec{e_w} - \varepsilon \vec{e_u} \tag{15}$$

the SIF after perturbation at point z^- are $k_{mx}(a'; w^-; u, 0) + \varepsilon k_{mz}(a'; w^-; u, 0)$ for $i = x$ and $k_{mz}(a'; w^-; u, 0) - \varepsilon k_{mx}(a'; w^-; u, 0)$ for $i = z$, where a' again denotes the new half-width of the crack. It is easy to show that

$$a' = 1 + \frac{z}{2}\varepsilon, \quad u = x + \frac{z}{2}\varepsilon, \quad w = z - (1 + x)\varepsilon \tag{16}$$

Hence, Eq. (5) applied at point z^- yields for $m = 2, 3$: for $i = x$,

$$\begin{aligned} &k_{mx}\left(1 + \frac{z}{2}\varepsilon; [z - (1 + x)\varepsilon]^-; x + \frac{z}{2}\varepsilon, 0\right) - k_{mx}(1; z^-; x, 0) + \varepsilon k_{mz}(1; z^-; x, 0) = -\varepsilon N_{mn} k_{nx}(1; z^-; x, 0) \\ &\quad + \varepsilon \,\mathrm{PV} \int_{-\infty}^{+\infty} f_{mn}(z' - z) k_{nx}(1; z'^-; x, 0) \frac{\mathrm{d}z'}{z - z'} + \varepsilon \int_{-\infty}^{+\infty} g_{mn}(z' - z) k_{nx}(1; z'^+; x, 0) z'\, \mathrm{d}z' \end{aligned} \tag{17}$$

and for $i = z$:

$$k_{mz}\Big(1+\frac{z}{2}\varepsilon;[z-(1+x)\varepsilon]^-;x+\frac{z}{2}\varepsilon,0\Big)-k_{mz}(1;z^-;x,0)-\varepsilon k_{mx}(1;z^-;x,0)=-\varepsilon N_{mn}k_{nz}(1;z^-;x,0)$$
$$+\varepsilon\,\mathrm{PV}\int_{-\infty}^{+\infty}f_{mn}(z'-z)k_{nz}(1;z'^-;x,0)\frac{\mathrm{d}z'}{z-z'}+\varepsilon\int_{-\infty}^{+\infty}g_{mn}(z'-z)k_{nz}(1;z'^+;x,0)z'\,\mathrm{d}z' \tag{18}$$

3.3. Equations on the functions $k_{mi}(a;z^\pm;z'^\pm)$, $m = 2,3$, $i = x,z$

These equations are obtained by dividing Eqs. (14), (17), (18) by $\sqrt{1-x}$ and then taking the limit $x \to 1$, using the definition (8) of the $k_{mi}(a;z^\pm;z'^\pm)$.

For $m = 2$, 3 and $i = x$, z, one obtains:

$$\lim_{x\to1}\int_{-\infty}^{+\infty}g_{mn}(z'-z)\frac{k_{ni}(1;z'^-;x,0)}{\sqrt{1-x}}\mathrm{d}z'=\int_{-\infty}^{+\infty}g_{mn}(z'-z)k_{ni}(1;z'^-;0^+)\mathrm{d}z' \tag{19}$$

$$\lim_{x\to1}\mathrm{PV}\int_{-\infty}^{+\infty}f_{mn}(z'-z)\frac{k_{ni}(1;z'^-;x,0)}{\sqrt{1-x}}\frac{\mathrm{d}z'}{z-z'}=\mathrm{PV}\int_{-\infty}^{+\infty}f_{mn}(z'-z)k_{ni}(1;z'^-;0^+)\frac{\mathrm{d}z'}{z-z'} \tag{20}$$

These equations mean that the symbols $\lim_{x\to1}$ and $(\mathrm{PV})\int_{-\infty}^{+\infty}$ simply commute. This is because when $x \to 1$, the points $(x,0^\pm,0)$ of application of the forces do not approach the point of observation $M^-(z'^-)$ of the SIF $k_{ni}(1;z'^-;x,0)$ so that these SIF remain bounded for all z'.

However, when $x \to 1$, the points $(x,0^\pm,0)$ of application of the forces do approach the point of observation $M^+(z'^+)$ of the SIF $k_{ni}(1;z'^+;x,0)$ for the special value $z' = 0$. Thinks then become more intricate. It is thus shown in Appendix A that

$$\lim_{x\to1}\int_{-\infty}^{+\infty}g_{m2}(z'-z)\frac{k_{2x}(1;z'^+;x,0)}{\sqrt{1-x}}z'\,\mathrm{d}z'=\mathrm{PV}\int_{-\infty}^{+\infty}g_{m2}(z'-z)k_{2x}(1;z'^+;0^+)z'\,\mathrm{d}z', \tag{21}$$

a similar result holding with the substitutions $g_{m2} \to g_{m3}$, $k_{2x} \to k_{3z}$; also,

$$\lim_{x\to1}\int_{-\infty}^{+\infty}g_{m2}(z'-z)\frac{k_{2z}(1;z'^+;x,0)}{\sqrt{1-x}}z'\,\mathrm{d}z'=\mathrm{PV}\int_{-\infty}^{+\infty}g_{m2}(z'-z)k_{2z}(1;z'^+;0^+)z'\,\mathrm{d}z'+\frac{4}{\sqrt{2\pi}}\frac{v}{2-v}g_{m2}(-z), \tag{22}$$

and similarly with the substitutions $g_{m2} \to g_{m3}$, $k_{2z} \to k_{3x}$.

Combination of Eqs. (14), (17), (18) and (19)–(22) then yields the following equations on the functions $k_{mi}(a;z^\pm;z'^\pm)$, for $m = 2,3$:

$$k_{mi}(1+\varepsilon/2;z^+;0^+)-k_{mi}(1;z^+;0^+)=\varepsilon\int_{-\infty}^{+\infty}g_{mn}(z'-z)k_{ni}(1;z'^-;0^+)\,\mathrm{d}z' \tag{23}$$

for $i = x,z$, and

$$k_{mx}\Big(1+\frac{z}{2}\varepsilon;[z-2\varepsilon]^-;0^+\Big)-k_{mx}(1;z^-;0^+)+\varepsilon k_{mz}(1;z^-;0^+)$$
$$=-\varepsilon N_{mn}k_{nx}(1;z^-;0^+)+\varepsilon\frac{4}{\sqrt{2\pi}}\frac{v}{2-v}g_{m3}(-z)+\varepsilon\,\mathrm{PV}\int_{-\infty}^{+\infty}f_{mn}(z'-z)k_{nx}(1;z'^-;0^+)\frac{\mathrm{d}z'}{z-z'}$$
$$+\varepsilon\mathrm{PV}\int_{-\infty}^{+\infty}g_{mn}(z'-z)k_{nx}(1;z'^+;0^+)z'\,\mathrm{d}z' \tag{24}$$

$$k_{mz}\left(1+\frac{z}{2}\varepsilon;[z-2\varepsilon]^{-};0^{+}\right)-k_{mz}(1;z^{-};0^{+})-\varepsilon k_{mx}(1;z^{-};0^{+})$$
$$=-\varepsilon N_{mn}k_{nz}(1;z^{-};0^{+})+\varepsilon\frac{4}{\sqrt{2\pi}}\frac{v}{2-v}g_{m2}(-z)+\varepsilon\,\mathrm{PV}\int_{-\infty}^{+\infty}f_{mn}(z'-z)k_{nz}(1;z'^{-};0^{+})\frac{\mathrm{d}z'}{z-z'}$$
$$+\varepsilon\,\mathrm{PV}\int_{-\infty}^{+\infty}g_{mn}(z'-z)k_{nz}(1;z'^{+};0^{+})z'\,\mathrm{d}z' \tag{25}$$

3.4. Equations on the functions f_{22}, f_{33}, f_{23}, g_{22}, g_{33}, g_{23}

Using relations (10) and (11) and identifying terms of order ε in Eqs. (23)–(25), one obtains the following integrodifferential equations on the functions:

$$f'_{22}(z)=-2z\int_{-\infty}^{+\infty}[g_{22}(z-z')g_{22}(z')-(1-v)g_{23}(z-z')g_{23}(z')]\,\mathrm{d}z' \tag{26}$$

$$f'_{33}(z)=-2z\int_{-\infty}^{+\infty}[g_{33}(z-z')g_{33}(z')-(1-v)g_{23}(z-z')g_{23}(z')]\,\mathrm{d}z' \tag{27}$$

$$f'_{23}(z)=-2z\int_{-\infty}^{+\infty}g_{23}(z-z')(g_{22}+g_{33})(z')\,\mathrm{d}z' \tag{28}$$

$$\left[\left(1+\frac{z^2}{4}\right)g_{22}(z)\right]'+\frac{2(1-v)}{2-v}g_{23}(z)=(1-v)\int_{-\infty}^{+\infty}g_{23}(z-z')\frac{f_{23}(z')}{z'}\,\mathrm{d}z'$$
$$-\,\mathrm{PV}\int_{-\infty}^{+\infty}g_{22}(z-z')\frac{f_{22}(z')}{z'}\,\mathrm{d}z' \tag{29}$$

$$\left[\left(1+\frac{z^2}{4}\right)g_{33}(z)\right]'+\frac{2(1-v)}{2-v}g_{23}(z)=(1-v)\int_{-\infty}^{+\infty}g_{23}(z-z')\frac{f_{23}(z')}{z'}\,\mathrm{d}z'$$
$$-\,\mathrm{PV}\int_{-\infty}^{+\infty}g_{33}(z-z')\frac{f_{33}(z')}{z'}\,\mathrm{d}z' \tag{30}$$

$$\left[\left(1+\frac{z^2}{4}\right)g_{23}(z)\right]'-\frac{1}{2-v}(g_{22}+g_{33})(z)=-\int_{-\infty}^{+\infty}(g_{22}+g_{33})(z-z')\frac{f_{23}(z')}{2z'}\,\mathrm{d}z'$$
$$-\,\mathrm{PV}\int_{-\infty}^{+\infty}g_{23}(z-z')\frac{(f_{22}+f_{33})(z')}{2z'}\,\mathrm{d}z' \tag{31}$$

where use has been made of relations (6) and parity properties of the f_{mn} and g_{mn} (see Section 2.1).

4. Differential equations and initial conditions on the functions $\widehat{F}_{22}$, $\widehat{F}_{33}$, $\widehat{F}_{23}$, $\hat{g}_{22}$, $\hat{g}_{33}$, $\hat{g}_{23}$

The definition adopted for the Fourier transform $\hat{\varphi}(p)$ of some function $\varphi(z)$ is the same as in Part I:

$$\hat{\varphi}(p)\equiv\int_{-\infty}^{+\infty}\varphi(z)\mathrm{e}^{\mathrm{i}pz}\,\mathrm{d}z \tag{32}$$

Note that since f_{22}, f_{33}, g_{22}, g_{33} are even and f_{23}, g_{23} odd, $\hat{f}_{22}$, $\hat{f}_{33}$, $\hat{g}_{22}$, $\hat{g}_{33}$ are even and real, and $\hat{f}_{23}$, $\hat{g}_{23}$ odd and purely imaginary.

4.1. Differential equations

Taking the Fourier transform of Eqs. (26)–(31) is elementary except for terms of the form

$$(\mathrm{PV})\int_{-\infty}^{+\infty} g_{mn}(z-z')\frac{f_{rs}(z')}{z'}\,\mathrm{d}z',$$

which are envisaged in Appendix B. The resulting equations read as follows:

$$\widehat{F}'_{22} = -\tfrac{2}{p}[\hat{g}_{22}^2 - (1-\nu)\hat{g}_{23}^2]' \tag{33}$$

$$\widehat{F}'_{33} = -\tfrac{2}{p}[\hat{g}_{33}^2 - (1-\nu)\hat{g}_{23}^2]' \tag{34}$$

$$\widehat{F}'_{23} = -\tfrac{2}{p}[\hat{g}_{23}(\hat{g}_{22}+\hat{g}_{33})]' \tag{35}$$

$$\hat{g}_{22} - \frac{\hat{g}''_{22}}{4} = \tfrac{1}{p}[\widehat{F}_{22}\hat{g}_{22} - (1-\nu)\widehat{F}_{23}\hat{g}_{23}] \tag{36}$$

$$\hat{g}_{33} - \frac{\hat{g}''_{33}}{4} = \tfrac{1}{p}[\widehat{F}_{33}\hat{g}_{33} - (1-\nu)\widehat{F}_{23}\hat{g}_{23}] \tag{37}$$

$$\hat{g}_{23} - \frac{\hat{g}''_{23}}{4} = \frac{1}{p}\left[\frac{\widehat{F}_{22}+\widehat{F}_{33}}{2}\hat{g}_{23} + \widehat{F}_{23}\frac{\hat{g}_{22}+\hat{g}_{33}}{2}\right] \tag{38}$$

In these expressions, the functions $\widehat{F}_{mn}$ are the definite integrals of the functions $\hat{f}_{mn}$ defined by

$$\widehat{F}_{mn}(p) \equiv \int_0^p \hat{f}_{mn}(q)\,\mathrm{d}q + \begin{cases} 0, & (m,n) = (2,2),(3,3) \\ \mathrm{i}\frac{2-\nu}{2(1-\nu)}, & (m,n) = (2,3) \end{cases} \tag{39}$$

Note that since $\hat{f}_{22}$, $\hat{f}_{33}$ are even and $\hat{f}_{23}$ odd, $\widehat{F}_{22}$, $\widehat{F}_{33}$ are odd and $\widehat{F}_{23}$ even. Because of these parity properties and those of the $\hat{g}_{mn}$, it suffices to determine all functions on the interval $(0,+\infty)$. Also, note that functions $\widehat{F}_{22}$, $\widehat{F}_{33}$ are real and $\widehat{F}_{23}$ purely imaginary.

Eqs. (33)–(38) form a system of six non-linear differential equations (on the interval $(0,+\infty)$), on the six unknown functions $\widehat{F}_{22}$, $\widehat{F}_{33}$, $\widehat{F}_{23}$, $\hat{g}_{22}$, $\hat{g}_{33}$, $\hat{g}_{23}$, of order 1 with respect to the $\widehat{F}_{mn}$ and order 2 with respect to the $\hat{g}_{mn}$. Hence, to (numerically) get these functions on any interval $[p_0, p_\infty]$ with $0 < p_0 \ll 1$ and $p_\infty \gg 1$, one may proceed in two ways:

- integrate "forwards", from p_0 to p_∞; this requires knowing the values of the $\widehat{F}_{mn}$, $\hat{g}_{mn}$ and $\hat{g}'_{mn}$ at p_0, that is near 0;
- integrate "backwards", from p_∞ to p_0; the values of the $\widehat{F}_{mn}$, $\hat{g}_{mn}$ and $\hat{g}'_{mn}$ are then needed at p_∞, that is near $+\infty$.

The next sections are therefore devoted to the necessary asymptotic study of the functions near 0 and $+\infty$.

4.2. Values of $\widehat{F}_{22}(0)$, $\widehat{F}_{33}(0)$, $\widehat{F}_{23}(0)$, $\hat{g}_{22}(0)$, $\hat{g}_{33}(0)$, $\hat{g}_{23}(0)$

From the definition (39) of the $\widehat{F}_{mn}$, it is clear that:

$$\widehat{F}_{22}(0) = \widehat{F}_{33}(0) = 0, \quad \widehat{F}_{23}(0) = \mathrm{i}\frac{2-\nu}{2(1-\nu)} \tag{40}$$

Moreover, values of $\hat{g}_{22}(0)$, $\hat{g}_{33}(0)$, $\hat{g}_{23}(0)$ are given by relations (14) of Part I, recalled here for the sake of completeness:

$$\hat{g}_{22}(0) = -\hat{g}_{33}(0) = \frac{1}{4}, \quad \hat{g}_{23}(0) = 0 \tag{41}$$

Finally, the derivatives $\hat{g}'_{mn}(0)$ are given by $\hat{g}'_{mn}(0) = i\int_{-\infty}^{+\infty} z g_{mn}(z)\,\mathrm{d}z$. For $(m,n) = (2,3)$, this integral is given by Eq. (18) of Part I. For $(m,n) = (2,2), (3,3)$, it is zero since $\hat{g}_{mn}$ is even. In conclusion,

$$\hat{g}'_{22}(0) = \hat{g}'_{33}(0) = 0, \quad \hat{g}'_{23}(0) = \mathrm{i}\frac{\nu}{2(1-\nu)} \tag{42}$$

4.3. Asymptotic behavior of $\widehat{F}_{22}(p)$, $\widehat{F}_{33}(p)$, $\widehat{F}_{23}(p)$, $\hat{g}_{22}(p)$, $\hat{g}_{33}(p)$, $\hat{g}_{23}(p)$ for $p \to 0^+$

As a first approximation, the values of the $\widehat{F}_{mn}(p_0)$, $\hat{g}_{mn}(p_0)$ and $\hat{g}'_{mn}(p_0)$ may be taken equal to those of the $\widehat{F}_{mn}(0)$, $\hat{g}_{mn}(0)$ and $\hat{g}'_{mn}(0)$. However, more refined values can be found by studying the asymptotic behavior of the functions near 0. Such a study will also be needed to derive asymptotic formulae for the $f_{mn}(z)$ and $g_{mn}(z)$ for $z \to +\infty$, which will nicely supplement the numerical values found over some necessary finite interval.

Let us suppose that just as the function $\hat{g}_{11}(p)$ (Leblond et al., 1996), $\hat{g}_{22}(p)$, $\hat{g}_{33}(p)$, $\hat{g}_{23}(p)$ admit, for $p \to 0^+$, a development involving terms of the form $p^\alpha \ln^\beta p$, $\alpha, \beta \in \mathbb{N}$. With this hypothesis, it is shown in Appendix C that:

$$\hat{g}_{22}(p) = \frac{1}{4} + \frac{1-2\nu}{4}p^2 \ln p + \mathrm{O}(p^2) \tag{43}$$

$$\hat{g}_{33}(p) = -\frac{1}{4} - \frac{1+\nu}{4(1-\nu)}p^2 \ln p + \mathrm{O}(p^2) \tag{44}$$

$$\hat{g}_{23}(p) = \mathrm{i}\frac{\nu}{2(1-\nu)}p + \mathrm{i}\frac{\nu(\nu^2-2\nu+2)}{4(1-\nu)^2}p^3 \ln p + \mathrm{O}(p^3) \tag{45}$$

$$\widehat{F}_{22}(p) = -\frac{1-2\nu}{2}p \ln p + \mathrm{O}(p) \tag{46}$$

$$\widehat{F}_{33}(p) = -\frac{1+\nu}{2(1-\nu)}p \ln p + \mathrm{O}(p) \tag{47}$$

$$\widehat{F}_{23}(p) = \mathrm{i}\frac{2-\nu}{2(1-\nu)} + \mathrm{i}\frac{3\nu^2(2-\nu)}{4(1-\nu)^2}p^2 \ln p + \mathrm{O}(p^2) \tag{48}$$

for $p \to 0^+$.

4.4. Asymptotic behavior of $\widehat{F}_{22}(p)$, $\widehat{F}_{33}(p)$, $\widehat{F}_{23}(p)$, $\hat{g}_{22}(p)$, $\hat{g}_{33}(p)$, $\hat{g}_{23}(p)$ for $p \to +\infty$

For $p \to +\infty$, the set of Eqs. (33)–(38) approximately reads as follows:

$$\widehat{F}'_{mn} = 0, \quad \hat{g}_{mn} - \frac{\hat{g}''_{mn}}{4} = 0, \quad (m,n) = (2,2),(3,3),(2,3) \tag{49}$$

Eq. $(49)_1$ strongly suggests that the $\widehat{F}_{mn}(p)$ tend toward some finite limits for $p \to +\infty$. The determination of these limits, noted $\widehat{F}^{\infty}_{mn}$, is expounded in Appendix D. The results are as follows:

$$\widehat{F}^{\infty}_{22} = \frac{2-3\nu}{2(2-\nu)}, \quad \widehat{F}^{\infty}_{33} = \frac{2+\nu}{2(2-\nu)}, \quad \widehat{F}^{\infty}_{23} = \mathrm{i}\frac{2}{2-\nu} \tag{50}$$

Eq. $(49)_2$ shows that the $\hat{g}_{mn}(p)$ behave like $\mathrm{e}^{\pm 2p}$ for $p \to +\infty$. However, the increasing component e^{2p} is obviously physically inadmissible, so that the $\hat{g}_{mn}(p)$ must behave like e^{-2p}. Unfortunately, Eq. $(49)_2$ fails to provide the values of the pre-exponential factors here.

5. Determination of functions f_{22}, f_{33}, f_{23}, g_{22}, g_{33}, g_{23}

Prior to giving numerical results, we briefly discuss here how the functions f_{mn} and g_{mn} can be obtained from the $\widehat{F}_{mn}$ and $\hat{g}_{mn}$.

5.1. Inverse Fourier transform

The g_{mn} are readily deduced from the $\hat{g}_{mn}$ through Fourier inversion:

$$g_{mn}(z) = \frac{1}{2\pi}\int_{-\infty}^{+\infty} \hat{g}_{mn}(p)\mathrm{e}^{-\mathrm{i}pz}\,\mathrm{d}p = \frac{1}{\pi}\int_{0}^{+\infty} \hat{g}_{mn}(p)\cos pz\,\mathrm{d}p, \quad (m,n) = (2,2),(3,3) \tag{51}$$

$$g_{23}(z) = \frac{1}{2\pi}\int_{-\infty}^{+\infty} \hat{g}_{23}(p)\mathrm{e}^{-\mathrm{i}pz}\,\mathrm{d}p = -\frac{1}{\pi}\int_{0}^{+\infty} i\hat{g}_{23}(p)\sin pz\,\mathrm{d}p \tag{52}$$

where parity properties of the $\hat{g}_{mn}$ have been used.

Also, $\hat{f}_{mn} = \widehat{F}'_{mn}$, so that:

$$f_{mn}(z) = \frac{1}{2\pi}\int_{-\infty}^{+\infty} \widehat{F}'_{mn}(p)\mathrm{e}^{-\mathrm{i}pz}\,\mathrm{d}p = \frac{1}{\pi}\int_{0}^{+\infty} \widehat{F}'_{mn}(p)\cos pz\,\mathrm{d}p, \quad (m,n) = (2,2),(3,3) \tag{53}$$

$$f_{23}(z) = \frac{1}{2\pi}\int_{-\infty}^{+\infty} \widehat{F}'_{23}(p)\mathrm{e}^{-\mathrm{i}pz}\,\mathrm{d}p = -\frac{1}{\pi}\int_{0}^{+\infty} i\widehat{F}'_{23}(p)\sin pz\,\mathrm{d}p \tag{54}$$

where parity properties have again been used.

The functions f_{mn} and g_{mn} will be determined numerically from these formulae over some finite interval, say for $0 \leqslant z \leqslant z_{\infty}$, $z_{\infty} \gg 1$. For values of $z > z_{\infty}$, one may use the asymptotic expressions given below.

5.2. Asymptotic behavior of f_{22}, f_{33}, f_{23}, g_{22}, g_{33}, g_{23} for $z \to +\infty$

The derivation of these behaviors is a little complex and hence relegated to Appendix E. Only the final results are given below:

$$g_{22}(z) \sim \frac{1-2\nu}{4z^3}, \quad g_{33}(z) \sim -\frac{1+\nu}{4(1-\nu)z^3}, \quad g_{23}(z) \sim \frac{3\nu(\nu^2-2\nu+2)}{4(1-\nu)^2 z^4} \tag{55}$$

$$f_{22}(z) \sim \frac{1-2\nu}{4z}, \quad f_{33}(z) \sim \frac{1+\nu}{4(1-\nu)z}, \quad f_{23}(z) \sim -\frac{3\nu^2(2-\nu)}{4(1-\nu)^2 z^2} \tag{56}$$

6. Numerical procedure and results

6.1. Calculation of $\widehat{F}_{22}$, $\widehat{F}_{33}$, $\widehat{F}_{23}$, $\hat{g}_{22}$, $\hat{g}_{33}$, $\hat{g}_{23}$

As mentioned above, the set of differential equations (33)–(38) can be solved on any interval $[p_0, p_\infty]$ with $0 < p_0 \ll 1$ and $p_\infty \gg 1$, by integrating "forwards", from p_0 to p_∞, or "backwards", from p_∞ to p_0. Let us compare these two methods:

- Integrating "forwards" seems, a priori, more suitable since the values of the $\widehat{F}_{mn}(p_0)$, $\hat{g}_{mn}(p_0)$, $\hat{g}'_{mn}(p_0)$ are known (Eqs. (43)–(48)), in contrast to the precise asymptotic behavior of the $\hat{g}_{mn}(p)$ and $\hat{g}'_{mn}(p)$ for $p \to +\infty$. However, due to the behavior in $e^{\pm 2p}$ of the $\hat{g}_{mn}(p)$ at infinity, any (inevitable) numerical error in the initial conditions or the integration method will yield a spurious component in e^{2p} in the $\hat{g}_{mn}(p)$ that will quickly "blow up", thus prohibiting to reach large values of p.
- Hence the only possibility is to integrate "backwards". The values of the $\widehat{F}_{mn}(p_\infty)$, $\hat{g}_{mn}(p_\infty)$, $\hat{g}'_{mn}(p_\infty)$ are then needed, but only these of the $\widehat{F}_{mn}(p_\infty)$ are known (Eq. (50)). To determine those of the $\hat{g}_{mn}(p_\infty)$ and $\hat{g}'_{mn}(p_\infty)$, one can use a Newton method aimed at matching the values of the $\hat{g}_{mn}(p_0)$ and $\hat{g}'_{mn}(p_0)$ given by Eqs. (43)–(45). (One can show that the values obtained for the $\widehat{F}_{mn}(p_0)$ necessarily then match conditions (46)–(48).) This task is not straightforward because one must first find good "initial values" for the $\hat{g}_{mn}(p_\infty)$ and $\hat{g}'_{mn}(p_\infty)$ in the Newton method, ensuring convergence of the algorithm. Indeed, for many choices of these initial values, the functions diverge toward infinity when p approaches p_0, due to the singularity in $1/p$ of the differential equations.

In practice, the Runge–Kutta method of order four is used to integrate from $p_\infty = 50$ to $p_0 = 10^{-6}$ with an accuracy of 10^{-5}. The solutions obtained for $\nu = 0.1$ and $\nu = 0.3$ are given in Figs. 2–5.

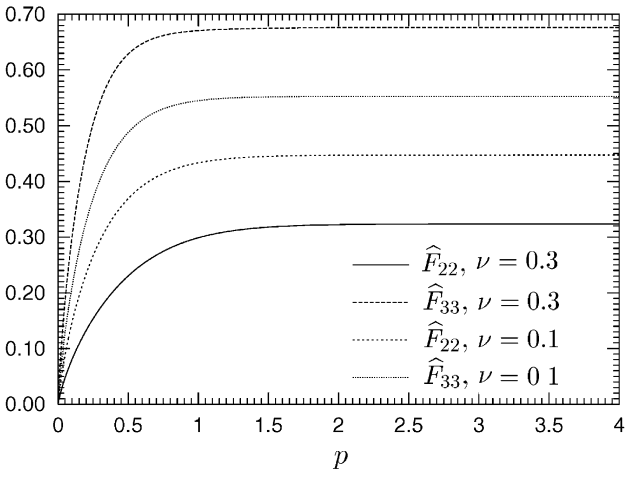

Fig. 2. Functions $\widehat{F}_{22}(p)$, $\widehat{F}_{33}(p)$.

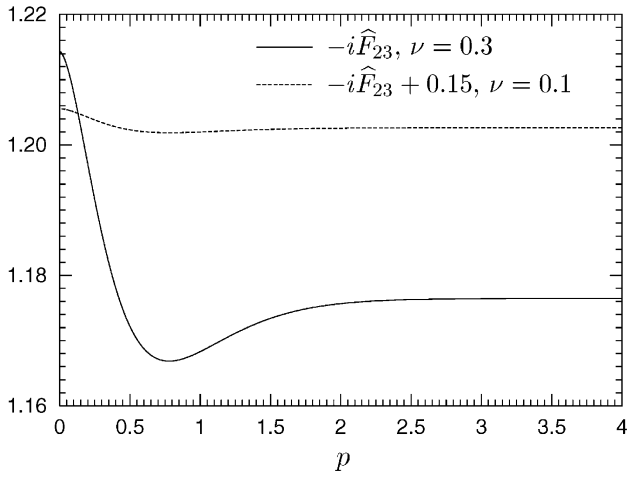

Fig. 3. Function $\widehat{F}_{23}(p)$.

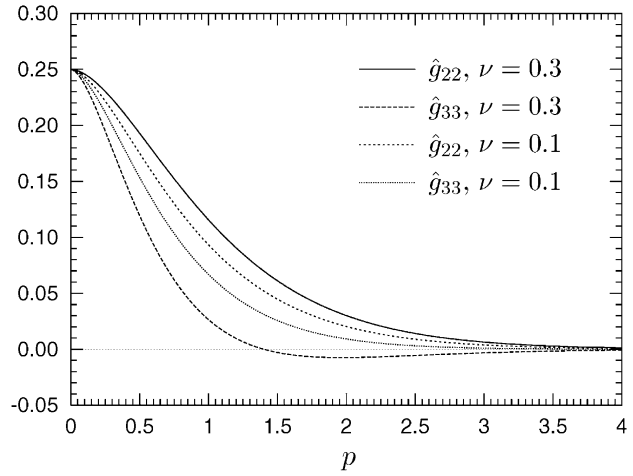

Fig. 4. Functions $\hat{g}_{22}(p)$, $\hat{g}_{33}(p)$.

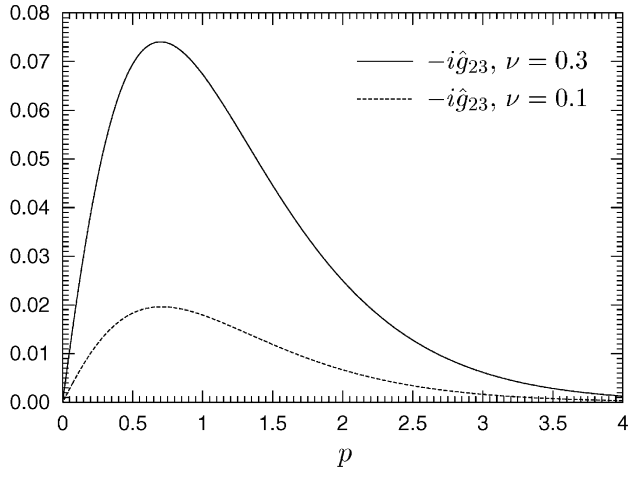

Fig. 5. Function $\hat{g}_{23}(p)$.

6.2. Calculation of $\bar{f}_{22}$, $\bar{f}_{33}$

Functions $\bar{f}_{22}$, $\bar{f}_{33}$ (in addition to $\hat{g}_{22}$, $\hat{g}_{33}$ and $\hat{g}_{23}$) were needed in Part I for the study of the bifurcation and stability problems. They are defined by Eq. (23) of Part I. One can easily show that $\bar{f}_{mn}(0) = 1/4$, $\bar{f}'_{mn} = -\widehat{F}_{mn}$, $(m,n) = (2,2), (3,3)$. Thus $\bar{f}_{22}$ and $\bar{f}_{33}$ can be obtained numerically through integration of $\widehat{F}_{22}$ and $\widehat{F}_{33}$. The results are given in Fig. 3 of Part I.

6.3. Calculation of operators **f** and **g**

It is recalled that the operators **f** and **g** are linked to the fundamental kernel **Z** by relations (1) and (2), that their components 11 are given in Leblond et al. (1996) and that their components 12, 21, 13, 31 are zero. The other components are obtained by using Eqs. (51)–(54) and (4). In practice, the integration interval $[0, +\infty)$ is replaced by the interval $[10^{-6}, 50]$, and calculations are performed for $z \in [0, 50]$. Functions f_{22}, f_{33}, f_{23} are presented in Figs. 6 and 7 for $z \in [0, 20]$, and functions g_{22}, g_{33}, g_{23} in Figs. 8 and 9 for $z \in [0, 6]$. Beyond these limits, the asymptotic expressions (55) and (56) are found to fit very well to the numerical results.

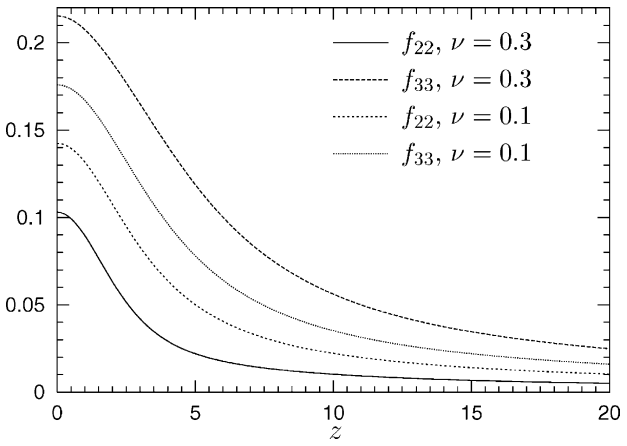

Fig. 6. Functions $f_{22}(z)$, $f_{33}(z)$.

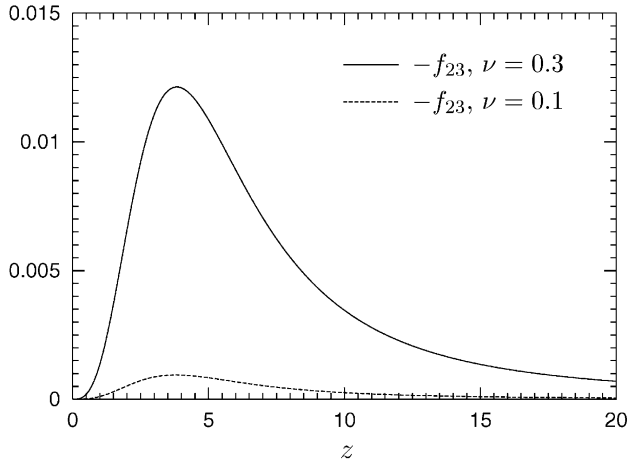

Fig. 7. Function $f_{23}(z)$.

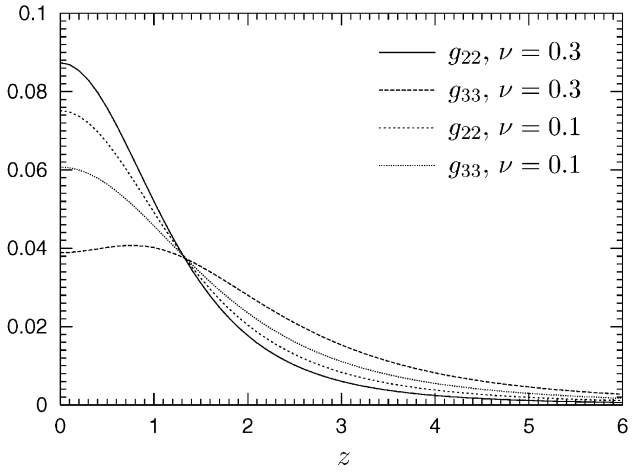

Fig. 8. Functions $g_{22}(z)$, $g_{33}(z)$.

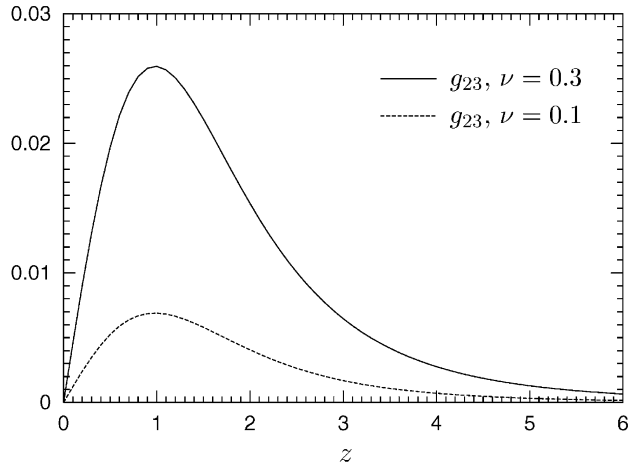

Fig. 9. Function $g_{23}(z)$.

One can observe that components 23 of operators **f** and **g**, which represent the coupling effect between modes 2 and 3, are all the smaller as Poisson's ratio v is low. Also, it is somewhat surprising that for $v = 0.3$, $g_{33}(z)$, which is tied to the 3rd SIF at point z^- of the rear part of the front when point forces $\pm\vec{e}_z$ are applied close to the point 0^+ of the fore part of the front, is *not* maximum for $z = 0$. Note, however, that a similar phenomenon is known to occur for the half-plane crack: the mode 3 SIF generated by point forces $\pm\vec{e}_z$ exerted on the crack faces is not maximum at that point of the crack front located closest to the points of application of the forces. Also, this effect can be observed to vanish for sufficiently small Poisson's ratios.

Appendix A. Justification of formulae (21), (22)

To calculate $\lim_{x\to 1}\int_{-\infty}^{+\infty} g_{mn}(z'-z)((k_{ni}(1;z'^{+};x,0))/(\sqrt{1-x}))z'\,\mathrm{d}z'$, split the integration domain $(-\infty,+\infty)$ into $(-\infty,-\eta)\cup(\eta,+\infty)$ and $[-\eta,\eta]$, η being a momentarily fixed arbitrary positive number. For $z'\in(-\infty,-\eta)\cup(\eta,+\infty)$, $((k_{ni}(1;z'^{+};x,0))/(\sqrt{1-x}))$ has a finite limit for $x\to 1$, equal to $k_{ni}(1;z'^{+};0^+)$ by definition, since the observation point z'^{+} of the SIF differs from the limit-points $(x=1,y=0^{\pm},z=0)$ of application of the point forces. Hence

$$\lim_{x\to 1}\int_{(-\infty,-\eta)\cup(\eta,+\infty)} g_{mn}(z'-z)\frac{k_{ni}(1;z'^{+};x,0)}{\sqrt{1-x}}z'\,\mathrm{d}z' = \int_{(-\infty,-\eta)\cup(\eta,+\infty)} g_{mn}(z'-z)k_{ni}(1;z'^{+};0^{+})z'\,\mathrm{d}z' \tag{A.1}$$

To evaluate the limit, for $x\to 1$, of the integral over $[-\eta,\eta]$, let us perform a first order Taylor expansion of the quantity $g_{mn}(z'-z)$ around the point $z'=0$:

$$\int_{-\eta}^{\eta} g_{mn}(z'-z)\frac{k_{ni}(1;z'^{+};x,0)}{\sqrt{1-x}}z'\,\mathrm{d}z' = g_{mn}(-z)\int_{-\eta}^{\eta}\frac{k_{ni}(1;z'^{+};x,0)}{\sqrt{1-x}}z'\,\mathrm{d}z' + \int_{-\eta}^{\eta}\mathrm{O}(z')\frac{k_{ni}(1;z'^{+};x,0)}{\sqrt{1-x}}z'\,\mathrm{d}z' \tag{A.2}$$

The examples of the semi-infinite crack, the penny-shaped crack and the tunnel-crack in mode 1 strongly suggest that $(k_{ni}(1;z'^{+};x,0)/\sqrt{1-x})$ is bounded by $Cst.z'^{-2}$ for $z'\to 0$. Therefore the integrand in the second term of the right-hand side of Eq. (A.2) is O(1), so that this equation may be rewritten as:

$$\int_{-\eta}^{\eta} g_{mn}(z'-z)\frac{k_{ni}(1;z'^{+};x,0)}{\sqrt{1-x}}z'\,\mathrm{d}z' = g_{mn}(-z)\int_{-\eta}^{\eta}\frac{k_{ni}(1;z'^{+};x,0)}{\sqrt{1-x}}z'\,\mathrm{d}z' + \mathrm{O}(\eta) \tag{A.3}$$

The integral in the right-hand side of (A.3) is zero if $k_{ni}(1;z'^{+};x,0)$ is even with respect to z', that is for $(n,i)=(2,x),(3,z)$. On the other hand, if $k_{ni}(1;z'^{+};x,0)$ is odd, i.e. for $(n,i)=(2,z),(3,x)$, one gets upon use of the homogeneity property of $k_{ni}(1;z'^{+};x,0)$ and the change of variable $z''=z'/(1-x)$:

$$\int_{-\eta}^{\eta}\frac{k_{ni}(1;z'^{+};x,0)}{\sqrt{1-x}}z'\,\mathrm{d}z' = \int_{-\eta/(1-x)}^{\eta/(1-x)} k_{ni}(1/(1-x);z''^{+};x/(1-x),0)z''\,\mathrm{d}z''$$

The $k_{ni}(1/(1-x);z''^{+};x/(1-x),0)$ are the weight functions of the tunnel-crack of width $2/(1-x)$ at point z''^{+} when the forces are applied at a distance $1/(1-x)-x/(1-x)=1$ from the fore part of the front. Since when $x\to 1$, this width becomes infinity, the $k_{ni}(1/(1-x);z''^{+};x/(1-x),0)$ behave as the weight functions of a half-plane crack when the forces are applied at a distance of unity from the front. Using the well-known expressions of these weight functions (see for instance Gao and Rice (1986)), one then gets for $(n,i)=(2,z),(3,x)$:

$$\lim_{x\to 1}\int_{-\eta/(1-x)}^{\eta/(1-x)} k_{ni}(1/(1-x);z''^{+};x/(1-x),0)z''\,\mathrm{d}z'' = \sqrt{\frac{1}{2\pi}}\frac{4v}{2-v}$$

It follows from these elements that (A.3) finally reads, in the limit $x\to 1$:

$$\lim_{x\to 1}\int_{-\eta}^{\eta} g_{mn}(z'-z)\frac{k_{ni}(1;z'^{+};x,0)}{\sqrt{1-x}}z'\,\mathrm{d}z' = \begin{cases}\mathrm{O}(\eta) & \text{if } (n,i)=(2,x) \text{ or } (3,z)\\ \sqrt{\frac{1}{2\pi}}\frac{4v}{2-v}g_{mn}(-z)+\mathrm{O}(\eta) & \text{if } (n,i)=(2,z) \text{ or } (3,x)\end{cases} \tag{A.4}$$

Combination of Eqs. (A.1) and (A.4), in the limit $\eta\to 0$, finally yields relations (21) and (22).

Appendix B. Calculation of some Fourier transforms

By definition, the symbol FT denoting the Fourier transform:

$$\begin{aligned}\mathrm{FT}\left[\mathrm{PV}\int_{-\infty}^{+\infty} g_{mn}(z-z')\frac{f_{rs}(z')}{z'}\mathrm{d}z'\right](p) &= \lim_{\eta\to 0}\int_{-\infty}^{+\infty}\mathrm{e}^{\mathrm{i}pz}\,\mathrm{d}z\int_{(-\infty,-\eta)\cup(\eta,+\infty)} g_{mn}(z-z')\frac{f_{rs}(z')}{z'}\mathrm{d}z'\\ (z''=z-z') &= \lim_{\eta\to 0}\int_{-\infty}^{+\infty} g_{mn}(z'')\mathrm{e}^{\mathrm{i}pz''}\,\mathrm{d}z''.\int_{(-\infty,-\eta)\cup(\eta,+\infty)}\frac{f_{rs}(z')}{z'}\mathrm{e}^{\mathrm{i}pz'}\,\mathrm{d}z'\\ &\quad\times\hat{g}_{mn}(p)\mathrm{PV}\int_{-\infty}^{+\infty}\frac{f_{rs}(z)}{z}\mathrm{e}^{\mathrm{i}pz}\,\mathrm{d}z\end{aligned} \tag{B.1}$$

Now,

$$\frac{\mathrm{d}}{\mathrm{d}p}\mathrm{PV}\int_{-\infty}^{+\infty}\frac{f_{rs}(z)}{z}\mathrm{e}^{\mathrm{i}pz}\,\mathrm{d}z=\int_{-\infty}^{+\infty}f_{rs}(z)\mathrm{i}\mathrm{e}^{\mathrm{i}pz}\,\mathrm{d}z=\mathrm{i}\hat{f}_{rs}(p)\Rightarrow\mathrm{PV}\int_{-\infty}^{+\infty}\frac{f_{rs}(z)}{z}\mathrm{e}^{\mathrm{i}pz}\,\mathrm{d}z$$
$$=\mathrm{i}\int_0^p\hat{f}_{rs}(q)\mathrm{d}q+\mathrm{PV}\int_{-\infty}^{+\infty}\frac{f_{rs}(z)}{z}\,\mathrm{d}z \tag{B.2}$$

Now, for $(r,s)=(2,2)$ or $(3,3)$, f_{rs} is even. Eqs. (B.1) and (B.2) then yield:

$$\mathrm{FT}\left[\mathrm{PV}\int_{-\infty}^{+\infty}g_{mn}(z-z')\frac{f_{rs}(z')}{z'}\mathrm{d}z'\right](p)=i\,\hat{g}_{mn}(p)\,\widehat{F}_{rs}(p), \tag{B.3}$$

$$\widehat{F}_{rs}(p)\equiv\int_0^p\hat{f}_{rs}(q)\,\mathrm{d}q \tag{B.4}$$

for $(r,s)=(2,2)$, $(3,3)$.

Similarly, for $(r,s)=(2,3)$, Eqs. (B.1) and (B.2) yield:

$$\mathrm{FT}\left[\int_{-\infty}^{+\infty}g_{mn}(z-z')\frac{f_{23}(z')}{z'}\mathrm{d}z'\right](p)=\hat{g}_{mn}(p)\left[i\int_0^p\hat{f}_{23}(q)\,\mathrm{d}q+\int_{-\infty}^{+\infty}\frac{f_{23}(z)}{z}\mathrm{d}z\right]$$

But $\int_{-\infty}^{+\infty}(f_{23}(z)/z)\,\mathrm{d}z$ is given by Eq. (17) of Part I. Thus,

$$\mathrm{FT}\left[\int_{-\infty}^{+\infty}g_{mn}(z-z')\frac{f_{23}(z')}{z'}\mathrm{d}z'\right](p)=\hat{g}_{mn}(p)\left[\mathrm{i}\widehat{F}_{23}(p)+\frac{2}{2-v}\right], \tag{B.5}$$

$$\widehat{F}_{23}(p)\equiv\int_0^p\hat{f}_{23}(q)\,\mathrm{d}q+\mathrm{i}\frac{2-v}{2(1-v)} \tag{B.6}$$

The choice of the additive constant $\mathrm{i}((2-v)/(2(1-v)))$ in the definition of $\widehat{F}_{23}$ here was made in order to simplify the differential equations (33)–(38) as much as possible.

Appendix C. Determination of the asymptotic behavior of $\widehat{F}_{22}(p)$, $\widehat{F}_{33}(p)$, $\widehat{F}_{23}(p)$, $\hat{g}_{22}(p)$, $\hat{g}_{33}(p)$, $\hat{g}_{23}(p)$ for $p\to 0^+$

It is assumed that $\hat{g}_{22}(p)$, $\hat{g}_{33}(p)$, $\hat{g}_{23}(p)$ admit, for $p\to 0^+$, expansions involving terms of the form $p^\alpha\ln^\beta p$ ($\alpha,\beta\in\mathbb{N}$). By Eqs. (41) and (42), these expansions read

$$\hat{g}_{22}(p)=1/4+a_2p^2\ln^{\beta_2}p+\mathrm{O}(p^2\ln^{\beta_2-1}p) \tag{C.1}$$

$$\hat{g}_{33}(p)=-1/4+a_3p^2\ln^{\beta_3}p+\mathrm{O}(p^2\ln^{\beta_3-1}p) \tag{C.2}$$

$$\hat{g}_{23}(p)=\mathrm{i}\frac{v}{2(1-v)}p+a_4p^3\ln^{\beta_4}p+\mathrm{O}(p^3\ln^{\beta_4-1}p) \tag{C.3}$$

The absence of a term of the form $p^2\ln^\beta p$ in $\hat{g}_{23}(p)$ here can be checked to be compatible with the differential equations (33)–(38).

Inserting these equations into the set of differential equations (33)–(38) and identifying principal terms, one first gets

$$\beta_2=\beta_3=\beta_4=1 \tag{C.4}$$

To next determine the constants a_2, a_3, a_4, one must consider the terms proportional to p^2 in the expansions of $\hat{g}_{22}(p)$ and $\hat{g}_{33}(p)$, since the derivatives of both expressions $p^2 \ln p$ and p^2 involve terms of the same order p. Thus, let us write these expansions in the form

$$\hat{g}_{22}(p) = 1/4 + a_2 p^2 \ln p + b_2 p^2 + \mathrm{O}(p^3 \ln^{\gamma_2} p)$$

$$\hat{g}_{33}(p) = -1/4 + a_3 p^2 \ln p + b_3 p^2 + \mathrm{O}(p^3 \ln^{\gamma_3} p)$$

Eqs. (33)–(35) then yield, account being taken of (39):

$$\widehat{F}_{22}(p) = -2a_2 p \ln p - \left(2b_2 - a_2 + \frac{v^2}{1-v}\right)p + \mathrm{O}(p^2 \ln^{\gamma_2} p) \tag{C.5}$$

$$\widehat{F}_{33}(p) = 2a_3 p \ln p + \left(2b_3 - a_3 - \frac{v^2}{1-v}\right)p + \mathrm{O}(p^2 \ln^{\gamma_3} p) \tag{C.6}$$

$$\widehat{F}_{23}(p) = \mathrm{i}\frac{2-v}{2(1-v)} - \mathrm{i}\frac{3v}{2(1-v)}(a_2 + a_3)p^2 \ln p + \mathrm{O}(p^2) \tag{C.7}$$

Inserting these expressions into (36)–(38), we finally get, after a long but straightforward calculation, by identifying terms of identical order:

$$a_2 = \frac{1-2v}{4}, \quad a_3 = -\frac{1+v}{4(1-v)}, \quad a_4 = \mathrm{i}\frac{v(v^2-2v+2)}{4(1-v)^2} \tag{C.8}$$

Although the introduction of coefficients b_2, b_3 in the reasoning was necessary for the reason explained above, they are found to finally cancel out in the calculation, which therefore fails to yield their values.

Eqs. (C.1)–(C.4) and (C.8) justify Eqs. (43)–(45) of the text, and Eqs. (C.5)–(C.8) justify Eqs. (46)–(48).

Appendix D. Determination of constants $\widehat{F}_{22}^{\infty}$, $\widehat{F}_{33}^{\infty}$, $\widehat{F}_{23}^{\infty}$

Eqs. (B.2) and (B.4) yield, since f_{22} is an even function:

$$\widehat{F}_{22}^{\infty} \equiv \lim_{p\to+\infty} \widehat{F}_{22}(p) = \lim_{p\to+\infty} 2\int_0^{+\infty} \frac{\sin pz}{z} f_{22}(z)\,\mathrm{d}z$$

$$\overset{pz\equiv u}{=} \lim_{p\to+\infty} 2\int_0^{+\infty} \frac{\sin u}{u} f_{22}(u/p)\,\mathrm{d}u = \pi f_{22}(0)$$

It then follows from Eq. (7) of Part I that:

$$\widehat{F}_{22}^{\infty} = \frac{2-3v}{2(2-v)} \tag{D.1}$$

A similar reasoning for $\widehat{F}_{33}$ yields:

$$\widehat{F}_{33}^{\infty} = \frac{2+v}{2(2-v)} \tag{D.2}$$

Finally, Eqs. (B.2), (B.6) and (17) of Part I yield, since f_{23} is odd:

$$\widehat{F}_{23}^{\infty} \equiv \lim_{p\to+\infty} \widehat{F}_{23}(p) = -\lim_{p\to+\infty} 2\mathrm{i}\int_0^{+\infty} \frac{f_{23}(z)}{z}\cos pz\,\mathrm{d}z + \mathrm{i}\frac{2}{2-v}$$

Now Riemann–Lebesgue's theorem, applied to the function $(f_{23}(z)/z)$ (which is regular at $z = 0$ since f_{23} is odd), implies that the limit here is 0. The value of $\widehat{F}_{23}^{\infty}$ follows:

$$\widehat{F}_{23}^{\infty} = \mathrm{i}\frac{2}{2-\nu} \tag{D.3}$$

Appendix E. Determination of the asymptotic behavior of $f_{22}(z)$, $f_{23}(z)$, $f_{33}(z)$, $g_{22}(z)$, $g_{23}(z)$, $g_{33}(z)$ for $z \to +\infty$

These asymptotic behaviors can be deduced from those of $\widehat{F}_{22}(p)$, $\widehat{F}_{33}(p)$, $\widehat{F}_{23}(p)$, $\hat{g}_{22}(p)$, $\hat{g}_{33}(p)$, $\hat{g}_{23}(p)$ for $p \to 0^+$. Indeed, with regard to $\hat{g}_{22}(p)$ for instance, repeated integration by parts of Eq. (51) yields:

$$\begin{aligned} g_{22}(z) &= \frac{1}{\pi}\left[\hat{g}_{22}(p)\frac{\sin pz}{z}\right]_0^{+\infty} - \frac{1}{\pi}\int_0^{+\infty}\hat{g}'_{22}(p)\frac{\sin pz}{z}\,\mathrm{d}p \\ &= \frac{1}{\pi z}\left[\hat{g}'_{22}(p)\frac{\cos pz}{z}\right]_0^{+\infty} - \frac{1}{\pi z}\int_0^{+\infty}\hat{g}''_{22}(p)\frac{\cos pz}{z}\,\mathrm{d}p \\ &= -\frac{1}{\pi z^2}\left[\hat{g}''_{22}(p)\frac{\sin pz}{z}\right]_0^{+\infty} + \frac{1}{\pi z^2}\int_0^{+\infty}\hat{g}'''_{22}(p)\frac{\sin pz}{z}\,\mathrm{d}p = \frac{1}{\pi z^4}\int_0^{+\infty}\hat{g}'''_{22}(u/z)\sin u\,\mathrm{d}u \quad (pz \equiv u) \end{aligned}$$

The bracketed terms here vanish because of the behavior of $\hat{g}_{22}$ near 0^+ and $+\infty$ (see Sections 4.2 and 4.4). Now Eq. (43) implies that for $p \to 0^+$,

$$\hat{g}'''_{22}(p) \sim \frac{1-2\nu}{2p}$$

Insertion of this result into the preceding expression yields:

$$g_{22}(z) \sim \frac{1-2\nu}{4z^3} \text{ for } z \to +\infty$$

References

Bueckner, H.F., 1987. Weight functions and fundamental fields for the penny-shaped and the half-plane crack in three-space. International Journal of Solids and Structures 23 (1), 57–93.

Gao, H., 1988. Nearly circular shear mode cracks. International Journal of Solids and Structures 24 (2), 177–193.

Gao, H., Rice, J.R., 1986. Shear stress intensity factors for planar crack with slightly curved front. ASME Journal of Applied Mechanics 53 (4), 774–778.

Gao, H., Rice, J.R., 1987a. Nearly circular connections of elastic half spaces. ASME Journal of Applied Mechanics 54 (4), 627–634.

Gao, H., Rice, J.R., 1987b. Somewhat circular tensile cracks. International Journal of Fracture 33 (3), 155–174.

Kassir, M.K., Sih, G., 1975. Three Dimensional Crack Problems. Nordhoff International Publishing, Leyden, The Netherlands.

Lazarus, V., Leblond, J.-B., 1998. Three-dimensional crack-face weight functions for the semi-infinite interface crack. II. Integrodifferential equations on the weight functions and resolution. Journal of the Mechanics and Physics of Solids 46 (3), 513–536.

Leblond, J.-B., Lazarus, V., Mouchrif, S.-E., 1999. Crack paths in three-dimensional elastic solids. II. Three-term expansion of the stress intensity factors—Applications and perspectives. International Journal of Solids and Structures 36 (1), 105–142.

Leblond, J.-B., Mouchrif, S.-E., Perrin, G., 1996. The tensile tunnel-crack with a slightly wavy front. International Journal of Solids and Structures 33 (14), 1995–2022.

Meade, K.P., Keer, L.M., 1984. On the problem of a pair of point forces applied to the faces of a semi-infinite plane crack. Journal of Elasticity 14 (1), 3–14.

Rice, J.R., 1985. First-order variation in elastic fields due to variation in location of a planar crack front. ASME Journal of Applied Mechanics 52 (3), 571–579.

Stallybrass, M., 1981. On the concentrated loading of certain elastic half-space problems and related external crack problems. A new approach. International Journal of Engineering Science 19 (8), 1123–1144.

Tada, H., Paris, P.C., Irwin, G.R., 1973. The Stress Analysis of Cracks Handbook. Del Research Corporation, Hellertown, USA.

International Journal of Fracture **122:** 23–46, 2003.

Brittle fracture and fatigue propagation paths of 3D plane cracks under uniform remote tensile loading

VÉRONIQUE LAZARUS
Laboratoire de Modélisation en Mécanique, Université Pierre et Marie Curie, Boîte 162, 4 Place Jussieu, 75252 Paris Cedex 05, France; e-mail: vlazarus@ccr.jussieu.fr

Received 31 October 2002; accepted in revised form 18 August 2003

Abstract. Fatigue and brittle fracture propagation paths of arbitrary plane cracks, loaded in mode I, embedded in an infinite isotropic elastic body, are investigated. The crack advance is supposed to be governed by the stress intensity factor, for instance through Paris' law in fatigue or Irwin's criterion in brittle fracture. The method used is based on successive iterations of the three-dimensional weight-function theory of Bueckner-Rice, that gives the variation of the stress intensity factor along the crack front arising from some small arbitrary coplanar perturbation of the front. Its main advantage is that only one dimensional integrals along the crack front are involved so that only the one dimensional meshing of the crack front is needed, and not the 3D meshing of the whole body as in the finite-element method. It is closely linked to previous works of Bower and Ortiz (1990, 1991, 1993). The differences lie on the one hand, in the simplified numerical implementation; on the other hand, in the simplified treatment of brittle fracture, Irwin's criterion being regularized by Paris' law by a procedure analogous to the 'viscoplastic regularization' in plasticity; and finally in the applications studied: propagation paths of an initially elliptical, rectangular or heart shaped crack in an homogeneous media and of a penny shape crack in an heterogeneous one.

Key words: Linear elasticity, stress intensity factor, mode I crack, tridimensional, weight function, plane/flat crack, perturbation method, angular point, fatigue, brittle fracture, propagation path, hydraulic fracturing.

1. Introduction

Let us consider a plane crack, such as the one depicted in Figure 1, contained in plane (O, x, z) with arbitrary contour $\mathcal{F}$, embedded in an infinite isotropic elastic body. The aim of this paper is to study the in-plane propagation path of this crack when it is subjected to mode I loading by uniform tensile stress σ_∞ at infinity in both fatigue and brittle fracture. For instance, this model may be of practical interest for the study of hydraulic fracturing problems. In fatigue, the crack propagation rate is supposed to be given by Paris' law; in brittle fracture, by Irwin's criterion. Hence the determination of the stress intensity factor along the front for all the stages of propagation is necessary. A classical method would be to use the finite element method but then a three-dimensional meshing of the body at each step of propagation is necessary. This may be very tedious if the propagation is studied over a long distance. Nevertheless, recently Sukumar et al. (2000), Stolarska et al. (2001), Sukumar et al. (2003) by coupling the level set method and the eXtended FEM for three-dimensional crack problems have limited the meshing operations to that of the initial three dimensional geometry. An other possibility is to use surface integral formulations as in Fares (1989) or Xu and Ortiz (1993). Two dimensional meshings of the crack surfaces are then necessary. Here an alternative method is used whose further advantage is to restrict the meshing operations to that of the one-dimensional initial

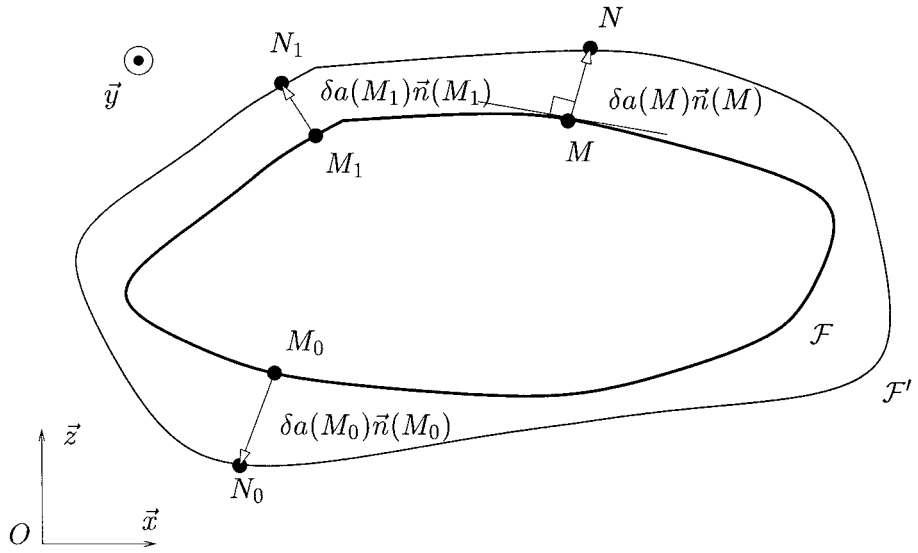

Figure 1. Arbitrary plane tensile crack and small (magnified on the figure for the sake of visibility) inplane perturbation of its crack front $\mathcal{F}$.

crack front. It is based on the three-dimensional weight-function theory derived by Rice (1985, 1989) and first adapted for numerical purposes by Bower and Ortiz (1990).

This three-dimensional theory is the extension of the bidimensional weight-function theory introduced by Bueckner (1970) and Rice (1972). The variation of the stress intensity factor along the crack front arising from some small arbitrary coplanar perturbation of the front is given by an integral along the initial front involving among other simple geometrical quantities, a function W linked to the weight-function. This variation was first derived by Rice (1985) for the half-plane crack, then by Gao and Rice (1987a) for the circular connection and Gao and Rice (1987b) for the penny-shaped crack. In all these papers, the weight-function of the initial crack was known and thus function W appears in the variation of the SIF in an explicit form. Finally Rice (1989) generalized these works to the case of any planar crack; in addition to the variation of the SIF, he gave the variation of the function W arising from the same coplanar perturbation, also in the form of an integral along the initial front.

In the previous mentioned papers, Gao and Rice applied the theory to small perturbations of the crack front. Bower and Ortiz (1990) extended the method to the study of arbitrary large perturbations of the front leading the way to the numerical resolution of some complex three-dimensional crack problems. It consists in applying numerically the three-dimensional weight-function theory to a succession of small perturbations arising in arbitrary large ones. As applications, they studied several problems involving half plane cracks propagating through heterogeneous media: fatigue crack propagating through a particle, crack trapped by an array of particles in brittle fracture, and crack growing through a material of decreasing toughness. Bower and Ortiz (1991) performed a more precise study of crack trapping and bridging by tough particles based on the same method. Bower and Ortiz (1993) extended the method to cracks loaded by non uniform remote stresses.

The aim of this paper is to study fatigue and brittle propagation paths under uniform remote loading by using the same method as Bower and Ortiz (1990). However, the originality of our work lies in three facets. First, the numerical implementation is different and notably

simplified. Secondly, for brittle fracture, a formulation is proposed that gives the advance of the crack front in *explicit* form once the stress intensity factor is known and so avoids the inversion of heavily *implicit* systems of equations as the ones used in Bower and Ortiz (1990, 1991, 1993). And finally, the originality lies in the applications studied: the asymptotic behavior of the SIF near an angular point of the front, the fatigue and brittle propagation paths of some special crack shapes (elliptical, rectangular, heart shaped ones) in an homogeneous material, brittle fracture of a penny shaped crack in a material with heterogeneous toughness. In homogeneous materials, it appears that in all the cases studied, the crack becomes circular after a certain time and that it advances slightly faster in fatigue and for a slightly lower loading in brittle fracture, than the penny-shaped one. In materials of heterogeneous toughness, the circular crack first propagates at points where the tenacity is lower. Then either, the SIF at the other points increases to attain themselves the threshold so that the crack front shape reaches a stable configuration for which the SIF equals the tenacity along all the front, or there exists some points of the front where the SIF decreases so that the tenacity is never attained and the crack front propagates by changing continuously its shape. It appears in the examples studied, that a stable crack front shape configuration is always reached.

2. Principle of the method

2.1. Bueckner-Rice weight function theory

Let us denote $K_{\mathcal{F}}(M)$ the SIF at point M of the crack front $\mathcal{F}$ when the body is subjected to uniform tensile stress σ_∞ at infinity and write, to separate the contributions of the loading and of the geometry:

$$K_{\mathcal{F}}(M) = \sigma_\infty \widehat{K}_{\mathcal{F}}(M). \tag{1}$$

Then, by linearity, $\widehat{K}_{\mathcal{F}}(M)$ corresponds to the SIF with loading unity at infinity and hence depends only on the geometry of the crack front $\mathcal{F}$.

Let us suppose now that the crack geometry is slightly perturbed in its plane, that is that the crack front advances, by a small distance $\delta a(M)$ in the direction perpendicular to the front $\mathcal{F}$ like in Figure 1. Rice (1989) has shown that to first order in δa, the SIF $\widehat{K}_{\mathcal{F}'}(N_0)$ at point N_0 of the new front $\mathcal{F}'$ defined by

$$\overrightarrow{M_0N_0} = \delta a(M_0)\vec{n}(M_0), \tag{2}$$

is given by $\widehat{K}_{\mathcal{F}}(M_0) + \delta\widehat{K}_{\mathcal{F}}(M_0)$ where

$$\delta\widehat{K}_{\mathcal{F}}(M_0) = \frac{1}{2\pi} PV \int_{\mathcal{F}} \frac{W_{\mathcal{F}}(M, M_0)}{D^2(M, M_0)} \widehat{K}_{\mathcal{F}}(M)[\delta a(M) - \delta_* a(M)]\mathrm{d}s(M). \tag{3}$$

In this expression, $s(M)$ is some curvilinear abscissa along the crack front, $D(M, M_0)$ is the distance between the points M and M_0, $W_{\mathcal{F}}(M, M_0)$ is a two-variable function linked to the weight function of the crack $\mathcal{F}$, more exactly to the SIF at the point M of $\mathcal{F}$ induced by unit point forces exerted on the point M' of the crack lips in the direction $\pm\vec{y}$, when M' approaches M_0 (see Rice, 1989 for the exact definition). $W_{\mathcal{F}}$ depends only on the crack geometry $\mathcal{F}$ and not on the loading. The quantity $\delta_* a(M)$ will be described further.

The function $W_{\mathcal{F}'}$ along the new crack front $\mathcal{F}'$ can be itself updated as $W_{\mathcal{F}'}(N_0, N_1) = W_{\mathcal{F}}(M_0, M_1) + \delta W_{\mathcal{F}}(M_0, M_1)$ where the variation of $W_{\mathcal{F}}$ is given, also to first order in δa, by:

$$\delta W_{\mathcal{F}}(M_0, M_1) = \frac{D^2(M_0, M_1)}{2\pi} PV \int_{\mathcal{F}} \frac{W_{\mathcal{F}}(M, M_0)\, W_{\mathcal{F}}(M, M_1)}{D^2(M, M_0)\, D^2(M, M_1)} [\delta a(M) - \delta_{**} a(M)] \mathrm{d}s(M). \tag{4}$$

Formulae (3) and (4) are legitimate for special normal advances $\delta_* a(M)$ and $\delta_{**} a(M)$ that preserve the shape of the front and such that $\delta_* a(M_0) = \delta a(M_0)$, $\delta_{**} a(M_0) = \delta a(M_0)$ and $\delta_{**} a(M_1) = \delta a(M_1)$ so as to ensure the existence of the integrals in Principal Value (PV). It can easily be shown, that one can always define a unique transformation, combination of translation, rotation and scaling that verifies all these conditions. It yields:

$$\delta_* a(M) = \delta a(M_0) \overrightarrow{n}(M_0).\overrightarrow{n}(M) \tag{5}$$

and

$$\delta_{**} a(M) = \frac{1}{2}\left((\overline{z' - z}) z_n + (z' - z)\overline{z_n}\right) \tag{6}$$

with,

$$z' = \frac{z'_0(z_1 - z) + z'_1(z - z_0)}{z_1 - z_0}, \tag{7}$$

where z, z_0, z_1, are the affixes[1] of points M, M_0, M_1; z'_0, z'_1, the affixes of points N_0, N_1; z_n the affix of the normal vector $\overrightarrow{n}(M)$, $\overline{z}$ the complex conjugate of z.

Suppose now that the SIF $\widehat{K}_{\mathcal{F}}$ and the function $W_{\mathcal{F}}$ are known for a given front $\mathcal{F}$. Since the quantities in the right-hand side of Equations (3) and (4) concern only the front $\mathcal{F}$, this theory allows to calculate the SIF $\widehat{K}_{\mathcal{F}'}$ and function $W_{\mathcal{F}'}$ along any crack front $\mathcal{F}'$ close to $\mathcal{F}$.

Numerically, one can repeat this procedure to any succession of crack fronts very close to each other. This can be applied to:

- the determination of the SIF and the function W along some arbitrary crack front (stage denoted *step I* in the sequel), starting from some crack shape for which they are known,
- the determination of the propagation path of any arbitrary crack (stage denoted *step II* in the sequel), the initial crack being that corresponding to the end of step I.

Instead of working on the couple of functions $\widehat{K}_{\mathcal{F}}$ and $W_{\mathcal{F}}$, Bower and Ortiz (1990, 1991, 1993) have worked with the couple of functions $\widehat{K}_{\mathcal{F}}$ and $W_{\mathcal{F}}/D$. The expression replacing Equation (4), giving $\delta(W_{\mathcal{F}}/D)$ is however a little more complicated since, in addition to the PV integral term, a supplementary term due to the normal advance $\delta_{**} a(M)$ then appears. This term is zero in Equation (4) since $W_{\mathcal{F}}$ is homogeneous of degree 0, hence is not changed by any scaling, that is by the composition of translation, rotation, scaling defining $\delta_{**} a(M)$. But this term is not zero for $\delta(W_{\mathcal{F}}/D)$ since D homogeneous of degree 2 is changed by any scaling hence for the normal advance $\delta_{**} a(M)$.

2.2. Step I: Determination of the SIF $\widehat{K}_{\mathcal{F}}$ and of the function $W_{\mathcal{F}}$ along some arbitrary crack front $\mathcal{F}$

Consider any crack front $\mathcal{F}$ subjected to uniform remote loading σ_∞. To determine the SIF and the function W along this front, one may proceed as follows:

1. Take as starting point a crack front $\mathcal{C}$ for which functions $\widehat{K}_{\mathcal{C}}(M)$ and $W_{\mathcal{C}}(M, M_0)$ are known and as close as possible to the front $\mathcal{F}$ studied.
2. Construct a succession of intermediate cracks very close to each other $\mathcal{F}_k$, $k = 0 \ldots n$, such that $\mathcal{F}_0 = \mathcal{C}$ and $\mathcal{F}_n = \mathcal{F}$, between $\mathcal{C}$ and $\mathcal{F}$.

3. Apply Equations (3) and (4) iteratively between $\mathcal{F}_k$ and $\mathcal{F}_{k+1}$, for $k = 0$ to $n-1$ to obtain the SIF $\widehat{K}_{\mathcal{F}_k}$ and the function $W_{\mathcal{F}_k}$ for $k = 1$ to n hence finally along the desired front $\mathcal{F}_n = \mathcal{F}$.

In practice, the SIF $\widehat{K}$ and the function W are known in a simple form only for some simple geometries: the half-plane crack (see for instance, Meade and Keer, 1984), the circular internal (see for instance, Tada et al., 1973) and external cracks (see for instance, Stallybrass, 1981) and the tunnel-crack (see Leblond et al., 1996). In the examples studied by Bower and Ortiz (1990, 1991, 1993) the half plane crack has been taken as starting point. The examples studied in the present paper can all be derived from circular internal ones $\mathcal{C}$ for which $\widehat{K}_{\mathcal{C}}(M) = 2\sqrt{R/\pi}$ and $W_{\mathcal{C}}(M, M_0) = 1$ where R denotes the radius of the crack (see for instance, Rice, 1989). Examples derived from the tunnel-crack are left for further work.

2.3. Step II: Determination of the propagation path of any arbitrary crack

One can now study crack propagation from that configuration corresponding to the end of step I. For numerical purposes, the crack advance is described stepwise each time that the maximum of the crack advance equal a given small quantity $\delta a_{\max}$. Let us consider the crack front in the position $\mathcal{F}$ and denote $\delta a_{\mathcal{F}}(M)$ the normal advance of the point M corresponding to one such step.

Suppose that the crack advance is governed by the SIF hence that $\delta a_{\mathcal{F}}(M)$ can be expressed as a function of the SIF along the front by a law of the form:

$$\delta a_{\mathcal{F}}(M) = \delta a_{\max} \mathcal{L}_M \left(\widehat{K}_{\mathcal{F}}(N), N \in \mathcal{F}\right) \text{ with } \mathcal{L}_M \left(\widehat{K}_{\mathcal{F}}(N), N \in \mathcal{F}\right) \leq 1 \tag{8}$$

Then, once the SIF $\widehat{K}_{\mathcal{F}}$ and function $W_{\mathcal{F}}$ are known for a given front $\mathcal{F}$, one can determine the propagation path of this crack by

1. applying law (8) to determine the displacement $\delta a_{\mathcal{F}}(M)$ of the front $\mathcal{F}$ and update its position,
2. using equations (3) and (4) to update the SIF $\widehat{K}_{\mathcal{F}}$ and function $W_{\mathcal{F}}$,
3. repeat, as many times as required, the two preceding operations to the new fronts obtained.

Examples of propagation laws (8) are given in Sections 2.4 for fatigue and 2.5 for brittle fracture.

2.4. Propagation law in fatigue

The crack is now subjected to some uniform and constant cyclic loading of amplitude $\Delta\sigma_\infty$. Suppose that the crack propagation rate $\frac{\mathrm{d}a(M)}{\mathrm{d}n_c}$, n_c denoting the number of loading cycles, at the point M of the front $\mathcal{F}$ is given by Paris' law, that is

$$\frac{\mathrm{d}a(M)}{\mathrm{d}n_c} = C(M)\,[\Delta K(M)]^{\beta(M)}\,, \tag{9}$$

where $\Delta K(M)$ is the amplitude of the SIF at the point M. By Equation (1),

$$\Delta K(M) = \Delta\sigma_\infty \widehat{K}(M). \tag{10}$$

$C(M)$ and $\beta(M)$ are material constants that depend on point M if the fracture properties of the material are heterogenous.

Now, consider the front at a given position $\mathcal{F}$ and suppose that during the advance $\delta a_{\mathcal{F}}(M)$ defined in the previous Section 2.3, $\widehat{K}(M)$ can be considered as constant equal to $\widehat{K}_{\mathcal{F}}(M)$. Then using (10) and integrating equation (9), one gets:

$$\delta a_{\mathcal{F}}(M) = n_c\, C(M) \Delta\sigma_{\infty}^{\beta(M)} \widehat{K}_{\mathcal{F}}(M)^{\beta(M)}, \tag{11}$$

where n_c is the number of cycles necessary to have $\max\limits_{M\in\mathcal{F}} \delta a_{\mathcal{F}}(M) = \delta a_{\max}$; by (11), this number is given by:

$$n_c = \frac{\delta a_{\max}}{\max\limits_{M\in\mathcal{F}} \left(C(M) \Delta\sigma_{\infty}^{\beta(M)} \widehat{K}_{\mathcal{F}}(M)^{\beta(M)} \right)}. \tag{12}$$

Notice, that since $C(M)\Delta\sigma_{\infty}^{\beta(M)} \widehat{K}_{\mathcal{F}}(M)^{\beta(M)}$ depends on the front position $\mathcal{F}$, n_c may change during propagation.

By introducing equation (12) into (11), it is easy to show that (11) can be written in the generic form (8) with:

$$\mathcal{L}_M \left(\widehat{K}_{\mathcal{F}}(N), N \in \mathcal{F} \right) = \frac{C(M) \Delta\sigma_{\infty}^{\beta(M)} \widehat{K}_{\mathcal{F}}(M)^{\beta(M)}}{\max\limits_{N\in\mathcal{F}} \left(C(N) \Delta\sigma_{\infty}^{\beta(N)} \widehat{K}_{\mathcal{F}}(N)^{\beta(N)} \right)}. \tag{13}$$

If $C(M) = Cst. \equiv C$ and $\beta(M) = Cst. \equiv \beta$, this simplifies into:

$$\mathcal{L}_M \left(\widehat{K}_{\mathcal{F}}(N), N \in \mathcal{F} \right) = \left(\frac{\widehat{K}_{\mathcal{F}}(M)}{\max\limits_{N\in\mathcal{F}} \widehat{K}_{\mathcal{F}}(N)} \right)^{\beta}. \tag{14}$$

2.5. Propagation law in brittle fracture

In brittle fracture, it is assumed that the propagation law is given by Irwin's criterion:

$$\begin{cases} \delta a_{\mathcal{F}}(M) = 0 \text{ if } K_{\mathcal{F}}(M) < K_c(M) \\ \delta a_{\mathcal{F}}(M) \geq 0 \text{ if } K_{\mathcal{F}}(M) = K_c(M), \end{cases} \tag{15}$$

where $K_c(M)$ is the fracture toughness at point M.

The crack is supposed to advance quasi-statically under remote loading σ_∞ varying in order to have at each moment $\max_{M\in\mathcal{F}} \frac{K_{\mathcal{F}}(M)}{K_c(M)} = 1$. This condition ensures that $K_{\mathcal{F}}(M) \leq K_c(M)$ for all points M of the front and that there is always a part of the front that propagates. By using Equation (1), this implies that the loading verifies:

$$\sigma_\infty = \frac{1}{\max\limits_{M\in\mathcal{F}} \dfrac{\widehat{K}_{\mathcal{F}}(M)}{K_c(M)}}, \tag{16}$$

hence, changes during propagation. Increasing σ_∞ means that one should increase the loading in order that the crack advances, in other word that the crack advances in a *stable* manner. Decreasing σ_∞ means that the crack advances in an *unstable* manner.

It is easy to show that the criterion (15) is satisfied by:

$$\delta a_{\mathcal{F}}(M) = \delta\tau \left(\frac{K_{\mathcal{F}}(M)}{K_c(M)} \right)^{\beta}, \beta \to \infty, \tag{17}$$

where $\delta\tau$ denotes the kinematical time increment corresponding to the advance $\delta a_{\mathcal{F}}(M)$. Indeed, if $K_{\mathcal{F}}(M) < K_c(M)$ then $\lim_{\beta\to\infty}\left(\frac{K_{\mathcal{F}}(M)}{K_c(M)}\right)^{\beta} = 0$ that is $\delta a_{\mathcal{F}}(M) = 0$, if $K_{\mathcal{F}}(M) = K_c(M)$ then $\left(\frac{K_{\mathcal{F}}(M)}{K_c(M)}\right)^{\beta} = 1$, that is $\delta a_{\mathcal{F}}(M) = \delta\tau \geq 0$ is undefined, and if $K_{\mathcal{F}}(M) > K_c(M)$ then $\delta a_{\mathcal{F}}(M) = +\infty$ hence this case is not admissible. Same trick is used for writing perfect plastic constitutive laws as viscoplastic ones for FEM applications. An other possible viscoplastic-type regularization was used by Gao and Rice (1989), but the advantage of ours is that, as will be more detailed below, fatigue and brittle fracture can both be treated by a Paris-type law.

Choosing the time increment $\delta\tau$ to have $\max_{M\in\mathcal{F}} \delta a_{\mathcal{F}}(M) = \delta a_{\max}$ implies by Equation (17):

$$\delta\tau = \frac{\delta a_{\max}}{\max\limits_{M\in\mathcal{F}}\left(\dfrac{K_{\mathcal{F}}(M)}{K_c(M)}\right)^{\beta}},$$

so that:

$$\delta a_{\mathcal{F}}(M) = \delta a_{\max}\left(\frac{\widehat{K}_{\mathcal{F}}(M)}{K_c(M)\max\limits_{N\in\mathcal{F}}\dfrac{\widehat{K}_{\mathcal{F}}(N)}{K_c(N)}}\right)^{\beta}, \beta\to\infty. \tag{18}$$

Equation (18) can be identified to the law (8) by taking:

$$\mathcal{L}_M\left(\widehat{K}_{\mathcal{F}}(N), N\in\mathcal{F}\right) = \left(\frac{\widehat{K}_{\mathcal{F}}(M)}{K_c(M)\max\limits_{N\in\mathcal{F}}\dfrac{\widehat{K}_{\mathcal{F}}(N)}{K_c(N)}}\right)^{\beta}, \beta\to\infty. \tag{19}$$

If the toughness $K_c(M)$ is independent of point M this simplifies into:

$$\mathcal{L}_M\left(\widehat{K}_{\mathcal{F}}(N), N\in\mathcal{F}\right) = \left(\frac{\widehat{K}_{\mathcal{F}}(M)}{\max\limits_{N\in\mathcal{F}}\widehat{K}_{\mathcal{F}}(N)}\right)^{\beta}, \beta\to\infty. \tag{20}$$

One advantage of this formulation is that in fact, Irwin' criterion can be formally seen as a Paris-type law. Hence the fatigue law (9) and the brittle fracture law (15) can be described by the same *explicit* law:

$$\delta a_{\mathcal{F}}(M) = \delta a_{\max}\frac{\left[f(M)\widehat{K}_{\mathcal{F}}(M)\right]^{\alpha(M)}}{\max\limits_{M\in\mathcal{F}}\left(\left[f(M)\widehat{K}_{\mathcal{F}}(M)\right]^{\alpha(M)}\right)} \tag{21}$$

with $\alpha(M) = \beta(M)$ and $f(M) = C(M)^{1/\beta(M)}\Delta\sigma_{\infty}$ in fatigue and, $\alpha(M) = \beta \gg 1$ and $f(M) = 1/K_c(M)$ in brittle fracture.

Bower and Ortiz (1990, 1991, 1993) proposed an other way to satisfy Irwin's criterion (15). They search by an iterative procedure the 'active' zone of the crack front where the crack advance is not zero. On each postulated 'active' zone, the crack advance $\delta a(M)$ is obtained by inversion of a linear equations system derived from the condition $K(M)+\delta K(M) = K_c(M)+$

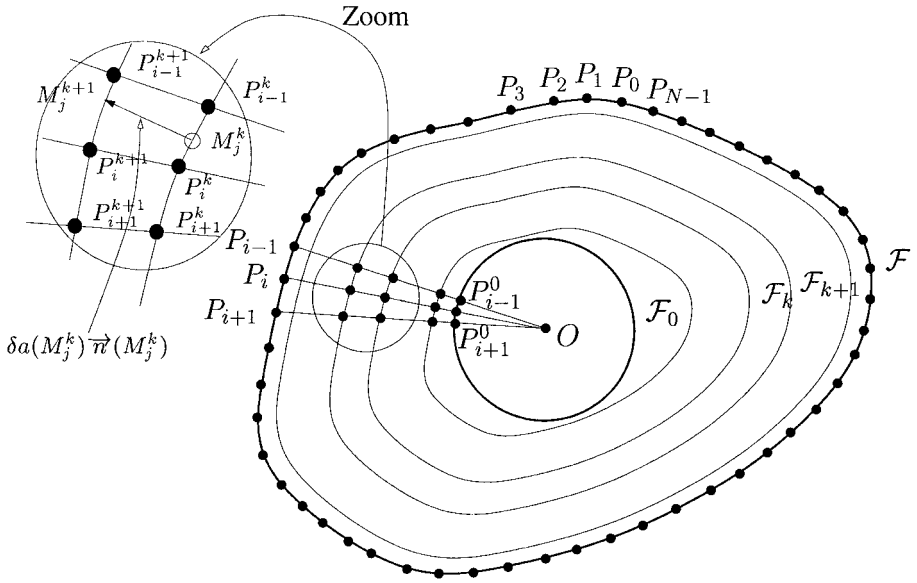

Figure 2. Intermediate cracks between the reference front $\mathcal{C}$ and the final one $\mathcal{F}$.

$\delta K_c(M)$. This makes their procedure quiet heavy. In contrary, our formulation presents the advantage to give explicitly $\delta a_{\mathcal{F}}(M)$ along the front once the SIF are known, without any iteration nor linear system inversion.

3. Numerical Procedure

3.1. Meshing operations and determination of the normal advance $\delta a(M)$

3.1.1. *During step I*

The initial crack front $\mathcal{F}$ is meshed with N points P_i, $i = 0 \dots N-1$. The N nodes P_i^0 of the reference circle $\mathcal{C}$ of center O are constructed through intersection of $\mathcal{C}$ with the lines $(O\,P_i)$. The segments $[P_i^0 P_i]$ are then cut into n subsegments to create $n-1$ intermediate meshes $P_{i,i=0\dots N-1}^k$ of the crack fronts $\mathcal{F}_k$, $k = 1 \dots n-1$.

As the vector $\overrightarrow{P_i^k P_i^{k+1}}$ is not in general, normal to the front $\mathcal{F}_k$ (see Figure 2), the equations (3) and (4) don't give the SIF and function W at points $P_{i,i=0\dots N-1}^{k+1}$ as a function of their values on nodes $P_{j,j=0\dots N-1}^k$ of $\mathcal{F}_k$. Therefore a second set of meshes $M_{i,i=0\dots N-1}^k$ of $\mathcal{F}_k$, $k = 0 \dots n$, where the SIF and function W are computed, is constructed by recurrence, by normal projection of the nodes M_i^k of $\mathcal{F}_k$ onto the front $\mathcal{F}_{k+1}$ with, as initialization, $M_i^0 = P_i^0$, $i = 0 \dots N-1$.

More precisely, suppose that the nodes M_i^k are known for the crack front $\mathcal{F}_k$. At this stage, the front $\mathcal{F}_{k+1}$ is known only by its nodes P_j^{k+1}. Two alternatives, depicted in Figure 3, are envisaged:

1. the linear one: the nodes $P_{j=0\dots N-1}^{k+1}$ are supposed to be linked by straight lines and for each i, the node M_i^{k+1} is constructed by normal projection of the node M_i^k on these straight lines (depicted by black arrows in Figure 3);

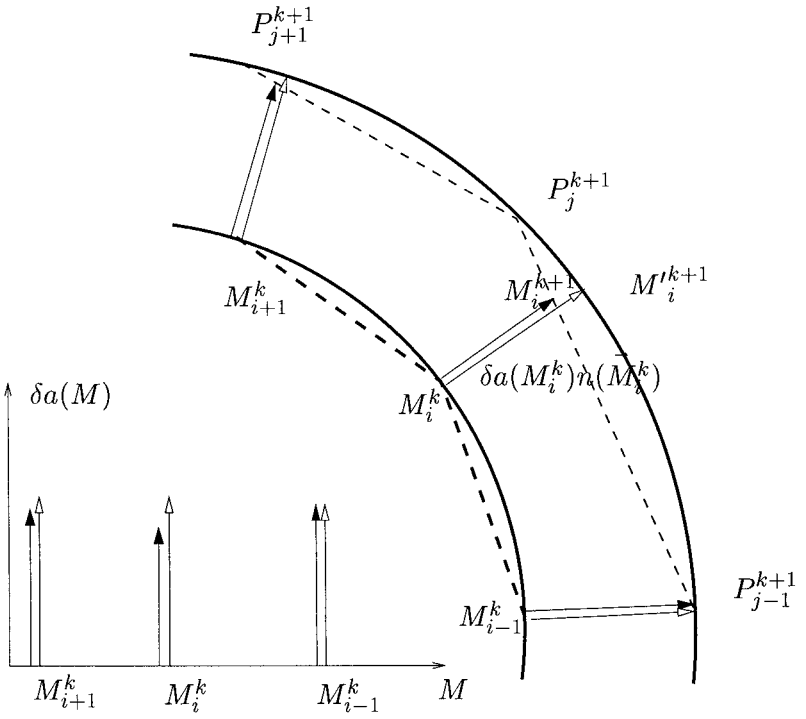

Figure 3. Computation of the normal advance.

2. the more precise quadratic one: the nodes $P_{j=0\ldots N-1}^{k+1}$ are supposed to be linked by arcs of circle and the node M_i^{k+1} (denoted M'^{k+1}_i in Figure 3) is constructed by projection of the node M_i^k on these arcs of circle (depicted by white arrows in Figure 3);

The normal advance $\delta a(M_i^k)$ is then simply given by $\delta a(M_i^k) = ||\overrightarrow{M_i^k M_i^{k+1}}||$.

Linear approximation is of course simpler but unfortunately appears to be numerically unstable so that in practice only the quadratic solution can be used. More precisely, the missing contribution in $\delta a(M)$ arising from the linear approximation may generate some corners even in smooth crack fronts, for instance at points M_i^k for which the projected point M_i^{k+1} is at the middle of a segment $[P_{j-1}^{k+1} P_j^{k+1}]$ (see Figure 3, black arrows). Now Leblond and Leguillon (1999) have shown that at these points, the SIF may become infinite giving rise to numerical peaks in function $\widehat{K}(M)$ which develop due to the incremental nature of the calculations making any further computation impossible. Thus it is necessary to use the more precise quadratic solution. Then, one verifies that irregularities just mentioned no more appear (see for instance Figure 3, white arrows).

It should be noticed that the SIF and function W along front $\mathcal{F}$ are not finally computed at the nodes $P_{i,i=0\ldots N-1}$ constructed by the user but at the nodes $M^n_{i,i=0\ldots N-1}$. Never mind, since $M^n_{i,i=0\ldots N-1}$ is a meshing of the final front as acceptable than $P_{i,i=0\ldots N-1}$.

For some simple crack shapes, one can construct a set of intermediate cracks analytically, so that the normal crack advance can also be known analytically. It is the case for instance for the elliptical crack. The results are then, of course, more precise. But in general, such a construction is not possible and has to be done numerically. Also, in all the results given below, except if the contrary is mentioned, it is always the numerical construction that is used, even in the few cases where analytical determination would be possible.

3.1.2. *During step II*

For the calculation of the propagation path, $\delta a(M_i^k)$, $k \geq n$ is given by the propagation law (8). Nodes $M^k_{i=0\ldots N-1}$ of the further fronts $\mathcal{F}_k$, $k > n$ are then simply obtained by the relation $\overrightarrow{M_i^k M_i^{k+1}} = \delta a(M_i^k)\overrightarrow{n}(M_i^k)$. Here a second set of meshes is not necessary since (3) and (4) give $\widehat{K}$ and W directly at the nodes M_i^k.

During both step I and II, if the meshes become too distorted, re-meshing is done. Nevertheless, it should be mentioned that re-meshing also introduces numerical errors. Hence, it should not be done at each step of calculation, but only when the meshes become too distorted.

3.2. Computation of the linear abscissa and of the normals

Linear abscissa and normals are simply computed by assuming that the points M_i^k are linked by straight lines. In particular, the normal $\overrightarrow{n}(M_i^k)$ is constructed to be normed, directed toward the exterior of the crack along the bisector of lines (M_{i-1}^k, M_i^k) and (M_i^k, M_{i+1}^k).

An alternative is to consider that the nodes are linked by arc of circles instead of straight lines. But computations have then shown that the results are not significantly improved.

3.3. Calculation of the SIF $\widehat{K}$ and of the function W

Let us recall that $\widehat{K}$ and W are computed on the set of meshes $M^k_{i,i=0\ldots N-1}$. The process is incremental. Suppose that for a given k, these functions are known at nodes $M^k_{i,i=0\ldots N-1}$. Then the SIF at nodes $M^{k+1}_{i,i=0\ldots N-1}$ of crack front $\mathcal{F}_{k+1}$ are given by $\widehat{K}(M_i^{k+1}) = \widehat{K}(M_i^k) + \delta\widehat{K}(M_i^k)$ where $\delta\widehat{K}(M_i^k)$ is derived from (3) with $\mathcal{F} = \mathcal{F}_k$, $M_0 = M_i^k$. Besides, $W(M_i^{k+1}, M_j^{k+1}) = W(M_i^k, M_j^k) + \delta W(M_i^k, M_j^k)$ where $\delta W(M_i^k, M_j^k)$ is given by (4) with $\mathcal{F} = \mathcal{F}_k$, $M_0 = M_i^k$ and $M_1 = M_j^k$.

To calculate each $\delta\widehat{K}(M_i^k)$, the PV part on segment $[M_{i-1}^k M_{i+1}^k]$ around M_i^k is extracted from Equation (3). The quantity $W(M, M_i^k)\widehat{K}(M)[\delta a(M) - \delta_* a(M)]$ is approximated by a quadratic function. Since $\delta a(M_i^k) - \delta_* a(M_i^k) = 0$ (see Equation (5)), this function is zero at point M_i^k hence takes the form $a(s(M) - s(M_i^k))(s(M) - b)$. In the neighborhood of M_i^k, the distance $D(M, M_i^k) \sim |s(M) - s(M_i^k)|$ so that:

$$PV \int_{[M_{i-1}^k M_{i+1}^k]} \frac{W(M, M_i^k)}{D^2(M, M_i^k)} \widehat{K}(M)[\delta a(M) - \delta_* a(M)]\mathrm{d}s(M) =$$

$$PV \int_{[M_{i-1}^k M_{i+1}^k]} a \frac{(s(M) - s(M_i^k))(s(M) - b)}{(s(M) - s(M_i^k))^2}\mathrm{d}s(M) = \tag{22}$$

$$a\left[s(M_{i+1}^k) - s(M_{i-1}^k) + (s(M_i^k) - b)\ln\frac{s(M_{i+1}^k) - s(M_i^k)}{s(M_i^k) - s(M_{i-1}^k)}\right]$$

Over the rest of the front, since $D^2(M, M_i^k)$ does not become zero, the integrand is regular. On each intervals $[M_j^k M_{j+1}^k]$, $j \neq i-1, i$ the integrand $\frac{W(M,M_i^k)}{D^2(M,M_i^k)}\widehat{K}(M)[\delta a(M) - \delta_* a(M)]$ is approximated by quadratic interpolation on nodes M_j^k, M_{j+1}^k and M_h^k, the third node M_h^k being either the previous one M_{j-1}^k if it is different from M_i^k, either the next one M_{j+2}^k.

To calculate $\delta W(M_i^k, M_j^k)$, a similar procedure is employed. Nevertheless, attention must be paid to the fact that the PV concerns both points M_i^k and M_j^k.

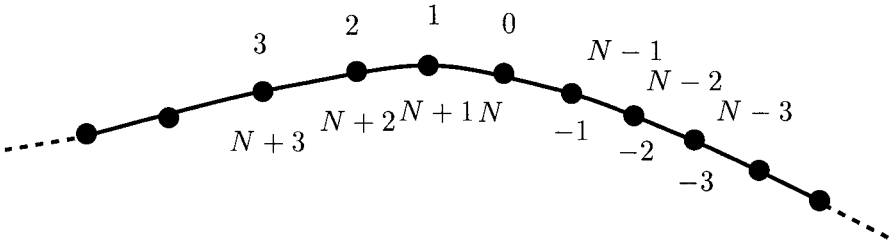

Figure 4. Double nodes.

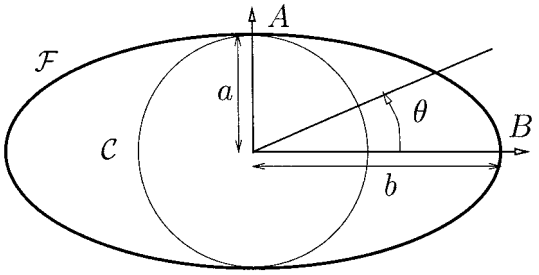

Figure 5. Elliptical crack.

Linear interpolation on nodes M_j^k, M_{j+1}^k, for the calculation of these integrals on each segment $[M_j^k M_{j+1}^k]$ is also possible, but then one verifies that one should increase the number of nodes to obtain comparable errors.

The procedure is less sophisticated, hence less complicated than the one developed by Bower and Ortiz (1990). For instance, no difference is made between collocation points (noted t_j in Bower and Ortiz (1990)) where $\delta\widehat{K}$ and δW are computed, and the nodes (noted s_i) used to evaluate the integrals. Besides, the procedure used to calculate the PV integrals is clearly outlined. Moreover, the regular integrals are computed by quadratic interpolation of all the integrand, no distinction is done in the choice of the interpolation functions between $\frac{W(M,M_i^k)}{D^2(M,M_i^k)}\widehat{K}(M)$ and $[\delta a(M) - \delta_* a(M)]$ as in Bower and Ortiz (1990). Nevertheless, our procedure gives comparable results, as will be shown below in Section 4.1.

3.4. Management of the end of meshes nodes problems

The closed front $\mathcal{F}$ has no beginning and no end, but the meshes begins at node 0 and finishes at node $N-1$. This discrepancy involves heavy management of exceptions in the writing of the loops $i = 0$ to $N-1$ on the nodes M_i^k. To avoid them, the meshes are extended, as in Figure 4, by the creation of *double nodes* in the neighborhood of nodes 0 and $N-1$.

3.5. CPU times

At each step, the integrals (3) and (4) have to be computed for each nodes of the meshing, that is $N + N^2$ times. Roughly the calculation of one of those integrals corresponds to N operations. Hence the CPU time is approximately proportional to N^3. For instance, with a CELERON processor 333 MHz, this time is about proportional to $10^{-5}N^3$ seconds. Hence a step of calculation involving 100 nodes takes approximately 10 sec, time that shrinks to 1 sec for 50 nodes. This makes the method very economical in time versus the FEM one.

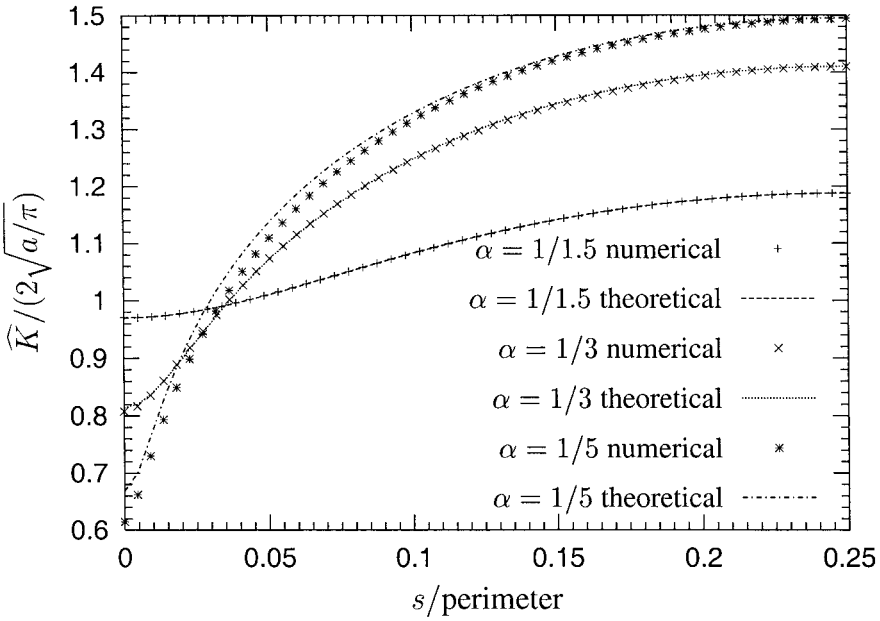

Figure 6. SIF along elliptical cracks ($s(B) = 0$, B defined in Figure 5).

4. Validation

4.1. Elliptical crack

For an elliptic crack with major axis b and minor axis a (see Figure 5), it is well known that (see for instance Irwin, 1962):

$$\widehat{K}(M) = \frac{\sqrt{\pi a}}{\mathrm{E}(k)} \left(\frac{\sin^2(\theta) + \alpha^4 \cos^2(\theta)}{\sin^2(\theta) + \alpha^2 \cos^2(\theta)} \right)^{1/4} \tag{23}$$

where θ is the polar angle of M, $\alpha = a/b < 1$, $k = \sqrt{1-\alpha^2}$ and $\mathrm{E}(k)$ denotes the complete elliptic integral of the second kind. The numerical results obtained for different values of α are shown in Figure 6. They are in good agreement with the analytical result (23). Nevertheless, one should notice two obvious facts:

- the errors increase when α decreases, that is the crack studied is the more distant from the circular starting circle of radius a;
- the error is the higher where the curvature of the front is the more important that is near point B.

To compare our results to those of Bower and Ortiz (1990), the case $\alpha = 1/3$ is considered. Figure 7 shows the value of the error E, defined by :

$$E = \sqrt{\frac{1}{L} \int_0^L \frac{\left(\widehat{K}_{num}(M) - \widehat{K}_{theo}(M)\right)^2}{\widehat{K}_0^2} \mathrm{d}s(M)} \tag{24}$$

as a function of the number of nodes N, a constant maximum step size of $\delta a_{\max} = 0.005a$ between the intermediate fronts $\mathcal{F}_k$ and $\mathcal{F}_{k+1}$ being used. In formula (24), L is the perimeter of the crack front and $\widehat{K}_0 = 2\sqrt{a/\pi}$ is the SIF for the initial circle of radius a. Figure 8 shows

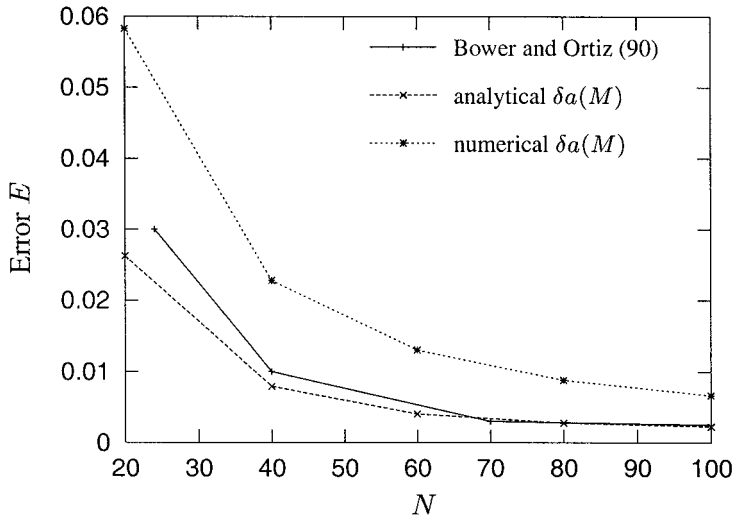

Figure 7. Error E obtained by different methods with $\delta a_{\max} = 0.005a$.

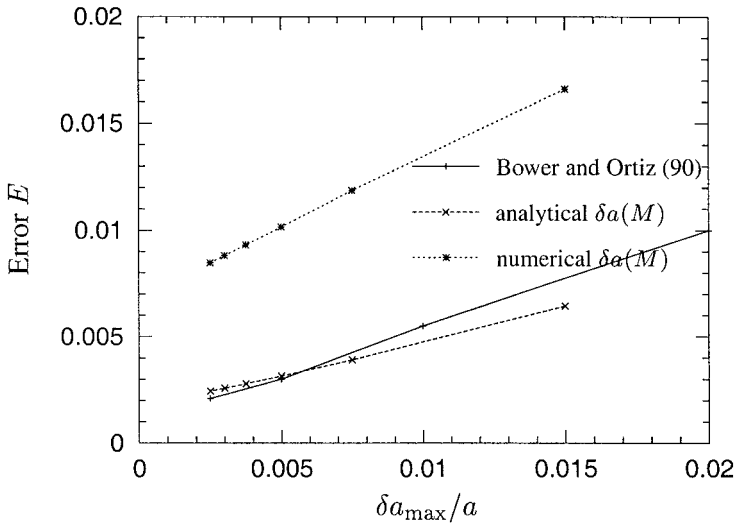

Figure 8. Error E obtained by different methods with $N = 72$.

the same error E as a function of $\delta a_{\max}/a$ with $N = 72$. In Figures 7 and 8, the lines with key 'Bower and Ortiz (1990)' correspond to the results of Bower and Ortiz (1990) obtained by giving the normal advance in analytical form. The others correspond to the results obtained by ourselves: 'Analytical $\delta a(M)$' means that $\delta a(M)$ has been given analytically by the same formula as in Bower and Ortiz (1990) and 'Numerical $\delta a(M)$' that $\delta a(M)$ has been computed by the systematic method depicted in Section 3.1.1.

One may verify in Figures 7 and 8 that:

(1) when the advance of the front is given analytically like in the work of Bower and Ortiz (1990), E is of the same order although our method is simpler. However, when the advance is computed numerically, the error is obviously slightly increased, but nevertheless reasonable enough to allow us to study the propagation path of cracks with more complex

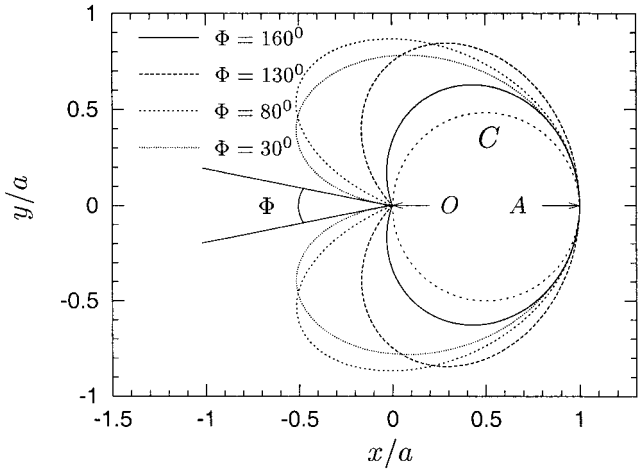

Figure 9. Heart shaped cracks.

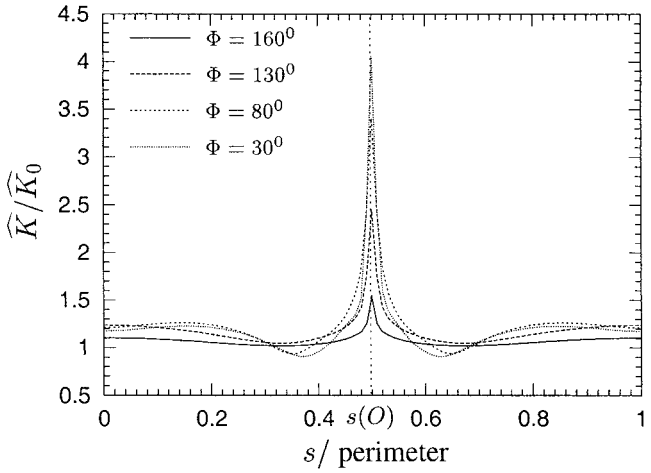

Figure 10. SIF along the heart shaped cracks depicted in Figure 9.

shapes as the ones studied below for which analytical determination of $\delta a(M)$ is not possible.

(2) the finer the discretization, that is the smaller $\delta a_{\max}/a$ is and the higher N is, the more the error decreases. Nevertheless, one is limited by the CPU time that, as has been seen in Section 3.5, may become very high for high N or number of steps, that is small $\delta a_{\max}/a$.

One can also compare the results with some results obtained by other numerical methods. For instance, for an elliptical crack of ratio $b/a = 2$, the error E obtained by Sukumar et al. (2003) using the FEM is about of $E = 0.02$ and the error E obtained by Xu et al. (1997) using a self-similar crack expansion method is about of $E = 0.006$. One can notice in Figures 7 and 8 that the error we obtained for a ratio $b/a = 3$ greater than theirs, is lower than 0.02 for relatively coarse discretization (for instance for $N > 50$ and $\delta a_{\max} = 0.005a$) and can be reduced to 0.006 for a sufficiently refined discretization ($N = 100$ and $\delta a_{\max} = 0.005a$).

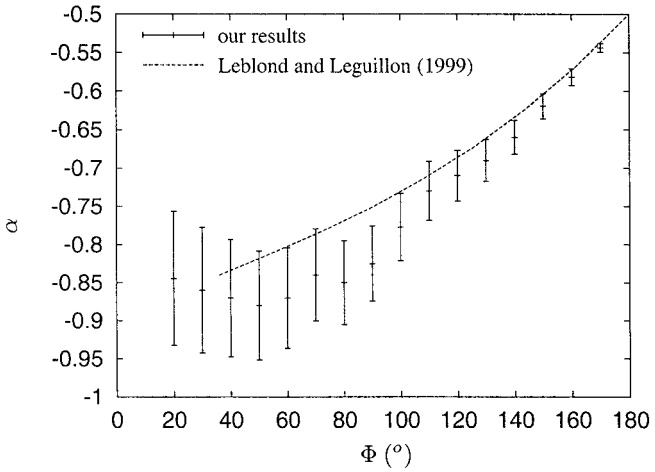

Figure 11. Computed values of the exponent α.

4.2. SIF IN THE VICINITY OF CORNER POINTS

The stress intensity factor $\widehat{K}$ along the front of several 'heart shaped cracks', like the ones depicted in Figure 9 (a denotes the minor width of the crack), with different opening angles Φ is given in Figure 10. It is normalized by the stress intensity factor $\widehat{K}_0 = \sqrt{2a/\pi}$ along the circle C of radius $a/2$ depicted in Figure 9. One can verify that in the vicinity of point A ($s = 0$) where the crack shape is close to the circle C, $\widehat{K}/\widehat{K}_0 \to 1$ when $\Phi \to 180^0$.

Leblond and Leguillon (1999) have shown that near the angular point O of the front, the SIF behaves in the following manner:

$$K(M) \propto |s(M) - s(O)|^{1/2+\alpha} \text{ when } M \to O, \tag{25}$$

where α depends only on the opening angle Φ and verifies $\alpha < -1/2$ so that the SIF becomes infinite at the notch point. The peak in Figure 10 is the numerical expression of this propriety. The scalar α can be computed by fitting the behavior (25) with the results of Figure 10 around the corner point O. The values obtained are given in Figure 11 for several angles Φ. Errors are due to the dependence of the results upon the points chosen for the fitting operations and to the numerical errors in the computation of the SIF. They are all the greater as the shape of the crack is more different from the initial circle $\mathcal{C}$, i.e., as Φ is smaller. Nevertheless, our values are relatively close to the ones obtained by Leblond and Leguillon (1999) by a more precise method in spite of the uncertainties linked to our method.

5. Some examples of propagation paths

Examples presented in Section 4.1, 4.2 have shown the efficiency of the method for compute SIF along given crack fronts. Let us now apply the method to prediction of fatigue (Section 5.1) and brittle fracture (Section 5.2) propagation paths of some particular cracks.

5.1. IN FATIGUE

Suppose now that the crack advance is governed by Paris' law (9) described in Section 2.4, fracture properties being homogeneous with $C(M) \equiv C$ and $\beta(M) \equiv \beta = 2$.

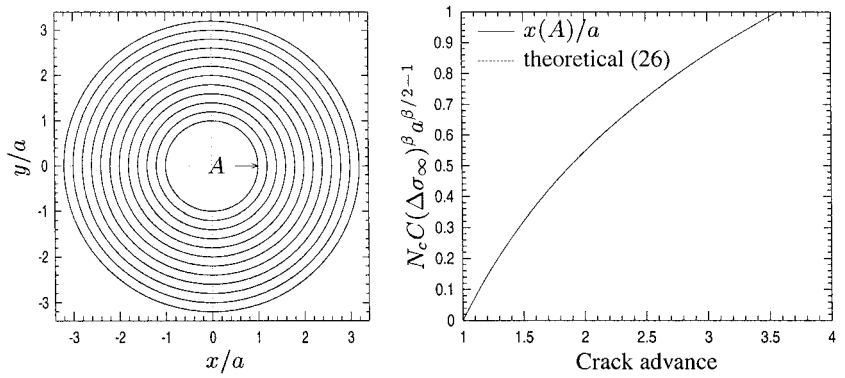

a. Propagation path b. Number of loading cycles versus advance

Figure 12. Penny shaped crack.

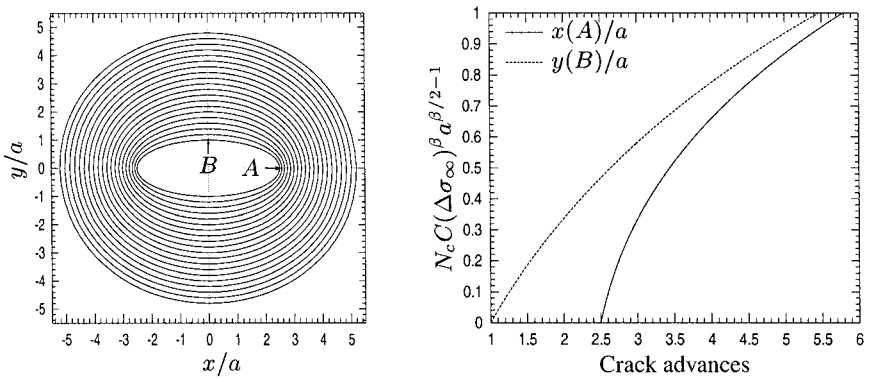

a. Propagation path b. Number of loading cycles versus advance

Figure 13. Elliptical crack.

Figures 12a, 13a, 14a, 15a show the propagation paths of a circular crack, an elliptical one with $b/a = 2.5$, a rectangular with $b/a = 1.5$ and a heart shaped one with $\Phi = 130^0$. In all these figures, a denotes the minimum width of the crack. The crack is chosen to be depicted until the initial area of the crack as been multiplied approximately by 10 since then the crack is circular and remains so in all the cases.

In Figures 12b, 13b, 14b, 15b, the quantity $N_c C(\Delta\sigma_\infty)^\beta a^{\beta/2-1}$ that is the number N_c of loading cycles between the initial and the actual configurations is given versus the advance of some particular points. This quantity is derived by summation from Equation (12) that gives the number of loading cycles between each numerical step.

The penny shaped crack is shown as a numerical test. Indeed, then $\widehat{K}(M) = 2\sqrt{x(A)/\pi}$ for all the points M of the crack front. Hence Paris' law (9) rises a uniform advance so that the crack remains circular and explicit integration of this law can be done. For $\beta = 2$, one obtains

$$N_c C(\Delta\sigma_\infty)^\beta a^{\beta/2-1} = N_c C(\Delta\sigma_\infty)^2 = \frac{\pi}{4} \ln \frac{x(A)}{a}. \tag{26}$$

One notices, in Figure 12, a very good adequacy between this theoretical result and the one obtained numerically.

Several facts can be noticed in these figures:

(1) It appears, as could be anticipated, that the crack becomes and remains circular after a

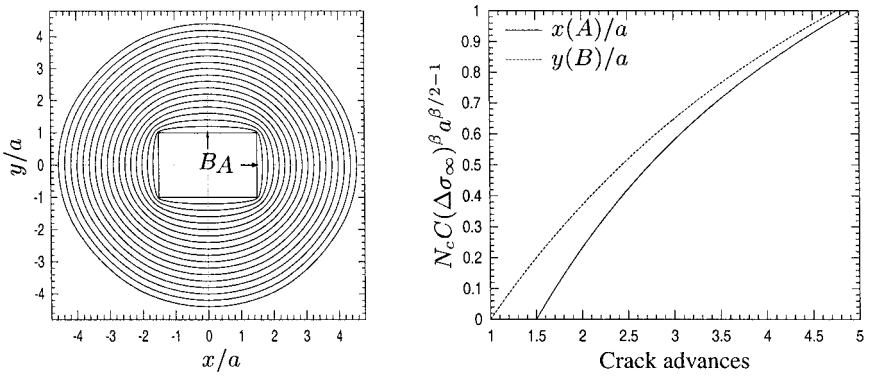

a. Propagation path b. Number of loading cycles versus advance

Figure 14. Rectangular crack.

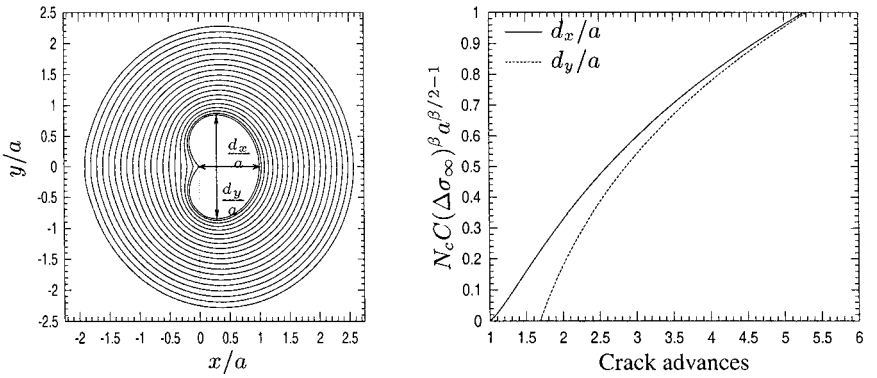

a. Propagation path b. Number of loading cycles versus advance

Figure 15. Heart shaped crack.

certain time. Hence one may conclude that it is a general feature of the fatigue propagation of *bounded* mode I cracks embedded in an infinite body propagating through a material of homogeneous fracture properties. Analogous results were reported by Sukumar et al. (2003) for fatigue propagation simulations of the elliptical crack, based on extended finite element method and the fast marching method.

(2) The curves 12b, 13b, 14b, 15b are concave. This means that the crack grows faster and faster. It is normal since when the crack growths, the SIF and the crack advance rate are, on average, also growing.

(3) Consider that the crack has undergone N_c loading cycles such as, for instance, $N_c C(\Delta\sigma_\infty)^\beta a^{\beta/2-1} = 1$. Then one can verify that the crack is, in all the cases considered, circular and that the ratio $r \equiv$ (Final Area)/(Initial Area) is $r \sim 12.7$ for the circular crack, $r \sim 12.8$ for the elliptical crack, $r \sim 12.6$ for the rectangular one, $r \sim 14$ for the heart shaped one. Hence the heart shaped crack has advanced slightly faster than the elliptical, the circular and the rectangular ones. That means that 2D crack rate advance calculations on penny shaped cracks instead of the real 3D shape may be not conservative. Nevertheless the value of r are very similar so that if one takes into account the numerical errors, one may conclude that the initial crack shape has no significant influence on the global crack advance rate. The differences between the advance rates are probably due, for the heart shape crack to the infinite, that is the

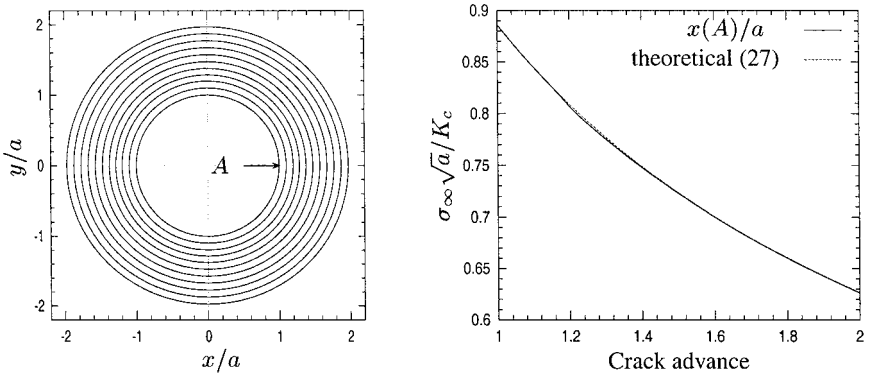

a. Propagation path b. Applied loading versus crack advance

Figure 16. Penny shaped crack.

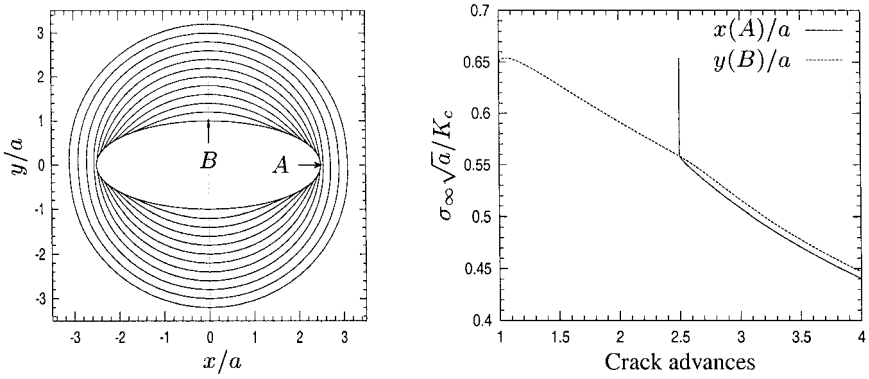

a. Propagation path b. Applied loading versus crack advance

Figure 17. Elliptical crack.

high numerical value of the SIF at the corner point (see Section 4.2) generating a high crack advance rate contribution; and oppositely, for the rectangular crack to the zero value of the SIF at the corner points generating a very small crack advance rate contribution.

5.2. In brittle fracture

The crack advances now in brittle fracture, in a material of homogeneous fracture toughness K_c under conditions (15) and (16) described in Section 2.5. In practice, numerically, (15) is replaced by (18) with $\beta = 50$.

Figures 16a, 17a, 18a, 19a show the propagation paths respectively of the circular, elliptical, rectangular, heart shaped cracks already studied in fatigue in Section 5.1. The crack is chosen to be depicted until the initial area of the crack as been multiplied approximately by 4, since then the crack is circular and subsequently, remains circular.

In Figures 16b, 17b, 18b, 19b, the normalized quantity $\sigma_\infty\sqrt{a}/K_c$ giving the remote loading σ_∞ is plotted *versus* the advance of some particular points. This quantity is derived from Equation (16).

Again, the example of the penny-shaped crack is given as a numerical example since then the crack remains circular, and the SIF along the crack front is given by $\widehat{K}(M) = 2\sqrt{x(A)/\pi}$ so that (16) gives:

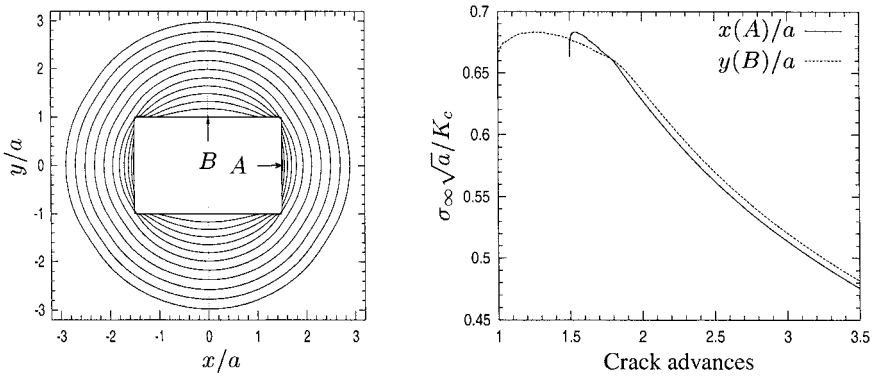

a. Propagation path b. Applied loading versus crack advance

Figure 18. Rectangular crack.

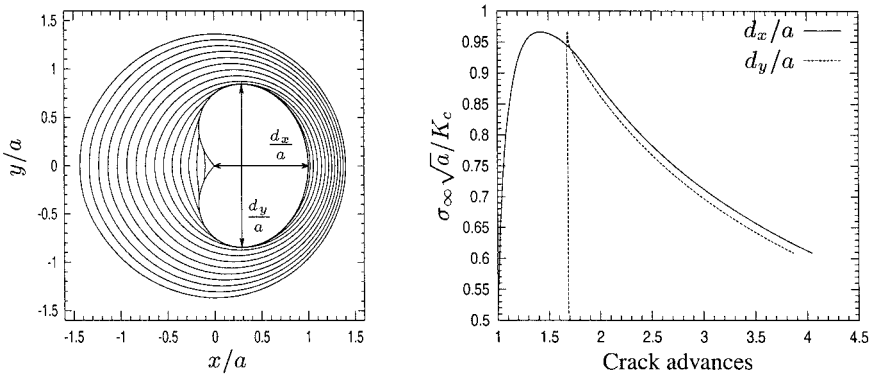

a. Propagation path b. Applied loading versus crack advance

Figure 19. Heart shaped crack.

$$\frac{\sigma_\infty \sqrt{a}}{K_c} = \frac{\sqrt{\pi a}}{2\sqrt{x(A)}} \tag{27}$$

One observes, in Figure 16, a good adequacy between this value and the computed ones.

Several things can be noticed in these figures:

(1) During a first stage where the SIF along the crack front is not uniform, one can verify that, in agreement with the criterion (15), the crack advances only where K is maximum and equal to K_c, that is for the elliptical and rectangular cracks, in the vicinity of points B defined in Figures 17a, 18a, for the heart shaped one in the vicinity of the corner point. Nevertheless, several numerical trials have shown that this is achieved only if β is high enough. In particular, one can verify that it is achieved for $\beta = 50$ but not for $\beta = 20$.

(2) During a second stage, the crack becomes circular hence the SIF is uniform along the crack front. The criterion then predicts a uniform advance of the front so that the crack remains circular.

(3) The elliptical, rectangular and heart shaped cracks advance first under increasing loading that is in a stable manner, then in an unstable manner. The stable phase is due to decreasing value of $\max_{M\in\mathcal{F}} \widehat{K}_{\mathcal{F}}(M)$ implying, according to (16), an increase in loading to have at each moment $\max_{M\in\mathcal{F}} K_{\mathcal{F}}(M) = \sigma_\infty \max_{M\in\mathcal{F}} \widehat{K}_{\mathcal{F}}(M) = K_c$. For the elliptical and rectangular cracks, the decreasing value of $\max_{M\in\mathcal{F}} \widehat{K}_{\mathcal{F}}(M) = \widehat{K}_{\mathcal{F}}(B)$ is due to the increase of curvature

around the point B that causes some screen effect. For the heart shaped crack, it is caused by the progressive vanishing of the corner.
(4) Among the loadings, the loading σ_∞^0 above which the propagation begins is of particular interest. To compare these loadings, one may consider cracks with same initial areas that is such as $a(\text{ellipse})/a(\text{circle}) \sim 0.63$, $a(\text{rectangle})/a(\text{circle}) \sim 0.72$, $a(\text{heart})/a(\text{circle}) \sim 1.41$. One founds

$$\frac{\sigma_\infty^0(\text{circle})\sqrt{a(\text{circle})}}{K_c} \sim 0.89,$$

$$\frac{\sigma_\infty^0(\text{ellipse})\sqrt{a(\text{circle})}}{K_c} \sim 0.82, \quad \frac{\sigma_\infty^0(\text{rectangle})\sqrt{a(\text{circle})}}{K_c} \sim 0.78$$

Hence, the rectangular crack begins to propagate for a lower loading than the elliptical and circular ones. Again, predictions made on circular cracks instead of the real crack shape may be slightly not conservative. For the heart shape crack, it has no real significance to read such a value since the value obtained numerically for the maximum SIF corresponds to a theoretical infinite value of the SIF at the corner point (see Section 4.2) which means that the crack starts to propagate theoretically instantaneously, that is with $\sigma_\infty = 0$, so that in practice, the corner never exists because it is instantaneously wiped out.
(5) The loading σ_∞^i above which the crack starts to propagate in an unstable manner is also of practical interest. Again for cracks with same initial areas, one obtains:

$$\frac{\sigma_\infty^i(\text{circle})\sqrt{a(\text{circle})}}{K_c} \sim 0.89, \quad \frac{\sigma_\infty^i(\text{ellipse})\sqrt{a(\text{circle})}}{K_c} \sim 0.83,$$

$$\frac{\sigma_\infty^i(\text{rectangle})\sqrt{a(\text{circle})}}{K_c} \sim 0.80, \quad \frac{\sigma_\infty^i(\text{heart})\sqrt{a(\text{circle})}}{K_c} \sim 0.82,$$

Again values are very close to each other showing a small effect of the initial crack shapes. Nevertheless, the small effect is such that predictions made on circular cracks instead of the real 3D shape may be not conservative. Indeed, it appears that if the body is loaded by an increasing remote loading starting from zero, the crack begins to propagate unstably, that is the body breaks, for a loading slightly smaller for the elliptical, rectangular, heart shaped cracks than for the circular crack.

5.3. Brittle fracture in an heterogeneous media

To illustrate the capacity of the regularized form of Irwin's criterion to perform calculations of propagation paths into heterogenous medias, let us consider a penny shaped crack of radius a with a periodical toughness such as:

$$K_c(M) = \overline{K_c}\,[1 + \lambda \cos(k\,\theta(M))]\,, \tag{28}$$

where $\theta(M)$ denotes the polar angle of any point M.

Figures 20, 21, 22 show the propagation paths and the corresponding loading for $k = 2$, $k = 3$, $k = 6$ respectively, λ being equal to 0.2.
One can distinguish several stages in the propagation paths:
(1) At the beginning of the propagation, the crack is circular hence $\widehat{K}$ is constant along the crack front, so that only the points where K_c is minimum propagate (points denoted B in the figures).

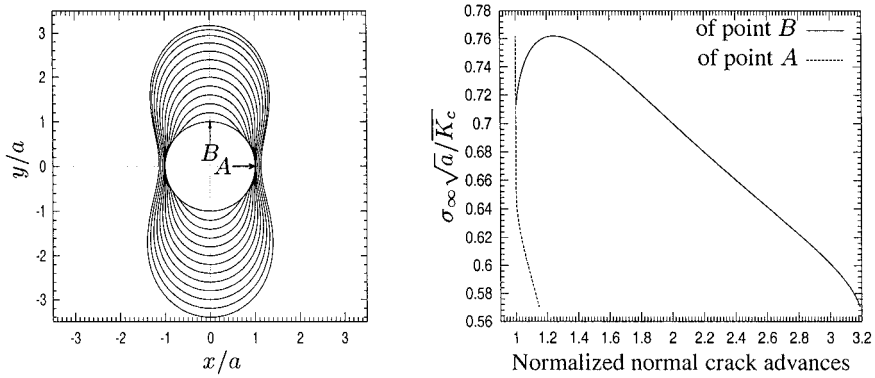

a. Propagation path b. Applied loading versus crack advance

Figure 20. Case $k = 2$.

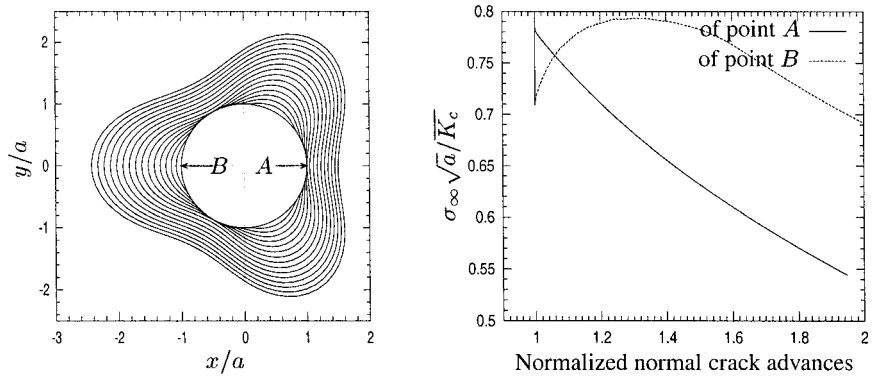

a. Propagation path b. Applied loading versus crack advance

Figure 21. Case $k = 3$.

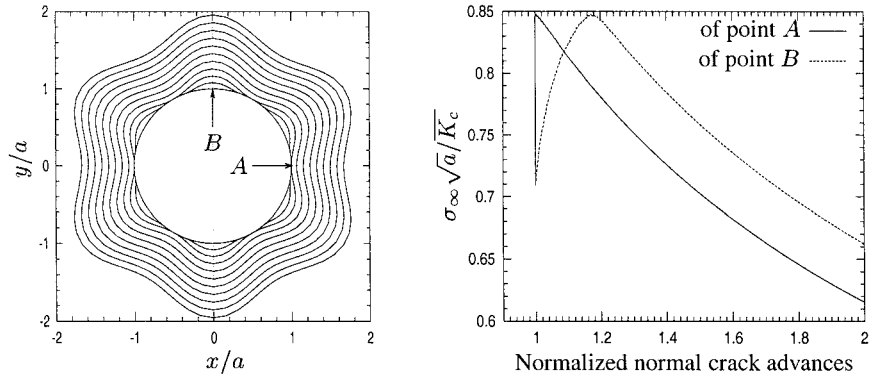

a. Propagation path b. Applied loading versus crack advance

Figure 22. Case $k = 6$.

(2) Then, more and more points reach the critical threshold that is more and more points propagate at the same time.
(3) Finally, the crack front attains a shape for which all of its points satisfy Irwin's criterion. From this stage, the crack propagates uniformly, hence the shape stays the same.

After stage 1, the same screen effect still mentioned in Sections 5.2, was susceptible to produce around points A, a shrinking of the SIF so that propagation around these points may have not occured. Hence, stage 2 was not obvious, a priori.

During the final stage 3, one can verify that the polar equation of the crack front is approximatively of the form $r(\theta) = a_0 + A\cos(k\theta + \pi)$ and the SIF of the form $\widehat{K}(\theta) = K_0 + B^2\cos(k\theta)$, which imply in particular that the SIF at the more advanced points of the fronts is lower than at the less advanced ones. These results agree with Gao and Rice (1987).

For $k = 3, 6$, one remarks that until the points A propagate, the loading has to be increased for crack propagation to occur. This means, by Equation (16), that $\frac{1}{\max_{M\in\mathcal{F}} \frac{\widehat{K}_{\mathcal{F}}(M)}{K_c(M)}} = \frac{K_c(B)}{\widehat{K}_{\mathcal{F}}(B)}$ increases, that is, since $K_c(B)$ is constant during propagation that $\widehat{K}_{\mathcal{F}}(B)$ decreases. This effect is probably due to a shielding effect, the opening displacement at points B being screened by the surrounding crack front. Then, once the crack front around the points B becomes 'open enough' to see the average growing of the front, $\widehat{K}_{\mathcal{F}}(B)$ increases, hence the loading decreases. The same effect exists for $k = 2$, but the loading begins to decrease before the point A begins to propagate. One can also notice that the higher the value of k, that is the more heterogeneous the fracture toughness is, the more the screen effect is present, the more the loading has to be increased to reach the instable phase. This means that the more the material has irregular fracture properties, the more it resists to fracture. One may wonder whether this a general rule?

6. Conclusion

Since only the meshing of the initial front is needed, the procedure depicted above is an efficient tool for solving problems concerning a flat crack subjected to mode I loading.

Several properties, some of common knowledge, have been noticed on the cases studied:
(1) For closed cracks (that can be derived from the penny shaped one through continuous deformation) propagating in a material of homogeneous fracture properties, the crack propagates to become circular.
(2) In material of heterogenous toughness, the crack appears to propagate to ensure the condition $K = K_c$ along the whole front.
(3) The influence of the initial crack shape on the loading seems to be small. Nevertheless, it is outlined that calculations make on 2D penny shaped cracks instead of the real 3D shape may be not conservative.
(4) In brittle fracture in the simple case studied, it appears that the more heterogenous the toughness is, the more the loading has to be increased to reach unstable crack propagation.

One may ask if these properties applied to any crack shape, hence are universal properties? One can reasonably answer yes for the two first ones even if no rigorous demonstration or experimental result are known. To answer yes for the two last properties would be more hazardous since it relies to some very particular examples that are moreover subjected to numerical errors.

Endnotes

[1]the affix z of a point M of the plane $(0, \vec{x}, \vec{z})$ is the complex number $x_M + iz_M$ where $(x_M, 0, z_M)$ are the cartesian coordinates of M and i the square root of -1.

References

Bower, A. F. and Ortiz, M. (1990). Solution of Three-Dimensional Crack Problems by a Finite Perturbation Method. *Journal of the Mechanics and Physics of Solids* **38**(4), 443–480.

Bower, A. F. and Ortiz, M. (1991). A Three-Dimensional Analysis of Crack Trapping and Bridging by Tough Particles. *Journal of the Mechanics and Physics of Solids* **39**(6), 815–858.

Bower, A. F. and Ortiz, M. (1993). An Analysis of Crack Trapping by Residual Stresses in Brittle Solids. *ASME Journal of Applied Mechanics* **60**, 175–182.

Bueckner, H. F. (1970). A Nover Principle for the Computation of Stress Intensity Factors. *Zeitschrift fur Angewandte Mathematik und Mechanik* **50**(9), 529–546.

Fares, N. (1989). Crack Fronts Trapped by Arrays of Obstacles: Numerical Solutions based on Surface Integral Representation. *Transactions of the ASME. Journal of Applied Mechanics* **56**(4), 837–843.

Gao, H. and Rice, J.R. (1987a). Nearly Circular Connections of Elastic Half Spaces. *ASME Journal of Applied Mechanics* **54**(4), 627–634.

Gao, H. and Rice, J.R. (1987b). Somewhat Circular Tensile Cracks. *International Journal of Fracture* **33**(3), 155–174.

Gao, H. and Rice, J.R. (1989). A First-Order Perturbation Analysis of Crack Trapping by Arrays of Obstacles. *Transactions of the ASME* **56**, 828–836.

Irwin, G. R. (1962). Crack-Extension Force for a Part-Through Crack in a Plate. *ASME Journal of Applied Mechanics* **29**, 654–661.

Leblond, J.-B. and Leguillon, D. (1999). Asymptotic behavior of stress intensity factors near an angular point of a crack front. *European Journal of Mechanics, A/Solids* **18**(1), 135–145.

Leblond, J.-B., Mouchrif, S.-E. Perrin, G. (1996). The Tensile Tunnel-Crack with a Slightly Wavy Front. *International Journal of Solids and Structures* **33**(14), 1995–2022.

Meade, K. P. and Keer, L. M. (1984). On the problem of a pair of point forces applied to the faces of a semi-infinite plane crack. *Journal of Elasticity* **14**(1), 3–14.

Rice, J. R. (1972). Some remarks on elastic crack-tip stress fields. *International Journal of Solids and Structures* **8**(6), 751–758.

Rice, J. R. (1985). First-Order Variation in Elastic Fields Due to Variation in Location of a Planar Crack Front. *ASME Journal of Applied Mechanics* **52**(3), 571–579.

Rice, J. R. (1989). Weight Function Theory for Three-Dimensional Elastic Crack Analysis. In: R. P. Wei and R. P. Gangloff (eds.): *Fracture Mechanics: Perspectives and Directions (Twentieth Symposium)*. Philadelphia, USA, pp. 29–57.

Stallybrass, M. (1981). ON the concentrated loading of certain elastic half-space problems and related external crack problems. A new approach. *International Journal of Engineering Science* **19**(8), 1123–1144.

Stolarska, M., Chopp, D., Noes, N. and Belytschko, T. (2001). Modelling crack growth by level sets in the extended finite element method. *International Journal for Numerical Methods in Engineering* **51**, 943–960.

Sukumar, N., Chopp, D. L. and Moran, B. (2003). Extended finite element method and fast marching method for three-dimensional fatigure crack propagation. *Engineering Fracture Mechanics* **70**(1), 29–48.

Sukumar, N., Moes, N., Moran, B. and Belytschko, T. (2000). Extended finite element method for three-dimensional crack modellins. *International Journal for Numerical Methods in Engineering* **48**(11), 1549–1570.

Tada, H., Paris, P. C. and Irwin, G. R. (1973). *The Stress Analysis of Cracks Handbook*. Del Research Corporation, Hellertown, USA.

Weaver, J. (1977). Three-dimensional crack analysis. *International Journal of Solids and Structures* **13**(4), 321–330.

Xu, G. and Ortiz, M. (1993). A variational boundary integral method for the analysis of 3-D cracks of arbitrary geometry modelled as continuous distributions of dislocation loops. *International Journal for Numerical Methods in Engineering* **36**(1), 3675–3701.

46 *Véronique Lazarus*

Xu, Y., Moran, B. and Belytschko, T. (1997). Self similar crack expansion method for three-dimensional crack analysis. *ASME Journal of Applied Mechanics* **64**(4), 729–739.

Available online at www.sciencedirect.com
SCIENCE DIRECT®
International Journal of Solids and Structures 43 (2006) 2091–2109
INTERNATIONAL JOURNAL OF SOLIDS and STRUCTURES
www.elsevier.com/locate/ijsolstr

Coplanar propagation paths of 3D cracks in infinite bodies loaded in shear

Elie Favier, Véronique Lazarus *, Jean-Baptiste Leblond

Laboratoire de Modélisation en Mécanique, Université Pierre et Marie Curie (Paris VI), Tour 65-55, Case 162, 4 place Jussieu, 75252 Paris Cedex 05, France

Received 15 December 2004; received in revised form 15 June 2005
Available online 18 August 2005

Abstract

Bower and Ortiz, recently followed by Lazarus, developed a powerful method, based on a theoretical work of Rice, for numerical simulation of planar propagation paths of mode 1 cracks in infinite isotropic elastic bodies. The efficiency of this method arose from the need for the sole 1D meshing of the crack front. This paper presents an extension of Rice's theoretical work and the associated numerical scheme to mixed-mode (2 + 3) shear loadings. Propagation is supposed to be channeled along some weak planar layer and to remain therefore coplanar, as in the case of a geological fault for instance. The capabilities of the method are illustrated by computing the propagation paths of cracks with various initial contours (circular, elliptic, rectangular, heart-shaped) in both fatigue and brittle fracture. The crack quickly reaches a stable, almost elliptic shape in all cases. An approximate but accurate analytic formula for the ratio of the axes of this stable shape is derived.

Keywords: 3D fracture mechanics; Coplanar crack propagation paths; Mode 2 + 3; Brittle fracture; Fatigue; Stable shape; Perturbation method; Weight functions

1. Introduction

There are several more or less efficient methods for numerical simulation of propagation paths of 3D cracks in elastic media. The most classical and general one is the finite element method (FEM). A

* Corresponding author. Tel.: +33 144278717; fax: +33 144275259.
E-mail addresses: favier@lmm.jussieu.fr (E. Favier), vlazarus@ccr.jussieu.fr (V. Lazarus), leblond@lmm.jussieu.fr (J.-B. Leblond).

0020-7683/$ - see front matter
doi:10.1016/j.ijsolstr.2005.06.041

non-trivial example involving a complex, non-planar crack shape is provided in the work of Xu et al. (1994). But the FEM requires meshing the whole 3D cracked body at each step of the crack propagation, and it is difficult to do this automatically. A recent and efficient variant of the FEM consists of coupling the level set method and the extended finite element method (XFEM); see for instance, Sukumar et al. (2003), Moes et al. (2002), Gravouil et al. (2002).

The sole meshing of the initial geometry is then required. Another alternative consists of using the boundary element method (BEM), which requires only 2D meshing of the crack surface and the outer boundary. Several examples of such an approach are provided in Chapter 5 of Bonnet (1994)'s book. Methods based on integral equations are especially attractive for infinite bodies since the sole meshing of the crack surface is then necessary; see for instance the examples provided by Fares (1989) and Xu and Ortiz (1993). If, in addition, the crack propagates along a plane, compelling methods requiring the sole 1D meshing of the crack front are envisageable. Using an earlier theoretical work of Rice (1989) and Bower and Ortiz (1990, 1991, 1993) proposed such an approach and applied it to various problems of practical interest. Lazarus (2003) later defined a simplified variant of this method which resulted in no significant loss of numerical accuracy.

More specifically, the basis of Bower and Ortiz' method and Lazarus' variant was Bueckner–Rice's weight function theory. The 2D version of this theory was expounded by Bueckner (1970) and Rice (1972), and its extension to the 3D case by Rice (1972) (in the appendix of this reference) and Bueckner (1973). It was applied by Rice (1989) to planar cracks with arbitrary contours loaded in mode 1. The theory yielded, to first order, the variation of the mode 1 stress intensity factor (SIF) along the crack front arising from some small but otherwise arbitrary coplanar perturbation of this front, under conditions of constant prescribed loading. This variation was expressed as a line integral over the unperturbed front which involved, in addition to the perturbation, some geometry-dependent "kernel" linked to the mode 1 weight function. The theory also provided the variation of this kernel, again to first order, in a similar form. Bower and Ortiz (1990, 1991, 1993)'s method consisted of applying Rice's two formulae to some sequence of small perturbations of the front resulting in arbitrary deformation of its initial shape. They applied it to the study of the propagation paths of semi-infinite tensile cracks in heterogeneous media, in both fatigue and brittle fracture.

In Lazarus (2003)'s variant, the numerical procedure was greatly simplified by using linear instead of quadratic elements, calculating the crack advance and the various integrals at the same discretization points instead of distinguishing between nodes and collocation points, etc. Validation tests based on numerical calculation of SIFs for crack geometries for which some analytical solution existed showed that such simplifications did not affect the overall numerical accuracy. In fact, the only point that was found to really require special care was accurate evaluation of some integrals in principal value. Also, Lazarus replaced the Irwin–Griffith propagation law for brittle fracture used by Bower and Ortiz by that of Paris. Nothing was lost by doing so since as noted by Lazarus, in addition to being a good propagation law for fatigue, Paris' law "simulates" Irwin–Griffith's law in the limit of very large Paris exponent. The advantage of using Paris' law was that the crack advance at all time steps and discretization points was directly provided by some explicit formula. In contrast, deducing the crack advance at the discretization points from the Irwin–Griffith criterion, as was done by Bower and Ortiz, was more difficult in two respects. First, iterations were required to determine the "active" part of the front, that is that portion which effectively propagates at the instant considered. Second, for each iteration, it was necessary to solve a large system of linear equations on the unknown values of the crack front advance at the discretization points of this active part. Lazarus applied her method to the study of the propagation paths, in fatigue and brittle fracture, of initially elliptic, rectangular and heart-shaped cracks loaded through some uniform remote tensile stress. She found that for all of these initial configurations, the crack quickly reached a stable, circular shape.

Bower and Ortiz' method and Lazarus' variant were developed only for mode 1 cracks. The aim of this paper is to extend Lazarus' method to mixed-mode (2 + 3) loadings, and to illustrate it through several examples of simulation of propagation of shear mode cracks with simple initial shapes, in both fatigue and brittle fracture. Propagation will be assumed to be coplanar; this is reasonable provided that the crack is channeled along a weak planar layer, which is the case, for instance, for a geological fault.

The first step consists of extending Rice (1989)'s results to planar cracks with arbitrary contour loaded in mode 2 + 3. This is done in Section 2. Our starting point here is Rice (1985)'s general formula (applicable to all modes) for the first-order variation of the displacement discontinuity across the crack plane resulting from some small coplanar advance of the front, under conditions of constant prescribed loading. The first-order variation of the SIFs is deduced from there by letting the observation point of this discontinuity tend toward the crack front. The treatment here extends both that of Rice (1989), which applied to planar mode 1 cracks with arbitrary contour, and those of Gao and Rice (1986) and Gao (1988), which applied to planar shear mode cracks with straight or circular contour. The first-order variation of the relevant kernels is also derived in a similar way, using their relation to the weight functions. Section 3 then briefly presents the extension of Lazarus (2003)'s numerical method to shear loadings. This extension is straightforward in principle, but the extended method is notably heavier than the original one for mode 1, because of the inevitable coupling of modes 2 and 3. Section 4 expounds validation tests based on numerical calculation of the distribution of SIFs along the front of elliptic cracks loaded in shear. Finally, Section 5 presents applications in the form of computation of planar propagation paths of shear mode cracks with simple (circular, elliptic, rectangular and heart-shaped) initial contours, in fatigue and brittle fracture. It is found that the crack front quickly reaches some stable, almost elliptic shape in all cases. An approximate but accurate analytic formula for the ratio of the axes of this stable shape is derived.

2. Extension of Rice's formulae to modes 2 and 3

2.1. Definitions and notations—Elementary properties of weight functions

2.1.1. Stress intensity factors

Consider a plane crack of arbitrary shape embedded in some infinite isotropic elastic medium subjected to some arbitrary loading (Fig. 1). Let $\mathscr{F}$ denote the crack front and s some curvilinear abscissa along it. At each point s of $\mathscr{F}$, define a local basis of vectors $(\vec{e}_1(s), \vec{e}_2(s), \vec{e}_3(s))$ in the following way:

(1) $\vec{e}_3(s)$ is tangent to $\mathscr{F}$ and oriented in the same direction as the curvilinear abscissa s;
(2) $\vec{e}_2(s)$ is in the crack plane, orthogonal to $\mathscr{F}$ and oriented in the direction of propagation;

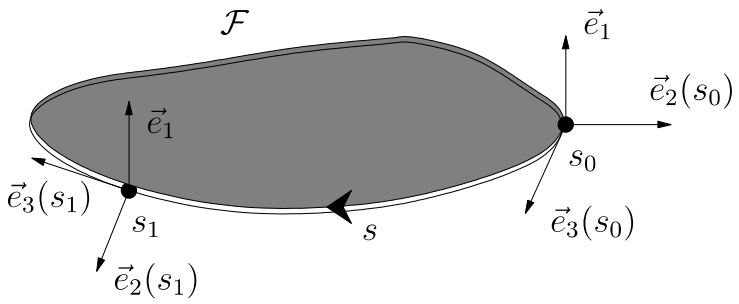

Fig. 1. Notations for a planar crack with arbitrary contour.

(3) $\vec{e}_1(s) \equiv \vec{e}_1$ is orthogonal to the crack plane and oriented in such a way that the basis $(\vec{e}_2(s), \vec{e}_1, \vec{e}_3(s))$ is direct.[1]

The SIFs $K_j(s)$, $j = 1, 2, 3$ at point s are then defined by the following formula, where Einstein's summation convention is employed:

$$\lim_{r\to 0} \sqrt{\frac{2\pi}{r}} [\![\vec{u}(s,r)]\!] \equiv 8 \Lambda_{ij} K_j(s) \vec{e}_i(s) \tag{1}$$

In this expression $[\![\vec{u}(s,r)]\!]$ denotes the displacement discontinuity across the crack plane, oriented by the vector $\vec{e}_1$, at the distance r behind the point s of $\mathscr{F}$, in the direction of the vector $-\vec{e}_2(s)$. Also, $(\Lambda_{ij})_{1\leqslant i\leqslant 3, 1\leqslant j\leqslant 3} \equiv \mathbf{\Lambda}$ is the diagonal matrix defined by

$$\mathbf{\Lambda} \equiv \frac{1}{E} \begin{pmatrix} 1-\nu^2 & 0 & 0 \\ 0 & 1-\nu^2 & 0 \\ 0 & 0 & 1+\nu \end{pmatrix} \tag{2}$$

where E denotes Young's modulus and ν, Poisson's ratio.[2]

2.1.2. Crack face weight functions and fundamental kernels

Let $k_{ij}(\mathscr{F}; s'; s, r)$ denote the ith SIF at the point s' of the crack front $\mathscr{F}$ resulting from application of a pair of opposite unit point forces equal to $\pm\vec{e}_j(s)$ on the upper (+) and lower (−) crack surfaces at a distance r behind the point s of the crack front. These nine scalar functions are called the *crack face weight functions* (CFWFs).

The functions $k_{ij}(\mathscr{F}; s'; s, r)/\sqrt{r}$ are known to have a well-defined limit for $r \to 0$ (see for instance, Leblond et al. (1999)). We then define the matrix $(W_{ij}(s', s))_{1\leqslant i\leqslant 3, 1\leqslant j\leqslant 3} \equiv \mathbf{W}(s', s)$ by the formula

$$W_{ij}(s', s) \equiv \pi \sqrt{\frac{\pi}{2}} D^2(s, s') \lim_{r\to 0} \frac{k_{ij}(\mathscr{F}; s'; s, r)}{\sqrt{r}} \tag{3}$$

where $D(s, s')$ denotes the cartesian distance between points s and s'. The functions $W_{ij}(s', s)$ in fact depend on the crack front shape, just like the CFWFs, but the argument $\mathscr{F}$ is omitted here for conciseness. They will be called the *fundamental kernels* or more shortly the *kernels*.

The CFWFs are positively homogeneous of degree −3/2; that is, if all distances are multiplied by some positive factor λ, the CFWFs are multiplied by $\lambda^{-3/2}$. The definition (3) of the functions $W_{ij}(s', s)$ then implies that they are positively homogeneous of degree 0.

Since tensile and shear problems are uncoupled for a planar crack in an infinite body, whatever the shape of the crack front, the components k_{12}, k_{13}, k_{21} and k_{31} of the CFWFs are zero, so that by Eq. (3):

$$W_{12}(s', s) \equiv W_{13}(s', s) \equiv W_{21}(s', s) \equiv W_{31}(s', s) \equiv 0. \tag{4}$$

Finally, considering two problems, one with point forces equal to $\pm\vec{e}_i$ exerted on the crack faces at (s, r) and one with point forces equal to $\pm\vec{e}_j$ exerted on the crack faces at (s', r'), applying Betti's theorem, and using Eqs. (1) and (3), one sees that the kernels obey the following "symmetry" property:

$$\Lambda_{im} W_{mj}(s, s') = \Lambda_{jm} W_{mi}(s', s) \tag{5}$$

[1] This choice differs from the usual one but coincides with that made by Rice (1989). Its advantage is that the basis vectors are labelled to agree with mode number designations for the SIFs, and this simplifies the reasoning below leading to the expressions of the variations of these SIFs when the crack front is perturbed.

[2] A similar formula holds for an arbitrary anisotropic medium but the matrix $\mathbf{\Lambda}$ is then no longer diagonal.

2.2. Principle of the derivation of the variations of the stress intensity factors and fundamental kernels

Let us now assume that the crack advances, under constant loading, by a small distance $\delta a(s)$ within its plane in the direction perpendicular to its front. The variation of the displacement discontinuity $\delta[\![\vec{u}(s_0,r)]\!]$ at point (s_0,r) is given, to first order in the perturbation, by the following formula Rice (1985):

$$\delta[\![\vec{u}(s_0,r)]\!] = 2\Lambda_{jm}\vec{e}_i(s_0)\int_{\mathscr{F}} k_{ji}(\mathscr{F};s;s_0,r)K_m(s)\delta a(s)\,\mathrm{d}s. \tag{6}$$

The variations of the SIFs will be obtained from there by taking the limit $r \to 0$ in this expression, using their relation to the variation of the displacement discontinuity. In fact, the formula for $\delta K_1(s_0)$ was given by Rice (1989) for a planar crack with arbitrary contour, and those for $\delta K_2(s_0)$ and $\delta K_3(s_0)$, which are of more interest here, by Leblond et al. (1999) for arbitrary, not necessarily planar initial crack geometries, and arbitrary, even possibly kinked, small crack extensions. (Leblond et al. (1999)'s formula in fact extended previous formulae of Gao and Rice (1986) and Gao (1988) which applied to planar shear mode cracks with coplanar extension and straight or circular contour.) However we shall re-derive Leblond et al. (1999)'s formulae here, for two reasons.

(1) The hypothesis of coplanar crack extension makes it possible to greatly simplify Leblond et al. (1999)'s intricate reasoning. Presenting the simple[3] reasoning proposed below offers the advantage that the paper is self-contained at little additional cost.
(2) It will also be necessary to calculate the variations of the kernels since these kernels appear in the formulae for the variations of the SIFs. The derivation of these additional formulae will use a similar, albeit somewhat more complex reasoning, based on the fact that the kernels are related to the CFWFs and thus to some SIFs generated by special loadings. The presentation of the derivation of the formulae for the variations of the SIFs will serve as a useful introduction there.

The formulae for $\delta W_{22}(s_0,s_1)$, $\delta W_{33}(s_0,s_1)$, $\delta W_{23}(s_0,s_1)$ and $\delta W_{32}(s_0,s_1)$ provided below are new. In contrast, it has already been mentioned in Section 1 that the formula for $\delta W_{11}(s_0,s_1)$ was provided by Rice (1989). We shall however re-derive it at no additional cost, since the reasoning presented below applies indifferently to all modes.

2.3. Variation of the stress intensity factors

In a first step, we assume that δa is zero at that point s_0 where the δK_i are to be evaluated (Fig. 2). The basis $(\vec{e}_1^*(s_0)\equiv\vec{e}_1,\vec{e}_2^*(s_0),\vec{e}_3^*(s_0))$ "adapted" to the perturbed crack front at this point is obtained, to first order in the perturbation, through rotation of the old one $(\vec{e}_1(s_0)\equiv\vec{e}_1,\vec{e}_2(s_0),\vec{e}_3(s_0))$ by an angle $\mathrm{d}\delta a(s_0)/\mathrm{d}s \equiv \delta a'(s_0)$ about the vector $\vec{e}_1$. Hence

$$\vec{e}_i^*(s_0) = \vec{e}_i(s_0) + \delta a'(s_0)\vec{e}_1\times\vec{e}_i(s_0) \tag{7}$$

where the symbol $\times$ denotes the vector product. (Note that since the basis $(\vec{e}_1,\vec{e}_2(s_0),\vec{e}_3(s_0))$ is left-handed, $\vec{e}_1\times\vec{e}_2(s_0) = -\vec{e}_3(s_0)$ and $\vec{e}_1\times\vec{e}_3(s_0) = \vec{e}_2(s_0)$).

Let $[\![\vec{u}^*(s_0,r^*)]\!]$ denote the displacement discontinuity across the crack plane in the perturbed crack configuration, at a small distance r^* behind the point s_0 in the direction of the vector $-\vec{e}_2^*(s_0)$ (Fig. 2). By Eq. (1),

$$\lim_{r^*\to 0}\sqrt{\frac{2\pi}{r^*}}[\![\vec{u}^*(s_0,r^*)]\!] = 8\Lambda_{ij}[K_j(s_0)+\delta K_j(s_0)]\vec{e}_i^*(s_0) \tag{8}$$

[3] In principle, less so in details.

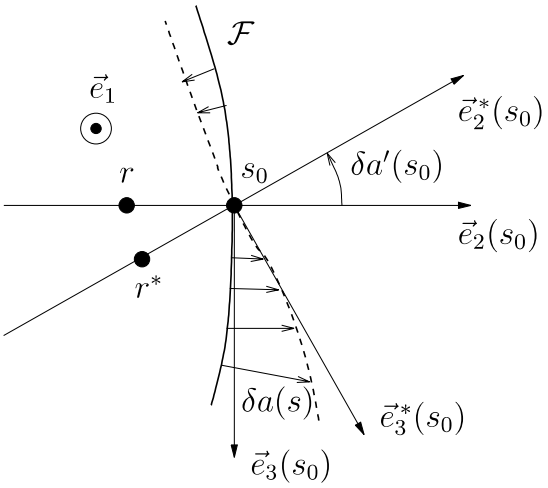

Fig. 2. Motion of the crack front around the immobile point s_0.

Now, by definition,

$$\delta[\![\vec{u}(s_0,r)]\!] \equiv [\![\vec{u}^*(s_0,r)]\!] - [\![\vec{u}(s_0,r)]\!] \tag{9}$$

where $[\![\vec{u}^*(s_0,r)]\!]$ is the displacement discontinuity in the perturbed crack configuration at a distance r behind the point s_0 in the direction of the vector $-\vec{e}_2(s_0)$, *not* $-\vec{e}_2^*(s_0)$ (Fig. 2). However the vector $-\vec{e}_2(s_0)$ here may be replaced by $-\vec{e}_2^*(s_0)$ because the resulting displacement of the observation point is of second order in the perturbation, as is obvious from Fig. 2. Using Eqs. (7) and (8), one then gets

$$\lim_{r\to 0}\sqrt{\frac{2\pi}{r}}\delta[\![\vec{u}(s_0,r)]\!] = 8\left[\Lambda_{ij}\delta K_j(s_0) + \varepsilon_{1ij}\Lambda_{jm}K_m(s_0)\delta a'(s_0)\right]\vec{e}_i(s_0) \tag{10}$$

where the ε_{ijm} denote the permutation symbols.[4]

We shall now use Eq. (6) in the limit $r \to 0$. It is shown in Appendix A that in this limit, the asymptotic behaviour of the integrals in the right-hand side is given by the following formula:

$$\begin{aligned}&\frac{\sqrt{2\pi}}{4}\lim_{r\to 0}\frac{1}{\sqrt{r}}\int_{\mathscr{F}} k_{ji}(\mathscr{F};s;s_0,r)K_m(s)\delta a(s)\,\mathrm{d}s \\ &\quad = \frac{v}{2-v}(\delta_{j2}\delta_{i3}+\delta_{j3}\delta_{i2})K_m(s_0)\delta a'(s_0) + \frac{1}{2\pi}\mathrm{PV}\int_{\mathscr{F}}\frac{W_{ji}(s,s_0)}{D^2(s_0,s)}K_m(s)\delta a(s)\,\mathrm{d}s\end{aligned} \tag{11}$$

where the δ_{ij} denote Kronecker's symbols and the integral in the right-hand side is to be understood as a Cauchy principal value (PV). Dividing then Eq. (6) by $\sqrt{r}$ and taking the limit $r \to 0$ using Eqs. (10) and (11), one obtains after some algebraic manipulations the following formula:

$$\delta\mathbf{K}(s_0) = \mathbf{N}\cdot\mathbf{K}(s_0)\delta a'(s_0) + \frac{1}{2\pi}\mathrm{PV}\int_{\mathscr{F}}\frac{\mathbf{W}(s_0,s)}{D^2(s_0,s)}\cdot\mathbf{K}(s)\delta a(s)\,\mathrm{d}s \tag{12}$$

The quantities $\mathbf{K}(s) \equiv (K_i(s))_{1\leqslant i\leqslant 3}$ and $\delta K(s) \equiv (\delta\mathbf{K}_i(s))_{1\leqslant i\leqslant 3}$ here are the column vectors of initial SIFs and variations of these SIFs, and $\mathbf{N} \equiv (N_{ij})_{1\leqslant i\leqslant 3,1\leqslant j\leqslant 3}$ is the matrix defined by

[4] $\varepsilon_{ijm} = 0$ if two indices are equal, 1 if $\{i,j,m\}$ is a positive permutation of $\{1,2,3\}$, -1 if it is a negative permutation.

$$\mathbf{N} \equiv \frac{2}{2-\nu}\begin{pmatrix} 0 & 0 & 0 \\ 0 & 0 & -1 \\ 0 & 1-\nu & 0 \end{pmatrix} \tag{13}$$

Eq. (12) is identical to Leblond et al. (1999)'s general equation (30)' (with the notation $\frac{1}{2\pi}\frac{\mathbf{W}(s_0,s)}{D^2(s,s_0)}$ instead of $\mathbf{Z}(s_0,s)$), in the special case of a planar crack with coplanar extension (and zero crack advance at the point s_0).

The restriction $\delta a(s_0)=0$ will now be removed by using a trick of Rice (1989). This trick consists of decomposing an arbitrary motion of the crack front defined by the normal advance $\delta a(s)$ into two steps:

(1) A translatory motion of displacement vector $\delta a(s_0)\vec{e}_2(s_0)$. This motion brings the point s_0 to its correct final position while leaving the crack front shape unchanged. The corresponding normal advance $\delta_* a(s)$ is given, to first order in $\delta a(s)$, by
$$\delta_* a(s) = \delta a(s_0)\vec{e}_2(s_0)\cdot\vec{e}_2(s) \tag{14}$$
The associated variation of $\mathbf{K}(s)$ will be denoted $\boldsymbol{\delta}_*\mathbf{K}(s)$.
(2) A motion with normal advance given by $\delta a(s)-\delta_* a(s)$. This advance is zero at point s_0 so that the corresponding variation of $\mathbf{K}(s_0)$ is given by Eq. (12), with $\delta a'(s_0)-\delta_* a'(s_0)=\delta a'(s_0)$ since $\delta_* a'(s_0)=0$ by Eq. (14).

Adding up the contributions from these two motions, one gets the final expression of the variation of the SIFs under constant loading in the general case:

$$\delta\mathbf{K}(s_0) = \delta_*\mathbf{K}(s_0) + \mathbf{N}\cdot\mathbf{K}(\mathbf{s_0})\delta a'(s_0) + \frac{1}{2\pi}\mathrm{PV}\int_{\mathscr{F}}\frac{\mathbf{W}(s_0,s)}{D^2(s_0,s)}\cdot\mathbf{K}(s)[\delta a(s)-\delta_* a(s)]\,\mathrm{d}s \tag{15}$$

2.4. Variation of the fundamental kernels

The method of derivation of the first-order formula for $\delta\mathbf{W}(s_0,s_1)$ consists of applying Eq. (12) to those special loadings defining the kernels, that is, pairs of opposite, unit point forces exerted on the crack faces close to the crack front.

We first make the assumption that the crack advance δa is zero at points s_0 and s_1. We also define the following CFWFs pertaining to the perturbed crack configuration:

(1) $k^*_{ij}(\mathscr{F}^*;s_0;s_1,r^*)$ is the ith SIF at point s_0 on the perturbed crack front $\mathscr{F}^*$ when point forces equal to $\pm\vec{e}^*_j(s_1)$ are applied at a distance r^* behind point s_1 on this front in the direction of the vector $-\vec{e}^*_2(s_1)$;
(2) $k^*_{ij}(\mathscr{F}^*;s_0;s_1,r)$ is defined in the same way except that the forces are exerted at a distance r behind point s_1 in the direction of the vector $-\vec{e}_2(s_1)$ instead of $-\vec{e}^*_2(s_1)$;
(3) $k_{ij}(\mathscr{F}^*;s_0;s_1,r)$ is defined in the same way as $k^*_{ij}(\mathscr{F}^*;s_0;s_1,r)$ except that the forces are equal to $\pm\vec{e}_j(s_1)$ instead of $\pm\vec{e}^*_j(s_1)$.

Suppose that forces equal to $\pm\vec{e}_j(s_1)$ are applied at a distance r behind point s_1 in the direction of the vector $-\vec{e}_2(s_1)$, and compare the ith resulting SIFs at point s_0 in the initial and perturbed configurations of the crack. Eq. (12) yields, in this specific case:

$$\begin{aligned} &k_{ij}(\mathscr{F}^*;s_0;s_1,r) - k_{ij}(\mathscr{F};s_0;s_1,r) \\ &\quad = N_{im}k_{mj}(\mathscr{F};s_0;s_1,r)\delta a'(s_0) + \frac{1}{2\pi}\mathrm{PV}\int_{\mathscr{F}}\frac{W_{im}(s_0,s)}{D^2(s_0,s)}k_{mj}(\mathscr{F};s;s_1,r)\delta a(s)\,\mathrm{d}s \end{aligned} \tag{16}$$

Now, by definition,

$$\delta W_{ij}(s_0,s_1)=\pi\sqrt{\frac{\pi}{2}}D^2(s_0,s_1)\left(\lim_{r^*\to 0}\frac{k^*_{ij}(\mathscr{F}^*;s_0;s_1,r^*)}{\sqrt{r^*}}-\lim_{r\to 0}\frac{k_{ij}(\mathscr{F};s_0;s_1,r)}{\sqrt{r}}\right) \tag{17}$$

In the first limit here, $k^*_{ij}(\mathscr{F}^*;s_0;s_1,r^*)$ may be replaced by $k^*_{ij}(\mathscr{F}^*;s_0;s_1,r)$ since the error thus introduced on the position of the point of application of the forces is of second order in the perturbation; thus

$$\delta W_{ij}(s_0,s_1)=\pi\sqrt{\frac{\pi}{2}}D^2(s_0,s_1)\lim_{r\to 0}\frac{k^*_{ij}(\mathscr{F}^*;s_0;s_1,r)-k_{ij}(\mathscr{F};s_0;s_1,r)}{\sqrt{r}} \tag{18}$$

Using now linearity with respect to the loading and Eq. (7) to express the $k^*_{ij}(\mathscr{F}^*;s_0;s_1,r)$ in terms of the $k_{ij}(\mathscr{F}^*;s_0;s_1,r)$, one gets after some manipulations

$$\begin{aligned}\delta W_{ij}(s_0,s_1)=&\pi\sqrt{\frac{\pi}{2}}D^2(s_0,s_1)\lim_{r\to 0}\frac{k_{ij}(\mathscr{F}^*;s_0;s_1,r)-k_{ij}(\mathscr{F};s_0;s_1,r)}{\sqrt{r}}\\&+\left[\delta_{j3}W_{i2}(s_0,s_1)-\delta_{j2}W_{i3}(s_0,s_1)\right]\delta a'(s_1)\end{aligned} \tag{19}$$

Inserting Eq. (16) in this result and taking the limit $r\to 0$ in the same way as in Section 2.3, using in particular equation (11), one then obtains

$$\begin{aligned}\delta\mathbf{W}(s_0,s_1)=&\mathbf{N}\cdot\mathbf{W}(s_0,s_1)\delta a'(s_0)-\mathbf{W}(s_0,s_1)\cdot\mathbf{N}\delta a'(s_1)\\&+\frac{D^2(s_0,s_1)}{2\pi}\ \mathrm{PV}\int_{\mathscr{F}}\frac{\mathbf{W}(s_0,s)\cdot\mathbf{W}(s,s_1)}{D^2(s_0,s)D^2(s_1,s)}\delta a(s)\,\mathrm{d}s\end{aligned} \tag{20}$$

In order to finally get rid of the hypothesis $\delta a(s_0)=\delta a(s_1)=0$, we use another trick of Rice (1989). This trick consists of now decomposing an arbitrary motion of the crack front, defined by the normal advance δa(s), into a motion corresponding to some advance $\delta_{**}a(s)$ and bringing points s_0 and s_1 to their correct final positions while leaving the kernels unchanged, plus a motion corresponding to the advance $\delta a(s)-\delta_{**}a(s)$, which is zero at s_0 and s_1. More specifically, one can always find a combination of a translatory motion, a rotation and a homothetical transformation bringing two distinct points s_0, s_1 from any initial positions to any final positions. (This is obvious using a complex variable formalism and noting that such transformations are of the form $f(z)=az+b$, where a and b are arbitrary complex parameters.) Such a combination does leave the kernels unaffected because they are independent of the position of the crack in its plane, its orientation and its size. Application of Eq. (20) to the second motion then yields the final expression of the variation of the kernels under constant loading in the general case:

$$\begin{aligned}\delta\mathbf{W}(s_0,s_1)=&\mathbf{N}\cdot\mathbf{W}(s_0,s_1)[\delta a'(s_0)-\delta_{**}a'(s_0)]-\mathbf{W}(s_0,s_1)\cdot\mathbf{N}[\delta a'(s_1)-\delta_{**}a'(s_1)]\\&+\frac{D^2(s_0,s_1)}{2\pi}\mathrm{PV}\int_{\mathscr{F}}\frac{\mathbf{W}(s_0,s)\cdot\mathbf{W}(s,s_1)}{D^2(s_0,s)D^2(s_1,s)}[\delta a(s)-\delta_{**}a(s)]\,\mathrm{d}s\end{aligned} \tag{21}$$

Note that quantities $\delta_{**}a'(s_0)$ and $\delta_{**}a'(s_1)$ here are nonzero, unlike quantity $\delta_{*}a'(s_0)$ in Eq. (15). The formula for the component $\delta W_{11}(s_0,s_1)$ is identical to that derived by Rice (1989).

3. Numerical procedure

3.1. General hypotheses

Formula (15) provides the first-order variation $\delta\mathbf{K}(s_0)$ of $\mathbf{K}(s_0)$ arising from some small coplanar perturbation of the crack front under conditions of constant prescribed loading, provided that the variation

$\delta_*\mathbf{K}(s_0)$ of $\mathbf{K}(s_0)$ for a translatory motion of the crack front is known. Such is notably the case for a loading consisting of uniform stresses applied at infinity; indeed $\delta_*\mathbf{K}(s_0) \equiv 0$ then. Attention is focused on this case in the sequel, and more specifically on shear loadings, since tensile ones have already been considered by Lazarus (2003).

Crack propagation is assumed to be coplanar, which is reasonable (for the shear loadings envisaged) if it is channeled along some weak planar layer. Such is the case for geological faults and certain cracks in composite materials. Propagation is assumed to be governed by the following Paris-type law:

$$\frac{\partial a}{\partial t}(s,t) = C[\mathscr{G}(s,t)]^{\beta/2} \tag{22}$$

In this expression $\partial a(s,t)/\partial t$ denotes the normal velocity of the crack front and $\mathscr{G}(s,t)$ the local energy release rate, related to the SIFs through Irwin's formula

$$\mathscr{G}(s,t) = \Lambda_{ij}K_i(s,t)K_j(s,t) \tag{23}$$

Also, C and β are material parameters called the *Paris constant* and the *Paris exponent*, respectively. Paris' law is adequate for sub-critical crack growth and fatigue, "t" being re-interpreted as "number of cycles" and "$\mathscr{G}$" as "$\Delta\mathscr{G}$" in the latter case. Following a remark of Lazarus (2003), it may also be considered, in the case of very large Paris exponent, as a kind of "regularization" of Griffith's propagation law for brittle fracture, just as, for instance, Norton's viscoplastic flow rule may be considered as a "viscoplastic regularization" of the Prandtl–Reuss plastic flow rule in the case of very large Norton exponent.

3.2. Lazarus' numerical procedure and its adaptation to shear mode cracks

If $\mathbf{K}(s_0)$ and $\mathbf{W}(s_0,s_1)$ are known for all points s_0, s_1 of some crack front, formula (15) (with $\delta_*\mathbf{K}(s_0) \equiv 0$) and (21) provide their values on any nearby front. Iterating the process, one can calculate them numerically for any arbitrarily deformed crack front. This is the common basis of Bower and Ortiz (1990)'s method for computation of the evolution of tensile cracks, of Lazarus (2003)'s variant of this method, and of the present extension to shear mode cracks.

Each simulation consists of two successive steps:

(1) Determination of the SIFs and kernels for the initial crack front considered. This is done using the incremental procedure just sketched, starting from a "reference" penny-shaped crack, for which they are known (see Section 3.3 below), and using a systematic automatic procedure to generate a sequence of successive crack front shapes ending up with that desired.
(2) Determination of the subsequent propagation path. The procedure is basically the same. However successive crack front shapes are no longer arbitrary but deduced sequentially from one another by using the propagation law (22) in the following time-discretized form:

$$\delta a(s,t_i) = \delta a_{\max}\left(\frac{\mathscr{G}(s,t_i)}{\mathscr{G}_{\max}(t_i)}\right)^{\beta/2} \tag{24}$$

The quantity $\delta a_{\max}$ here denotes the maximum crack advance imposed between consecutive steps, and $\mathscr{G}_{\max}(t_i)$ the maximum instantaneous value of the energy release rate along the crack front.[5] (Incidentally, Eq. (24) makes it clear why Paris' propagation law "simulates" that of Griffith in the case of very large exponent β; indeed in such a case $\delta a(s,t_i)$ is nonzero only if $\mathscr{G}(s,t_i)$ is equal to $\mathscr{G}_{\max}(t_i)$).

[5] Some information is lost in Eq. (24) with respect to Eq. (22), namely the instants corresponding to the successive configurations of the crack front. It is of course possible to calculate these instants, as was done by Lazarus (2003) in the case of tensile loadings, but we shall concentrate here on the sole sequence of successive crack front configurations and forget about the corresponding instants.

Details of the numerical procedure for shear loadings are quite similar to those of the procedure for tensile loadings, as expounded by Lazarus (2003), and will not be repeated here. The only significant difference is that the procedure for shear loadings is notably heavier, due to the inevitable coupling of modes 2 and 3. Advantage is however taken of the symmetry property (5), which relates $W_{23}(s,s')$ to $W_{32}(s',s)$ and thus allows to compute and store only W_{23}.

3.3. Initialization: stress intensity factors and fundamental kernels for a penny-shaped crack

The SIFs and kernels for a penny-shaped crack are needed as initial conditions for the numerical procedure just explained. Fig. 3 shows a top view of such a crack, of radius a. (An elliptic crack is also represented for future purposes.) We consider a global right-handed frame $Oxyz$ with origin O at the centre of the crack and axis Oz perpendicular to its plane, together with the associated polar angle θ in the Oxy plane. The curvilinear abscissa $s \equiv a\theta$ along the crack front is oriented in the same way as the polar angle θ. Fig. 3 also shows the local left-handed basis of vectors $(\vec{e}_1, \vec{e}_2(s), \vec{e}_3(s))$ (on the elliptic crack front for legibility), as defined in Section 2.1.1. Note that with the convention adopted, the normal vectors $\vec{e}_1, \vec{e}_z$ to the crack plane are not equal but opposite, so that $[\![\vec{u}]\!](x,y) \equiv \vec{u}(x,y,z=0^-) - \vec{u}(x,y,z=0^+)$. The loading consists of some uniform shear stress $\sigma_{xz} \equiv \tau$ imposed at infinity.

The SIFs and CFWFs for this geometry and loading were given by Tada et al. (1973) and Bueckner (1987), respectively. With the sign conventions adopted, they read as follows:

$$\begin{cases} K_2(\theta) &= -\dfrac{4}{2-\nu}\tau\sqrt{\dfrac{a}{\pi}}\cos\theta \\ K_3(\theta) &= \dfrac{4(1-\nu)}{2-\nu}\tau\sqrt{\dfrac{a}{\pi}}\sin\theta \end{cases} \tag{25}$$

$$\begin{cases} W_{22}(\theta_1,\theta_2) = \dfrac{2\cos(\theta_1-\theta_2)-3\nu}{2-\nu} \\ W_{33}(\theta_1,\theta_2) = \dfrac{2(1-\nu)\cos(\theta_1-\theta_2)+3\nu}{2-\nu} \\ W_{23}(\theta_1,\theta_2) = \dfrac{1}{1-\nu}W_{32}(\theta_2,\theta_1) = \dfrac{2\sin(\theta_1-\theta_2)}{2-\nu} \end{cases} \tag{26}$$

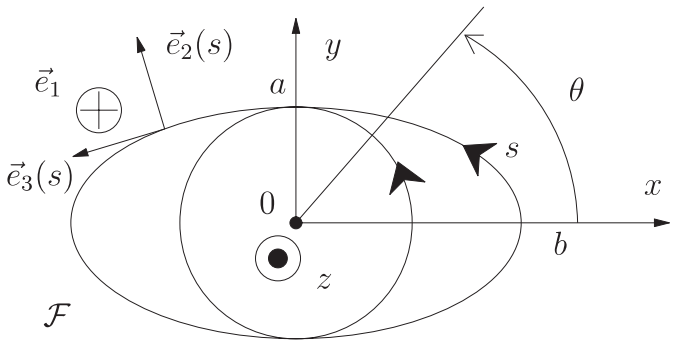

Fig. 3. Top views of penny-shaped and elliptic cracks.

4. Validation: calculation of shear mode stress intensity factors for an elliptic crack

In order to assess the accuracy of the numerical procedure proposed, we shall apply it to the calculation of the SIFs along the front of some elliptic crack obtained through gradual deformation of an initially penny-shaped crack, and compare the results with the known analytic solution. This solution was provided by Kassir and Sih (1966). For an elliptic crack of minor axis a, parallel to the Oy axis, and major axis b, parallel to the Ox axis (see Fig. 3), loaded through some uniform remote shear stress $\sigma_{xz} \equiv \tau$, it reads as follows:

$$\begin{cases} K_2(\theta) = -\dfrac{\alpha^2 f(k,\nu)\cos\theta}{(\sin^2\theta + \alpha^4\cos^2\theta)^{1/4}(\sin^2\theta + \alpha^2\cos^2\theta)^{1/4}}\tau\sqrt{\pi a} \\ K_3(\theta) = \dfrac{(1-\nu) f(k,\nu)\sin\theta}{(\sin^2\theta + \alpha^4\cos^2\theta)^{1/4}(\sin^2\theta + \alpha^2\cos^2\theta)^{1/4}}\tau\sqrt{\pi a} \end{cases} \tag{27}$$

In these expressions θ denotes the polar angle as above (*not* the angle of the classical parametric equations of the ellipse, $x = b\cos\phi$, $y = a\sin\phi$); also, α, k and $f(k,\nu)$ are defined by

$$\alpha \equiv \frac{a}{b}; \quad k \equiv \sqrt{1-\alpha^2}; \quad f(k,\nu) \equiv \frac{k^2}{(k^2-\nu)E(k) + \nu(1-k^2)K(k)} \tag{28}$$

where $K(k)$ and $E(k)$ are the complete elliptic integrals of the first and second kinds (Gradsteyn and Ryzhik, 1965).

Fig. 4 shows theoretical and numerical results for elliptic cracks of various shapes, for a Poisson's ratio of 0.25. The origin of the curvilinear abscissa here is taken at the right endpoint of the major axis. In the numerical calculations, each ellipse is discretized with 200 points, and the maximum stepsize for each increment of deformation of the crack front is $\delta a_{\max} = 2.5\times10^{-3}a$.

Table 1 also displays the mean errors E_2, E_3 defined as

$$E_i \equiv \left\{ \frac{1}{L}\int_0^L \frac{(K_i^{\text{num}}(s) - K_i^{\text{theor}}(s))^2}{4\tau^2 a/\pi}\,\mathrm{d}s \right\}^{1/2} \qquad (i = 2,3) \tag{29}$$

where L is the perimeter of the ellipse.

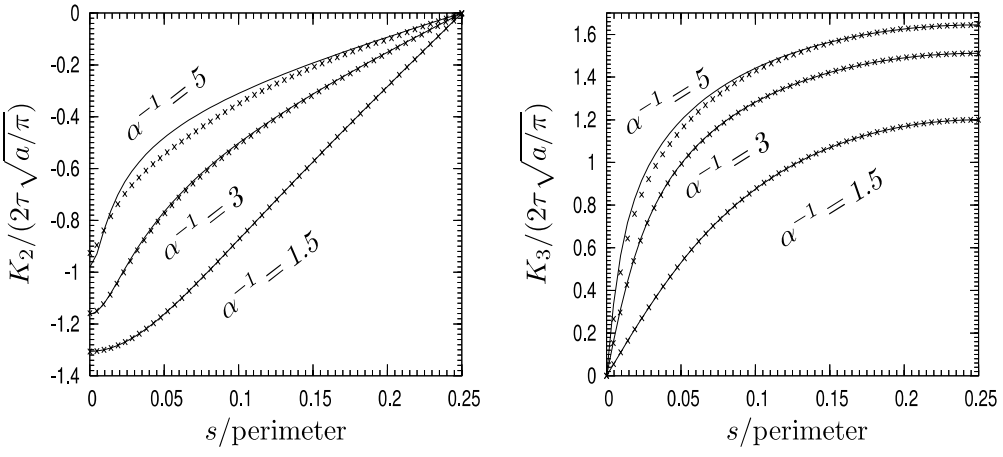

(a) Mode 2 SIF **(b)** Mode 3 SIF

Fig. 4. Shear mode SIFs along the front of various elliptic cracks—Lines: analytical formulae (27); discrete points: numerical results.

Table 1
Mean errors made in the numerical calculation of shear mode SIFs for elliptic cracks

	$\alpha^{-1}=1.5$	$\alpha^{-1}=3$	$\alpha^{-1}=5$
E_2	5.7×10^{-4}	8.7×10^{-3}	4.6×10^{-2}
E_3	3.3×10^{-4}	4.3×10^{-3}	3.2×10^{-2}

Fig. 4 and Table 1 exhibit a good agreement between numerical and theoretical results, even though the errors of course increase with the eccentricity of the ellipse. Also, these errors are larger than those found by Lazarus (2003) when performing similar calculations in mode 1. This can rationalized by the fact that more calculations, introducing more inaccuracies, are required in mode $2+3$: indeed for mode 1 two integrals must be evaluated at each step (one for δK_1 plus one for δW_{11}), versus ten for mode $2+3$ (two for each δK_i, $i=2,3$, plus two for each δW_{ij}, $(i,j)=(2,2),(3,3),(2,3)$).

The errors in Fig. 4 and Table 1 are comparable to those made using the FEM for ellipses with large eccentricities, and notably smaller for ellipses with moderate eccentricities. For instance Sukumar et al. (2003), using the level set method coupled with the XFEM, reported a relative error of 2×10^{-2} in the calculation of K_1 for an elliptic crack with $\alpha^{-1}=2$. This is notably larger than the error reported in Table 1 for mode $2+3$, which is itself larger than that reported by Lazarus (2003) for mode 1.

5. Application to simulation of propagation of shear mode cracks

5.1. Propagation of initially circular, elliptic, rectangular and heart-shaped cracks in fatigue and brittle fracture

We have computed the successive shapes of initially circular, elliptic, rectangular and heart-shaped cracks obeying the propagation law (22). The value of Poisson's ratio used was $\nu=0.25$, and that of Paris' exponent was $\beta=2$ for fatigue and $\beta=50$ ($\approx+\infty$) for brittle fracture. The simulations were stopped when the crack reached a stable shape. Figs. 5 and 6 show the successive crack configurations obtained. The quantity a here denotes a typical dimension of the initial crack shape, the precise definition of which depends on this shape and is conspicuous on the figures.

The difference between successive crack fronts in fatigue and brittle fracture clearly appears in these figures. In fatigue, all points of the crack front move simultaneously. In brittle fracture, propagation occurs only on some "active" part of the front. This active part starts from those points where the energy release rate is initially maximum, and gradually extends over the crack front. The stable crack shape is reached as soon as the whole front has become active.

The stable shape can be observed to be approximately elliptic in all cases; this question will be examined in more detail in the next section. However, in the cases of initially rectangular and heart-shaped cracks, which are numerically tricky because of the presence of angular points on the crack front, one can observe some slight perturbation of the regular shape of the front in the vicinity of these points. This perturbation is due to numerical errors, and therefore provides an appreciation of the accuracy of the method. It clearly appears here that numerical errors accumulate and cannot be corrected for once they are made. This unhappy feature of the numerical procedure of course arises from its incremental nature, and is in clear contrast with those of more classical procedures such as the FEM. It is a counterpart of the simplicity and efficiency of the method.

It is also interesting to note that in the case of propagation of an initially heart-shaped crack in brittle fracture (last diagram of Fig. 6), even when the crack front has reached its stable shape, it does not move symmetrically with respect to its vertical axis of symmetry; the propagation rate is larger on its right part than on its left one. The explanation of this apparent paradox is that in brittle fracture, the motion of the

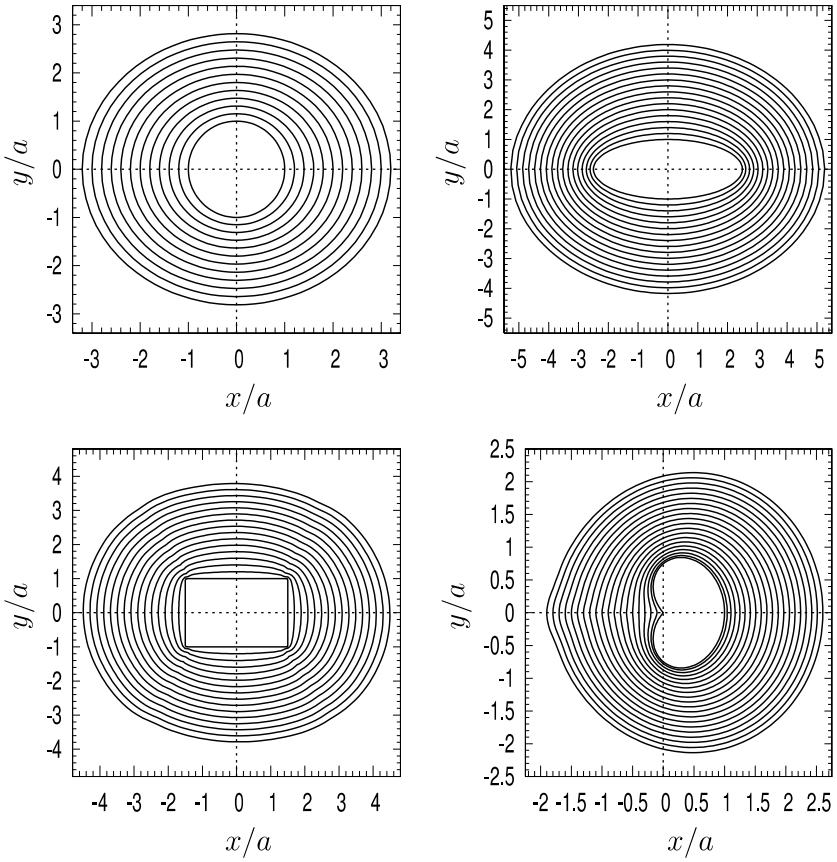

Fig. 5. Successive crack fronts of shear mode cracks in fatigue ($\beta = 2$).

crack front is not defined in a unique way, because the distribution of the energy release rate along the crack front is insensitive to global translational motions of this front; the simulation thus "selects" some possible solution among the very many envisageable, in which the left and right parts of the crack front happen to propagate at different rates. The selection of this specific solution is governed by the initial crack front shape, which is itself not symmetric. A subtle difference appears here between Griffith's original propagation law and its "regularized" variant used here, that is Paris' law with a very large exponent: Griffith's law implies some bifurcation, but this bifurcation is erased by the regularization, just as bifurcations occurring in plasticity are erased by viscoplastic regularizations of the flow rule.

5.2. Theoretical study of the stable shape of the crack front

The aim of this section is to show that the stable shape of the crack front is only *approximately* elliptic, and also to derive an approximate, but accurate analytical formula for the ratio of the axes of this stable shape based on the approximation that it *is* elliptic.

Let $\theta \mapsto r_0(\theta)$ denote the polar representation of the stable shape. Since this shape is preserved in time, the polar representation of the crack front is of the form $\theta \mapsto r(\theta, t) \equiv \lambda(t) r_0(\theta)$ at each instant. For such a propagation path, the normal velocity of the crack front is given by

$$\frac{\partial a}{\partial t}(\theta, t) \equiv \frac{\partial r}{\partial t}(\theta, t)\vec{e}_r(\theta, t) \cdot \vec{e}_2(\theta, t) = \lambda'(t) \frac{r_0^2(\theta)}{\sqrt{r_0'^2(\theta) + r_0^2(\theta)}} \tag{30}$$

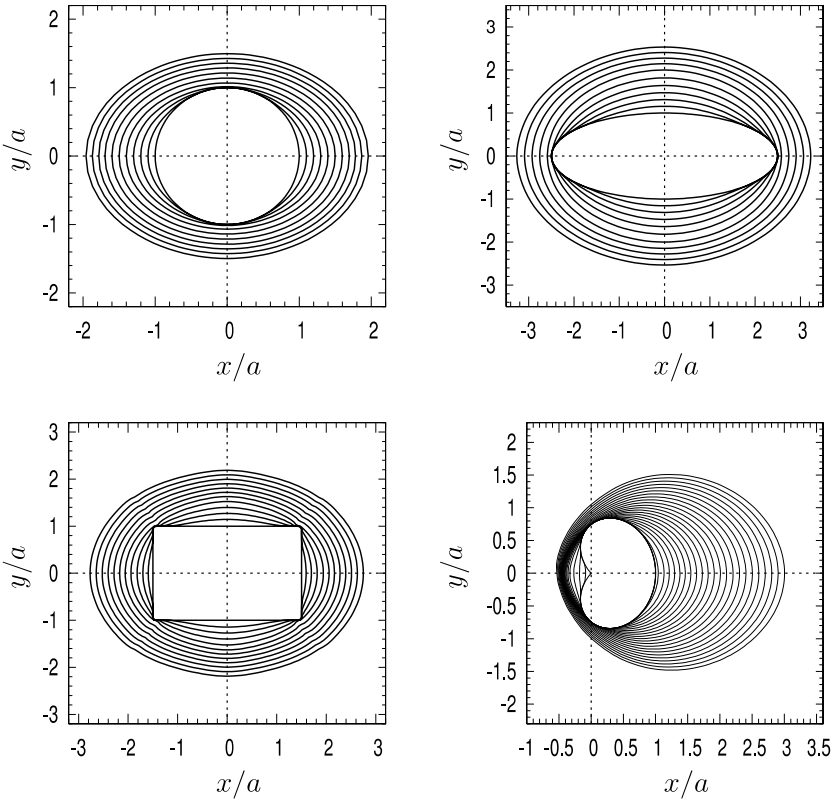

Fig. 6. Successive crack fronts of shear mode cracks in brittle fracture ($\beta = 50$).

Paris' propagation law (22) then implies that

$$\mathscr{G}(\theta,t) \propto \left(\frac{r_0^2(\theta)}{\sqrt{r_0'^2(\theta) + r_0^2(\theta)}} \right)^{2/\beta} \tag{31}$$

Now, for an elliptic crack,

$$r(\theta) = \frac{a}{\sqrt{\sin^2\theta + \alpha^2\cos^2\theta}} \tag{32}$$

and, by Eqs. (23) and (27)

$$\frac{E\mathscr{G}(\theta)}{(1-\nu^2)\tau^2\pi a} = [f(k,\nu)]^2 \frac{\alpha^4\cos^2\theta + (1-\nu)\sin^2\theta}{(\sin^2\theta + \alpha^4\cos^2\theta)^{1/2}(\sin^2\theta + \alpha^2\cos^2\theta)^{1/2}} \tag{33}$$

Eq. (31), with $r_0(\theta)$ given by an expression of type (32), and Eq. (33) stipulate different types of dependence of $\mathscr{G}$ upon θ, whatever the value of Paris' exponent β. Hence the stable shape cannot be elliptic.

However, it has already been noted upon inspection of Figs. 5 and 6 that the elliptic shape is a good approximation to the true stable shape. Accepting this approximation, one can derive an again approximate but accurate formula for the ratio of the axes of the stable shape. Indeed, since this ratio does not vary in time,

$$\frac{(\partial a/\partial t)(\theta = \pi/2, t)}{(\partial a/\partial t)(\theta = 0, t)} = \frac{a}{b} \tag{34}$$

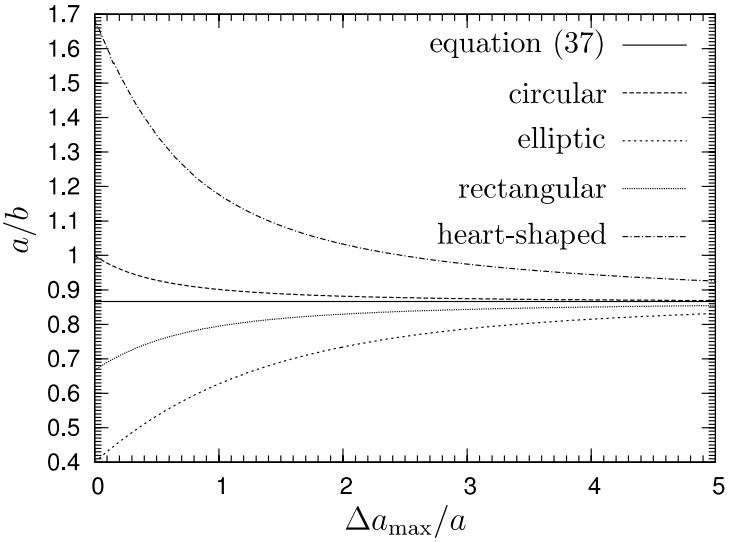

Fig. 7. Evolution of the ratio of the axes of the crack in fatigue ($\beta = 2$).

Also, Paris' propagation law (22) implies that

$$\frac{(\partial a/\partial t)(\theta = \pi/2, t)}{(\partial a/\partial t)(\theta = 0, t)} = \left(\frac{\mathcal{G}(\theta = \pi/2, t)}{\mathcal{G}(\theta = 0, t)}\right)^{\beta/2} \tag{35}$$

Now if the crack is nearly elliptic,

$$\frac{\mathcal{G}(\theta = \pi/2)}{\mathcal{G}(\theta = 0)} \approx (1 - \nu)\frac{b}{a} \tag{36}$$

by Eq. (33). Combining Eqs. (34)–(36), one gets

$$\frac{a}{b} \approx (1 - \nu)^{\frac{\beta}{\beta+2}} \tag{37}$$

The special case where $\beta = +\infty$ (brittle fracture) was considered by Gao (1988), using a first-order perturbation approach based on the assumption of a nearly circular stable shape. He found that for this stable shape,

$$\frac{a}{b} \approx 1 - 2A, \quad A \equiv \frac{\nu(2 - \nu)}{2(2 - 2\nu - \nu^2)} \tag{38}$$

The deviation from a circular shape in this formula is proportional to A and therefore to ν. Thus the perturbation approach is valid only provided that Poisson's ratio is much smaller than unity, and only zeroth- and first-order terms in ν must in fact be retained in formula (38).[6] This formula then reduces to

$$\frac{a}{b} \approx 1 - \nu \tag{39}$$

and this agrees with Eq. (37) for $\beta = +\infty$.

Figs. 7 and 8 show the evolution of the ratio a/b as a function of $\Delta a_{\max}/a$, $\Delta a_{\max}$ denoting the maximum crack advance, for the various initial crack shapes envisaged, in both fatigue and brittle fracture. This ratio

[6] This point seems to have been overlooked by Gao (1988).

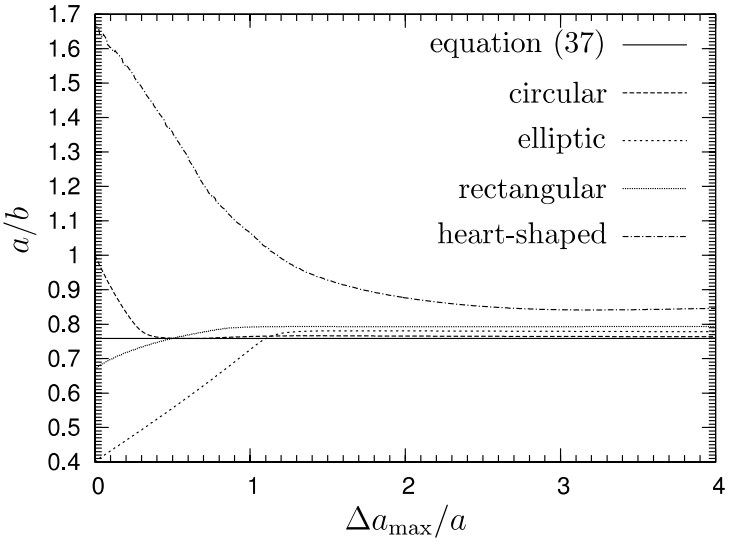

Fig. 8. Evolution of the ratio of the axes of the crack in brittle fracture ($\beta = 50$).

Table 2
Values of $\frac{|(a/b)_{num} - (a/b)_{lim}|}{(a/b)_{lim}}$ in fatigue and brittle fracture

	$\beta = 2$ (%)	$\beta = 50$ (%)
Circular	0.3	0.7
Elliptic	4	2.8
Rectangular	1.3	4.8
Heart-shaped	6.8	11.6

can be observed to tend toward some limit independent of the initial crack shape and in acceptable agreement with the theoretical value provided by Eq. (37).

Table 2 allows to better appreciate the convergence of numerical values of a/b toward their theoretical limit given by Eq. (37). It shows the relative gap between this theoretical limit value and that obtained numerically after an maximum advance of $5a$ in the case of fatigue, and $4a$ in the case of brittle fracture. It can be observed that convergence is slowest for the initially heart-shaped crack in both fatigue and brittle fracture. The obvious explanation is that this is the initial crack shape that differs most markedly from the stable, quasi-elliptic crack shape. Also, the agreement between numerical and theoretical limit values of a/b is better for $\beta = 2$ than for $\beta = 50$. This is again no surprise because for very large values of β, the local propagation rate is very sensitive to the local value of the energy release rate, and this enhances the impact of numerical errors.

6. Summary and conclusion

This paper was devoted to numerical simulation of coplanar propagation (channeled along some weak planar layer) of shear mode cracks with arbitrary contour. The crack was assumed to be embedded in some infinite body loaded through uniform remote stresses. Propagation laws pertaining to both brittle fracture and fatigue were envisaged.

We first derived formulae providing, to first order, the variations of the three stress intensity factors resulting from a small but otherwise arbitrary coplanar perturbation of the crack front, under conditions of constant prescribed loading. The expressions of these variations consisted of integrals along the crack front involving some matrix "kernel" linked to the crack face weight functions, plus some "local" terms. The first-order expressions of the variations of the components of this kernel were also derived.

These results were then used to extend Lazarus (2003)'s simplified variant of Bower and Ortiz (1990, 1991, 1993)'s method for numerical simulation of coplanar propagation of mode 1 cracks to mixed-mode (2 + 3) cracks. The propagation paths of initially circular, elliptic, rectangular and heart-shaped shear mode cracks were studied in both fatigue and brittle fracture. These simulations evidenced the existence of some almost elliptic stable crack front shape, toward which all the crack fronts considered were observed to evolve. An approximate but accurate formula providing the ratio of the axes of this stable shape as a function of Poisson's ratio and Paris' exponent was finally derived.

Appendix A. Justification of formula (11)

The aim of this appendix is to calculate the limit in the left-hand side of Eq. (11) of the text.

It is recalled that the crack advance δa in this formula is assumed to be zero at the point s_0. Without any loss of generality, we can assume that $s_0 = 0$. Also, we split the integration domain $(-\infty, +\infty)$ into $[(-\infty, -\eta) \cup (\eta, +\infty)] \cup [-\eta, \eta]$, η being an arbitrary positive number. This number is fixed for the moment but will go to zero at the end of the reasoning.

Consider the integral over $(-\infty, -\eta) \cup (\eta, +\infty)$ first. For any fixed s in this domain, the quantity $k_{ji}(\mathscr{F}; s; s_0, r)/\sqrt{r} \equiv k_{ji}(\mathscr{F}; s; 0, r)/\sqrt{r}$ has a finite limit for $r \to 0$ given by Eq. (3). Hence

$$\lim_{r\to 0} \frac{1}{\sqrt{r}} \int_{(-\infty,-\eta)\cup(\eta,+\infty)} k_{ji}(\mathscr{F}; s; 0, r) K_m(s) \delta a(s)\, \mathrm{d}s = \frac{1}{\pi}\sqrt{\frac{2}{\pi}} \int_{(-\infty,-\eta)\cup(\eta,+\infty)} \frac{W_{ji}(s,0)}{D^2(s,0)} K_m(s) \delta a(s)\, \mathrm{d}s \tag{A.1}$$

Note that the term $D^2(s, 0)$ in the denominator here does not raise any problem of convergence of the integral since it never becomes zero in the domain $(-\infty, -\eta) \cup (\eta, +\infty)$.

Taking the limit of the integral over $[-\eta, \eta]$ is more difficult because $D^2(s, 0)$ vanishes on this interval at the point $s_0 = 0$. Performing a first-order Taylor expansion of the quantity $K_m(s)\delta a(s)$ around this point in this integral, one gets

$$\begin{aligned} &\frac{1}{\sqrt{r}} \int_{-\eta}^{\eta} k_{ji}(\mathscr{F}; s; 0, r) K_m(s) \delta a(s)\, \mathrm{d}s \\ &\quad = K_m(0)\delta a'(0) \int_{-\eta}^{\eta} \frac{k_{ji}(\mathscr{F}; s; 0, r)}{\sqrt{r}} s\, \mathrm{d}s + \int_{-\eta}^{\eta} \frac{k_{ji}(\mathscr{F}; s; 0, r)}{\sqrt{r}} \mathrm{O}(s^2)\, \mathrm{d}s \end{aligned} \tag{A.2}$$

Now in the special cases where the CFWFs are known explicitly, that is for a semi-infinite crack (Gao and Rice, 1986), a penny-shaped crack (Gao, 1988) and an external circular crack loaded in mode 1 (Gao and Rice, 1987), the quantities $k_{ji}(\mathscr{F}; s; 0, r)/\sqrt{r}$ are bounded by a constant times s^{-2} for $s \to 0$. Making the reasonable assumption that this is true in general, we conclude that the integrand in the second term of the right-hand side of Eq. (A.2) is O(1) for $s \to 0$, so that this equation may be rewritten as

$$\frac{1}{\sqrt{r}} \int_{-\eta}^{\eta} k_{ji}(\mathscr{F}; s; 0, r) K_m(s) \delta a(s)\, \mathrm{d}s = K_m(0)\delta a'(0) \int_{-\eta}^{\eta} \frac{k_{ji}(\mathscr{F}; s; 0, r)}{\sqrt{r}} s\, \mathrm{d}s + \mathrm{O}(\eta) \tag{A.3}$$

In order to calculate the limit of the integral in the right-hand side of Eq. (A.3), let us use the property of positive homogeneity of degree $-3/2$ of the CFWFs and the change of variable $s' \equiv s/r$; we thus get

$$\int_{-\eta}^{\eta} \frac{k_{ji}(\mathscr{F};s;0,r)}{\sqrt{r}} s\,\mathrm{d}s = \int_{-\eta/r}^{\eta/r} k_{ji}(\mathscr{F}/r;s';0,1)s'\,\mathrm{d}s' \tag{A.4}$$

The $k_{ji}(\mathscr{F}/r;s';0,1)$ here represent the CFWFs at the observation point s', when unit point forces are exerted on the crack faces at a distance of unity from the point $s_0 = 0$ of the crack front $\mathscr{F}$, this front being "dilated" by a factor of $1/r$. In the limit $r \to 0$, the curvature of this dilated front becomes zero, so that the $k_{ji}(\mathscr{F}/r;s';0,1)$ become identical to the CFWFs of a half-plane crack. Also, the lower and upper bounds $\pm\eta/r$ of the integral go to $\pm\infty$. Using the well-known expressions of the CFWFs for a half-plane crack (Gao and Rice, 1986), one then gets

$$\lim_{r\to 0} \int_{-\eta}^{\eta} \frac{k_{ji}(\mathscr{F};s;0,r)}{\sqrt{r}} s\,\mathrm{d}s = \begin{cases} 0 & \text{if } (j,i) = (2,2) \text{ or } (3,3) \\ \sqrt{\dfrac{1}{2\pi}}\dfrac{4\nu}{2-\nu} & \text{if } (j,i) = (2,3) \text{ or } (3,2) \end{cases} \tag{A.5}$$

Combination of Eqs. (A.3) and (A.5) then yields

$$\lim_{r\to 0} \frac{1}{\sqrt{r}} \int_{-\eta}^{\eta} k_{ji}(\mathscr{F};s;0,r) K_m(s)\delta a(s)\,\mathrm{d}s = \sqrt{\frac{1}{2\pi}}\frac{4\nu}{2-\nu}(\delta_{j2}\delta_{i3} + \delta_{j3}\delta_{i2})K_m(0)\delta a'(0) + \mathrm{O}(\eta) \tag{A.6}$$

Combining Eqs. (A.1) and (A.6), and then letting η go to zero, one finally gets Eq. (11) of the text (with $s_0 = 0$).

References

Bonnet, M., 1994. Equations intégrates et éléments de frontière en mécanique des solides. Ecole Polytechnique (Palaiseau), Ch. 2 et 5.

Bower, A.F., Ortiz, M., 1990. Solution of three-dimensional crack problems by a finite perturbation method. Journal of the Mechanics and Physics of Solids 38 (4), 443–480.

Bower, A.F., Ortiz, M., 1991. A three-dimensional analysis of crack trapping and bridging by tough particles. Journal of the Mechanics and Physics of Solids 39 (6), 815–858.

Bower, A.F., Ortiz, M., 1993. An analysis of crack trapping by residual stresses in brittle solids. Transactions of the ASME. Journal of Applied Mechanics 60 (1), 175–182.

Bueckner, H.F., 1970. A novel principle for the computation of stress intensity factors. Zeitschrift fur Angewandte Mathematik und Mechanik 50 (9), 529–546.

Bueckner, H.F., 1973. Field singularities and related integral representations (crack analysis). In: Sih, G.C. (Ed.), Mechanics of Fracture, vol. 1, Methods of Analysis and Solutions of Crack Problems. Noordhoff, Leyden, The Netherlands.

Bueckner, H.F., 1987. Weight functions and fundamental fields for the penny-shaped and the half-plane crack in three-space. International Journal of Solids and Structures 23 (1), 57–93.

Fares, N., 1989. Crack fronts trapped by arrays of obstacles: numerical solutions based on surface integral representation. Transactions of the ASME. Journal of Applied Mechanics 56 (4), 837–843.

Gao, H., 1988. Nearly circular shear mode cracks. International Journal of Solids and Structures 24 (2), 177–193.

Gao, H., Rice, J.R., 1986. Shear stress intensity factors for planar crack with slightly curved front. ASME Journal of Applied Mechanics 53 (4), 774–778.

Gao, H., Rice, J.R., 1987. Nearly circular connections of elastic half spaces. ASME Journal of Applied Mechanics 54 (4), 627–634.

Gradsteyn, I.S., Ryzhik, I.M., 1965. Tables of Integrals Series, and Products. Academic Press, New York.

Gravouil, A., Moes, N., Belytschko, T., 2002. Non-planar 3d crack growth by the extended finite element and level sets. II. Level set update. International Journal for Numerical Methods in Engineering 53 (11), 2569–2586.

Kassir, M.K., Sih, G.C., 1966. Three-dimensional stress distribution around an elliptical crack under arbitrary loadings. ASME Journal of Applied Mechanics 33 (3), 601–611.

Lazarus, V., 2003. Brittle fracture and fatigue propagation paths of 3D plane cracks under uniform remote tensile loading. International Journal of Fracture 112 (1–2), 23–46.

Leblond, J.-B., Lazarus, V., Mouchrif, S.-E., 1999. Crack paths in three-dimensional elastic solids. II. Three-term expansion of the stress intensity factors—Applications and perspectives. International Journal of Solids and Structures 36 (1), 105–142.

Moes, N., Gravouil, A., Belytschko, T., 2002. Non-planar 3d crack growth by the extended finite element and level sets. I. Mechanical model. International Journal for Numerical Methods in Engineering 53 (11), 2549–2568.

Rice, J.R., 1972. Some remarks on elastic crack-tip stress fields. International Journal of Solids and Structures 8 (6), 751–758.

Rice, J.R., 1985. First-order variation in elastic fields due to variation in location of a planar crack front. ASME Journal of Applied Mechanics 52 (3), 571–579.

Rice, J.R., 1989. Weight function theory for three-dimensional elastic crack analysis. In: Wei, R.P., Gangloff, R.P. (Eds.), Fracture Mechanics: Perspectives and Directions (Twentieth Symposium). American Society for Testing and Materials STP 1020, Philadelphia, USA.

Sukumar, N., Chopp, D.L., Moran, B., 2003. Extended finite element method and fast marching method for three-dimensional fatigure crack propagation. Engineering Fracture Mechanics 70 (1), 29–48.

Tada, H., Paris, P.C., Irwin, G.R., 1973. The Stress Analysis of Cracks Handbook. Del Research Corporation, Hellertown, USA.

Xu, G., Ortiz, M., 1993. A variational boundary integral method for the analysis of 3-d cracks of arbitrary geometry modelled as continuous distributions of dislocation loops. International Journal for Numerical Methods in Engineering 36 (21), 3675–3701.

Xu, G., Bower, A., Ortiz, M., 1994. An analysis of non-planar crack growth under mixed mode loading. International Journal of Solids and Structures 31 (16), 2167–2193.

Available online at www.sciencedirect.com
ScienceDirect
Journal of the Mechanics and Physics of Solids 56 (2008) 1269–1295
JOURNAL OF THE MECHANICS AND PHYSICS OF SOLIDS
www.elsevier.com/locate/jmps

The deformation of the front of a 3D interface crack propagating quasistatically in a medium with random fracture properties

Nadjime Pindra, Véronique Lazarus, Jean-Baptiste Leblond*

Université Pierre et Marie Curie-Paris 6, CNRS, UMR 7190 (Institut Jean Le Rond d'Alembert), Boîte courrier 161-2, 4 place Jussieu, F-75005 Paris, France

Received 19 June 2007; received in revised form 13 September 2007; accepted 14 September 2007

Abstract

One studies the evolution in time of the deformation of the front of a semi-infinite 3D interface crack propagating quasistatically in an infinite heterogeneous elastic body. The fracture properties are assumed to be lower on the interface than in the materials so that crack propagation is channelled along the interface, and to vary randomly within the crack plane. The work is based on earlier formulae which provide the first-order change of the stress intensity factors along the front of a semi-infinite interface crack arising from some small but otherwise arbitrary in-plane perturbation of this front. The main object of study is the long-time behavior of various statistical measures of the deformation of the crack front. Special attention is paid to the influences of the mismatch of elastic properties, the type of propagation law (fatigue or brittle fracture) and the stable or unstable character of 2D crack propagation (depending on the loading) upon the development of this deformation.

Keywords: Crack mechanics; Inhomogeneous material; Asymptotic analysis; 3D interface crack

1. Introduction

Three-dimensional interfacial fracture mechanics is not an easy subject, and the literature devoted to this topic is still very scarce. The first contributions in this field were due to Willis (1971, 1972) and contained solutions for internal and external circular interface cracks subjected to polynomial (not necessarily axisymmetric) loads. Then almost 30 years elapsed before Lazarus and Leblond (1998a, b) considered the problem of small coplanar perturbation of the front of a semi-infinite interface crack.

Lazarus and Leblond (1998a) first analyzed the variation of the stress intensity factors (SIFs) along the front of such a crack. Their method of solution was, in Bueckner's (1987) terminology, "special" rather than "general" since it did not yield the full solution of the elasticity problem implied but concentrated on the sole distribution of the SIFs along the crack front, at the expense of completeness but with the advantage of

*Corresponding author.
E-mail address: leblond@lmm.jussieu.fr (J.-B. Leblond).

0022-5096/$ - see front matter © 2007 Elsevier Ltd. All rights reserved.
doi:10.1016/j.jmps.2007.09.007

(relative) simplicity and elegance. This method basically stood as an extension of that devised in the work of Rice (1985), and used there and in the work of Gao and Rice (1986) to analyze the same problem but for an ordinary crack in an elastically homogeneous medium. The basis of Rice's (1985) method was a reformulation of Bueckner's weight function theory; Bueckner's 3D weight functions for a semi-infinite *ordinary* crack in an infinite body have been known for a long time, and this allowed Rice (1985) and Gao and Rice (1986) to derive explicit formulae for the perturbation of the SIFs for such a crack. In contrast, the 3D weight functions for a semi-infinite *interface* crack in an infinite body were unknown in 1998, and this prevented Lazarus and Leblond (1998a) from deriving similar fully explicit formulae for this type of crack. They nevertheless succeeded in establishing formulae containing only five unknown constants γ_+, γ_-, γ_{III}, γ_z, γ depending on the elastic properties of the materials, thus reducing the problem to the evaluation of these constants.

Lazarus and Leblond (1998b) then tried to calculate the "γ" constants, with mitigated success. The method they used was similar to that already employed by Leblond et al. (1996) to evaluate the 3D weight function of a tensile tunnel-crack embedded in an infinite body. The basic idea was to apply the formulae established previously to special motions of the crack front preserving its shape while modifying its position and orientation, namely translatory motions and rotations. The output of this procedure consisted of differential equations on the Fourier transforms of the weight functions in the direction of the crack front which, in theory, allowed to evaluate these functions, together with the "γ" constants. Unfortunately, these differential equations were too complex to be solvable analytically in general. As a consequence, analytical expressions of the weight functions and the "γ" constants could be found only for small values of the "bielastic constant" ε, to first order in this constant. For arbitrary values of ε, the weight functions and the "γ" constants could only be calculated numerically.

A few years later, the problem of the semi-infinite interface crack with a slightly wavy front was re-investigated completely independently by Bercial-Velez et al. (2005), using some techniques devised by Willis (1971, 1972), Willis and Movchan (1995) and Antipov (1999). Their elaborate method of solution was "general" in Bueckner's (1987) terminology since it yielded, in principle, the full solution of the elasticity problem implied, and in particular did not involve any unknown quantities analogous to Lazarus and Leblond's "γ" constants. Unfortunately the format in which the solution was expressed was not very explicit and did not allow for a comparison with Lazarus and Leblond's (1998a, b) results.

Very recently, the problem was again revisited by Piccolroaz et al. (2007) with the idea of filling this gap. The new work was inspired by that of Bercial-Velez et al. (2005), but rather than concentrating again on the perturbed crack problem, Piccolroaz et al. directly calculated the 3D weight functions of a semi-infinite interface crack. The formulae they obtained were sufficiently explicit to yield the exact analytic expressions of all "γ" constants, for arbitrary values of the bielastic constant ε. Detailed comparison with the numerical values of these constants obtained by Lazarus and Leblond (1998b) revealed an excellent agreement, thus validating the results obtained in both works.

It is therefore now possible to supplement Lazarus and Leblond's (1998a) formulae for the SIFs of a slightly perturbed semi-infinite interface crack with Piccolroaz et al.'s (2007) expressions of the "γ" constants appearing in these formulae. One thus gets fully explicit, analytic formulae for these SIFs, which be called the *LLPMM formulae*[1] in the sequel.

The aim of the present paper is to apply the LLPMM formulae to the study of the evolution in time of the deformation of the front of a semi-infinite interface crack propagating quasistatically in a medium whose fracture properties are random functions of position. These properties will be assumed to be lower on the interface than in the materials, thereby channelling crack propagation along the interface. Two types of propagation laws will be envisaged: fatigue governed by a Paris-type law and brittle fracture governed by a Griffith-type law. Several types of loadings will also be considered.

This work comes as a natural complement to a number of papers published in the past 15 years, which were devoted to similar studies of the deformation of the front of a crack propagating in a material with spatially variable fracture properties, but with different geometrical and mechanical hypotheses. All of these papers bore potential applications in the context of propagation of geological faults and cracks in composites.

[1]LLPMM: Lazarus–Leblond–Piccolroaz–Mishuris–Movchan.

Perrin and Rice (1994) and Wolfries and Willis (1999) first considered the case of a semi-infinite mode I crack propagating dynamically in a homogeneous elastic solid obeying a model scalar wave equation. Propagation was assumed to be governed by some Griffith-type law with a spatially variable fracture toughness. Using a previous work of Rice et al. (1994), Perrin and Rice (1994) studied several statistical measures of the deformation of the crack front. These measures were found to grow without bound at a moderate rate proportional to the logarithm of time. The emphasis of Wolfries and Willis's (1999) subsequent work was on the effect of the "next" term (proportional to the square root of the distance to the crack front) in the expansion of the tensile stress ahead of the crack front, which had been disregarded in the previous work. The conclusion was that this term has a major influence upon the rate of development of the "wavyness" of the crack front.

Perrin and Rice's (1994) work was also extended to true elastic solids obeying the vectorial equations of elastodynamics by Morrissey and Rice (1998, 2000), using Willis and Movchan's (1995) recent discovery of the exact expression of the 3D mode I dynamic weight function for a semi-infinite crack. They found that the deformation of the crack front increased proportionally to time. This implied a larger rate of growth of this deformation for the true equations of elastodynamics than for the model scalar equation, which was interpreted as being due to the existence of persistent "crack front waves".

The same problem but for quasistatic crack propagation was studied by Schmittbuhl et al. (1995) and Katzav and Adda-Bedia (2006), using some results of Rice (1985). The focus of these two works was on self-affine properties of the crack front.

One shortcoming of the semi-infinite crack geometry considered in all of these works was the lack of any characteristic lengthscale. This was the motivation for Favier et al.'s (2006) study of the same problem but for a tunnel-crack of finite width. This work was based on Leblond et al.'s (1996) earlier study of coplanar perturbation of such a crack. For technical reasons, propagation had to be assumed to be quasistatic and the problem could only be treated in the case of fatigue, using a Paris-type propagation law. The "wavyness" of the crack front was found to increase much more quickly than in the case of a semi-infinite crack. This phenomenon was interpreted as being due to an effect of instability of sinusoidal perturbations of the front of large wavelength typical of such finite crack geometries.

In the present work, the focus will again be on the development of the "wavyness" of the crack front, with special emphasis on the influences of the following factors:

- The mismatch of elastic properties between the two materials, for an interface crack. This factor was not envisaged at all in previous studies which considered only ordinary cracks in elastically homogeneous materials.
- The type of loading. We shall consider a typical class of loadings depending on a parameter whose sign will govern the stable or unstable character of 2D crack propagation[2] under constant loading. There will be a strong connection here with the work of Wolfries and Willis (1999) in spite of the differences in the hypotheses made.
- The type of propagation law (fatigue versus brittle fracture). Previous works did consider different propagation laws, but there were other differences in the hypotheses made so that it was difficult to separate the influences of the various factors.

The paper is organized as follows. Section 2 is devoted to preliminaries and notations for 3D interface cracks. Section 3 provides the LLPMM formulae for the variation of the SIFs arising from some slight coplanar perturbation of a semi-infinite interface crack. These formulae are used in Section 4 to determine the distribution of the energy release rate along the perturbed front for the class of loadings considered. From there, Section 5 studies the statistical evolution in time of the deformation of the front of a semi-infinite crack propagating in fatigue along some heterogeneous interface. Section 6 re-considers the same problem but in brittle fracture. Finally Section 7 provides a synthesis of the results obtained.

[2]That is, propagation within a medium with uniform fracture properties. In this case the crack front remains straight at all instants so that the problem is 2D in the perpendicular plane.

2. Preliminaries and notations

The notations adopted are similar to those in the work of Hutchinson et al. (1987). We consider an infinite heterogeneous body made of two isotropic elastic materials bonded together on their planar interface. Materials "+" and "−", with shear moduli μ_+ and μ_- and Poisson ratios ν_+ and ν_-, occupy the half-spaces $y>0$ and $y<0$ respectively. The "bielastic constant" ε and the "equivalent Poisson ratio" ν are defined by

$$\begin{cases} \varepsilon \equiv \dfrac{1}{2\pi}\ln\dfrac{(3-4\nu_+)/\mu_+ + 1/\mu_-}{(3-4\nu_-)/\mu_- + 1/\mu_+}, \\ 1-\nu \equiv \dfrac{(1-\nu_+)/\mu_+ + (1-\nu_-)/\mu_-}{(1/\mu_+ + 1/\mu_-)\cosh^2(\pi\varepsilon)}. \end{cases} \tag{1}$$

The definition of the bielastic constant is classical. That of the equivalent Poisson ratio, which was introduced by Lazarus and Leblond (1998a), is less standard but will reveal very convenient for the problem considered here. The notation ν is logical in the sense that for a homogeneous body ($\mu_+=\mu_-$, $\nu_+=\nu_-$, $\varepsilon=0$), this quantity is identical to the common Poisson ratios of the materials. Also, it is shown in Appendix A that it satisfies the inequalities (which will be needed in the sequel)

$$0<\nu<\tfrac{1}{2}, \tag{2}$$

analogous to those satisfied by the individual Poisson ratios.

Now consider, within the interface, a crack with arbitrary smooth contour and some arbitrary point M on this contour (Fig. 1). Define a frame $Mxyz$ with origin at this point and axes Mx, My, Mz parallel to the direction of crack propagation, perpendicular to the crack plane and coincident with the local tangent to the crack front, respectively.

The SIFs at the point M are defined *via* the local expressions of the displacement discontinuity across the crack faces and the stresses on the interface ahead of the crack front. The displacement discontinuity $[\![\mathbf{u}]\!] \equiv \mathbf{u}_+ - \mathbf{u}_-$ across the crack faces, in the plane Mxy locally perpendicular to the crack front and near the point M, is given by the following asymptotic formulae:

$$\begin{cases} [\![u_y + \mathrm{i}u_x]\!](x<0,z=0) \sim 2(1-\nu)\dfrac{\cosh(\pi\varepsilon)}{1+2\mathrm{i}\varepsilon}\left(\dfrac{1}{\mu_+}+\dfrac{1}{\mu_-}\right)K(M)\sqrt{\dfrac{|x|}{2\pi}}\,|x|^{\mathrm{i}\varepsilon}, \\ [\![u_z]\!](x<0,z=0) \sim 2\left(\dfrac{1}{\mu_+}+\dfrac{1}{\mu_-}\right)K_{III}(M)\sqrt{\dfrac{|x|}{2\pi}}. \end{cases} \tag{3}$$

In these expressions,

$$K(M) \equiv K_I(M) + \mathrm{i}K_{II}(M) \tag{4}$$

is the local complex SIF ($K_I(M)$ and $K_{II}(M)$ are the local mode I and mode II SIFs), and $K_{III}(M)$ is the local mode III SIF. The asymptotic expressions of the stress components σ_{yx}, σ_{yy} and σ_{yz} on the interface ahead of

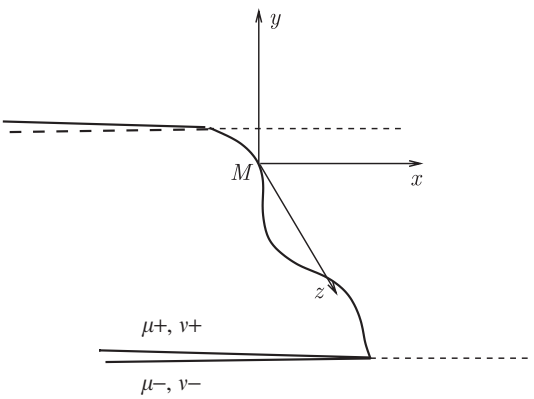

Fig. 1. Planar interface crack with arbitrary contour in an infinite body.

the crack front, in the plane Mxy and near the point M, are given by

$$\begin{cases} (\sigma_{yy} + \mathrm{i}\sigma_{yx})(x>0, y=0, z=0) \sim \dfrac{K(M)\, x^{\mathrm{i}\varepsilon}}{\sqrt{2\pi x}}, \\ \sigma_{yz}(x>0, y=0, z=0) \sim \dfrac{K_{III}(M)}{\sqrt{2\pi x}}. \end{cases} \tag{5}$$

Finally the energy release rate $G(M)$ at the point M is given by Irwin's formula:

$$G(M) = \frac{1}{4}\left(\frac{1}{\mu_+} + \frac{1}{\mu_-}\right)\{(1-\nu)|K(M)|^2 + [K_{III}(M)]^2\}. \tag{6}$$

3. The LLPMM formulae

We now envisage, within some infinite heterogeneous elastic body, a semi-infinite interface crack lying in the Ozx plane, with a straight front parallel to the Oz axis (Fig. 2). Let a denote the distance from the reference Oz axis to the crack front. Let the crack be loaded through some arbitrary system of forces exerted anywhere in the body and/or on the crack faces. This loading generates a distribution of SIFs $K(M) \equiv K(z) \equiv K_I(z) + \mathrm{i}K_{II}(z)$, $K_{III}(M) \equiv K_{III}(z)$ along the crack front.

Consider first *translatory* motions of the crack front in the direction x under constant loading (Fig. 2). For such motions, let $\frac{\mathrm{d}K}{\mathrm{d}a}(z) \equiv \frac{\mathrm{d}K_I}{\mathrm{d}a}(z) + \mathrm{i}\frac{\mathrm{d}K_{II}}{\mathrm{d}a}(z)$ and $\frac{\mathrm{d}K_{III}}{\mathrm{d}a}(z)$ denote the derivatives of the SIFs at the point z with respect to the position of the front.

Consider now small, *non-uniform* motions of the crack front in the direction x under constant loading; let $\delta a(z)$ denote the local distance from the original front to the new one at the point z (Fig. 3). Then, to first

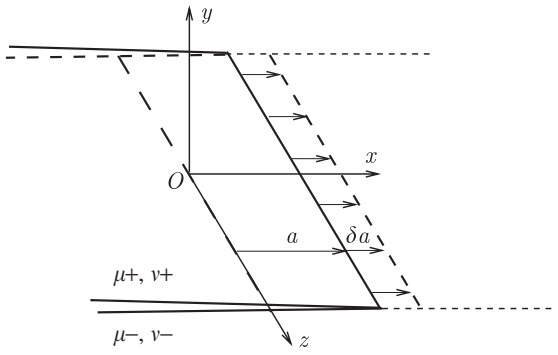

Fig. 2. Semi-infinite interface crack with straight front.

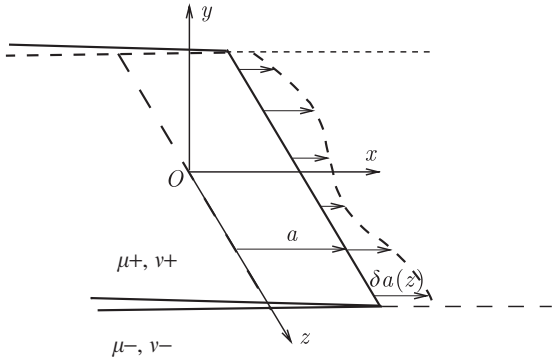

Fig. 3. Semi-infinite interface crack with slightly perturbed front.

order in the perturbation, the variations of the SIFs $\delta K(z)$, $\delta K_{III}(z)$ are given by the following formulae (Lazarus and Leblond, 1998a):

$$\begin{cases} \delta K(z) = \dfrac{\mathrm{d}K}{\mathrm{d}a}(z)\delta a(z) + \dfrac{1+2\mathrm{i}\varepsilon}{8\cosh(\pi\varepsilon)}\left\{ PV\int_{-\infty}^{+\infty}\left[\dfrac{\gamma_+}{|z'-z|^{2\mathrm{i}\varepsilon}}\overline{K(z')} + \gamma_-\, K(z')\right]\dfrac{\delta a(z')-\delta a(z)}{(z'-z)^2}\mathrm{d}z' \right. \\ \qquad \left. + \dfrac{2\gamma_{III}}{1-\nu} FP\int_{-\infty}^{+\infty}\mathrm{sgn}(z'-z)K_{III}(z')\dfrac{\delta a(z')-\delta a(z)}{|z'-z|^{2+\mathrm{i}\varepsilon}}\mathrm{d}z'\right\}, \\ \delta K_{III}(z) = \dfrac{\mathrm{d}K_{III}}{\mathrm{d}a}(z)\delta a(z) + \dfrac{\gamma}{4} PV\int_{-\infty}^{+\infty} K_{III}(z')\dfrac{\delta a(z')-\delta a(z)}{(z'-z)^2}\mathrm{d}z' \\ \qquad + \dfrac{1-\nu}{4}\mathrm{Re}\left[\gamma_z FP\int_{-\infty}^{+\infty}\mathrm{sgn}(z'-z)\,\overline{K(z')}\dfrac{\delta a(z')-\delta a(z)}{|z'-z|^{2+\mathrm{i}\varepsilon}}\mathrm{d}z'\right]. \end{cases} \tag{7}$$

In these expressions the symbols $PV\int$ and $FP\int$ denote the Cauchy principal value and Hadamard finite part of the integral considered, respectively, and γ_+, γ_-, γ_{III}, γ_z, γ are quantities which depend only on the bielastic constant ε and the equivalent Poisson ratio ν. Note that for a translatory motion of the front ($\delta a(z) \equiv Cst. \equiv \delta a$), $\delta K(z)$ and $\delta K_{III}(z)$ reduce to $\frac{\mathrm{d}K}{\mathrm{d}a}(z)\delta a$ and $\frac{\mathrm{d}K_{III}}{\mathrm{d}a}(z)\delta a$, as desired.

The values of the "γ" constants, as provided by Piccolroaz et al. (2007), are

$$\begin{cases} \gamma_+ = -\dfrac{4}{\sqrt{\pi}}\dfrac{\Gamma(1+\mathrm{i}\varepsilon)}{\Gamma(1/2+\mathrm{i}\varepsilon)}\cosh(\pi\varepsilon)\dfrac{\cosh(\pi\varepsilon)-1/(1-\nu)}{\cosh(\pi\varepsilon)+1/(1-\nu)}, \\ \gamma_- = \dfrac{8}{\pi(1+2\mathrm{i}\varepsilon)}\dfrac{\cosh^2(\pi\varepsilon)}{\cosh(\pi\varepsilon)+1/(1-\nu)}, \\ \gamma_{III} = -\dfrac{2^{2-\mathrm{i}\varepsilon}}{\sqrt{\pi}}\dfrac{\varepsilon(1+\mathrm{i}\varepsilon)}{1+2\mathrm{i}\varepsilon}\dfrac{\Gamma(1/2-\mathrm{i}\varepsilon)}{\Gamma(1-\mathrm{i}\varepsilon)}\dfrac{\cosh^2(\pi\varepsilon)}{\cosh(\pi\varepsilon/2)[\cosh(\pi\varepsilon)+1/(1-\nu)]}, \\ \gamma_z = -\dfrac{1+2\mathrm{i}\varepsilon}{(1-\nu)\cosh(\pi\varepsilon)}\gamma_{III}, \\ \gamma = -\dfrac{2}{\pi}\dfrac{\cosh(\pi\varepsilon)-3/(1-\nu)}{\cosh(\pi\varepsilon)+1/(1-\nu)}, \end{cases} \tag{8}$$

where the notation ν introduced in Eq. $(1)_2$ is used and Γ is the gamma function.

4. Distribution of the energy release rate along the crack front

4.1. Class of loadings considered

For simplicity, we shall only consider distributions of forces invariant in the direction z. For such loadings and a straight crack front, the distributions of the SIFs and the energy release rate are uniform along the front. Thus, if the fracture properties are uniform and the crack front is initially straight, it remains straight at all instants. We shall then speak of *2D crack propagation* (in the plane perpendicular to the crack front). This kind of propagation is said to be "stable" or "unstable", under constant loading, according to whether the energy release rate is a decreasing or an increasing function of the distance of propagation.[3]

The loading being invariant in the direction z and the crack front being straight and located at the distance a from the reference Oz axis, let the (uniform) SIFs be denoted $K(a)$ and $K_{III}(a)$, or simply K and K_{III}. Similarly, let the (uniform) energy release rate be denoted $G(a)$ or simply G. For definiteness, we introduce the extra

[3]This terminology makes an implicit reference to Griffith's propagation law for which crack propagation occurs when the energy release rate reaches some critical value. For such a law and under constant loading, after the onset of crack propagation, the velocity of the crack goes immediately down to zero if the energy release rate decreases with distance, but continuously increases in the opposite case; hence the expressions "stable propagation", "unstable propagation".

assumption that $K(a)$ and $K_{III}(a)$ vary according to the formulae

$$\begin{cases} K(a) \equiv k a^{\alpha - i\varepsilon}, \\ K_{III}(a) \equiv k_{III} a^{\alpha}, \end{cases} \tag{9}$$

where k and k_{III} are constants independent of a and α some real exponent. Such dependences can be achieved, for various values of the exponent α, through suitable distributions of forces exerted on the crack faces:

- The value $\alpha = -\frac{1}{2}$ is obtained by exerting uniform line tractions $\pm\mathbf{P}$ on the lines $x = 0, y = 0^{\pm}$ (Fig. 4). Indeed the SIFs are then given by (Hutchinson et al., 1987)

$$\begin{cases} K(a) = (P_y + iP_x)\cosh(\pi\varepsilon)\sqrt{\dfrac{2}{\pi a}}\, a^{-i\varepsilon}, \\ K_{III}(a) = P_z\sqrt{\dfrac{2}{\pi a}}. \end{cases} \tag{10}$$

- The value $\alpha = \frac{1}{2}$ is obtained by exerting uniform surface tractions $\pm\mathbf{p}$ on the regions $0 < x < a, y = 0^{\pm}$ of the crack faces (Fig. 5). Indeed integration of formulae (10), immediately shows that the SIFs are then given by

$$\begin{cases} K(a) = 2(p_y + ip_x)\dfrac{\cosh(\pi\varepsilon)}{1 - 2i\varepsilon}\sqrt{\dfrac{2a}{\pi}}\, a^{-i\varepsilon}, \\ K_{III}(a) = 2p_z\sqrt{\dfrac{2a}{\pi}}. \end{cases} \tag{11}$$

- More generally, all values of α larger than $-\frac{1}{2}$ can be obtained by exerting surface tractions of the form $\pm\mathbf{p}(x) = \pm\mathbf{C}x^{\alpha - 1/2}$ on the regions $0 < x < a, y = 0^{\pm}$ of the crack faces. Indeed use of formulae (10) and the

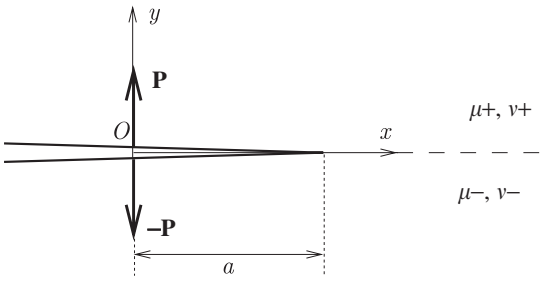

Fig. 4. Semi-infinite interface crack with uniform line tractions (the picture is 2D in the plane Oxy and the tractions are drawn parallel to the direction y).

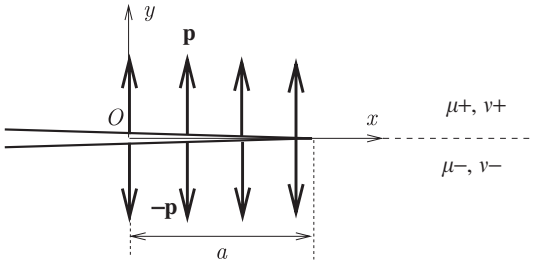

Fig. 5. Semi-infinite interface crack with uniform surface tractions (the picture is 2D in the plane Oxy and the tractions are drawn parallel to the direction y).

change of variable $u \equiv x/a$ then yields

$$\begin{cases} K(a) = \int_0^a (C_y + \mathrm{i}C_x) x^{\alpha-1/2} \cosh(\pi\varepsilon) \sqrt{\dfrac{2}{\pi(a-x)}} (a-x)^{-\mathrm{i}\varepsilon} \,\mathrm{d}x \\ \qquad = (C_y + \mathrm{i}C_x) \cosh(\pi\varepsilon) \sqrt{\dfrac{2}{\pi}} a^{\alpha-\mathrm{i}\varepsilon} \int_0^1 u^{\alpha-1/2} (1-u)^{-1/2-\mathrm{i}\varepsilon} \,\mathrm{d}u, \\ K_{III}(a) = \int_0^a C_z \, x^{\alpha-1/2} \sqrt{\dfrac{2}{\pi(a-x)}} \,\mathrm{d}x \\ \qquad = C_z \sqrt{\dfrac{2}{\pi}} a^{\alpha} \int_0^1 u^{\alpha-1/2} (1-u)^{-1/2} \,\mathrm{d}u. \end{cases} \tag{12}$$

The practical realization of the majority of loadings belonging to the class considered would obviously be problematic, but this is of little importance since they only serve as typical examples. One advantage of this class is that it encompasses loadings leading to stable propagation (for $\alpha<0$) as well as unstable propagation (for $\alpha>0$) of the crack. Note also that although the semi-infinite crack geometry considered does not involve any characteristic lengthscale, such a lengthscale comes into play *via* the loading, as clearly appears in Eq. (9) (except for $\alpha = 0$). The importance of introduction of some characteristic lengthscale in studies of the development of the deformation of crack fronts has been underlined by Leblond et al. (1996).

4.2. Calculation of the energy release rate

We shall use Fourier transforms of various functions in the direction z of the crack front. The Fourier transform $\widehat{\phi}(k)$ of an arbitrary function $\phi(z)$ is defined by

$$\widehat{\phi}(k) \equiv \int_{-\infty}^{+\infty} \phi(z) \, \mathrm{e}^{\mathrm{i}kz} \,\mathrm{d}z \;\Leftrightarrow\; \phi(z) \equiv \frac{1}{2\pi} \int_{-\infty}^{+\infty} \widehat{\phi}(k) \, \mathrm{e}^{-\mathrm{i}kz} \,\mathrm{d}k. \tag{13}$$

A few double Fourier transforms, denoted with a tilde instead of a hat, will also be encountered.

As a prerequisite to the discussion of crack propagation, one must calculate the distribution of the local energy release rate along the perturbed crack front for an arbitrary perturbation $\delta a(z)$, $-\infty<z<+\infty$. The first task consists of taking the Fourier transforms of Eq. (7). The elements required to do so have been provided by Lazarus and Leblond (1998a) and will not be repeated here. The final expressions of the Fourier transforms $\widehat{\delta K}(k)$, $\widehat{\delta K_{III}}(k)$ of the perturbations of the SIFs $\delta K(z)$, $\delta K_{III}(z)$ are

$$\begin{cases} \widehat{\delta K}(k) = \left\{ \dfrac{\mathrm{d}K}{\mathrm{d}a} - \dfrac{1+2\mathrm{i}\varepsilon}{8\cosh(\pi\varepsilon)} \left[\gamma_+ \dfrac{\sinh(\pi\varepsilon)}{\varepsilon} \Gamma(1-2\mathrm{i}\varepsilon) \dfrac{|k|^{1+2\mathrm{i}\varepsilon}}{1+2\mathrm{i}\varepsilon} \overline{K} + \pi\gamma_- |k| K \right.\right. \\ \qquad \left.\left. - \dfrac{4\gamma_{III}}{1-\nu} \dfrac{\cosh(\pi\varepsilon/2)}{\varepsilon} \Gamma(1-\mathrm{i}\varepsilon) \operatorname{sgn}(k) \dfrac{|k|^{1+\mathrm{i}\varepsilon}}{1+\mathrm{i}\varepsilon} K_{III} \right] \right\} \widehat{\delta a}(k), \\ \widehat{\delta K_{III}}(k) = \left\{ \dfrac{\mathrm{d}K_{III}}{\mathrm{d}a} - \dfrac{\pi\gamma}{4} |k| K_{III} \right. \\ \qquad \left. + \mathrm{i} \dfrac{1-\nu}{2} \dfrac{\cosh(\pi\varepsilon/2)}{\varepsilon} \operatorname{sgn}(k) \operatorname{Im} \left[\gamma_z \Gamma(1-\mathrm{i}\varepsilon) \dfrac{|k|^{1+\mathrm{i}\varepsilon}}{1+\mathrm{i}\varepsilon} \overline{K} \right] \right\} \widehat{\delta a}(k). \end{cases} \tag{14}$$

The next step consists of evaluating the Fourier transform $\widehat{\delta G}(k)$ of the perturbation of the energy release rate $\delta G(z)$ from Eqs. (6) and (14). The calculation is lengthy but straightforward. Using Eqs. (8) and (9) and formulae (8.332.3) and (8.335.1) of Gradshteyn and Ryzhik (1980), one gets

$$\frac{\widehat{\delta G}(k)}{G} = \frac{2}{a} [\alpha - f(ka)] \widehat{\delta a}(k), \tag{15}$$

where G is recalled to denote the energy release rate for a straight front and f is the function defined by

$$f(p) \equiv A|p| + \mathrm{Re}(B|p|^{1+2i\varepsilon}); \tag{16}$$

in this expression A and B are constants given by

$$\begin{cases} A \equiv H^{-1}\left\{(1-\nu)\cosh(\pi\varepsilon)|k|^2 + \dfrac{1}{2}\left[\dfrac{3}{1-\nu} - \cosh(\pi\varepsilon)\right]k_{III}^2\right\}, \\ B \equiv H^{-1}[1-(1-\nu)\cosh(\pi\varepsilon)]\dfrac{\Gamma(1/2-i\varepsilon)}{\Gamma(1/2+i\varepsilon)}\dfrac{\overline{k}^2}{2^{1+2i\varepsilon}}, \end{cases} \tag{17}$$

where,

$$H \equiv [1+(1-\nu)\cosh(\pi\varepsilon)]\left(|k|^2 + \frac{k_{III}^2}{1-\nu}\right). \tag{18}$$

It is shown in Appendix B that the constants A and B defined by Eq. (17) satisfy the inequality (will be needed in the sequel)

$$A > |B(1+2i\varepsilon)| = |B|\sqrt{1+4\varepsilon^2}. \tag{19}$$

5. Deformation of the crack front in fatigue

5.1. Paris-type propagation law

Let $a(z,t)$ denote the distance from the Oz axis to the perturbed crack front at location z along this axis and time t. Also, let $G(z,t)$ denote the energy release rate at the point $(x = a(z,t), y = 0, z)$ of the perturbed crack front at time t. In this section, propagation of this front is assumed to be governed by the following Paris-type law[4]:

$$\frac{\partial a}{\partial t}(z,t) = C(z,t)[G(z,t)]^{N/2}, \tag{20}$$

where $C(z,t)$ (the *Paris constant*) and N (the *Paris exponent*) are material parameters. The inhomogeneity of the interface is modelled by assuming the Paris constant to be a function of position, the Paris exponent being considered as uniform for simplicity. The simple notation $C(z,t)$ in fact represents the value of the Paris constant at the position $(x = a(z,t), y = 0, z)$; it is assumed to vary only slightly so that it can be written as

$$C(z,t) \equiv C[1+\delta c(z,t)], \quad |\delta c(z,t)| \ll 1, \tag{21}$$

where C represents its mean value and $\delta c(z,t)$ its "normalized", dimensionless fluctuation.

The fluctuations of the position of the crack front and the energy release rate arising from the fluctuations of the Paris constant are also naturally assumed to be small at each instant, so that

$$\begin{cases} a(z,t) \equiv a(t) + \delta a(z,t), \quad |\delta a(z,t)| \ll a(t), \\ G(z,t) \equiv G(t) + \delta G(z,t), \quad |\delta G(z,t)| \ll G(t), \end{cases} \tag{22}$$

where the quantities $a(t)$ and $G(t)$ denote the mean position of the crack and the mean energy release rate at time t.

5.2. Evolution of the perturbation of the crack front

The evolution of the perturbation $\delta a(z,t)$ of the crack front will now be obtained by combining the expression (15) of the perturbed energy release rate and the propagation law (20).

[4]Eq. (20) is written formally as a propagation law for subcritical crack growth. In the case of fatigue "t" must be re-interpreted as "number of cycles" and "G" as "amplitude of variation of the energy release rate during one cycle".

Expanding first the propagation law to first order in $\delta a(z,t)$, $\delta c(z,t)$, $\delta G(z,t)$ and identifying terms of order 0 and 1, one gets

$$\begin{cases} \dfrac{\mathrm{d}a}{\mathrm{d}t}(t) = C[G(t)]^{N/2}, \\ \dfrac{\partial \delta a}{\partial t}(z,t) = C[G(t)]^{N/2}\left[\dfrac{N}{2}\dfrac{\delta G(z,t)}{G(t)} + \delta c(z,t)\right]. \end{cases}$$

Eliminating then $\mathrm{d}t$ between these expressions and considering henceforward all perturbations as functions of the mean position $a(t) \equiv a$ of the crack instead of time, one gets

$$\frac{\partial \delta a}{\partial a}(z,a) = \frac{N}{2}\frac{\delta G(z,a)}{G(a)} + \delta c(z,a).$$

Upon use of the Fourier decompositions of $\delta a(z,a)$, $\delta G(z,a)$, $\delta c(z,a)$ and Eq. (15), this yields the evolution equation of the Fourier transform $\widehat{\delta a}(k,a)$ of the perturbation of the crack front:

$$\frac{\partial \widehat{\delta a}}{\partial a}(k,a) = \frac{N}{a}[\alpha - f(ka)]\widehat{\delta a}(k,a) + \widehat{\delta c}(k,a). \tag{23}$$

Assuming the crack to be initially straight and integrating the linear, inhomogeneous, first-order differential Eq. (23) by standard methods, one gets

$$\widehat{\delta a}(k,a) = \int_{a_0}^{a} \left(\frac{a}{a'}\right)^{N\alpha}\left[\frac{\psi(ka)}{\psi(ka')}\right]^{N} \widehat{\delta c}(k,a')\,\mathrm{d}a', \tag{24}$$

where a_0 denotes the initial value of a and ψ the function defined by

$$\psi(p) \equiv \exp\left[-\int_0^p f(p')\frac{\mathrm{d}p'}{p'}\right] = \exp\left[-A|p| - \mathrm{Re}\left(B\frac{|p|^{1+2\mathrm{i}\varepsilon}}{1+2\mathrm{i}\varepsilon}\right)\right] \tag{25}$$

(where Eq. (16) has been used).

5.3. Statistical hypotheses

Using Eq. (24) for the perturbation of the crack front, we shall now study some features of this perturbation for a statistical ensemble of possible "realizations" of the heterogeneous interface. Basic elements of the mathematical description of such an ensemble are provided in Appendix C. These elements include precise definitions of the *mathematical expectation* $E[F(z)]$ of any observable $F(z)$ defined on the crack front (Eq. (C.1)) and of its *two-point autocorrelation function* $E[F(z_1)F(z_2)]$ (Eq. (C.2)).

If the observable is statistically invariant in the direction z of the crack front, its two-point autocorrelation function depends only on the relative distance between points z_1 and z_2:

$$E[F(z_1)F(z_2)] \equiv \mathscr{F}(z_2 - z_1). \tag{26}$$

The function $\mathscr{F}$ here is obviously even and is called the *autocorrelation function* of F. It is shown in Appendix C that the following relations then hold:

$$E[\widetilde{F_1 F_2}](k_1,k_2) = E[\widehat{F}(k_1)\widehat{F}(k_2)] = 2\pi\delta(k_1+k_2)\widehat{\mathscr{F}}(k_2), \tag{27}$$

where δ is Dirac's function and $E[\widetilde{F_1 F_2}](k_1,k_2)$ the double Fourier transform of the function $E[F(z_1)F(z_2)]$. The function $\widehat{\mathscr{F}}$ in Eq. $(27)_2$ is called the *power spectrum* of the observable and is the Fourier transform of its autocorrelation function.

We shall make the hypothesis of statistical homogeneity and isotropy of the distribution of the Paris constant within the interface. This implies that its two-point autocorrelation function is of the form

$$E[\delta c(z_1,a_1)\delta c(z_2,a_2)] \equiv \mathscr{C}(z_2 - z_1, a_2 - a_1). \tag{28}$$

The function $\mathscr{C}(z_2 - z_1, a_2 - a_1)$ here depends only on the distance $\sqrt{(z_2-z_1)^2 + (a_2-a_1)^2}$, which notably implies that it is even in its first argument. It is assumed to decrease down to zero over some characteristic

distance b (the "fluctuation distance" of the Paris constant) much smaller than the characteristic lengthscale a introduced by the loading.

Since the perturbation of the crack front arises from the fluctuations of the Paris constant, hypothesis (28) implies that is also statistically invariant in the direction of this front, which means that

$$E[\delta a(z_1,a)\delta a(z_2,a)] \equiv \mathscr{A}(z_2-z_1,a). \tag{29}$$

The function $\mathscr{A}$ here is obviously even in its first argument.

5.4. General formula for the power spectrum of the perturbation of the crack front

The first task is to derive the general expression, valid for all times, of the power spectrum $\widehat{\mathscr{A}}(k,a)$ of the perturbation of the crack front. By the expression (24) of $\widehat{\delta a}(k,a)$ and the definition (C.2) of the two-point autocorrelation function,

$$\begin{aligned} &E[\widehat{\delta a}(k_1,a)\,\widehat{\delta a}(k_2,a)] \\ &= \int_{a_0}^{a}\int_{a_0}^{a}\left(\frac{a^2}{a_1a_2}\right)^{N\alpha}\left[\frac{\psi(k_1a)\psi(k_2a)}{\psi(k_1a_1)\psi(k_2a_2)}\right]^N E[\widehat{\delta c}(k_1,a_1)\,\widehat{\delta c}(k_2,a_2)]\,\mathrm{d}a_1\,\mathrm{d}a_2 \\ &= 2\pi\delta(k_1+k_2)\int_{a_0}^{a}\int_{a_0}^{a}\left(\frac{a^2}{a_1a_2}\right)^{N\alpha}\left(\frac{[\psi(k_2a)]^2}{\psi(k_2a_1)\psi(k_2a_2)}\right)^N \widehat{\mathscr{C}}(k_2,a_2-a_1)\,\mathrm{d}a_1\,\mathrm{d}a_2. \end{aligned}$$

Use has been made here of Eq. $(27)_2$ for the observable δc. Also, since the right-hand side is nonzero only for $k_1+k_2=0$ and the function ψ defined by Eq. (25) is even, we have safely replaced $\psi(k_1a)/\psi(k_1a_1)$ by $\psi(-k_2a)/\psi(-k_2a_1)=\psi(k_2a)/\psi(k_2a_1)$.

On the other hand, Eq. $(27)_2$ for the observable δa implies that

$$E[\widehat{\delta a}(k_1,a)\,\widehat{\delta a}(k_2,a)] = 2\pi\delta(k_1+k_2)\,\widehat{\mathscr{A}}(k_2,a).$$

Comparison between these two expressions of $E[\widehat{\delta a}(k_1,a)\widehat{\delta a}(k_2,a)]$ reveals that

$$\widehat{\mathscr{A}}(k,a) = \int_{a_0}^{a}\int_{a_0}^{a}\left(\frac{a^2}{a_1a_2}\right)^{N\alpha}\left(\frac{[\psi(ka)]^2}{\psi(ka_1)\psi(ka_2)}\right)^N \widehat{\mathscr{C}}(k,a_2-a_1)\,\mathrm{d}a_1\,\mathrm{d}a_2, \tag{30}$$

which is the expression looked for.

5.5. Asymptotic expression of the power spectrum of the perturbation of the crack front

We shall now derive the asymptotic expression of the power spectrum $\widehat{\mathscr{A}}(k,a)$ of the perturbation of the crack front for large times, that is for $a \gg a_0$. Just like in the works of Perrin and Rice (1994) and Favier et al. (2006), the treatment will basically rely on some argument of domination of the diagonal $a_1=a_2$ in integration over the square $[a_0,a]\times[a_0,a]$.

Use of the change of variables defined by

$$r \equiv \tfrac{1}{2}(a_1+a_2); \quad s \equiv a_2-a_1 \tag{31}$$

in Eq. (30) yields

$$\widehat{\mathscr{A}}(k,a) = \int_{a_0}^{a}\left[\int_{-s_m(r)}^{s_m(r)}\left(\frac{a^2}{r^2-s^2/4}\right)^{N\alpha}\left(\frac{[\psi(ka)]^2}{\psi[k(r-s/2)]\,\psi[k(r+s/2)]}\right)^N \widehat{\mathscr{C}}(k,s)\,\mathrm{d}s\right]\mathrm{d}r, \tag{32}$$

where $-s_m(r)$ and $s_m(r)$ are the minimum and maximum values of s allowed by the inequalities $a_0 \leqslant a_1 = r-s/2 \leqslant a$, $a_0 \leqslant a_2 = r+s/2 \leqslant a$. Now the function $\widehat{\mathscr{C}}(k,s)$ takes non-negligible values only when $|s| \lesssim b$. On the other hand $r \geqslant a_0 \gg b$. Therefore, the integrand in Eq. (32) takes non-negligible values only when $|s| \ll r$ (domination of the diagonal). One may therefore safely replace $r^2-s^2/4$, $\psi[k(r-s/2)]$, $\psi[k(r+s/2)]$ by r^2, $\psi(kr)$, $\psi(kr)$ in the integral. Also, if $a \gg a_0$, $s_m(r) \sim a \gg b$ for almost every $r \in [a_0,a]$, so that $|s| \ll s_m(r)$ for those

values of s for which the integrand is non-negligible; hence the integral over the interval $[-s_m(r), s_m(r)]$ may safely be extended to the entire real line. The integral of $\widehat{\mathscr{C}}(k,s)$ then becomes identical to $\widetilde{\mathscr{C}}(k,0)$ where $\mathscr{C}$is the double Fourier transform of the function $\mathscr{C}$, so that, Eq. (32) becomes

$$\widehat{\mathscr{A}}(k,a)\sim\widetilde{\mathscr{C}}(k,0)a^{2N\alpha}[\psi(ka)]^{2N}\mathscr{I}(a),\quad \mathscr{I}(a)\equiv\int_{a_0}^{a} r^{-2N\alpha}\,[\psi(kr)]^{-2N}\,\mathrm{d}r. \tag{33}$$

It now becomes necessary to distinguish between the cases $k=0$ and $k\neq 0$.

- *Special case*: $k=0$.
  Then $\psi(kr)=\psi(0)=1$ so that
  $$\mathscr{I}(a)=\frac{a^{1-2N\alpha}-a_0^{1-2N\alpha}}{1-2N\alpha}.$$
  Therefore, there are two sub-cases according to whether the exponent $1-2N\alpha$ here is negative or positive:
  - If $\alpha>\frac{1}{2N}$,
    $$\widehat{\mathscr{A}}(0,a)\sim\frac{\widetilde{\mathscr{C}}(0,0)}{2N\alpha-1}a_0\left(\frac{a}{a_0}\right)^{2N\alpha}. \tag{34}$$
  - If $\alpha<\frac{1}{2N}$,
    $$\widehat{\mathscr{A}}(0,a)\sim\frac{\widetilde{\mathscr{C}}(0,0)}{1-2N\alpha}a. \tag{35}$$

- *General case*: $k\neq 0$.
  It is clear, by Eq. (25) and inequality (19), that the function $\psi(p)$ goes to zero for $|p|\to+\infty$ not less quickly than $\exp(-C|p|)$ where $C\equiv A-|B|/|1+2\mathrm{i}\varepsilon|>0$. Therefore $[\psi(kr)]^{-2N}$ goes to infinity for $r\to+\infty$ not less quickly than $\exp(2NC|k|r)$. Since $r^{-2N\alpha}$ varies much less quickly, it may safely be replaced by $a^{-2N\alpha}$ in the expression $(33)_2$ of $\mathscr{I}(a)$ which thus becomes
  $$\mathscr{I}(a)\sim a^{-2N\alpha}\int_{a_0}^{a}[\psi(kr)]^{-2N}\,\mathrm{d}r=a^{-2N\alpha}\int_{a_0}^{a}\exp\left[2NA|k|r+2N\mathrm{Re}\left(B\frac{|kr|^{1+2\mathrm{i}\varepsilon}}{1+2\mathrm{i}\varepsilon}\right)\right]\mathrm{d}r.$$
  Integration by parts of this integral now yields
  $$\mathscr{I}(a)\sim a^{-2N\alpha}\left\{\frac{\exp(2NA|k|a)}{2NA|k|}\exp\left[2N\mathrm{Re}\left(B\frac{|ka|^{1+2\mathrm{i}\varepsilon}}{1+2\mathrm{i}\varepsilon}\right)\right]-\int_{a_0}^{a}\frac{\exp(2NA|k|r)}{A|k|}\exp\left[2N\mathrm{Re}\left(B\frac{|kr|^{1+2\mathrm{i}\varepsilon}}{1+2\mathrm{i}\varepsilon}\right)\right]\mathrm{Re}(B|k|^{1+2\mathrm{i}\varepsilon}r^{2\mathrm{i}\varepsilon})\,\mathrm{d}r\right\}.$$
  Replacing the term $r^{2\mathrm{i}\varepsilon}$ in the expression Re(...) here by $a^{2\mathrm{i}\varepsilon}$ since it varies much less quickly than the exponentials, one gets
  $$\mathscr{I}(a)\sim a^{-2N\alpha}\frac{\exp\left[2NA|k|a+2N\mathrm{Re}\left(B\frac{|ka|^{1+2\mathrm{i}\varepsilon}}{1+2\mathrm{i}\varepsilon}\right)\right]}{2NA|k|}-\frac{\mathrm{Re}(B|k|^{1+2\mathrm{i}\varepsilon}a^{2\mathrm{i}\varepsilon})}{A|k|}\mathscr{I}(a),$$
  which implies that
  $$\mathscr{I}(a)\sim a^{-2N\alpha}\frac{\exp\left[2NA|k|a+2N\mathrm{Re}\left(B\frac{|ka|^{1+2\mathrm{i}\varepsilon}}{1+2\mathrm{i}\varepsilon}\right)\right]}{2N[A|k|+\mathrm{Re}(B|k|^{1+2\mathrm{i}\varepsilon}a^{2\mathrm{i}\varepsilon})]}=\frac{a^{-2N\alpha}[\psi(ka)]^{-2N}}{2N|k|[A+\mathrm{Re}(B|ka|^{2\mathrm{i}\varepsilon})]}.$$

Insertion of this result into Eq. $(33)_1$ finally yields

$$\widehat{\mathscr{A}}(k,a)\sim\frac{\widetilde{\mathscr{C}}(k,0)}{2N|k|[A+\mathrm{Re}(B|ka|^{2i\varepsilon})]},\quad (k\neq 0). \tag{36}$$

Note that the denominator here does not vanish, since $A+\mathrm{Re}(B|ka|^{2i\varepsilon})\geqslant A-|B|>0$ by inequality (19).

Eqs. (34)and (35) show that in the limit of large times, $\widehat{\mathscr{A}}(0,a)$ goes to infinity in all cases; the larger the value of α, the quicker the divergence. In contrast, Eq. (36) shows that for $k\neq 0$, $\widehat{\mathscr{A}}(k,a)$ asymptotically oscillates indefinitely between finite values (except if $\varepsilon=0$, in which case it tends toward a constant), and therefore remains bounded. This means that Fourier components of the perturbation of the crack front with small wavenumbers (large wavelengths) gradually develop in time at the expense of Fourier components with large wavenumbers (small wavelengths); the higher the value of α, the larger the effect. This phenomenon will be referred to as the *gradual selection of Fourier components of the perturbation of large wavelength* in the sequel.

5.6. Comments

Some useful qualitative understanding of the phenomenon just evidenced can be gained by considering the evolution Eq. (23) of $\widehat{\delta a}(k,a)$.

- *Assume first that 2D crack propagation is unstable, that is,* $\alpha>0$.
  The function f defined by Eq. (16) is even and its derivative is given, for positive values of its argument, by $f'(p)=A+\mathrm{Re}[B(1+2i\varepsilon)p^{2i\varepsilon}]\geqslant A-|B(1+2i\varepsilon)|>0$ by inequality (19). Therefore f is an increasing function over the interval $[0,+\infty)$. Also, $f(0)=0$ and $\lim_{p\to+\infty}f(p)=+\infty$ since f' is bounded from below by a positive constant. Therefore the equation $f(p)=\alpha$ has a unique solution p_0 over the interval $(0,+\infty)$.[5] The quantity $\alpha-f(ka)$ is positive for $|k|<p_0/a$ and negative for $|k|>p_0/a$. In the first case, that is if the wavelength $\lambda\equiv 2\pi/|k|$ is larger than $\lambda_0\equiv 2\pi a/p_0$, the Fourier component $\widehat{\delta a}(k,a)$ tends to "explode" because of the term $\frac{N}{a}[\alpha-f(ka)]\widehat{\delta a}(k,a)$ in its evolution equation (23). In the second case, that is if λ is smaller than λ_0, this term tends to reduce the value of $\widehat{\delta a}(k,a)$, which therefore remains bounded. In other words, there is a effect of unstable growth of Fourier components of the perturbation of wavelength greater than the "critical" wavelength λ_0.
  However, the picture is made a bit more complex by the fact that for any given $k\neq 0$, the wavelength λ is fixed and finite, and thus *always* ultimately becomes smaller than λ_0 which increases proportionally to a. The implication is that if $k\neq 0$, unstable growth of $\widehat{\delta a}(k,a)$ always stops after a certain time. This is why $\widehat{\delta a}(k,a)$ diverges only for $k=0$.
- *Assume now that 2D crack propagation is stable, that is,* $\alpha<0$.
  Then the equation $f(p)=\alpha$ has no solution. The quantity $\alpha-f(ka)$ is negative for all values of k, and does not generate any dramatic "explosion" of $\widehat{\delta a}(k,a)$. In other words, there is no effect of unstable growth of Fourier components of the perturbation of wavelength greater than the critical wavelength, because such a critical wavelength no longer exists. However the phenomenon of gradual selection of Fourier components of large wavelength is still present, although less spectacular. Indeed the term $\frac{N}{a}[\alpha-f(ka)]\widehat{\delta a}(k,a)$ in Eq. (23) tends to reduce the value of $\widehat{\delta a}(k,a)$, and the effect is maximum for large $|k|$ (small λ) since $\alpha-f(ka)$ goes to $-\infty$ then; hence Fourier components of the perturbation of small wavelength are more attenuated in time than components of large wavelength.

The conclusion is that the selection of Fourier components of the perturbation of large wavelength occurs for all values of the coefficient α characterizing the stability or instability of 2D crack propagation. However it is more dramatic in the unstable case, because it is enhanced then by an effect of "explosion" of Fourier components of wavelength greater than some critical value proportional to the characteristic lengthscale a.

[5]This solution is connected to the existence of a bifurcated solution in brittle fracture, as will be seen in Section 6 below.

Similar phenomena have been reported at least twice in the literature. Favier et al. (2006) recently performed a similar study of the deformation of the front of a tensile tunnel-crack propagating in some elastically homogeneous medium with random fracture properties. This study evidenced both gradual selection of Fourier components of the perturbation of large wavelength and unstable development of components of wavelength greater than some critical value. However, a single loading consisting of uniform stresses at infinity was considered; the value of α, namely $\frac{1}{2}$ (implying unstable 2D crack propagation) was fixed, and this precluded any study of the influence of this parameter.

There is also a strong connection with the work of Wolfries and Willis (1999), in spite of the fact that the situation considered by these authors (dynamic crack propagation of an ordinary crack governed by a Griffith-type law) was somewhat different from that studied here (quasistatic propagation of an interface crack governed by a Paris-type law). Wolfries and Willis's (1999) major conclusion was that the sign of the quantity M appearing in the "next" term (proportional to the square root of the distance to the crack front) in the expansion of the tensile stress ahead of the front had a paramount influence on the evolution of Fourier components of the perturbation of large wavelength. This is in line with our own observations on the influence of the exponent α, since for an ordinary mode I crack, as considered by Wolfries and Willis (1999), the parameter M is directly related to the derivative $\mathrm{d}K_I/\mathrm{d}a$ of the SIF for a uniform advance of the crack front[6] and hence to the exponent α.

The strong influence of the sign of M or α, which governs the stable or unstable character of 2D crack propagation, upon the possible "explosion" of Fourier components of the perturbation of sufficiently large wavelength, obviously arises from the fact that when this wavelength goes to infinity, the perturbation ultimately becomes uniform along the front so that the problem becomes 2D in the perpendicular plane.

In contrast, the fact that the gradual selection of Fourier components of the perturbation of large wavelength has been found to occur for both the tensile tunnel-crack and the semi-infinite interface crack *for all values of* α, even in the absence of dramatic "explosion" of such components, strongly suggests that it must be a pretty general phenomenon. This conclusion is confirmed by the following qualitative reasoning. Consider Fourier components of the perturbation of the crack front of small wavelength. For such components, the front oscillates over distances much smaller than the characteristic lengthscales of the geometry and the loading. Therefore, the distributions of the SIFs and the energy release rate along the perturbed front, which govern the evolution in time of the Fourier component considered, are determined by the local geometry of the front and do not depend much on the details of the far geometry and the loading. A simple argument presented in Appendix D confirms that independently of the far geometry and loading, for sinusoidal undulations of the crack front of short wavelength, the energy release rate is larger at these points where the crack advance is minimum than at those points where it is maximum; the smaller the wavelength, the larger the difference. The implication is that such undulations tend to disappear in time at a rate which increases when the wavelength decreases, independently of the far geometry and loading.

5.7. Asymptotic expression of the autocorrelation function of the perturbation

We shall now derive the asymptotic expression of the autocorrelation function $\mathscr{A}(z,a)$ of the perturbation of the crack front for large times. This will be done by taking the inverse Fourier transform of the power spectrum $\widehat{\mathscr{A}}(k,a)$. Unfortunately it does not suffice here to simply replace $\widehat{\mathscr{A}}(k,a)$ by its asymptotic expression (36) for $a \to +\infty$. Indeed the fact that this expression goes to infinity when k goes to 0 makes it clear that the convergence of $\widehat{\mathscr{A}}(k,a)$ toward its asymptotic expression is non-uniform with respect to k. It is thus necessary to come back to the original form (30) of $\widehat{\mathscr{A}}(k,a)$. Following then the same steps as at the beginning of Section 5.5, based on the inequalities $b \ll a_0 \ll a$, one gets

$$\mathscr{A}(z,a) \sim \frac{1}{2\pi}\int_{-\infty}^{+\infty} \widetilde{\mathscr{C}}(k,0)\,\mathrm{e}^{-\mathrm{i}kz}\left\{\int_{a_0}^{a}\left(\frac{a}{r}\right)^{2N\alpha}\left[\frac{\psi(ka)}{\psi(kr)}\right]^{2N}\mathrm{d}r\right\}\mathrm{d}k.$$

[6]This relation was evidenced by Amestoy and Leblond (1992). For a semi-infinite crack in an infinite body, as considered here, $\mathrm{d}K_I/\mathrm{d}a$ is simply proportional to M.

This expression is readily transformed, upon use of the change of variables defined by

$$u \equiv \frac{r}{a}; \quad p \equiv ka \tag{37}$$

and change of the order of integration, into

$$\mathscr{A}(z,a) \sim \frac{1}{2\pi} \int_{a_0/a}^{1} u^{-2N\alpha} \left\{ \int_{-\infty}^{+\infty} \widetilde{\mathscr{C}}\left(\frac{p}{a}, 0\right) \mathrm{e}^{-\mathrm{i}pz/a} \left[\frac{\psi(p)}{\psi(pu)}\right]^{2N} \mathrm{d}p \right\} \mathrm{d}u. \tag{38}$$

Detailed inspection of the integral on u here reveals that both its lower and upper bounds can generate divergent behaviors, depending on the value of α, in the limit $a \to +\infty$. It is thus necessary to express $\mathscr{A}(z,a)$ in the form

$$\mathscr{A}(z,a) \sim \mathscr{J}_1(a) + \mathscr{J}_2(a), \tag{39}$$

where[7]

$$\begin{cases} \mathscr{J}_1(a) \equiv \dfrac{1}{2\pi} \displaystyle\int_{a_0/a}^{1/2} u^{-2N\alpha} \left\{ \int_{-\infty}^{+\infty} \widetilde{\mathscr{C}}\left(\frac{p}{a}, 0\right) \mathrm{e}^{-\mathrm{i}pz/a} \left[\frac{\psi(p)}{\psi(pu)}\right]^{2N} \mathrm{d}p \right\} \mathrm{d}u, \\ \mathscr{J}_2(a) \equiv \dfrac{1}{2\pi} \displaystyle\int_{1/2}^{1} u^{-2N\alpha} \left\{ \int_{-\infty}^{+\infty} \widetilde{\mathscr{C}}\left(\frac{p}{a}, 0\right) \mathrm{e}^{-\mathrm{i}pz/a} \left[\frac{\psi(p)}{\psi(pu)}\right]^{2N} \mathrm{d}p \right\} \mathrm{d}u, \end{cases} \tag{40}$$

and to study the behavior of the integrals $\mathscr{J}_1(a)$ and $\mathscr{J}_2(a)$ separately.

- *Study of the integral $\mathscr{J}_1(a)$.*
  This integral may or may not, depending on the value of α, go to infinity in the limit $a \to +\infty$ because of its lower bound on u. Indeed, replacing $\widetilde{\mathscr{C}}(p/a, 0)$ by $\widetilde{\mathscr{C}}(0,0)$ and $\mathrm{e}^{-\mathrm{i}pz/a}$ by unity in the limit $a \to +\infty$ and using the fact that the function $\psi(p)$ is even, one gets

  $$\mathscr{J}_1(a) \sim \frac{\widetilde{\mathscr{C}}(0,0)}{\pi} \int_{a_0/a}^{1/2} u^{-2N\alpha} \left\{ \int_{0}^{+\infty} \left[\frac{\psi(p)}{\psi(pu)}\right]^{2N} \mathrm{d}p \right\} \mathrm{d}u.$$

  There are again two cases here according to whether the exponent $-2N\alpha$ of u is larger or smaller than -1:
  - If $\alpha > \frac{1}{2N}$, considering the integral as a function of the small parameter $\xi \equiv a_0/a$ instead of a and differentiating it, one gets

    $$\frac{\mathrm{d}\mathscr{J}_1}{\mathrm{d}\xi} \sim -\frac{\widetilde{\mathscr{C}}(0,0)}{\pi} \xi^{-2N\alpha} \int_{0}^{+\infty} \left[\frac{\psi(p)}{\psi(p\xi)}\right]^{2N} \mathrm{d}p \sim -\frac{\widetilde{\mathscr{C}}(0,0)}{\pi} \xi^{-2N\alpha} \int_{0}^{+\infty} [\psi(p)]^{2N} \mathrm{d}p$$

    (since $\psi(0) = 1$), which yields upon integration

    $$\mathscr{J}_1(a) \sim \frac{\widetilde{\mathscr{C}}(0,0)}{\pi(2N\alpha - 1)} \left(\frac{a}{a_0}\right)^{2N\alpha - 1} \int_{0}^{+\infty} [\psi(p)]^{2N} \mathrm{d}p. \tag{41}$$

    Therefore $\mathscr{J}_1(a)$ goes to infinity in this case.
  - If $\alpha < \frac{1}{2N}$, $\mathscr{J}_1(a)$ goes to a finite limit:

    $$\mathscr{J}_1(a) \to \frac{\widetilde{\mathscr{C}}(0,0)}{\pi} \int_{0}^{1/2} u^{-2N\alpha} \left\{ \int_{0}^{+\infty} \left[\frac{\psi(p)}{\psi(pu)}\right]^{2N} \mathrm{d}p \right\} \mathrm{d}u. \tag{42}$$

- *Study of the integral $\mathscr{J}_2(a)$.*
  We shall see, at the expense of a somewhat elaborate reasoning, that this integral goes to infinity in all cases in the limit $a \to +\infty$ because of its upper bound on u.

[7] The "intermediary" bound of $\frac{1}{2}$ here is arbitrary, and could be replaced by any number in the interval $(0,1)$.

One difficulty is that $\widetilde{\mathscr{C}}(p/a,0)$ cannot simply be replaced by $\widetilde{\mathscr{C}}(0,0)$ in Eq. $(40)_2$. Indeed it is easy to check, using the definition (25) of the function ψ, that what is obtained then is a divergent (infinite) integral on u, because of the upper bound of unity. It becomes necessary here to account for the fact that it is the decrease of the function $\widetilde{\mathscr{C}}(k,0)$ down to zero at infinity which ensures the convergence of the integral on u in Eq. $(40)_2$. It will be assumed more precisely, for definiteness, that this function is of the form

$$\widetilde{\mathscr{C}}(k,0) \equiv \widetilde{\mathscr{C}}(0,0)\mathrm{e}^{-b|k|}, \tag{43}$$

where b is recalled to denote the "fluctuation distance" of the Paris constant. Inserting this expression into Eq. $(40)_2$ and using the fact that the function ψ is even, one gets

$$\mathscr{J}_2(a) = \frac{\widetilde{\mathscr{C}}(0,0)}{\pi}\mathrm{Re}\left\{\int_{1/2}^{1} u^{-2N\alpha}\left[\int_0^{+\infty}\mathrm{e}^{-\eta(1+\mathrm{i}\theta)p}\left(\frac{\psi(p)}{\psi(pu)}\right)^{2N}\mathrm{d}p\right]\mathrm{d}u\right\},$$

where

$$\eta \equiv \frac{b}{a}; \quad \theta \equiv \frac{z}{b}. \tag{44}$$

Note that η is a small parameter whereas θ is fixed and finite. To study the singular behavior of this integral in the limit $\eta \to 0^+$ due to the upper bound of unity on u, one may safely replace $u^{-2N\alpha}$ by unity, define $v \equiv 1-u$ and expand $\psi(pu) \equiv \psi[p(1-v)]$ to first order in v using the definition (25) of the function ψ. This leads to

$$\begin{aligned}\mathscr{J}_2(a) &\sim \frac{\widetilde{\mathscr{C}}(0,0)}{\pi}\mathrm{Re}\left\{\int_0^{1/2}\left[\int_0^{+\infty}\mathrm{e}^{-\eta(1+\mathrm{i}\theta)p}\exp[-2NvAp - 2Nv\,\mathrm{Re}(Bp^{1+2\mathrm{i}\varepsilon})]\,\mathrm{d}p\right]\mathrm{d}v\right\}\\ &= \frac{\widetilde{\mathscr{C}}(0,0)}{2\pi N}\mathrm{Re}\left\{\int_0^{+\infty}\mathrm{e}^{-\eta(1+\mathrm{i}\theta)p}\frac{1-\exp[-NAp - N\,\mathrm{Re}(Bp^{1+2\mathrm{i}\varepsilon})]}{Ap + \mathrm{Re}(Bp^{1+2\mathrm{i}\varepsilon})}\mathrm{d}p\right\}.\end{aligned}$$

Considering now $\mathscr{J}_2(a)$ as a function of the small parameter η, differentiating it, and using the change of variable $q \equiv \eta p$, one gets

$$\frac{\mathrm{d}\mathscr{J}_2}{\mathrm{d}\eta} \sim \frac{\widetilde{\mathscr{C}}(0,0)}{2\pi N}\mathrm{Re}\left\{\int_0^{+\infty}(1+\mathrm{i}\theta)\,\mathrm{e}^{-(1+\mathrm{i}\theta)q}\frac{\exp[-NAq/\eta - N\,\mathrm{Re}(B(q/\eta)^{1+2\mathrm{i}\varepsilon})]-1}{A+\mathrm{Re}(B(q/\eta)^{2\mathrm{i}\varepsilon})}\frac{\mathrm{d}q}{\eta}\right\}.$$

The exponential in the ratio here can be discarded in the limit $\eta \to 0^+$, so that

$$\frac{\mathrm{d}\mathscr{J}_2}{\mathrm{d}\eta} \sim -\frac{\widetilde{\mathscr{C}}(0,0)}{2\pi N\eta}\mathrm{Re}\left[\int_0^{+\infty}\frac{(1+\mathrm{i}\theta)\,\mathrm{e}^{-(1+\mathrm{i}\theta)q}}{A+\mathrm{Re}(B(q/\eta)^{2\mathrm{i}\varepsilon})}\mathrm{d}q\right]. \tag{45}$$

To study the behavior of the integral here in the limit $\eta \to 0^+$, let us define the function (depending upon the parameter θ)

$$F_\theta(\lambda) \equiv \int_0^{+\infty}\frac{(1+\mathrm{i}\theta)\mathrm{e}^{-(1+\mathrm{i}\theta)q}}{A+\mathrm{Re}(B\mathrm{e}^{-2\mathrm{i}\varepsilon\lambda}q^{2\mathrm{i}\varepsilon})}\mathrm{d}q. \tag{46}$$

This function is periodic of period $\pi/|\varepsilon|$. It may therefore be written in the form $F_\theta(\lambda) \equiv \overline{F} + \widetilde{F_\theta}(\lambda)$ where $\overline{F}$ denotes its mean value and the function $\widetilde{F_\theta}(\lambda)$ is periodic with zero mean value. The calculation of $\overline{F}$ is presented in Appendix E, and the result is

$$\overline{F} = \begin{cases}\dfrac{1}{A+\mathrm{Re}(B)} & \text{if } \varepsilon = 0,\\ \dfrac{1}{\sqrt{A^2-|B|^2}} & \text{if } \varepsilon \neq 0.\end{cases} \tag{47}$$

Note that $\overline{F}$ is real and independent of the parameter θ. We also denote $\widetilde{\mathscr{F}_\theta}(\lambda)$ some indefinite integral of the function $\widetilde{F_\theta}(\lambda)$. Since $\widetilde{F_\theta}(\lambda)$ is periodic and its mean value is zero, $\widetilde{\mathscr{F}_\theta}(\lambda)$ is periodic.

With these notations, Eq. (45) yields

$$\frac{\mathrm{d}\mathscr{J}_2}{\mathrm{d}\eta}\sim -\frac{\widetilde{\mathscr{C}}(0,0)}{2\pi N\eta}\mathrm{Re}[F_\theta(\ln\eta)]$$

$$\Rightarrow \mathrm{d}\mathscr{J}_2\sim -\frac{\widetilde{\mathscr{C}}(0,0)}{2\pi N}\{\overline{F}+\mathrm{Re}[\widetilde{F_\theta}(\ln\eta)]\}\,\mathrm{d}(\ln\eta)$$

$$\Rightarrow \mathscr{J}_2(a)\sim -\frac{\widetilde{\mathscr{C}}(0,0)}{2\pi N}\{\overline{F}\ln\eta+\mathrm{Re}[\widetilde{\mathscr{F}}_\theta(\ln\eta)]\}+Cst.$$

Since the function $\widetilde{\mathscr{F}}_\theta(\lambda)$ is periodic, the term $\mathrm{Re}[\widetilde{\mathscr{F}}_\theta(\ln\eta)]$ here is bounded, like the constant, and therefore both are negligible compared to the term $\overline{F}\ln\eta$ which goes to infinity in the limit $\eta\to 0^+$. It follows that

$$\mathscr{J}_2(a)\sim -\frac{\widetilde{\mathscr{C}}(0,0)}{2\pi N}\overline{F}\,\ln\left(\frac{b}{a}\right)\sim\frac{\widetilde{\mathscr{C}}(0,0)}{2\pi N}\overline{F}\,\ln a. \tag{48}$$

Combining Eqs. (39), (41), (42) and (48), we see that there are two cases:

- If $\alpha>\frac{1}{2N}$, the integral $\mathscr{J}_2(a)$ is negligible compared to the integral $\mathscr{J}_1(a)$, so that

$$\mathscr{A}(z,a)\sim\mathscr{J}_1(a)\sim\frac{\widetilde{\mathscr{C}}(0,0)}{\pi(2N\alpha-1)}\left(\frac{a}{a_0}\right)^{2N\alpha-1}\int_0^{+\infty}[\psi(p)]^{2N}\,\mathrm{d}p. \tag{49}$$

- If $\alpha<\frac{1}{2N}$, the integral $\mathscr{J}_1(a)$ is negligible compared to the integral $\mathscr{J}_2(a)$, so that

$$\mathscr{A}(z,a)\sim\mathscr{J}_2(a)\sim\frac{\widetilde{\mathscr{C}}(0,0)}{2\pi N}\overline{F}\,\ln a, \tag{50}$$

  where the quantity $\overline{F}$ is recalled to be given by Eq. (47).

Several comments are in order here. The first observation is that the autocorrelation function $\mathscr{A}(z,a)$ of the perturbation of the crack front goes to infinity in the limit $a\to+\infty$ in all cases; the larger the value of the parameter α, the quicker the divergence. These effects obviously arise from similar features apparent in the behavior of the Fourier component $\widehat{\mathscr{A}}(0,a)$ (see Eqs. (34) and (35)). The role of the other Fourier components $\widehat{\mathscr{A}}(k,a)$, $k\neq 0$, is less important since they remain bounded (see Eq. (36)).

It is also worth noting in this context that the decomposition of $\mathscr{A}(z,a)$ into $\mathscr{J}_1(a)+\mathscr{J}_2(a)$ followed by separate study of the behavior of these integrals in the limit $a\to+\infty$, far from being a mere mathematical procedure, possesses a nice physical interpretation. Indeed we have noted that the divergence of $\mathscr{A}(z,a)$ in the limit $a\to+\infty$ arises from the lower bound of a_0/a in the expression $(40)_1$ of $\mathscr{J}_1(a)$ for large values of α, but from the upper bound of unity in the expression $(40)_2$ of $\mathscr{J}_2(a)$ for small values of α. This means that this divergence is due to the far past ($r\simeq a_0$, see Eq. $(37)_1$) if α is large, but from the near past ($r\simeq a$) if α is small. In other words, quite naturally, the influence of the far past upon the development of the perturbation of the crack front is more important when 2D crack propagation is unstable (α large) than when it is stable (α small).

Another observation is that $\mathscr{A}(z,a)$ becomes independent of z in the limit $a\to+\infty$. Thus correlations between values of δa at different points of the crack front ultimately become independent of the distance between these points, that is exactly as strong as if they coincided. The explanation lies in the gradual selection of Fourier components of δa of large wavelength evidenced in Section 5.6, which implies that long-range correlations develop in time at the expense of short-range ones.

5.8. Asymptotic expression of the autocorrelation function of the slope of the perturbation

Although the autocorrelation function of δa does provide informations about the geometric evolution of the crack front, it is not a good measure of its "wavyness", because it depends on all Fourier components of δa,

including that corresponding to $k=0$ which represents a mere translatory motion of the front. It is thus interesting to study the autocorrelation function of the "slope" $\partial\delta a/\partial z$, which is independent of this particular Fourier component.

By Eqs. $(27)_1$ and (29),

$$\begin{aligned} E\left[\frac{\partial\delta a}{\partial z}(z_1,a)\frac{\partial\delta a}{\partial z}(z_2,a)\right] &= \frac{1}{4\pi^2}\int_{-\infty}^{+\infty}\int_{-\infty}^{+\infty} E\left[\widehat{\frac{\partial\delta a}{\partial z}}(k_1,a)\widehat{\frac{\partial\delta a}{\partial z}}(k_2,a)\right]\mathrm{e}^{-\mathrm{i}k_1z_1-\mathrm{i}k_2z_2}\,\mathrm{d}k_1\,\mathrm{d}k_2 \\ &= -\frac{1}{4\pi^2}\int_{-\infty}^{+\infty}\int_{-\infty}^{+\infty} k_1k_2\,E[\widehat{\delta a}(k_1,a)\widehat{\delta a}(k_2,a)]\,\mathrm{e}^{-\mathrm{i}k_1z_1-\mathrm{i}k_2z_2}\,\mathrm{d}k_1\,\mathrm{d}k_2 \\ &= \frac{1}{2\pi}\int_{-\infty}^{+\infty} k^2\widehat{\mathscr{A}}(k,a)\,\mathrm{e}^{-\mathrm{i}k(z_2-z_1)}\,\mathrm{d}k. \end{aligned} \tag{51}$$

From this point, the reasoning is basically similar to that made in Section 5.7 for the autocorrelation function of δa, so that a mere sketch of the procedure will be sufficient. One first gets, in the limit $a\to+\infty$,

$$E\left[\frac{\partial\delta a}{\partial z}(z_1,a)\frac{\partial\delta a}{\partial z}(z_2,a)\right]\sim\mathscr{K}_1(a)+\mathscr{K}_2(a), \tag{52}$$

where,

$$\begin{cases} \mathscr{K}_1(a)\equiv\dfrac{1}{2\pi a^2}\displaystyle\int_{a_0/a}^{1/2}u^{-2N\alpha}\left\{\int_{-\infty}^{+\infty}p^2\,\widetilde{\mathscr{C}}\left(\frac{p}{a},0\right)\mathrm{e}^{-\mathrm{i}p(z_2-z_1)/a}\left[\frac{\psi(p)}{\psi(pu)}\right]^{2N}\mathrm{d}p\right\}\mathrm{d}u, \\ \mathscr{K}_2(a)\equiv\dfrac{1}{2\pi a^2}\displaystyle\int_{1/2}^{1}u^{-2N\alpha}\left\{\int_{-\infty}^{+\infty}p^2\,\widetilde{\mathscr{C}}\left(\frac{p}{a},0\right)\mathrm{e}^{-\mathrm{i}p(z_2-z_1)/a}\left[\frac{\psi(p)}{\psi(pu)}\right]^{2N}\mathrm{d}p\right\}\mathrm{d}u. \end{cases} \tag{53}$$

Detailed study of the integral $\mathscr{K}_1(a)$ reveals that

- If $\alpha>\frac{1}{2N}$,

$$\mathscr{K}_1(a)\sim\frac{\widetilde{\mathscr{C}}(0,0)}{\pi(2N\alpha-1)\,a_0^2}\left(\frac{a}{a_0}\right)^{2N\alpha-3}\int_0^{+\infty}p^2[\psi(p)]^{2N}\,\mathrm{d}p. \tag{54}$$

- If $\alpha<\frac{1}{2N}$,

$$\mathscr{K}_1(a)\sim\frac{\widetilde{\mathscr{C}}(0,0)}{\pi a^2}\int_0^{1/2}u^{-2N\alpha}\left\{\int_0^{+\infty}p^2\left[\frac{\psi(p)}{\psi(pu)}\right]^{2N}\mathrm{d}p\right\}\mathrm{d}u. \tag{55}$$

The study of the integral $\mathscr{K}_2(a)$ is again based on hypothesis (43) on the function $\widetilde{\mathscr{C}}(k,0)$. It is similar to that of the integral $\mathscr{J}_2(a)$ except that no derivation with respect to the parameter $\eta\equiv b/a$ is needed. The result is

$$\mathscr{K}_2(a)\sim\frac{\widetilde{\mathscr{C}}(0,0)}{2\pi Nb^2}\mathrm{Re}\left\{G_\theta\left[\left(\frac{a}{b}\right)^{2\mathrm{i}\varepsilon}\right]\right\},\quad G_\theta(\zeta)\equiv\int_0^{+\infty}\frac{q\mathrm{e}^{-(1+\mathrm{i}\theta)q}}{A+\mathrm{Re}(B\zeta q^{2\mathrm{i}\varepsilon})}\mathrm{d}q,\quad\theta\equiv\frac{z_2-z_1}{b}. \tag{56}$$

Combinating Eqs. (52), (54)–(56), one sees that there are again two cases:

- If $\alpha>\frac{3}{2N}$,

$$E\left[\frac{\partial\delta a}{\partial z}(z_1,a)\frac{\partial\delta a}{\partial z}(z_2,a)\right]\sim\mathscr{K}_1(a)\sim\frac{\widetilde{\mathscr{C}}(0,0)}{\pi(2N\alpha-1)\,a_0^2}\left(\frac{a}{a_0}\right)^{2N\alpha-3}\int_0^{+\infty}p^2[\psi(p)]^{2N}\,\mathrm{d}p. \tag{57}$$

- If $\alpha<\frac{3}{2N}$,

$$E\left[\frac{\partial\delta a}{\partial z}(z_1,a)\frac{\partial\delta a}{\partial z}(z_2,a)\right]\sim\mathscr{K}_2(a)\sim\frac{\widetilde{\mathscr{C}}(0,0)}{2\pi Nb^2}\mathrm{Re}\left\{G_\theta\left[\left(\frac{a}{b}\right)^{2i\varepsilon}\right]\right\}. \tag{58}$$

Note that the term $\mathrm{Re}\{G_\theta[(a/b)^{2i\varepsilon}]\}$ here is a periodic function of $\ln a$ of period $\pi/|\varepsilon|$. It cannot be expressed in a simple analytical form except if $\varepsilon=0$, in which case its value is $\frac{1}{A+\mathrm{Re}(B)}\frac{1-\theta^2}{(1+\theta^2)^2}=\frac{b^2}{A+\mathrm{Re}(B)}\frac{b^2-(z_2-z_1)^2}{[b^2+(z_2-z_1)^2]^2}$.

Thus, for large values of α, $E[\frac{\partial\delta a}{\partial z}(z_1,a)\frac{\partial\delta a}{\partial z}(z_2,a)]$ goes to infinity in the limit $a\to+\infty$, but the divergence is less quick than that of $\mathscr{A}(z,a)$ (compare Eqs. (49) and (57)). For small values of α, $E[\frac{\partial\delta a}{\partial z}(z_1,a)\frac{\partial\delta a}{\partial z}(z_2,a)]$ oscillates indefinitely between finite values for $a\to+\infty$ (except if $\varepsilon=0$, in which case it tends toward a finite limit), whereas $\mathscr{A}(z,a)$ goes to infinity (compare Eqs. (50) and (58)). Thus $E[\frac{\partial\delta a}{\partial z}(z_1,a)\frac{\partial\delta a}{\partial z}(z_2,a)]$ evolves less quickly than $\mathscr{A}(z,a)$ in all cases. The obvious explanation is that as noted in Section 5.7, the divergence of $\mathscr{A}(z,a)$ for $a\to+\infty$ essentially arises from that of the Fourier component $\widehat{\mathscr{A}}(0,a)$, and $E[\frac{\partial\delta a}{\partial z}(z_1,a)\frac{\partial\delta a}{\partial z}(z_2,a)]$ does not depend upon this particular component.

Another observation is that in the limit $a\to+\infty$, $E[\frac{\partial\delta a}{\partial z}(z_1,a)\frac{\partial\delta a}{\partial z}(z_2,a)]$ depends upon the distance z_2-z_1 between the points of observation of the slope for small values of α, but not for large ones. The explanation is that as noted in Section 5.7, the phenomenon responsible for the disappearance of the dependence upon this distance is the selection of Fourier components of δa of large wavelength, which is maximum for large values of α, as was explained in Section 5.6. The fact that for small values of α, $E[\frac{\partial\delta a}{\partial z}(z_1,a)\frac{\partial\delta a}{\partial z}(z_2,a)]$ depends on z_2-z_1 whereas $\mathscr{A}(z,a)$ is independent of z (compare Eqs. (50) and (58)) can be rationalized in a similar way: $\mathscr{A}(z,a)$ is more sensitive than $E[\frac{\partial\delta a}{\partial z}(z_1,a)\frac{\partial\delta a}{\partial z}(z_2,a)]$ to the selection of Fourier components of δa of large wavelength, since the former quantity depends upon the Fourier component $\widehat{\mathscr{A}}(0,a)$ contrary to the latter.

5.9. Asymptotic expression of the distance of correlation of the perturbation

The "distance of correlation" L of the perturbation of the crack front characterizes the distance over which correlations between values of δa at different points of this front can be felt. It can be given several definitions, the simplest being

$$L\equiv\sqrt{\frac{\int_{-\infty}^{+\infty}\widehat{\mathscr{A}}(k,a)\,\mathrm{d}k}{\int_{-\infty}^{+\infty}k^2\widehat{\mathscr{A}}(k,a)\,\mathrm{d}k}}=\sqrt{\frac{\mathscr{A}(0,a)}{E\{[(\partial\delta a/\partial z)(z,a)]^2\}}}. \tag{59}$$

There are three cases here in the limit $a\to+\infty$:

- If $\alpha>\frac{3}{2N}$, by Eqs. (49) and (57),

$$L\sim a\sqrt{\frac{\int_0^{+\infty}[\psi(p)]^{2N}\,\mathrm{d}p}{\int_0^{+\infty}p^2[\psi(p)]^{2N}\,\mathrm{d}p}}. \tag{60}$$

- If $\frac{1}{2N}<\alpha<\frac{3}{2N}$, by Eqs. (49) and (58),

$$L\sim b\left(\frac{a}{a_0}\right)^{N\alpha-1/2}\sqrt{\frac{2N}{2N\alpha-1}\frac{\int_0^{+\infty}[\psi(p)]^{2N}\,\mathrm{d}p}{\mathrm{Re}\{G_0[(a/b)^{2i\varepsilon}]\}}}. \tag{61}$$

- If $\alpha<\frac{1}{2N}$, by Eqs. (50) and (58),

$$L\sim b\sqrt{\frac{\overline{F}\,\ln a}{\mathrm{Re}\{G_0[(a/b)^{2i\varepsilon}]\}}}. \tag{62}$$

In Eqs. (61) and (62), G_0 is the function defined by Eq. $(56)_2$ with $\theta \equiv 0$.

Eqs. (60)–(62) show that the correlation distance of the perturbation goes to infinity in the limit $a \to +\infty$ in all cases (with superimposed oscillations if $\varepsilon \neq 0$ and $\alpha < \frac{3}{2N}$); the larger the value of α, the quicker the divergence. This again illustrates the selection of Fourier components of the perturbation of large wavelength and the dependence of this phenomenon upon the value of α.

6. Deformation of the crack front in brittle fracture

6.1. Generalities

In this section, we assume that crack propagation is governed by Griffith's law:

$$G(z,a) = G_c(z,a) \equiv G_c[1 + \delta g_c(z,a)], \quad |\delta g_c(z,a)| \ll 1. \tag{63}$$

In this equation the x-coordinate of the point of the crack front considered is denoted a as above, and $\delta g_c(z,a)$ represents the "normalized", dimensionless fluctuation of the critical energy release rate $G_c(z,a)$. The distribution of this fluctuation is assumed to be statistically homogeneous and isotropic within the interface, so that its two-point autocorrelation function is given by

$$E[\delta g_c(z_1,a)\,\delta g_c(z_2,a)] \equiv \mathscr{G}_c(z_2 - z_1), \tag{64}$$

where $\mathscr{G}_c$ is an even function. The fluctuations of the crack advance resulting from those of the critical energy release rate are also statistically invariant in the direction of the crack front, so that Eq. (29) still applies.

Taking the Fourier transform of Eq. (63) and identifying terms of order 0 and 1 in the perturbation, one gets

$$\begin{cases} G(a) = G_c, \\ \dfrac{\widehat{\delta G}(k,a)}{G(a)} = \widehat{\delta g_c}(k,a). \end{cases} \tag{65}$$

Note that Eq. $(65)_1$ implies that $G(a)$ must remain invariable, which requires a continuous adjustment in time of the quantities k and k_{III} of Eq. (9), that is of the loading. This condition being assumed to be fulfilled, combination of Eqs. (15) and $(65)_2$ yields

$$\widehat{\delta a}(k,a) = \frac{a}{2}\frac{\widehat{\delta g_c}(k,a)}{\alpha - f(ka)} \;\Rightarrow\; \delta a(z,a) = \frac{a}{4\pi}\int_{-\infty}^{+\infty} \frac{\widehat{\delta g_c}(k,a)}{\alpha - f(ka)} \mathrm{e}^{-\mathrm{i}kz}\,\mathrm{d}k. \tag{66}$$

Unfortunately, if $\alpha > 0$, the expression $(66)_2$ of $\delta a(z,a)$ is meaningless because the integral is divergent. Indeed, referring to Section 5.6 above, one sees that for such values of α, the denominator has simple poles at the points $k = \pm p_0/a$. This means that *the problem is intractable in brittle fracture in the case of unstable 2D crack propagation.*

The origin of the problem can be best understood by considering the special case of a uniform distribution of the critical energy release rate within the interface. The condition of uniformity of G is then obviously met by a straight front. But if $\alpha > 0$, this is not the sole solution, because by Eq. (15), a sinusoidal perturbation of the front having $k = \pm p_0/a$, that is of wavelength $\lambda_0 \equiv 2\pi a/p_0$, generates a zero perturbation of G. The implication is existence of a bifurcation. Worse, new bifurcations continuously appear, since the reasoning just made applies at every instant. The consequence is that the problem is ill-posed, resulting in the divergent integral of Eq. $(66)_2$.

We shall therefore consider the sole case of stable 2D crack propagation ($\alpha < 0$) henceforward. Eq. (66) then takes the form

$$\widehat{\delta a}(k,a) = -\frac{a}{2}\frac{\widehat{\delta g_c}(k,a)}{|\alpha| + f(ka)} \;\Rightarrow\; \delta a(z,a) = -\frac{a}{4\pi}\int_{-\infty}^{+\infty} \frac{\widehat{\delta g_c}(k,a)}{|\alpha| + f(ka)} \mathrm{e}^{-\mathrm{i}kz}\,\mathrm{d}k, \tag{67}$$

where the integral is convergent. It is important to note that there is no integral from a_0 to a here, that is, the values of $\widehat{\delta a}(k,a)$ and $\delta a(z,a)$ depend on the distribution of δg_c at the sole position $x = a$. In other words, the shape of the crack front is entirely determined by the instantaneous distribution of the critical energy release rate; there is no memory of its past distributions or the past shapes of the crack front. This characteristic

feature of Griffith's propagation law will considerably simplify the mathematical treatment and bear important physical consequences, as will be seen.

6.2. Asymptotic expression of the power spectrum of the perturbation of the crack front

By the expression $(67)_1$ of $\widehat{\delta a}(k,a)$, the definition (C.2) of the two-point autocorrelation function, Eq. $(27)_2$ for the observable δg_c and the fact that the function $f(p)$ is even,

$$E[\widehat{\delta a}(k_1,a)\,\widehat{\delta a}(k_2,a)] = \frac{a^2}{4}\frac{E[\widehat{\delta g_c}(k_1,a)\,\widehat{\delta g_c}(k_2,a)]}{[|\alpha|+f(k_1 a)][|\alpha|+f(k_2 a)]} = \frac{a^2}{4}\frac{2\pi\delta(k_1+k_2)\widehat{\mathscr{G}_c}(k_2)}{[|\alpha|+f(k_2 a)]^2}.$$

Comparison with Eq. $(27)_2$ for the observable δa then reveals that

$$\widehat{\mathscr{A}}(k,a) = \frac{a^2}{4}\frac{\widehat{\mathscr{G}_c}(k)}{[|\alpha|+f(ka)]^2}. \tag{68}$$

Now consider the limit $a \to +\infty$. There are again two cases:

- If $k = 0$, since $f(0) = 0$, Eq. (68) reduces to

$$\widehat{\mathscr{A}}(0,a) = \frac{\widehat{\mathscr{G}_c}(0)}{4\alpha^2}a^2. \tag{69}$$

- If $k \neq 0$, using Eq. (16) and the fact that the term $|\alpha|$ in Eq. (68) is negligible compared to the term $f(ka)$ which goes to infinity, one gets

$$\widehat{\mathscr{A}}(k,a) \sim \frac{\widehat{\mathscr{G}_c}(k)}{4k^2[A+\mathrm{Re}(B|ka|^{2i\varepsilon})]^2}, \quad (k\neq 0). \tag{70}$$

Eqs. (69) and (70) show that in the limit of large times, $\widehat{\mathscr{A}}(0,a)$ goes to infinity, whereas $\widehat{\mathscr{A}}(k,a)$ remains bounded for $k \neq 0$. These features are analogous to those found in Section 5.5 in the case of fatigue, and again symptomatic of a gradual selection in time of Fourier components of the perturbation of the crack front of large wavelength.

However the divergence of $\widehat{\mathscr{A}}(0,a)$ for $a \to +\infty$ is quicker in brittle fracture than in fatigue (compare Eqs. (35) and (69)), and similarly the asymptotic formula for $\widehat{\mathscr{A}}(k,a)$, $k \neq 0$ goes to infinity in the limit $k \to 0$ more quickly in brittle fracture (compare Eqs. (36) and (70)).[8] This means that the selection of Fourier components of δa of large wavelength is stronger in brittle fracture. The explanation lies in the presence, in fatigue, of an effect of memory of previous configurations of the crack front, which is absent in brittle fracture, as was noted above. Such a memory effect delays the elimination of Fourier components of δa of short wavelength.

6.3. Asymptotic expression of the autocorrelation function of the perturbation

Fourier inversion of Eq. (68) and use of the change of variable $p \equiv ka$ yields

$$\mathscr{A}(z,a) = \frac{a}{8\pi}\int_{-\infty}^{+\infty}\frac{\widehat{\mathscr{G}_c}(p/a)}{[|\alpha|+f(p)]^2}\,\mathrm{e}^{-\mathrm{i}pz/a}\,\mathrm{d}p.$$

It follows that in the limit $a \to +\infty$,

$$\mathscr{A}(z,a) \sim \frac{\widehat{\mathscr{G}_c}(0)}{4\pi}a\int_0^{+\infty}\frac{\mathrm{d}p}{[|\alpha|+Ap+\mathrm{Re}(Bp^{1+2i\varepsilon})]^2}, \tag{71}$$

where use has been made of Eq. (16).

[8] Since the problem is tractable in brittle fracture only if $\alpha<0$, the comparison with fatigue can be made only in this case. The formulae for fatigue used here are therefore those pertaining to small values of α.

Comparison of Eqs. (50) and (71) shows that the divergence of $\mathscr{A}(z,a)$ for $a \to +\infty$ is quicker in brittle fracture than in fatigue. This is obviously because it essentially arises from the divergence of the Fourier component $\widehat{\mathscr{A}}(0,a)$ (other Fourier components remaining bounded), which was noted above to be stronger in brittle fracture.

6.4. Asymptotic expression of the autocorrelation function of the slope of the perturbation

By Eqs. (51) and (68),

$$E\left[\frac{\partial \delta a}{\partial z}(z_1,a)\frac{\partial \delta a}{\partial z}(z_2,a)\right] = \frac{a^2}{8\pi}\int_{-\infty}^{+\infty} \frac{\widehat{\mathscr{G}_c}(k)}{[|\alpha| + f(ka)]^2} k^2 \, \mathrm{e}^{-\mathrm{i}k(z_2-z_1)} \, \mathrm{d}k.$$

Discarding the term $|\alpha|$ which becomes negligible compared to $f(ka)$ in the limit $a \to +\infty$ and using Eq. (16), one gets from there

$$E\left[\frac{\partial \delta a}{\partial z}(z_1,a)\frac{\partial \delta a}{\partial z}(z_2,a)\right] \sim \frac{1}{8\pi}\int_{-\infty}^{+\infty} \frac{\widehat{\mathscr{G}_c}(k)}{[A + \mathrm{Re}(B|ka|^{2\mathrm{i}\varepsilon})]^2} \mathrm{e}^{-\mathrm{i}k(z_2-z_1)} \, \mathrm{d}k. \tag{72}$$

This expression cannot be simplified further, except if $\varepsilon = 0$, in which case it reduces to $\frac{\mathscr{G}_c(z_2-z_1)}{4[A+\mathrm{Re}(B)]^2}$.

Thus in the limit $a \to +\infty$, $E[\frac{\partial \delta a}{\partial z}(z_1,a)\frac{\partial \delta a}{\partial z}(z_2,a)]$ oscillates indefinitely between finite values (except if $\varepsilon = 0$, in which case it tends toward a constant). Also, it depends upon the distance $z_2 - z_1$ between the points of observation of the slope, unlike $\mathscr{A}(z,a)$ which is independent of z. Both of these features are analogous to those observed in fatigue for negative values of α (see Section 5.8).

6.5. Asymptotic expression of the distance of correlation of the perturbation

Using the definition (59) of the distance of correlation and Eqs. (71) and (72), one gets, in the limit $a \to +\infty$:

$$L \sim \sqrt{a \frac{\displaystyle\int_0^{+\infty} \frac{\widehat{\mathscr{G}_c}(0)\,\mathrm{d}p}{[|\alpha| + Ap + \mathrm{Re}(Bp^{1+2\mathrm{i}\varepsilon})]^2}}{\displaystyle\int_0^{+\infty} \frac{\widehat{\mathscr{G}_c}(k)\,\mathrm{d}k}{[A + \mathrm{Re}(B(ka)^{2\mathrm{i}\varepsilon})]^2}}}. \tag{73}$$

Thus L diverges for $a \to +\infty$ more quickly than in fatigue (compare to Eq. (62)). This is again connected to the fact that the selection of Fourier components of the perturbation of large wavelength is stronger in brittle fracture than in fatigue.

7. Synthesis

The main findings of this work can be summarized as follows:

- *General observations*:
  - Although the mismatch of elastic properties between the materials introduces oscillations in the long-time behavior of many of the quantities studied, its overall role is relatively minor. It never changes the basic, bounded or divergent character of these quantities.
  - The problem can be treated in fatigue for all values of the parameter α characterizing the stability or instability of 2D crack propagation. In brittle fracture, however, it can be treated only if 2D crack propagation is stable ($\alpha < 0$), because some apparently intractable bifurcation problem arises in the case of unstable 2D crack propagation ($\alpha > 0$).
- *In fatigue*:
  - There is an effect of gradual selection in time of Fourier components of the perturbation of the crack front of large wavelength. The effect is present for all values of α, but is enhanced for $\alpha > 0$ by a dramatic "explosion" of Fourier components of large wavelength.

- The "wavyness" of the crack front, as measured by the autocorrelation function of the slope (derivative of the perturbation in the direction of the front), grows in time without bound for large values of α and tends toward a constant or oscillates for small ones.
- The distance of correlation of the perturbation of the crack front increases in time without bound in all cases.

• *In brittle fracture*:

- The gradual selection of Fourier components of the perturbation of the crack front of large wavelength is stronger than in fatigue. This is because in fatigue, it is mitigated by an effect of "memory" of previous configurations of the crack front which delays the elimination of Fourier components of short wavelength.
- The autocorrelation function of the slope tends toward a constant or oscillates in time, like in fatigue.
- The distance of correlation of the perturbation of the crack front diverges in time more quickly than in fatigue.

Acknowledgments

We wish to express our warm thanks to Profs. L. Mishuris and A. Movchan for having provided us with the values of the "γ" constants, without which this work would have been incomplete, prior to publication. Their friendly welcome in Liverpool and interesting comments are also gratefully acknowledged.

We also wish to thank M. Adda-Bedia, D. Bonamy, E. Katzav, L. Ponson, J. Schmittbuhl and R. Toussaint for several enlightening discussions.

Appendix A. Inequalities on the equivalent Poisson ratio

The aim of this Appendix is to establish inequalities (2) of the text on the constant v (the "equivalent Poisson ratio") defined by Eq. $(1)_2$. Of course, the individual Poisson ratios v_+, v_+ will be assumed to verify the inequalities $0<v_+<\frac{1}{2}$, $0<v_-<\frac{1}{2}$.

Inequality $(2)_1$ is quite trivial; indeed, since v_+ and v_- are positive, $(1-v_+)/\mu_+<1/\mu_+$, $(1-v_-)/\mu_-<1/\mu_-$ so that, by Eq. $(1)_2$,

$$1-v<\frac{1}{\cosh^2(\pi\varepsilon)}\leqslant 1 \quad\Rightarrow\quad v>0.$$

To establish inequality $(2)_2$, one needs an explicit expression of $\cosh(\pi\varepsilon)$. By Eq. $(1)_1$,

$$e^{\pi\varepsilon}=\sqrt{\frac{\dfrac{3-4v_+}{\mu_+}+\dfrac{1}{\mu_-}}{\dfrac{3-4v_-}{\mu_-}+\dfrac{1}{\mu_+}}} \quad\Rightarrow\quad \cosh(\pi\varepsilon)=2\frac{\dfrac{1-v_+}{\mu_+}+\dfrac{1-v_-}{\mu_-}}{\sqrt{\left(\dfrac{3-4v_+}{\mu_+}+\dfrac{1}{\mu_-}\right)\left(\dfrac{3-4v_-}{\mu_-}+\dfrac{1}{\mu_+}\right)}}.$$

It then follows from Eq. $(1)_2$ that

$$1-v=\frac{1}{4}\frac{\left(\dfrac{3-4v_+}{\mu_+}+\dfrac{1}{\mu_-}\right)\left(\dfrac{3-4v_-}{\mu_-}+\dfrac{1}{\mu_+}\right)}{\left(\dfrac{1}{\mu_+}+\dfrac{1}{\mu_-}\right)\left(\dfrac{1-v_+}{\mu_+}+\dfrac{1-v_-}{\mu_-}\right)}.$$

Let us now write v_+ and v_- in the form

$$v_+\equiv\tfrac{1}{2}-\alpha_+;\quad v_-\equiv\tfrac{1}{2}-\alpha_-.$$

Then $\alpha_+ > 0$, $\alpha_- > 0$ and

$$1-\nu = \frac{1}{4}\frac{\left(\frac{1+4\alpha_+}{\mu_+}+\frac{1}{\mu_-}\right)\left(\frac{1+4\alpha_-}{\mu_-}+\frac{1}{\mu_+}\right)}{\left(\frac{1}{\mu_+}+\frac{1}{\mu_-}\right)\left(\frac{1/2+\alpha_+}{\mu_+}+\frac{1/2+\alpha_-}{\mu_-}\right)}$$
$$= \frac{1}{2}\frac{\left(\frac{1}{\mu_+}+\frac{1}{\mu_-}+\frac{4\alpha_+}{\mu_+}\right)\left(\frac{1}{\mu_+}+\frac{1}{\mu_-}+\frac{4\alpha_-}{\mu_-}\right)}{\left(\frac{1}{\mu_+}+\frac{1}{\mu_-}\right)\left(\frac{1}{\mu_+}+\frac{1}{\mu_-}+\frac{2\alpha_+}{\mu_+}+\frac{2\alpha_-}{\mu_-}\right)}$$
$$= \frac{1}{2}\frac{\left(\frac{1}{\mu_+}+\frac{1}{\mu_-}\right)^2+4\left(\frac{1}{\mu_+}+\frac{1}{\mu_-}\right)\left(\frac{\alpha_+}{\mu_+}+\frac{\alpha_-}{\mu_-}\right)+16\frac{\alpha_+}{\mu_+}\frac{\alpha_-}{\mu_-}}{\left(\frac{1}{\mu_+}+\frac{1}{\mu_-}\right)^2+2\left(\frac{1}{\mu_+}+\frac{1}{\mu_-}\right)\left(\frac{\alpha_+}{\mu_+}+\frac{\alpha_-}{\mu_-}\right)}.$$

The big ratio here is obviously larger than unity, so that $1-\nu > \frac{1}{2}$, which implies that $\nu < \frac{1}{2}$.

Appendix B. Inequality on the constants *A* and *B*

The aim of this appendix is to establish inequality (19) of the text on the constants A and B defined by Eqs. (17). The proof will rely on inequalities (2) on the equivalent Poisson ratio ν.

The following preliminary remark is in order: since $1-\nu < 1/\cosh^2(\pi\varepsilon)$, as noted at the beginning of Appendix A, and since $1-\nu > 0$ by inequality $(2)_2$,

$$(1-\nu)\cosh(\pi\varepsilon) \leqslant (1-\nu)\cosh^2(\pi\varepsilon) < 1.$$

Now since $1-\nu > 0$, the quantity H defined by Eq. (18) is positive. Also, $\frac{3}{1-\nu} - \cosh(\pi\varepsilon) = \frac{1}{1-\nu}[3-(1-\nu)\cosh(\pi\varepsilon)] > \frac{2}{1-\nu} > 0$ by the preliminary remark. Eq. $(17)_1$ then implies that

$$A \geqslant H^{-1}|k|^2(1-\nu)\cosh(\pi\varepsilon).$$

Also, Eq. $(17)_2$, combined with the preliminary remark, implies that

$$|B| = H^{-1}\frac{|k|^2}{2}[1-(1-\nu)\cosh(\pi\varepsilon)].$$

It follows from there that

$$A - |B|\sqrt{1+4\varepsilon^2} \geqslant H^{-1}|k|^2\left[(1-\nu)\cosh(\pi\varepsilon)\left(1+\frac{\sqrt{1+4\varepsilon^2}}{2}\right)-\frac{\sqrt{1+4\varepsilon^2}}{2}\right].$$

Since $(1-\nu)\cosh(\pi\varepsilon) \geqslant 1-\nu > \frac{1}{2}$, this implies that

$$A - |B|\sqrt{1+4\varepsilon^2} > H^{-1}\frac{|k|^2}{2}\left(1-\frac{\sqrt{1+4\varepsilon^2}}{2}\right).$$

The problem is reduced to proving that the term $(\ldots)$ here is non-negative, i.e. that $|\varepsilon| \leqslant \sqrt{3}/2$.

To show that this is indeed true, write Eq. $(1)_1$ defining ε in the form

$$e^{2\pi\varepsilon} = \frac{3-4\nu_+ + \frac{\mu_+}{\mu_-}}{(3-4\nu_-)\frac{\mu_+}{\mu_-}+1}.$$

The denominator in the right-hand side here does not vanish since $3-4\nu_- > 0$, so that this right-hand side is a monotone function of the ratio μ_+/μ_-. Hence its extremal values are $3-4\nu_+$, for $\mu_+/\mu_- = 0$, and $\frac{1}{3-4\nu_-}$, for

$\mu_+/\mu_- = +\infty$. Since $0<v_+<\frac{1}{2}$ and $0<v_-<1/2$, they are in the interval $(\frac{1}{3}, 3)$. Hence $\frac{1}{3}<e^{2\pi\varepsilon}<3$, which implies that $|\varepsilon|<\frac{\ln 3}{2\pi}<\frac{\sqrt{3}}{2}$. This concludes the proof.

Appendix C. Statistical description of an ensemble of cracked media

We consider a statistical ensemble of possible "realizations" of a medium made of two elastic half-spaces bonded together except on a semi-infinite interface crack. The elastic properties are the same for all realizations, but the fracture properties of the interface and the geometry of the crack front vary from one realization to another. To each realization is attached a specific real number ω, which is a random variable spanning some domain Ω of the real line. The *density of probability* of the variable ω is denoted $p(\omega)$. The probability that this variable lie in some neighborhood of ω of measure $d\omega$ is thus $p(\omega)\,d\omega$. The integral of $p(\omega)$ over Ω is unity by definition.

The *mathematical expectation* $E[F(z)]$ of any observable $F(z;\omega)$ defined on the crack front (depending upon the specific realization considered) is defined as

$$E[F(z)] \equiv \int_\Omega F(z;\omega)\,p(\omega)\,d\omega. \tag{C.1}$$

Its *two-point autocorrelation function* $E[F(z_1)F(z_2)]$ is similarly defined as

$$E[F(z_1)F(z_2)] \equiv \int_\Omega F(z_1;\omega)F(z_2;\omega)\,p(\omega)\,d\omega. \tag{C.2}$$

Similar formulae hold for functions defined in Fourier's space.

Let $E[\widetilde{F_1F_2}](k_1,k_2)$ denote the double Fourier transform of the function $E[F(z_1)F(z_2)]$. Then

$$\begin{aligned}
E[\widetilde{F_1F_2}](k_1,k_2) &\equiv \int_{-\infty}^{+\infty}\int_{-\infty}^{+\infty} E[F(z_1)F(z_2)]\,e^{ik_1z_1}\,e^{ik_2z_2}\,dz_1\,dz_2\\
&= \int_{-\infty}^{+\infty}\int_{-\infty}^{+\infty} e^{ik_1z_1}\,e^{ik_2z_2}\left(\int_\Omega F(z_1;\omega)F(z_2;\omega)p(\omega)\,d\omega\right)dz_1\,dz_2\\
&= \int_\Omega p(\omega)\left(\int_{-\infty}^{+\infty} F(z_1;\omega)\,e^{ik_1z_1}\,dz_1\right)\left(\int_{-\infty}^{+\infty} F(z_2;\omega)\,e^{ik_2z_2}\,dz_2\right)d\omega\\
&= \int_\Omega \widehat{F}(k_1;\omega)\widehat{F}(k_2;\omega)\,p(\omega)\,d\omega\\
&= E[\widehat{F}(k_1)\widehat{F}(k_2)].
\end{aligned}$$

This establishes Eq. $(27)_1$ of the text.

Moreover, if the observable is statistically invariant in the direction of the crack front, in which case its two-point autocorrelation function is of the form (26), one also gets

$$\begin{aligned}
E[\widetilde{F_1F_2}](k_1,k_2) &= \int_{-\infty}^{+\infty} \mathscr{F}(z_2-z_1)e^{ik_1z_1}\,e^{ik_2z_2}\,dz_1\,dz_2\\
&= \int_{-\infty}^{+\infty} \mathscr{F}(z_2-z_1)\,e^{i(k_1+k_2)z_1}\,e^{ik_2(z_2-z_1)}\,dz_1\,dz_2\\
&= \int_{-\infty}^{+\infty} 2\pi\delta(k_1+k_2)\mathscr{F}(z)\,e^{ik_2z}\,dz\\
&= 2\pi\delta(k_1+k_2)\,\widehat{\mathscr{F}}(k_2),
\end{aligned}$$

where δ denotes Dirac's function. This establishes Eq. $(27)_2$.

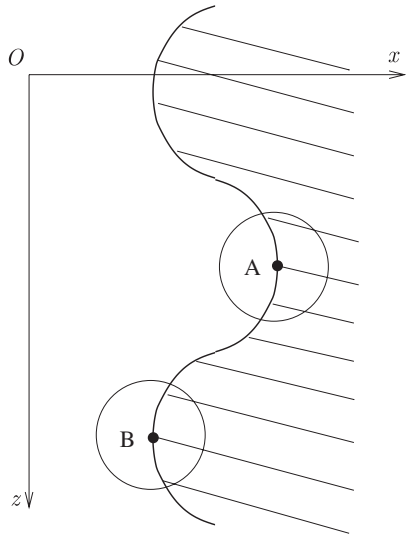

Fig. D.1. Planar interface crack with sinusoidal front.

Appendix D. Qualitative analysis of the evolution in time of a sinusoidal perturbation of the crack front of short wavelength

Fig. D.1 shows a picture of an interface crack with a sinusoidal front, as seen from above. The hatched region represents the still unbroken part of the interface. The crack advance is maximum at point A and minimum at point B.

Now draw small circles centered at points A and B. Because the sign of the curvature of the crack front is different at these two points, the relative proportion of the interior of the circle occupied by the unbroken interface is larger at point A than at point B. Thus relative motions of the crack faces are more hindered near point A than near point B. The implication is that the SIFs, and consequently the energy release rate, tend to be larger at point B than at point A. This phenomenon will be referred to as the "curvature effect".

The curvature effect is present whatever the value of the wavelength of the undulation. However, when this wavelength is large, the crack front is only weakly curved so that the curvature effect is small and bound to be overcome by other effects arising from the far geometry and loading. On the other hand, when the wavelength of the undulation is small, the crack front is strongly curved so that the curvature effect is important and must dominate over other ones. The implication is that for sinusoidal perturbations of the crack front of short wavelength, these points of the front where the crack advance is minimum will propagate more quickly than those where the crack advance is maximum. In other words, the amplitude of the perturbation will decrease in time; the smaller the wavelength, the larger the difference between the values of the energy release rate at points A and B, and therefore the faster the decay of the perturbation.

Appendix E. Calculation of the mean value of the function $F_\theta(\lambda)$

The purpose of this appendix is to establish Eq. (47) of the text, which provides the mean value $\overline{F}$ of the function $F_\theta(\lambda)$ defined by Eq. (46).

- If $\varepsilon = 0$, the function $F_\theta(\lambda)$ is constant and therefore identical to $\overline{F}$, and its value is

$$\int_0^{+\infty} \frac{(1+\mathrm{i}\theta)\mathrm{e}^{-(1+\mathrm{i}\theta)q}}{A+\mathrm{Re}(B)}\,\mathrm{d}q = \frac{1}{A+\mathrm{Re}(B)}.$$

This establishes Eq. $(47)_1$.

- If $\varepsilon \neq 0$, the function $F_\theta(\lambda)$ is periodic of period $\pi/|\varepsilon|$. Therefore,

$$\overline{F} \equiv \frac{\varepsilon}{\pi}\int_0^{\pi/\varepsilon}\left[\int_0^{+\infty}\frac{(1+\mathrm{i}\theta)\,\mathrm{e}^{-(1+\mathrm{i}\theta)q}}{A+\mathrm{Re}(Bq^{2\mathrm{i}\varepsilon}\mathrm{e}^{-2\mathrm{i}\varepsilon\lambda})}\mathrm{d}q\right]\mathrm{d}\lambda$$
$$= \frac{\varepsilon}{\pi}\int_0^{+\infty}(1+\mathrm{i}\theta)\,\mathrm{e}^{-(1+\mathrm{i}\theta)q}\left[\int_0^{\pi/\varepsilon}\frac{\mathrm{d}\lambda}{A+\mathrm{Re}(Bq^{2\mathrm{i}\varepsilon}\mathrm{e}^{-2\mathrm{i}\varepsilon\lambda})}\right]\mathrm{d}q.$$

Instead of integrating on λ from 0 to π/ε here, one may integrate from λ_0 to $\lambda_0+\pi/\varepsilon$ where λ_0 is an arbitrary number, and then use the change of variable $\mu \equiv \lambda - \lambda_0$. The integral on λ is then replaced by

$$\int_0^{\pi/\varepsilon}\frac{\mathrm{d}\mu}{A+\mathrm{Re}(Bq^{2\mathrm{i}\varepsilon}\mathrm{e}^{-2\mathrm{i}\varepsilon\lambda_0}\mathrm{e}^{-2\mathrm{i}\varepsilon\mu})}.$$

Choose λ_0 in such a way that $Bq^{2\mathrm{i}\varepsilon}\mathrm{e}^{-2\mathrm{i}\varepsilon\lambda_0} = |B|$. This integral then reduces to

$$\int_0^{\pi/\varepsilon}\frac{\mathrm{d}\mu}{A+|B|\cos(2\varepsilon\mu)},$$

the value of which is readily shown by standard methods to be $\frac{\pi}{\varepsilon\sqrt{A^2-|B|^2}}$. Inserting this value into the preceding expression of $\overline{F}$ and performing the integration on q, one gets Eq. $(47)_2$ of the text.

References

Amestoy, M., Leblond, J.B., 1992. Crack paths in plane situations—II: detailed form of the expansion of the stress intensity factors. Int. J. Solids Struct. 29, 465–501.

Antipov, Y.A., 1999. An exact solution to the 3D problem of an interface semi-infinite plane crack. J. Mech. Phys. Solids 47, 1051–1093.

Bercial-Velez, J.P., Antipov, Y.A., Movchan, A.B., 2005. High-order asymptotics and perturbation problems for 3D interfacial cracks. J. Mech. Phys. Solids 53, 1128–1162.

Bueckner, H.F., 1987. Weight functions and fundamental fields for the penny-shaped and the half-plane crack in three space. Int. J. Solids Struct. 23, 57–93.

Favier, E., Lazarus, V., Leblond, J.B., 2006. Statistics of the deformation of the front of a tunnel-crack propagating in some inhomogeneous medium. J. Mech. Phys. Solids 54, 1449–1478.

Gao, H., Rice, J.R., 1986. Shear stress intensity factors for a planar crack with slightly curved front. ASME J. Appl. Mech. 53, 774–778.

Gradshteyn, I.S., Ryzhik, I.M., 1980. Table of Integrals, Series, and Products. Academic Press, New York.

Hutchinson, J.W., Mear, M.E., Rice, J.R., 1987. Crack paralleling an interface between dissimilar materials. ASME J. Appl. Mech. 54, 828–832.

Katzav, E., Adda-Bedia, M., 2006. Roughness of tensile crack fronts in heterogenous materials. Europhys. Lett. 76, 450–456.

Lazarus, V., Leblond, J.B., 1998a. Three-dimensional crack-face weight functions for the semi-infinite interface crack—I: variation of the stress intensity factors due to some small perturbation of the crack front. J. Mech. Phys. Solids 46, 489–511.

Lazarus, V., Leblond, J.B., 1998b. Three-dimensional crack-face weight functions for the semi-infinite interface crack—II: integrodifferential equations on the weight functions and resolution. J. Mech. Phys. Solids 46, 513–536.

Leblond, J.B., Mouchrif, S.E., Perrin, G., 1996. The tensile tunnel-crack with a slightly wavy front. Int. J. Solids Struct. 33, 1995–2022.

Morrissey, J.W., Rice, J.R., 1998. Crack front waves. J. Mech. Phys. Solids 46, 467–487.

Morrissey, J.W., Rice, J.R., 2000. Perturbative simulations of crack front waves. J. Mech. Phys. Solids 48, 1229–1251.

Perrin, G., Rice, J.R., 1994. Disordering of a dynamic planar crack front in a model elastic medium of randomly variable toughness. J. Mech. Phys. Solids 42, 1047–1064.

Piccolroaz, A., Mishuris, G., Movchan, A.B., 2007. Evaluation of the Lazarus–Leblond constants in the asymptotic model of the interfacial wavy crack. J. Mech. Phys. Solids 55, 1575–1600.

Rice, J.R., 1985. First-order variation in elastic fields due to variation in location of a planar crack front. ASME J. Appl. Mech. 52, 571–579.

Rice, J.R., Ben-Zion, Y., Kim, K.S., 1994. Three-dimensional perturbation solution for a dynamic planar crack moving unsteadily in a model elastic solid. J. Mech. Phys. Solids 42, 813–843.

Schmittbuhl, J., Roux, S., Vilotte, J.P., Maloy, K.J., 1995. Interfacial crack pinning: effect of nonlocal interactions. Phys. Rev. Lett. 74, 1787–1790.

Willis, J.R., 1971. Interfacial stresses induced by arbitrary loading of dissimilar elastic half-spaces joined over a circular region. J. Inst. Math. Appl. 7, 179–197.

Willis, J.R., 1972. The penny-shaped crack on an interface. Q. J. Mech. Appl. Math. 25, 367–385.

Willis, J.R., Movchan, A.B., 1995. Dynamic weight functions for a moving crack. I. Mode I loading. J. Mech. Phys. Solids 43, 319–341.

Wolfries, S., Willis, J.R., 1999. Perturbation of a dynamic planar crack moving in a model elastic solid. J. Mech. Phys. Solids 47, 1633–1661.

A Letters Journal Exploring the Frontiers of Physics

January 2010

EPL, **89** (2010) 26002 www.epljournal.org
doi: 10.1209/0295-5075/89/26002

Shrinkage star-shaped cracks: Explaining the transition from 90 degrees to 120 degrees

G. Gauthier[1], V. Lazarus[2(a)] and L. Pauchard[3]

[1] *Univ Paris-Sud, UMR 7608, Lab FAST, Bat 502, Campus Univ - F-91405, Orsay, France, EU*
[2] *UPMC Univ Paris 6, UMR 7608, Lab FAST, Bat 502, Campus Univ - F-91405, Orsay, France, EU*
[3] *CNRS, UMR 7608, Lab FAST, Bat 502, Campus Univ - F-91405, Orsay, France, EU*

received 29 September 2009; accepted in final form 21 December 2009
published online 29 January 2010

PACS 62.20.M- – Structural failure of materials
PACS 91.60.Ba – Elasticity, fracture, and flow
PACS 83.80.Hj – Suspensions, dispersions, pastes, slurries, colloids

Abstract – Contraction due to drying or cooling of materials yields various self-organized crack patterns. The junctions between the cracks are complex and form in some conditions, star-shaped cracks with mostly 90 degrees or 120 degrees intersection angles. Any physical explanation of the selection of the angle is lacking. Here, we report directional drying of colloids experiments in capillary tubes allowing to obtain a reversible transition between 90 degrees and 120 degrees. We show that the transition is governed by a linear elastic fracture mechanics energy minimization principle hence by only one dimensionless parameter: the ratio between the Griffith length (balance between the energy needed to create cracks and to deform the material elastically) and the cell size. We give a straightforward characterization technique to estimate Griffith's length by changing the cell geometry. As a bonus, we deduce from it the toughness of drying colloidal suspensions. We underline that the method may be applied to a broad area of materials, from suspensions (colloids, paints or mud) to engineering (ceramics, coatings) and geological materials (basalt, sediments).

Introduction. – Giant's Causeway [1,2], Port Arthur tessellated pavement [3], Bimini Road [4], Mars polygons [5,6], septarias [7,8], fracture networks in muds, permafrost [9], paintings [10], gels [11], concrete [12], coatings are some more or less known examples of self-organized crack patterns that have intrigued people throughout history. These patterns are formed by constrained shrinking of the medium due, for instance, to cooling or drying leading to fracture. The crack networks form mostly 90° or 120° angles. Intersections at 90° angles form ⊤ or + shaped connections. ⊤ intersections are present in fracture networks formed in thin films due to sequential formation of the cracks [13]. The horizontal bar of the ⊤ is formed first and the vertical one later. On the other hand, + shaped connections are necessarily mostly formed simultaneously, since a crack cannot cross the free surface formed by another. They can be observed on Bimini Road formed by contraction of sedimentary rocks [4] or Port Arthur tessellated pavement (Eaglehawk Neck, Tasmania) (fig. 1(a)) whose formation is poorly understood but may be due to evaporation or cooling shrinkage of sedimentary rocks [3]. Intersections at 120° can be observed during the cooling of basalt [2]. They are formed simultaneously and appear as Y star-shaped connections. The Giant's Causeway, forming at some places a regular hexagonal tessellation (fig. 1(b)), is an example of such connections.

Intersections formed simultaneously, that is Y or + intersections, can be reproduced experimentally in different kinds of experiments. In experiments on drying of corn starch [14–16] or on cooling of ice [17], the fracture network is complex and forms a polygonal pattern with mainly Y intersections. + intersections have been observed in directional-drying experiments of colloidal suspensions in capillary tubes [18]. But to date, no experiments exist that allow to control the transition from Y to + intersections. In the lack of such experiments, previous theoretical predictions focused mainly on quasi-hexagonal crack patterns, in particular on their scaling [19–21] or the maturation of their shape [22–25]. In general, the hexagonal crack pattern is believed to be the solution of the energy minimization principle as in foams [22,26].

(a) E-mail: veronique.lazarus@upmc.fr

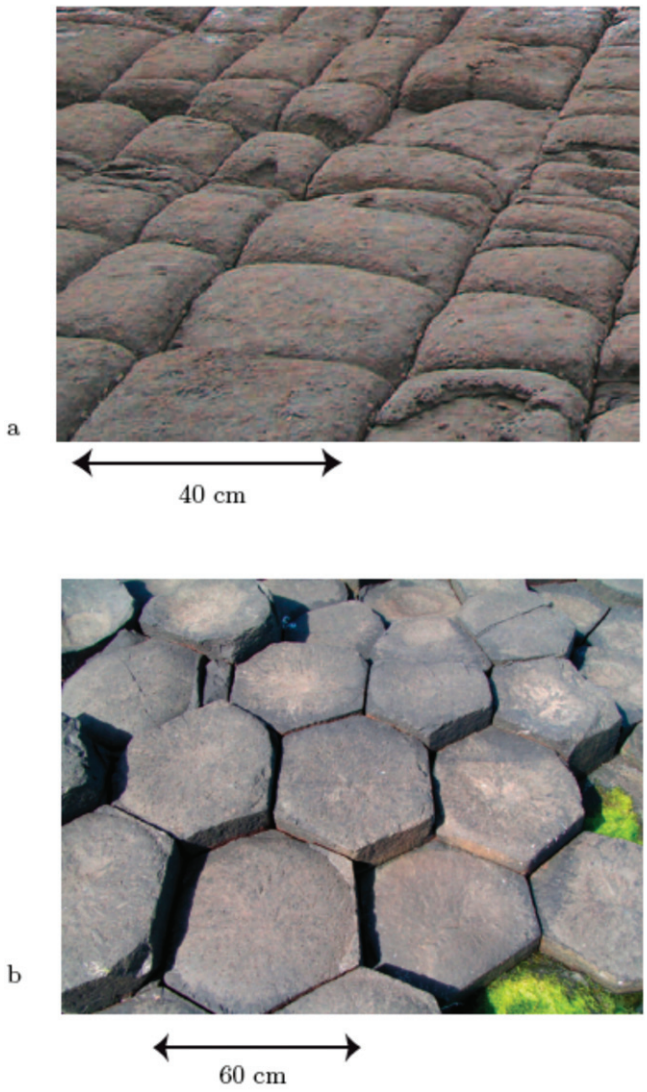

Fig. 1: (Colour on-line) Examples of polygonal patterns: (a) Port Arthur rectangular tessellated pavement, Tasmania (Courtesy of Wayne Bentley); (b) Giant's Causeway hexagonal tessellated pavement, Ireland (Courtesy of A. Davaille).

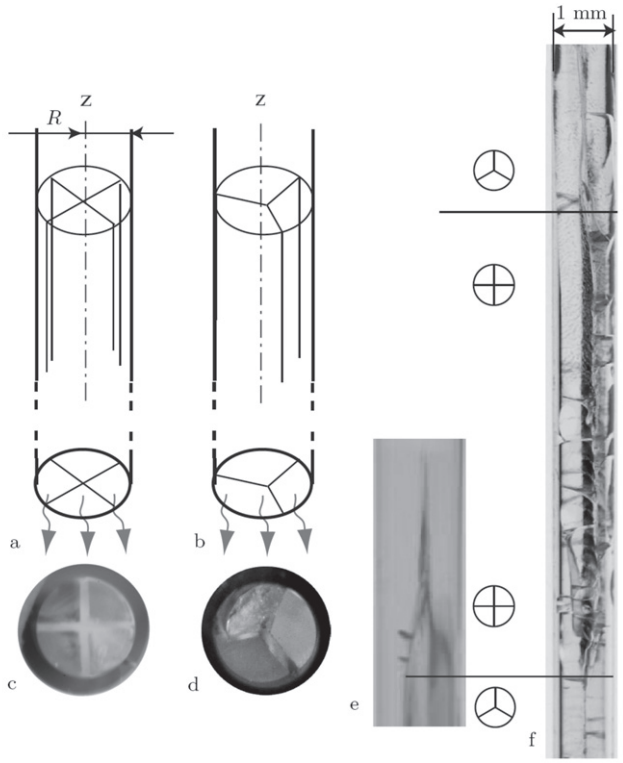

Fig. 2: The capillary tubes are filled with a colloidal suspension. The single bottom open edge allows for evaporation of the solvent. Cracks appear following the compaction front (front of the bottom-up growing gel). Their sectional shape depends on the controlled drying rate: (a,c) + intersection ($v \approx 64\,\mathrm{nm\,s^{-1}}$); (b,d) $\curlyvee$ intersection ($v \approx 31\,\mathrm{nm\,s^{-1}}$). (e,f) Pictures of the capillary tube at different times showing the reversible transition from $\curlyvee$ to + configuration: (e) the transition from $\curlyvee$ to + observed when the drying rate changes from $v \approx 31\,\mathrm{nm\,s^{-1}}$ to $v \approx 64\,\mathrm{nm\,s^{-1}}$; (f) followed by the transition + to $\curlyvee$ observed when the drying rate changes from $v \approx 64\,\mathrm{nm\,s^{-1}}$ to $v \approx 31\,\mathrm{nm\,s^{-1}}$ again (on this picture, the first secondary cracks have appeared explaining the finite observation scale).

In this letter, we report directional-drying experiments of colloidal suspensions in capillary tubes that allow to control the transition from $\curlyvee$ to + intersections. We show that the transition is governed by a Linear Elastic Fracture Mechanics (LEFM) energy minimization principle [27], hence by only one dimensionless parameter: the ratio between an internal length, the Griffith length, depending on the loading and the material, and an external length, the diameter of the tube. A straightforward method to estimate this parameter is given. This method is applied to the determination of the toughness of drying colloids (it seems that to date, only one such data exists [28]).

Experiments. – Directional-drying experiments are performed in circular capillary tubes [18], of length 12 cm and inner radius $R = 0.5\,\mathrm{mm}$, with an aqueous colloidal suspension (cf. fig. 2); namely Ludox® SM30 which is made of 30% in mass of silica spheroids particles of average diameter $2r = 7\,\mathrm{nm}$ (data given by the manufacturer Grace Davison). To ensure an unidirectional drying, the top extremity of each tube is closed. To balance the loss of water volume, tubes are only partially filled ($\approx 7\,\mathrm{cm}$ high) with suspension, so that the air trapped in the tube expands during the drying. After filling, the tubes dry in ambient condition for two hours, in order to form a 1 cm plug at the drying extremity, and then put in an airtight chamber. The drying rate is controlled either by the relative humidity RH or by the temperature T of the airtight chamber: changing T modifies the water viscosity and, according to Darcy's law, changes the water velocity through the porous medium formed by the gel. Experiments are performed at either 20 °C or 3 °C; the humidity rate is fixed either smaller than 10% using

desiccant or larger than 90% introducing water in the chamber.

Above the plug, vertical cracks appear that propagate following the compaction front (front of the bottom-up growing gel). These cracks are organized and clearly observable during a distance of propagation smaller than 3 cm. After this distance, the propagation becomes disordered and secondary cracks appear (fig. 2(f)). Experiments performed at $T = 20\,^{\circ}\mathrm{C}$ and $RH < 10\%$ give rise to 4 crack surfaces (fig. 2(a)), while drying at $T = 20\,^{\circ}\mathrm{C}$ and $RH > 90\%$ or at $T = 3\,^{\circ}\mathrm{C}$ and $RH < 10\%$ gives 3 crack surfaces. Changing the drying conditions changes the average velocity v of the crack tips. The velocities of the cracks tips are measured using a digital camera and are almost constant during the observation scale of the cracks (< 3 cm). Drying at $T = 20\,^{\circ}\mathrm{C}$ and $RH < 10\%$ corresponds to $v = 64 \pm 10\,\mathrm{nm\,s^{-1}}$, while drying at $T = 20\,^{\circ}\mathrm{C}$ and $RH > 90\%$ or at $T = 3\,^{\circ}\mathrm{C}$ and $RH < 10\%$ gives $v = 31 \pm 5\,\mathrm{nm\,s^{-1}}$. Errors on the velocity correspond to the scattering during one experiment and to the reproducibility on typically 10 experiments. Due to symmetry, the four cracks form a + connection. To check this point, the capillary tubes have been cut, at the crack tips, along a plane perpendicular to the tube axis (see fig. 2(c)). Similar cuts of tubes (fig. 2(d)) for slow-drying conditions ($v \approx 31\,\mathrm{nm\,s^{-1}}$) reveal a $\curlyvee$ shaped connection (fig. 2(b)). Changing the drying rate from $v \approx 31\,\mathrm{nm\,s^{-1}}$ to $v \approx 64\,\mathrm{nm\,s^{-1}}$ results in a reversible transition from + to $\curlyvee$ shape connections (fig. 2(e),(f)).

Fracture mechanics model. – From a mechanical point of view, the stationary behavior of the crack pattern in the crack tips reference frame allows to approximate the problem by using 2D plane strain linear elastic fracture mechanics. The medium is assumed to evolve quasistatically and to be subjected to a uniform isotropic tensile prestress σ_0 so that the Cauchy stress tensor $\boldsymbol{\sigma}$ is linked to the strain tensor $\boldsymbol{\varepsilon}$ by

$$\boldsymbol{\sigma} = \frac{E\nu}{(1+\nu)(1-2\nu)}\mathrm{tr}\boldsymbol{\varepsilon}\,\mathbf{1} + \frac{E}{(1+\nu)}\boldsymbol{\varepsilon} + \sigma_0\mathbf{1}, \qquad (1)$$

where E denotes the Young modulus and ν the Poisson ratio. The prestress σ_0 arises from the contraction of the medium due to capillary pore pressure in poro-elastic media during the drying process [29,30] and from thermal contraction during the cooling process [31]. Furthermore, our model assumes purely radial cracks, a perfect adhesion of the gel on the walls and traction-free boundary conditions on the cracks.

Then the local strain energy density $U(n)$ depends on the number n of radial cracks and is given as a function of the strain components ε_{ij} by (Einstein's implicit summation convention is employed for the indexes $i, j = 1, 2, 3$, see [31])

$$U(n) = \frac{E\nu}{2(1+\nu)(1-2\nu)}\varepsilon_{ii}^2 + \frac{E}{2(1+\nu)}\varepsilon_{ij}\varepsilon_{ij} + \sigma_0\varepsilon_{ii}. \qquad (2)$$

The total energy $\mathcal{E}(n)$, corresponding to the sum of the local strain energy and the crack energy, per unit height is

$$\mathcal{E}(n) = \int_S U(n)\,\mathrm{d}S + nG_cR\,. \qquad (3)$$

It depends on n, R, E, σ_0 and on G_c, which is the energy needed to create one unit area of crack [32]. Let us introduce the Griffith length L_c defined as

$$L_c = \frac{G_cE}{\sigma_0^2}. \qquad (4)$$

The dimensionless form [21] of $\mathcal{E}(n)$ reads

$$\frac{\mathcal{E}(n)E}{\sigma_0^2R^2} = \int_{\bar{S}} \bar{U}(n)\mathrm{d}\bar{S} + n\frac{L_c}{R}, \qquad (5)$$

where $\bar{S}$ is a the cross-sectional surface with $R = 1$ and $\bar{U}(n)$ is the local strain energy density in the presence of n radial cracks for a constraint elastic medium of unitary prestress $\sigma_0 = 1$, unitary Young's modulus $E = 1$ and radius $R = 1$.

Now we search among the radial crack configurations, the one that minimizes the total energy $\mathcal{E}(n)$ (some theoretical considerations about the principle can be found in [27,33]). Since the dimensionless form $\frac{\mathcal{E}(n)E}{\sigma_0^2R^2}$ of $\mathcal{E}(n)$ depends only on n and L_c/R (5), this minimization yields n_c as a function of a single dimensionless parameter L_c/R. L_c gives the ratio between the energy needed to create cracks ($\propto G_c$) and to deform the material elastically ($\propto \sigma_0^2/E$). The larger the critical energy release rate G_c (*i.e.* large value of L_c), the fewer the cracks. Hence the minimization of $\mathcal{E}$ in terms of n yields the critical number n_c as a decreasing function of L_c/R. This minimization is done numerically. For each given value of n, the mechanical stress and displacement fields, and then the strain energy density $\int_{\bar{S}} \bar{U}(n)\mathrm{d}\bar{S}$ corresponding to $E = 1$, $R = 1$ and $\sigma_0 = 1$ are calculated by finite elements using CAST3M. Minimization of (5) in terms of n yields n_c as a function of $\frac{L_c}{R}$. This function is plotted in fig. 3 for the typical value $\nu = 0.3$. It is a stairlike curve since the number of cracks can only be an integer.

Comparison with the experiments. – To compare numerical predictions with experiments, one needs to estimate Griffith's length L_c. For this, we use directional-drying experiments in flat (aspect ratio of $w/e = 20$, w being the width of the cell) Hele-Shaw cells [30,34], in the same drying conditions as above (cf. inset of fig. 4). The cells are 2 cm long for the 50, 100 and 200 μm thick, and 4 cm long for the ones of thickness 300 and 400 μm. The cells are half-filled with the suspension. During drying, a parallel array of cracks appears, with a crack spacing l which depends on the cell thickness e and the drying conditions. Applying again the minimization principle on these crack patterns, we obtain by 2D finite-elements computations, $l = a\sqrt{L_ce}$ with $a = 3.1$ for $\nu = 0.3$. The linear fit of l as a function of e gives the value of L_c

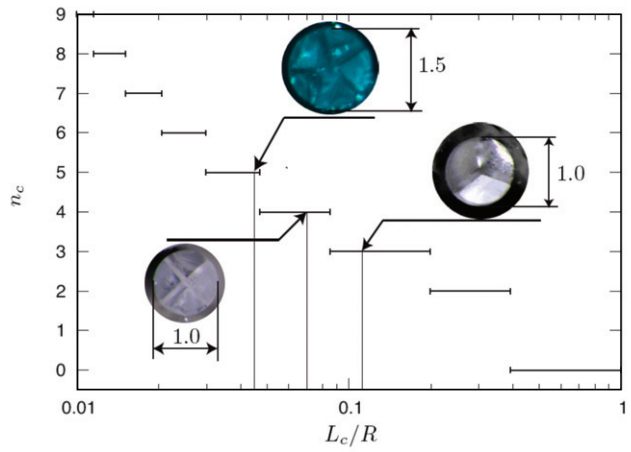

Fig. 3: (Colour on-line) Number of radial cracks in a capillary tube n_c as a function of Griffith's length L_c normalized with the radius of the capillary tube R ($n=1$ is not present for symmetry reasons) for $\nu=0.3$. The values are obtained by finite-element simulations: for each value L_c/R, the pattern with n_c radial cracks corresponds to the minimum of the total energy, which is the sum of the strain energy and the crack energy. Adhesion of the gel on the wall is supposed. The L_c/R and cross-section view of the experiments realized with Ludox®SM30 are shown.

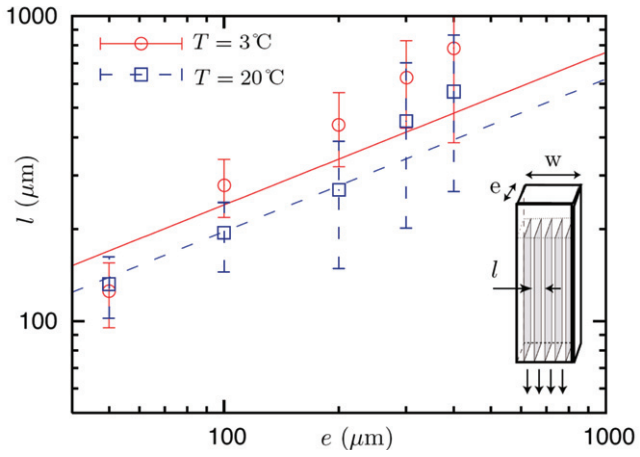

Fig. 4: (Colour on-line) Distance between cracks as a function of the thickness of the Hele-Shaw cell for drying of Ludox®SM30 at $T=3\,^\circ$C (○) and at $T=20\,^\circ$C (□). Griffith's length L_c is obtained by interpolation (lines) with the solution of the minimum-energy principle, that is $l=a\sqrt{L_c e}$, $a=3.1$ (obtained by FE for $\nu=0.3$). The linear fit is done systematically, in a least-square sense weighted by the error bars. The large scattering in the data points is due to the high variations in the crack spacing and the error bars correspond to the variability of l over more than 10 experiments.

for each suspension and drying condition: $L_c=60\pm18\,\mu$m for $v\approx31\,\mathrm{nm\,s^{-1}}$ and $L_c=34\pm10\,\mu$m for $v\approx64\,\mathrm{nm\,s^{-1}}$. Now reporting the corresponding values of L_c/R (0.12 and 0.068, respectively) on fig. 3 allows for the determination of n_c (3 and 4, respectively.) for the tube experiments. The predicted values are in good agreement with the experiments.

Moreover, the model predicts, for a fixed length L_c, that an increase of the radius R from 0.5 mm to 0.75 mm is expected to give rise to 5 radial cracks in the case $v\approx64\,\mathrm{nm\,s^{-1}}$: this transition is indeed observed ($L_c/R=0.045$ in fig. 3). The model also works for experiments on Ludox® HS 40 ($2r\approx12\,$nm). The values of L_c are then $L_c\simeq40\ \mu$m when drying rapidly and $L_c\simeq45\,\mu$m in cases of slow drying, and yield by minimization $n_c=4$ ($L_c/R=0.08$–0.09 in fig. 3) for both drying rates, that is a + shape intersection for $R\simeq0.5\,$mm, in agreement with the experiments. All these results allow to conclude that the transition between ϒ and + (and also 5 cracks) intersections is governed by energy minimization hence by the ratio of Griffith's length to the size of the cell.

Discussion. – Our study demonstrates that L_c depends on the drying rate. Several explanations can be proposed. The first explanation is that the stress σ_0 in the area of the crack tips is dependent on v because of diffusion effects [20]. The second explanation is that the porous medium formed by agglomeration of particles on the drying front has a different structure [35] as a function of v that induces a change of the values of E and G_c. The precise determination of the dependence of σ_0, E and G_c on the drying rate raises fundamental difficulties that are behind the scope of this article. We emphasize that by estimating directly L_c, we overcome these difficulties.

To simply derive L_c from Hele-Shaw experiments, the dependence of σ_0, that is L_c on the cell geometry, in particular on e, linked to 3D diffusion effects [25,36], has been neglected. The thicker the cells, the more important these effects are (fig. 4). Since [34], $l\propto e^{2/3}$, L_c varies as $e^{-1/3}$ which explains that the the slopes appear to be off in particular for larger values of e. But it can been disregarded here, e ranging from $50\,\mu$m to $400\,\mu$m, especially in the absence of more rigorous methods. For instance, the method consisting in translating measure of G_c and E from film measurements into directional drying is questionable, particularly since G_c and E are position and time dependent. Measuring L_c in the same kind of experiments overcomes these difficulties and allows to show that the transition between + and ϒ intersections is governed by the ratio of Griffith's length to the size of the cell.

The model can be used to estimate Griffith's length L_c. Since L_c depends on three parameters G_c, E and σ_0 (or two if one considers the mode I toughness defined by $K_{Ic}^2=\frac{E}{1-\nu^2}G_c$), this gives a method to obtain one parameter when the others are still known. For instance considering Ludox®SM30, assuming $\sigma_0=-2\gamma/r\simeq40\,$MPa, where $\gamma\simeq0.07\,$N/m is the air-water surface tension [30] and $2r=7\,$nm the particles diameter, the value of K_{Ic} can be derived from the measure of L_c: $K_{Ic}=\sigma_0\sqrt{L_c}\simeq0.2$–$0.3\,\mathrm{MPa\,m^{1/2}}$. This value seems reasonable compared to fused silica [37] for which $K_{Ic}\simeq1\,\mathrm{MPa\,m^{1/2}}$. It shall

however be noticed that it is significantly higher than the one often used in the literature for such material ($K_{Ic} \simeq 10^2\,\mathrm{Pa\,m^{1/2}}$ [28]). The discrepancy may be explained by the fact that the toughness seems to correspond to the fracture of solid/liquid interfaces in their experiments, and to the fracture of solid/solid ones in ours. Further discussion of this point is devoted to another article.

Conclusion. – We have observed a reversible transition ϒ and + during directional-drying experiments in capillary tubes. We show that the selection between ϒ and + intersections is controlled by the ratio of Griffith's length L_c to the diameter of the cell. It corresponds to a local minimum of the total energy, *i.e.* the sum of the elastic and crack energies. This is an experimental demonstration that the crack pattern satisfies the often used [21,22] principle of energy minimization. Directional-drying experiments in capillary tubes can be used to estimate Griffith's length L_c. Since L_c depends on three parameters G_c, E and σ_0 (or two if one considers the toughness defined by $K_{Ic}^2 = \frac{E}{1-\nu^2} G_c$), this gives a method to obtain one parameter when the others are still known. We applied it to estimate the toughness of consolidated Ludox®SM30. Extension from bounded to unbounded conditions is not straightforward and is the subject of further developments to infer new information on tessellated pavements formation on Earth or on other planets, as Mars where polygons are widely studied.

* * *

The authors thanks PPF *Processus physique en sciences de la terre* for funding, W. Bentley for the nice Port Arthur pictures, H. Auraldou, P. Gondret, N. Mangold, C. Maurini, E. Mittelstaedt, J. Levy and D. Salin for pertinent comments. The authors greatly appreciated A. Davaille comments and discussions on the geological patterns. The paper largely benefited from comments of referees.

REFERENCES

[1] O'Reilly J., *Trans. R. Ir. Acad.*, **26** (1878) 641.
[2] DeGraff J. M. and Aydin A., *Geol. Soc. Am.*, **99** (1987) 600.
[3] Branagan D. F. and Cairns H. C., *J. Proc. R. Soc. N. S. W.*, **126** (1993) 63.
[4] Shinn E. A., *Spec. Publ. Int. Assoc. Sedimentol.*, **41** (2009) 19.
[5] Mangold N., *Icarus*, **174** (2005) 336.
[6] Levy J., Head J. and Marchant D., *J. Geophys. Res.*, **114** (2009) E01007.
[7] Sellès-Martinez J., *Earth-Sci. Rev.*, **41** (1996) 177.
[8] Seilacher A., *Sediment. Geol.*, **143** (2001) 41.
[9] Plug L. J. and Werner B. T., *J. Geophys. Res.-Solid Earth*, **106** (2001) 8599.
[10] Pauchard L., Lazarus V., Abou B., Sekimoto K., Aitken G. and Lahanier C., *Reflets*, **3** (2007) 5.
[11] Atkinson A. and Guppy R. M., *J. Mater. Sci.*, **26** (1991) 3869.
[12] Colina H. and Roux S., *Eur. Phys. J. E*, **1** (2000) 189.
[13] Bohn S., Pauchard L. and Couder Y., *Phys. Rev. E*, **71** (2005) 046214.
[14] Muller G., *J. Geophys. Res.*, **103** (1998) 15239.
[15] Toramaru A. and Matsumoto T., *J. Geophys. Res.*, **109** (2004) B02205.
[16] Goehring L. and Morris S. W., *Europhys. Lett.*, **69** (2005) 739.
[17] Menger F. M., Zhang H., Caran K. L., Seredyuk V. A. and Apkarian R. P., *J. Am. Chem. Soc.*, **124** (2002) 1140.
[18] Gauthier G., Lazarus V. and Pauchard L., *Langmuir*, **23** (2007) 4715.
[19] Goehring L. and Morris S. W., *J. Geophys. Res.-Solid Earth*, **113** (2008) B10203.
[20] Goehring L., Mahadevan L. and Morris S. W., *Proc. Natl. Acad. Sci. U.S.A*, **106** (2009) 387.
[21] Jenkins D., *Int. J. Solids Struct.*, **46** (2009) 1078.
[22] Jagla E. A. and Rojo A. G., *Phys. Rev. E*, **65** (2002) 026203.
[23] Saliba R. and Jagla E. A., *J. Geophys. Res.-Solid Earth*, **108** (2003) 2476.
[24] Jagla E. A., *Phys. Rev. E*, **69** (2004) 056212.
[25] Bahr H.-A., Hofmann M., Weiss H.-J., Bahr U., Fischer G. and Balke H., *Phys. Rev. E*, **79** (2009) 056103.
[26] Weaire D. and Hutzler S., *The Physics of Foams* (Oxford University Press) 2000.
[27] Francfort G. A. and Marigo J. J., *J. Mech. Phys. Solids*, **46** (1998) 1319.
[28] Zarzycki J., *J. Non-Cryst. Solids*, **100** (1988) 359.
[29] Wang H. F., *Theory of Linear Poroelasticity with Applications to Geomechanics and Hydrogeology* (Princeton University Press, Princeton and Oxford) 2000.
[30] Dufresne E. R., Corwin E. I., Greenblatt N. A., Ashmore J., Wang D. Y., Dinsmore A. D., Cheng J. X., Xie X. S., Hutchinson J. W. and Weitz D. A., *Phys. Rev. Lett.*, **91** (2003) 224501.
[31] Timoshenko S. and Goodier J. N., *Theory of Elasticity* (McGraw-Hill, New-York) 1969.
[32] Griffith A. A., *Philos. Trans. R. Soc. London*, **221** (1920) 163.
[33] Bourdin B., Francfort G. and Marigo J.-J., *J. Elast.*, **91** (2008) 5.
[34] Allain C. and Limat L., *Phys. Rev. Lett.*, **74** (1995) 2981.
[35] Dong K., Yang R., Zou R. and Yu A., *Phys. Rev. Lett.*, **96** (2006) 145505.
[36] Hofmann M., Bahr H. A., Linse T., Bahr U., Balke H. and Weiss H. F., *Int. J. Fract.*, **141** (2006) 345.
[37] Michel M., Serbena F. and Lepienski C., *J. Non-Cryst. Solids*, **352** (2006) 3550.

Basalt Columns and Crack Formation during Directional Drying of Colloidal Suspensions in Capillary Tubes

V. Lazarus[1],G. Gauthier[1], L. Pauchard[1], C. Maurini[1], C. Valdivia[1,2]

[1]*UPMC Univ Paris 6, Univ Paris-Sud, CNRS, UMR 7608, Lab FAST, Bat 502, Campus Univ, F-91405, Orsay, France;*
[2] *UPMC Univ Paris 6, CNRS, UMR 7190, Institut Jean Le Rond d'Alembert, Boite courrier 161-2, 4 Place Jussieu, F-75005, Paris, France;*

Abstract: Formation of basalt columns during cooling of lava may be modeled by the drying of colloidal silica suspension confined in capillary cells (Allain and Limat 1995, Gauthier et al. 2007). During the drying process, particles aggregate at the open edge forming a growing drained gelled porous medium. High negative capillary pressure in the draining fluid (Dufresne et al., 2003) and adhesion to the walls of the cells generates high tensile stresses in the gel leading to crack formation. Depending on the experimental conditions and the shape of the cell (rectangular or circular), several crack morphologies appear. Here the aim is to compare the experimental morphologies with the ones predicted by fracture mechanics. For this purpose, the drained gelled porous medium is modeled by a linear elastic medium subjected to tensile prestresses and the cracks by the variational approach to fracture of Bourdin, Francfort and Marigo (1998, 2000, 2008).

1 Introduction

The basalt columns are formed during the directional cooling of a lava flow. Cooling can be simulated advantageously by experiments of drying, cooling like drying inducing similar fields of prestresses. Nevertheless the pilot experiments used until now, on nontransparent materials (cornstarch in particular, cf Goehring, Morris *al.* [11]) do not make it possible to observe the dynamics of formation of the fractures. On the other hand, experiments of directional drying carried out on transparent colloidal suspensions in circular capillary tubes (Gauthier *et al* [10]) allowed to reproduce and observe some of the still badly explained aspects of the columns: facies presenting a smooth and rough alternation, dynamics of propagation by jumps [13]. In this paper, we will consider such directional drying experiments and study the influence of the capillary tube cross section shape on the crack morphologies. The experimental morphologies obtained in circular, square and rectangular tubes will be retrieved by two dimensional non local

damage model simulations. In the present paper, we will concentrate on a qualitative comparison. A more quantitative study is underway but remains still to be completed.

Experiments of directional drying of colloidal suspension in flat rectangular capillary tubes have been performed first by Allain and Limat [1] and then by Dufresne *et al.* [7, 8]. For thin cells, they observed an array of parallel cracks perpendicular to the flat direction of the cell. In circular tubes, Gauthier *et al* [10] observed the formation of two perpendicular cracks containing the axis of the cylinder. In both cases, the cracks grows along the drying direction. In this paper, some new experiments on thick rectangular cells and on square ones will be presented. In the thick ones, some cracks parallel to the flat direction appear in addition to the array of parallel cracks; in the square ones, we observe two cracks cutting the cross-section along the diagonals.

For the numerical analysis, we will use the energetic approach to brittle fracture of Francfort and Marigo [9], which is able to approach the phenomena of initiation, multicracking and complex crack paths. In order to use the traditional finite elements, our work will be based on a regularized version of the energetic formulation, which may be mechanically interpreted as a non-local gradient damage model [5]. Two dimensional simulations on the cross section of the tubes allow us to retrieve qualitatively the experimental observed morphologies.

2 Experiments

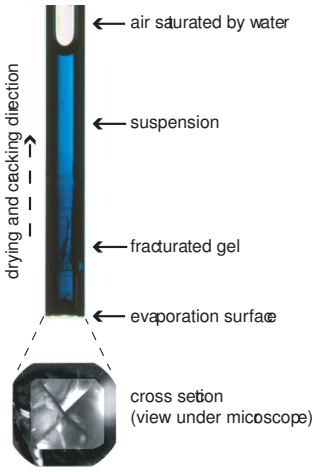

Figure 1: Experimental setup

Experiments are carried out, at room temperature, using aqueous suspensions of mono disperse silica spherical particles (Ludox HS 40) of radius $r = 15 \pm 2$ nm and volume fraction $\phi \simeq 0.2$. To investigate unidirectional drying, vertical glass capillary tubes are used; the top of the tube is closed and the bottom one is placed in a surrounding maintained at a constant humidity rate using a desiccant. The tube is only partially filled with the suspension so that the air and solvent vapor, located above the suspension can expand to compensate the loss of solvent during desiccation. As the sample loses solvent, particles aggregate at the open edge forming a growing drained gelled porous medium (fig. 1). High negative capillary pressure in the draining fluid generates high tensile stresses in the gel. This causes crack formation [7] following the drying direction. Depending on the tube morphology, several crack morphologies appear (see fig. 2):

- for circular cells (diameter ~ 1 mm), two vertical perpendicular cracks;
- for square cells (diagonal ~ 1 mm), two vertical perpendicular cracks along

the diagonals of the square (see also picture of figure 1);

- for flat rectangular cells (thickness < 100 μm, aspect ratio > 20), an array of parallel cracks perpendicular to the largest walls;
- for more thick rectangular cells (thickness > 200 μm, aspect ratio > 20), two sets of perpendicular cracks: as before, an array of parallel cracks and some crack parallel to the large walls. For technical reasons, it is difficult for the moment, to determine if this last crack corresponds to delamination between the porous medium and the wall or to a crack that is located inside the porous medium. Several clues indicates that the crack is located inside: if delamination occurs at both sides, the medium under tensile stresses becomes unloaded and cracks shall no more propagate, but this is not the case; the dynamics of crack propagation is the same as in circular or square tubes where the cracks are inside the medium; the numerical calculations predicts the presence of a crack at mid wall (see below).

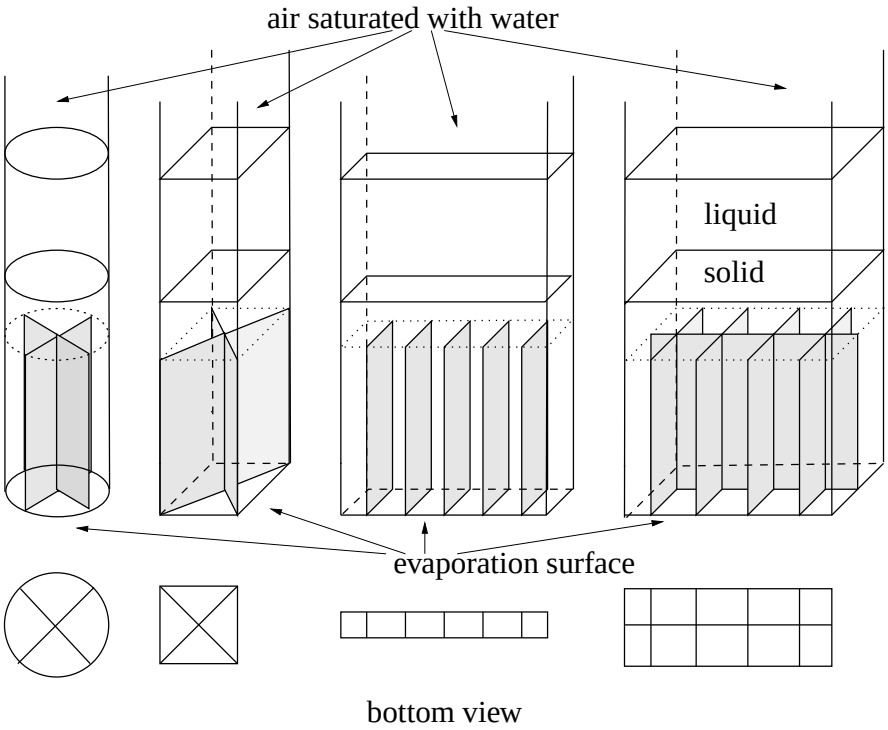

Figure 2: Different cells and cracks (in greyscale) morphologies

The dynamics of crack propagation undergoes an intriguing jerky crack motion described in [8, 10]. But the analysis of this interesting motion is not the aim of this paper. In the sequel, we will focus on the two dimensional problem of the crack morphologies in a cross section; hence we will try to retrieve the crack patterns depicted on the bottom view of figure 2.

3 A simplified model of drying during directional drying

3.1 A simplified mechanical model of drying

For the present qualitative study, the two dimensional horizontal cross section S problem is considered (bottom of figure 2). We suppose the material elastic and isotropic. We replace the loading due to high negative pressure that appears at the liquid meniscus formed by the particles at the bottom air/water evaporation interface [7] by a given tensile isotropic prestress $\sigma_0 > 0$ or an equivalent mismatch strain $\epsilon_0 > 0$, so that:

$$\boldsymbol{\sigma} = \lambda \mathrm{tr}\boldsymbol{\epsilon}\, \mathbf{1} + 2\mu\boldsymbol{\epsilon} + \sigma_0 \mathbf{1} \Leftrightarrow \boldsymbol{\epsilon} = \frac{1+\nu}{E}\boldsymbol{\sigma} - \frac{1}{E}\mathrm{tr}\boldsymbol{\sigma}\, \mathbf{1} - \epsilon_0 \mathbf{1} \tag{1}$$

where λ and μ are the material Lamé coefficients, E is the Young modulus and ν is the Poisson coefficient. The gel adheres to the wall, so that the displacement is zero at the boundary of the section: $\boldsymbol{u} = 0$.

3.2 Variational approach to fracture

Following the energetic approach of Francfort and Marigo [9], the fracture problem consists in finding the displacement field $\boldsymbol{u}$ satisfying the boundary conditions and the crack pattern Γ that minimizes the total energy $\mathcal{E}_t$ defined as the sum of the potential energy of the system, say $\mathcal{E}_p$, and the surface energy associated to the crack, say $\mathcal{E}_s$:

$$\mathcal{E}_t(\boldsymbol{u}, \Gamma) = \mathcal{E}_p(\boldsymbol{u}, \Gamma) + \mathcal{E}_s(\Gamma) \tag{2}$$

where:

$$\mathcal{E}_p(\boldsymbol{u}, \Gamma) = \int_{S/\Gamma} \left[\frac{\lambda}{2} (\mathrm{tr}\boldsymbol{\epsilon}(\boldsymbol{u}))^2 + \mu\, \boldsymbol{\epsilon}(\boldsymbol{u}) : \boldsymbol{\epsilon}(\boldsymbol{u}) + \sigma_0\, \mathrm{tr}\boldsymbol{\epsilon}(\boldsymbol{u}) \right] \mathrm{d}S \tag{3}$$

$$\mathcal{E}_s(\Gamma) = G_c\, \mathrm{length}(\Gamma), \tag{4}$$

G_c denoting the energy required to create a unit length crack.

The functional (2) should be minimized among all admissible displacement fields and crack surfaces. The associated minimization problem is referred to [2] as a *free discontinuity problem*. To solve it numerically by using standard finite elements we used a regularization technique originally developed for analog problems in image segmentation [12] and adapted to fracture mechanics by Bourdin et al. [4]. The energy functional (2) is approximated by the following family of elliptic functional depending on a regularized displacement field $\boldsymbol{u}$ and an addi-

tional scalar field $\alpha \in [0,1]$:

$$\mathcal{E}_t^\ell(\boldsymbol{u},\alpha) = \int_S \left[(1-\alpha)^2 \frac{\lambda}{2}(\mathrm{tr}\boldsymbol{\epsilon}(\boldsymbol{u}))^2 + \mu\,\boldsymbol{\epsilon}(\boldsymbol{u}) : \boldsymbol{\epsilon}(\boldsymbol{u}) + \sigma_0 \mathrm{tr}\boldsymbol{\epsilon}(\boldsymbol{u})\right] \mathrm{d}S + \\ + G_c \int_S \left[\frac{\alpha^2}{4\ell} + \ell\,\nabla\alpha\cdot\nabla\alpha\right] \mathrm{d}S \tag{5}$$

For $\ell \to 0$, the minimizers of (5) are characterized by bands with α close to 1 and high displacement gradients. Those bands, whose thickness is of the order of ℓ, are a regularized approximation of the cracks lines. Mathematically, it is possible to show (see [6]) that the global minimizers of (5) tends to the global minimizers of (2) when $\ell \to 0$. From the mechanical point of view, the functional (2) may be interpreted as the energy functional of a non-local gradient damage model, where α stays for the damage field and ℓ for the internal length.
For a given value of the loading parameter σ_0, we solved the regularized minimization problem for (5) by using standard linear triangular finite elements and the alternate minimization strategy detailed in [3]. The prestress σ_0 is assumed to be constant; the damage field α is set equal to zero at the boundary to simulate perfect bonding.

4 Qualitative comparison between experiments and numerical simulations

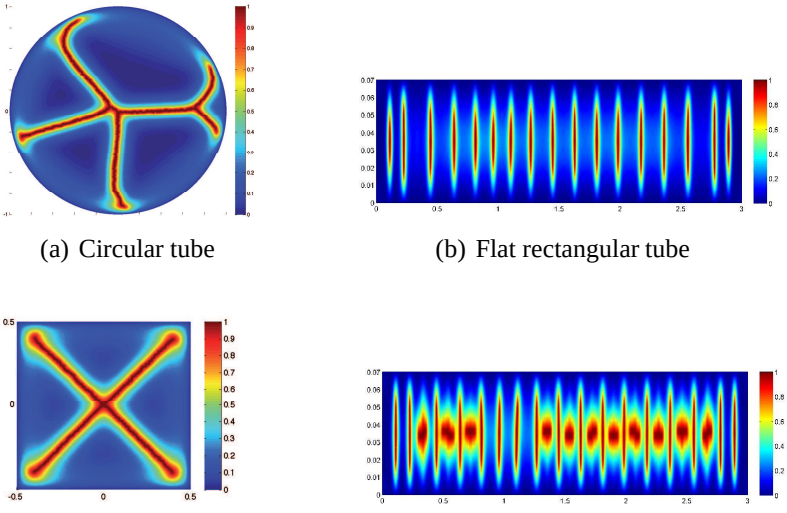

(a) Circular tube (b) Flat rectangular tube

(c) Squared tube (d) More thick rectangular tube

Figure 3: Non local damage model with gradient. Elastic medium with tensile prestresses.

Figure 3 reports the results of the numerical simulations for the cross sectional shapes of figure 2. All the patterns observed experimentally (bottom of figure 2) can be retrieved by the numerical model. In the case of thick rectangular cells, a crack at mid distance of the largest walls appears in the simulations. This leads to interpret the secondary cracks that appears in the experiments as a crack inside the medium and not a delamination crack. But this point merits further investigations.
By the moment, we are able to report only qualitative agreement between the numerical and experimental results. The challenge now is to perform more quantitative comparisons. This suppose a large amount of theoretical, experimental and numerical work. Experimentally, the control parameter of the experiments have to be varied (temperature, hygrometry, particle nature and size...) and the material has to be characterized mechanically. Numerically, the influence of the small parameter ℓ, which may be interpreted as an internal length, has to be analyzed in details. This will demand also a further theoretical groundwork for the analysis of the behavior of the underlying non-local damage model. This study is the subject of ongoing works.

5 Conclusion

By using the regularized formulation of the variational approach to fracture mechanics proposed by Bourdin, Francfort and Marigo and a simplified 2D mechanical model of directional drying of colloidal suspensions, we are able to retrieve, at least qualitatively, the crack morphologies. This first study is encouraging and will be completed by more quantitative experimental and numerical results. The experiments shall shed some new light on the basalt column formations. The numerical simulations may be complementary to the experiments by highlighting the pertinent experimental parameters.

References

[1] C. Allain and L. Limat. Regular patterns of cracks formed by directional drying of a colloidal suspension. *Physical Review Letters*, 74:2981–2984, 1995.

[2] L. Ambrosio, N. Fusco, and D. Pallara. *Functions of bounded variation and free discontinuity problems*. Oxford Mathematical Monographs. Oxford Science Publications, 2000.

[3] B. Bourdin. Numerical implementation of the variational formulation of quasi-static brittle fracture. *Interfaces and Free Boundaries*, 9:411–430, 2007.

[4] B. Bourdin, G. A. Francfort, and J. J. Marigo. Numerical experiments in revisited brittle fracture. *Journal of the Mechanics and Physics of Solids*, 48(4):797–826, 2000.

[5] Blaise Bourdin, Gilles Francfort, and Jean-Jacques Marigo. The variational approach to fracture. *Journal of elasticity*, 91(1):5 – 148, 2008.

[6] A. Braides. *Approximation of Free-Discontinuity Problems*, volume 1694 of *Lecture Notes in Mathematics*. Springer, 1998.

[7] E. R. Dufresne, E. I. Corwin, N. A. Greenblatt, J. Ashmore, D. Y. Wang, A. D. Dinsmore, J. X. Cheng, X. S. Xie, J. W. Hutchinson, and D. A. Weitz. Flow and fracture in drying nanoparticle suspensions. *Physical Review Letters*, 91(22):224501, 2003.

[8] E.R. Dufresne, D.J. Stark, N.A. Greenblatt, J.X. Cheng, J.W. Hutchinson, L. Mahadevan, and D.A. Weitz. Dynamics of fracture in drying suspensions. *Langmuir*, 22(17):7144–7147, 2006.

[9] G. A. Francfort and J. J. Marigo. Revisiting brittle fracture as an energy minimization problem. *Journal of the Mechanics and Physics of Solids*, 46:1319–1342, 1998.

[10] G. Gauthier, V. Lazarus, and L. Pauchard. Alternating crack propagation during directional drying. *Langmuir*, 23(9):4715–4718, 2007.

[11] Lucas Goehring, Stephen W. Morris, and Zhenquan Lin. Experimental investigation of the scaling of columnar joints. *Physical Review E (Statistical, Nonlinear, and Soft Matter Physics)*, 74(3):036115, 2006.

[12] D. Mumford and J. Shah. Optimal approximations by piecewise smooth functions and associated variational problems. *Comm. Pure Appl. Math*, 42:577–685, 1989.

[13] M. P. Ryan and C. G. Sammis. Cyclic fracture mechanisms in cooling basalt. *Geological Society of America Bulletin*, 89(9):1295–1308, 1978.

Analytical and 3D finite element study of the deflection of an elastic cantilever bilayer plate.

M. Chekchaki*
UPMC Univ Paris 6, Univ Paris-Sud, CNRS, UMR 7608,
Lab FAST, Bât 502, Campus Univ, F-91405 Orsay, France

V. Lazarus†
UPMC Univ Paris 6, Univ Paris-Sud, CNRS, UMR 7608,
Lab FAST, Bât 502, Campus Univ, F-91405 Orsay, France;

J. Frelat‡
UPMC Univ Paris 6, CNRS, UMR 7190, Institut Jean Le Rond d'Alembert,
Boite courrier 161-2, 4 Place Jussieu, F-75005, Paris, France

Abstract

The mechanical system considered is a bilayer cantilever plate. The substrate and the film are linear elastic. The film is subjected to isotropic uniform prestresses due for instance to volume variation associated with cooling, heating or drying. This loading yields deflection of the plate. We recall Stoney's analytical formula linking the total mechanical stresses to this deflection. We also derive a relationship between the prestresses and the deflection. We relax Stoney assumption of very thin films. The analytical formulas are derived by assuming that the stress and curvature states are uniform and biaxial. To quantify the validity of these assumptions, finite element calculations of the three-dimensional elasticity problem are performed for a wide range of plate geometries, Young's and Poisson's moduli. One purpose is to

*e-mail:mourad.chekchaki@etu.upmc.fr
†Corresponding author: e-mail:veronique.lazarus@upmc.fr
‡e-mail:joel.frelat@upmc.fr

help any user of the formulas to estimate their accuracy. In particular, we show that for very thin films, both formulas written either on the total mechanical stresses or on the prestresses, are equivalent and accurate. Error associated with the misfit between our theorical study and numerical results are also presented. For thicker films, the observed deflection is satisfactorily reproduced by the expression involving the prestresses, not the total mechanical stresses.

1 Introduction

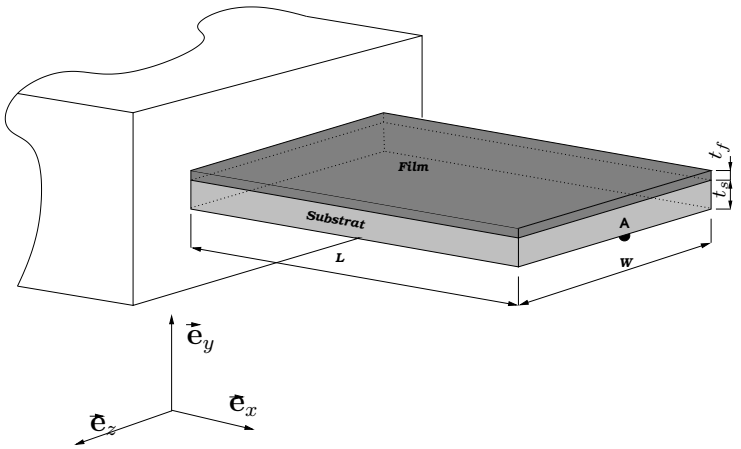

Figure 1: Bilayer cantilever plate

Thin films coated on a plate are currently used to perform several functions in thermal, tribological, mechanical or biological areas. Paintings or micro-electro-mechanical systems (MEMS) are other interesting examples of bilayers. They appear from the nano to the macro scale. In all these systems, undesirable consequences such as folds, cracking or delamination may occur due to the internal residual stresses that appear during the deposition process. It is thus crucial to evaluate these stresses. The cornerstone methodology used to infer them is to measure the deformation of a bilayer plate and to use Stoney's type [1] stress-deformation relations. Two methodologies are

currently used: the measure of the *local* curvature of a circular plate or the measure of the *global* deflection of a cantilever. While the first method requires sophisticated experimental set-up [2], the second method is very simple thus extensively used by different communities [3, 4, 5]. Moreover, the cantilever geometry often appears in MEMS and has recently be used in new nanoscale testing machines [6]. Thus the precise knowledge of the equations linking the free end deflection and the stresses in the film for this cantilever geometry is important. The main goal of the current work is to present such equations and to validate them by solving the 3D elasticity problem using finite element computations. One purpose is to give a practical guideline to anyone that uses the equation, so that one is able to answer questions such as "Can I use the formula for my framework and if yes, what is the accuracy of it?"

Several equations describing the relationship stress-deflection can be found in the literature. Stoney [1] was the first to propose such a formula for the cantilever setup. The underlying assumptions are that (i) the substrate is homogeneous, isotropic and linearly elastic (Young modulus E_s, Poisson's ratio ν_s); (ii) the film and substrate thicknesses t_f and t_s are small compared to the lateral extent of the system; (iii) t_f and t_s are uniform; (iv) the film thickness t_f is small relative to the thickness t_s of the substrate; (v) the displacements are infinitesimal in comparison with the plate width W and length L; (vi) edge effects are inconsequential; (vii) the curvature is uniform and uniaxial around the z-direction; (viii) the total stress state is uniform and uniaxial $\boldsymbol{\sigma} = \sigma_f \, \mathbf{e}_x \times \mathbf{e}_x$. It reads, using the notations of figure 1:

$$\delta = \frac{3\sigma_f t_f L^2}{E_s t_s^2}$$

where δ is the deflection at the free standing end $x = L$ of the plate. The uniaxial curvature (vii) and stress state (viii) is however, are not verified in practice as soon as $W \gg t_s$ and shall

be replaced by the assumption of (vii) uniform biaxial curvature and (viii) uniform stress states $\boldsymbol{\sigma} = \sigma_f \left(\mathbf{e}_x \times \mathbf{e}_x + \mathbf{e}_z \times \mathbf{e}_z\right)$. The formula then becomes (see for instance [7, 8]):

$$\delta = \frac{3(1-\nu_s)\sigma_f t_f L^2}{E_s t_s^2} \tag{1}$$

Numerous papers deal with extensions of this last formula to less restrictive assumptions. A nice overview can be found in [8] and [9]. All the points (i) to (vi) cited above have been less or more relaxed: see for instance [10] for nonuniform substrate thickness, [11, 12] for discontinuous films, [13, 14] for large displacements, [15] for non-uniform curvature, and [16] for anisotropic films. Points (vii) and (viii) of uniform biaxial curvature and stress states in the film have been relaxed keeping the assumption (iv) of thin films, for bilayer [17, 18, 19] and multilayer systems [20, 21]. The case of arbitrary film thickness (relaxation of point (iv)) has been addressed by [22, 23, 8], keeping the assumption (viii) of uniform biaxial stress state in the film, assumption that can be anticipated to be no longer valid in general. Here, both the assumptions (iv) of thin film and (viii) of uniform stress state are relaxed by considering the particular problem of an elastic bilayer, the film being subjected to uniform isotropic prestresses σ_0 (e.g due to thermal or drying processes.). It is worth noting here the distinction between the mechanical stresses $\boldsymbol{\sigma}$ and the prestresses $\sigma_0\mathbf{1}$: the prestresses $\sigma_0\mathbf{1}$ corresponds to the loading and are imposed to be isotropic and uniform, whereas $\boldsymbol{\sigma}$ are the resulting stresses, hence are point dependant and not generally isotropic or biaxial. In previous cited papers, the film is supposed to be subjected to uniform biaxial stresses $\boldsymbol{\sigma} = \sigma_f \left(\mathbf{e}_x \times \mathbf{e}_x + \mathbf{e}_y \times \mathbf{e}_y\right)$ and the plate deformations are linked to the single parameter σ_f such defined. Here, we link the deflection to the given prestress σ_0. Analytical equations are solved for the assumption of a uniform biaxial stress state, thus neither the boundary conditions and nor the stress inhomogeneities are taken into account. In the case of thin films as compared to the

substrate, the stress inhomogeneities in the film can be neglected and the boundary conditions can be taken into account using plate model finite element simulations [14, 24]. For thicker films, the plate approach is questionable since it consists in replacing the stresses state through the plate thickness by equivalent membrane forces and moments, so that possible stress inhomogeneities in the thickness due to the structural effect can not be studied. To determine the full displacement and stress fields in both the film and the substrate without any assumption on the shape of these fields, we solve the 3D complete elasticity problem, with perfect adhesion conditions on the interface, by Finite Element (FE) calculations. This approach permits consideration of the effect of boundary conditions on the deflection profile. It is the first time, to the best of our knowledge, that the Stoney formula is verified by 3D FE computations. Several plate geometries and layer materials properties are considered. We show that for very thin films, both formulas written either on the total mechanical stresses or on the prestresses, are equivalent and accurate; the error made on the formulas are also given. For thicker films, we show that only the formula based upon the prestresses is accurate.

2 Analytical approach

2.1 Material behavior

Let us suppose that the substrate and the film are linearly elastic both with Young's moduli E_s, E_f and Poisson's ratios ν_s, ν_f respectively. The film is loaded by uniform isotropic prestresses $\boldsymbol{\sigma_0} = \sigma_0 \mathbf{1}$, so that the constitutive laws between the stress $\boldsymbol{\sigma}$ and the strain $\boldsymbol{\varepsilon}$ tensors is at any point

of the film:

$$\boldsymbol{\sigma} = \Lambda_f(\boldsymbol{\varepsilon}) + \sigma_0 \mathbf{1} \tag{2}$$

and at any point of the substrate:

$$\boldsymbol{\sigma} = \Lambda_s(\boldsymbol{\varepsilon}) \tag{3}$$

where $\Lambda_i(\boldsymbol{\varepsilon})$, $i = f, s$ is defined by:

$$\Lambda_i(\boldsymbol{\varepsilon}) = \frac{E_i \nu_i}{(1+\nu_i)(1-2\nu_i)} \mathrm{tr}\boldsymbol{\varepsilon}\ \mathbf{1} + \frac{E_i}{(1+\nu_i)}\boldsymbol{\varepsilon} \tag{4}$$

2.2 Energy density

The infinitesimal internal work is in the film and in the substrate:

$$dU = \sigma : \mathrm{d}\boldsymbol{\varepsilon} = \begin{cases} \Lambda_f(\boldsymbol{\varepsilon}) : \mathrm{d}\boldsymbol{\varepsilon} + \boldsymbol{\sigma_0} : \mathrm{d}\boldsymbol{\varepsilon} \\ \\ \Lambda_s(\boldsymbol{\varepsilon}) : \mathrm{d}\boldsymbol{\varepsilon} \end{cases}$$

so that, by integration, the strain energy density is at any point of the film (using (2)),

$$U = \frac{1}{2}\Lambda_f(\boldsymbol{\varepsilon}) : \boldsymbol{\varepsilon} + \boldsymbol{\sigma_0} : \boldsymbol{\varepsilon} = \frac{1}{2}(\boldsymbol{\sigma} : \boldsymbol{\varepsilon} + \boldsymbol{\sigma_0} : \boldsymbol{\varepsilon})$$

and at any point of the substrate (using (3)):

$$U = \frac{1}{2}\Lambda_s(\boldsymbol{\varepsilon}) : \boldsymbol{\varepsilon} = \frac{1}{2}\boldsymbol{\sigma} : \boldsymbol{\varepsilon}$$

2.3 Boundary conditions

The elasticity problem with a clamped plate is, to our knowledge, not tractable analytically. In particular, it is obvious that the curvature is uniaxial near the clamped boundary but overall rather

biaxial. We search for an approximate solution by assuming that the stress and curvature states are uniform and biaxial around any direction in the (x,z)-plane : $\boldsymbol{\sigma} = \sigma_f \left(\mathbf{e}_x \times \mathbf{e}_x + \mathbf{e}_z \times \mathbf{e}_z\right)$ and $\boldsymbol{\varepsilon} = \varepsilon \left(\mathbf{e}_x \times \mathbf{e}_x + \mathbf{e}_z \times \mathbf{e}_z\right) + \varepsilon_{yy}\mathbf{e}_y \times \mathbf{e}_y$. This implies:

$$\sigma_f = \frac{E_f}{1-\nu_f}\varepsilon + \frac{1-2\nu_f}{1-\nu_f}\sigma_0. \tag{5}$$

The strain energy density in the film then becomes (the constant term proportional to σ_0^2 has been omitted since it disappears finally in the minimization process):

$$U = \frac{E_f}{1-\nu_f}\varepsilon^2 + 2\frac{1-2\nu_f}{1-\nu_f}\sigma_0\varepsilon \tag{6}$$

and in the substrate:

$$U = \frac{E_s}{1-\nu_s}\varepsilon^2 \tag{7}$$

2.4 Kinematic hypothesis and resolution

Now, supposing that the curvature κ is uniform in the plane (x,z), we search ε under the following form:

$$\varepsilon = \varepsilon_0 - y\kappa \tag{8}$$

and we determine the stationary point of the total potential energy V toward ε_0 and κ. Using the relation $\delta = \frac{1}{2}\kappa L^2$, it yields[1] for δ:

$$\delta = \frac{3(1-2\nu_f)\sigma_0 t_f L^2}{\left(\frac{1-\nu_f}{1-\nu_s}\right)E_s t_s^2}\frac{1+t}{1+2M(2t+3t^2+2t^3)+M^2t^4} \tag{9}$$

where $M = \frac{(1-\nu_s)E_f}{(1-\nu_f)E_s}$ and $t = t_f/t_s$.

[1]We choose $y = 0$ corresponding to the mid plane of the bilayer plate. Any other choice, would change the value of ε_0 but not the value of κ and δ which are of interest here.

If $E_f \ll E_s$ and $t_f \ll t_s$, one has

$$\delta = \frac{3(1-2\nu_f)\sigma_0 t_f L^2}{\left(\frac{1-\nu_f}{1-\nu_s}\right) E_s t_s^2}. \tag{10}$$

And in this case, the part $\frac{E_f}{1-\nu_f}\varepsilon$ of the stresses linked to the in-plane deformations ε can be neglected in comparison with σ_0 so that $\sigma_f \sim \frac{1-2\nu_f}{1-\nu_f}\sigma_0$ (equations (5), (8), (9)). Introducing this relation in (9), yields the classical Stoney formula (1).

If $E_f t_f / E_s t_s \ll 1$ but not necessarily $t_f \ll t_s$, the following formula, sometimes used in the literature (see [3]) holds:

$$\delta = \frac{3(1-2\nu_f)\sigma_0 t_f L^2 (1+t_f/t_s)}{\left(\frac{1-\nu_f}{1-\nu_s}\right) E_s t_s^2} \tag{11}$$

One may also be tempted to make the assumption that the mean biaxial stress is uniform and satisfies $\sigma_f \sim \frac{1-2\nu_f}{1-\nu_f}\sigma_0$ in order to express the deflection as a function of the stress state. This supposes that the term $\frac{E_f}{1-\nu_f}\varepsilon$ in equation (5) can be neglected in comparison to σ_0. Equation (9) then becomes:

$$\delta = \frac{3(1-\nu_s)\sigma_f t_f L^2}{E_s t_s^2} \frac{1+t}{1+2M(2t+3t^2+2t^3)+M^2 t^4} \tag{12}$$

which can also be found using the results derived in [22, 8] between the curvature κ and the mismatch strain ε_m using the relations $\delta = \frac{1}{2}\kappa L^2$ and $\varepsilon_m = \sigma_f(1-\nu_f)/E_f$. The validity of this formula is discussed in the next section.

3 3D Finite Element calculations

The 3D equilibrium elasticity problem, with perfect adhesion on the interface between the substrate and the film (zero displacement $[\![\boldsymbol{u}]\!] = \mathbf{0}$ and stress vector $[\![\boldsymbol{\sigma}]\!].\boldsymbol{n} = \mathbf{0}$ jumps), zero displacements conditions for the clamped boundary ($\boldsymbol{u} = \mathbf{0}$) and traction free ones on the remain boundary

($\boldsymbol{\sigma}.\boldsymbol{n} = \mathbf{0}$), has been solved by FE with Cast3M[2] using cubic elements (P2) containing 20 nodes each. The total number of degrees of freedom (number of nodes $\times$ 3) is approximately 40000. Two elements are put in the thickness of each layer (we have verified that more elements does not bring more accuracy).

The prestress σ_0 is the loading and the mechanical displacement and stress fields corresponding to this loading, are obtained by the FE calculation. The deflection δ is taken as the vertical displacement of the extremity mid point of the plate (point **A**, fig. 1). By taking into account the linearity of the problem, we can present the results in the following dimensionless form:

$$\delta = \frac{\sigma_0 L^2}{E_s t_s} f\left(\frac{t_f}{t_s}, \frac{E_f}{E_s}, \frac{W}{L}, \frac{t_s}{L}, \nu_s, \nu_f\right).$$

It is then easy to perform the comparison between the analytical formula on δ-σ_0 and the numerical results. It is less straightforward to work on the formula written on δ-σ_f since numerically σ_f is point dependent whereas analytically it is assumed to be uniform. Also, to perform the comparison, σ_f is taken as the mean value of the normal stress in the x-direction $\langle\sigma_{xx}\rangle$ over all the film, that is, where V_f is the film volume:

$$\sigma_f = \langle\sigma_{xx}\rangle = \frac{1}{V_f}\iiint_{V_f} \sigma_{xx}\mathrm{d}V \tag{13}$$

The validity of the formulas is demonstrated for a wide range of E_f/E_s, t_f/t_s, W/L. Finally, the influence of the Poisson's ratio is considered including the case of auxetics films [3].

[2] finite element code developed by the French Commissariat à l'Energie Atomique http://www-cast3m.cea.fr.

[3] materials with negative Poisson modulus.

3.1 Using the total stresses or the prestresses in the Stoney formulas ?

To compare complete Stoney formulas (9) written for δ and σ_0 and (12) written for δ and σ_f, we introduce the relative errors $\Delta_R\delta = \dfrac{\delta_{(9)} - \delta_{FE}}{\delta_{FE}}$ and $\Delta_R\delta_f = \dfrac{\delta_{(12)} - \delta_{FE}}{\delta_{FE}}$ between the values $\delta_{(9)}$ and $\delta_{(12)}$ of δ obtained using equation (9) and (12) resp. and the ones obtained by FE calculations for a given value of σ_0, σ_f being obtained by eq. (13). The results are given in figure 2 for $E_f/E_s = 10^{-2}$, $t_f/t_s = 10^{-2}$ and $W/L = 0.1$.

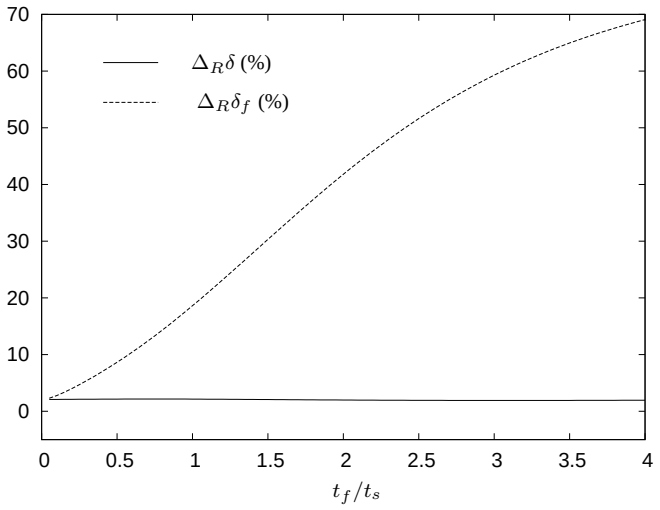

Figure 2: Relative error between the deflection obtained through the formulas (9) and (12) and the numerical values ($E_f/E_s = 10^{-2}$, $t_s/L = 10^{-2}$, $W/L = 0.1$, $\nu = 0.3$)

To understand the large disparity in error between the equations, in figure 3 we plot quantities relevant to the biaxiality state and uniformity of the stresses in the film : the biaxiality ratio defined by the ratio between the mean xx component of the stress tensor and the mean zz component; and the mean xx stress component divided by its value $\frac{1-2\nu_f}{1-\nu_f}\sigma_0$ when the term $\frac{E_f}{1-\nu_f}\varepsilon$ in equation (5) can be neglected. When their value is near 1, it means that the stress state is biaxial and uniform equal to $\frac{1-2\nu_f}{1-\nu_f}\sigma_0$; when their values depart from 1, the stress state is no longer biaxial and uniform.

One can notice that:

- for small enough t_f/t_s (here $t_f/t_s < 0.5$), both formulas (9) and (12) agree with the numerical values. This means that they can both be used equivalently. This is because the component of the stress field in the film linked to the inplane deformation can be neglected so that the film stresses are nearly uniform satisfying $\sigma_f \sim \frac{1-2\nu_f}{1-\nu_f}\sigma_0$ (see figure 3 for small values of t_f/t_s).

- for $t_f/t_s \ll 1$, since (1) and (10) are then equivalent to formula (9) and (12) resp., previous points implies that (1) and (10) can both be used equivalently.

- for bigger t_f/t_s (in the limit $t_{s,f} \ll L$), only formula (9) (and not (12)) can be used. This is not surprising. Since the stress state in the layer is then no more uniform (see figure 3 for arbitrary values of t_f/t_s), it is unreasonable to use only one scalar σ_f to describe the stress state in the film, even if one takes $\sigma_f = \langle\sigma_{xx}\rangle$. If a determination of the stress state in the film is desired, only a local approach using the local curvatures and the local stress state [9] may be used, but such a calculations is outside of the scope of the current work.

These results have been obtained in the case $W/L = 0.1$. For larger plates, it will be shown in the sequel that results are less accurate. One can conclude from these results, that only the formula written on the prestresses can be used for film thicknesses of the same order as the substrate thickness whatever the plate width. We will focus on those formula, namely (9) and (11), in the sequel.

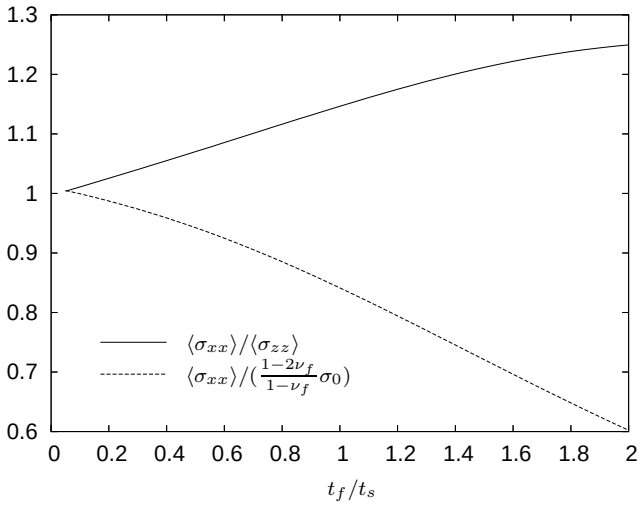

Figure 3: Increasing non uniformity of the film stresses with the film thickness ($E_f/E_s = 10^{-2}$, $t_s/L = 10^{-2}$, $W/L = 0.1$, $\nu = 0.3$).

3.2 Deflection versus film thickness

3.2.1 General case

In this section, we study the accuracy of formula (9) and (11) in the case of identical Poisson's ratio in the substrate and the film ($\nu_f = \nu_s = \nu = 0.3$). The dependence on ν is considered in next part. In figure 4, the dimensionless deflections $\delta E_s t_s/\sigma_0 L^2$ are plotted as a function of t_f/t_s for $t_s/L = 10^{-2}$, $W/L = 1$ and different values of E_f/E_s. The dashed lines correspond to the FE computations and the solid ones to the analytical equations (9). Some computations performed for smaller values of t_s/L show a weak dependence of the plot on this value, hence the influence of this parameter is not shown. The dependence on W/L is also weak, so that among the curves corresponding to $W/L = 0.1$ or $W/L = 1$ we have chosen to represent only the worst, that is $W/L = 1$. More details on the dependence of the results on the width of the plate is considered further.

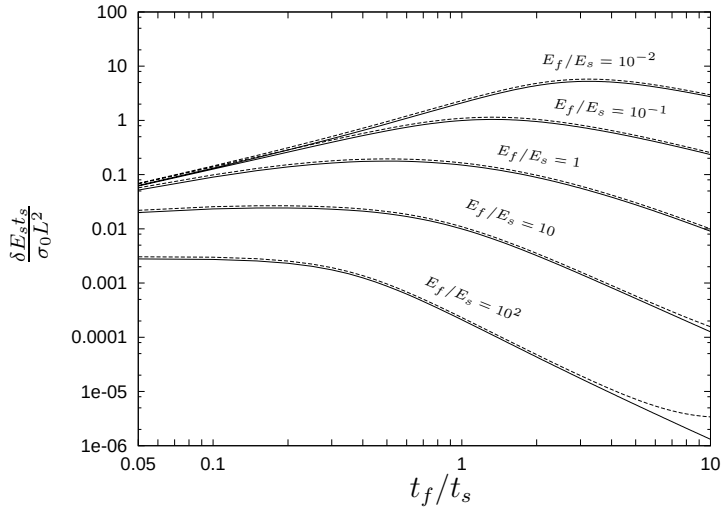

Figure 4: *Complete* analytical formula (9) (solid lines) compared with the FE computations (dashed lines) obtained for $t_s/L = 10^{-2}$, $W/L = 1$, $\nu = 0.3$.

One can notice several things on these curves:

- Good agreement is found between the Stoney formula (9) including the ratio of Young modulus influence even for a film much thicker than the substrate. The agreement is better for small ratio of E_f/E_s than for larger ones.

- The "mountain like" curve is due to the competition of two effects: when t_f/t_s increases, (i) as the membrane force proportional to $\sigma_0 t_f$ exerted by the film increases, the deflection increases, (ii) however, as the bending rigidity of the film proportional to t_f^3 increases, the deflection decreases. For thin films, the membrane force effect is predominant, and for thicker films, the rigidity effect.

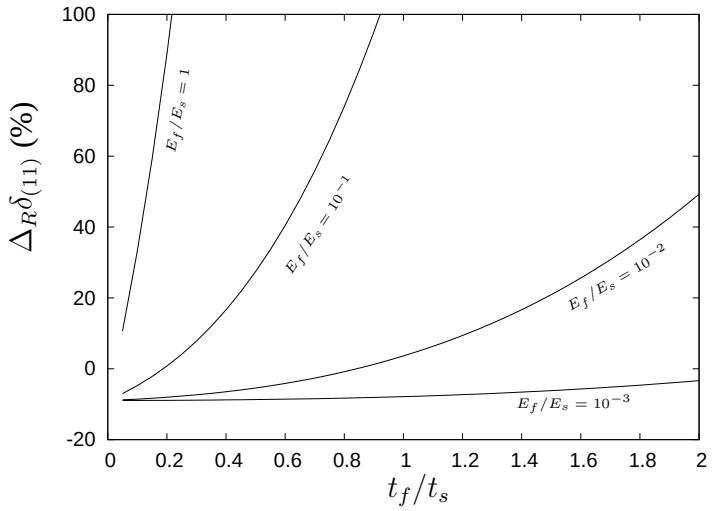

Figure 5: Relative error between the deflection obtained through the *simplified* equation (11) and the FE computations one for $t_s/L = 10^{-2}$, $W/L = 1$, $\nu = 0.3$.

3.2.2 Case $E_f t_f/E_s t_s \ll 1$

In practice, the Young modulus E_f of the film may be not known exactly [3], so that only the simplified Stoney formula (11) is useful. It is thus pratical to evaluate $\Delta_R\delta_{(11)} \equiv \frac{\delta_{(11)}-\delta_{FE}}{\delta_{FE}}$. Good agreement is found between this simplified formula and the numerical values only for not too thick films and not too stiff films. For $E_f/E_s = 1$, $t_f/t_s = 0.05$, $W/L = 1$, the relative error is still $\Delta_R\delta_{(11)} = 15\%$, so that we consider in fig. 5 only the most favorable cases corresponding to $E_f/E_s \leq 1$.

The maximum film/substrate thickness for which the agreement is acceptable depends on the ratio E_f/E_s: the smaller E_f/E_s the thicker the film can be. More precisely, figure 6 gives the domain for which the relative error between the simplified Stoney formula (11) and the numerical solution is less than 10 $\%$. The solid curve corresponds to the relative error between the simplified (11) and complete (9) Stoney formula, which has been shown to match the numerical values. It

is obtained by determining $M = \frac{(1-\nu_s)E_f}{(1-\nu_f)E_s}$ for each value of $t \equiv t_f/t_s$ satisfying the equation $\Delta_R\delta_{Stoney} \equiv \frac{\delta_{(11)}-\delta_{(9)}}{\delta_{(9)}} = 0.1$, that is:

$$M^2t^4 + 2M(2t + 3t^2 + 2t^3) = \Delta_R\delta_{Stoney} \tag{14}$$

with $\Delta_R\delta_{Stoney} = 0.1$. Some numerical points have been added corresponding to $\Delta_R\delta_{(11)} = 10\%$ which confirm the good agreement between formula (9) and the numerical results. Moreover it shows that the analytical graph obtained using equation (14) underestimates the maximum thickness ratio that can be considered so that the relative error $\Delta_R\delta_{(11)}$ made using simplified equation (11) can safely be estimated using $\Delta_R\delta_{Stoney}$ that is equation (14).

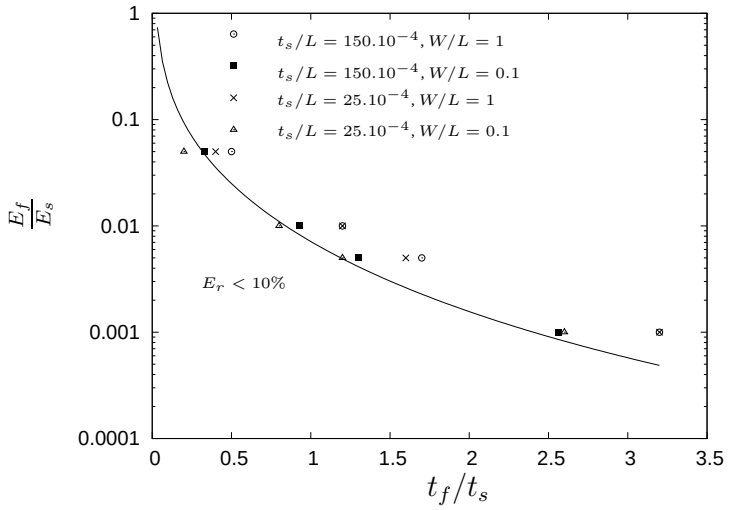

Figure 6: Thickness and Young's modulus ratios influence on the relative error. To the left of the solid line, the relative error between the simplified (11) and complete (9) Stoney formula is less than 10%. The points correspond to values of t_f/t_s, E_f/E_s for which the relative error between the simplified (11) formula and the numerical result is 10% (each point corresponds to different values of t_s/L and W/L).

3.3 Influence of Poisson's modulus

We have verified, in the previous section, that (9) is accurate if $\nu_s = \nu_f = 0.3$. To verify that the dependence of (9) on ν_f and ν_s is accurate, we consider $\nu_s = 0.3$ and $\nu_f \in (-1; 0.5)$ including auxetics [25, 26, 27] and the corresponding relative error between formula (9) and the FE values (figure 7, 8). These results allow moreover a quantified assesment of the error associated with the formula (9).

We see on figure 7 and 8 that:

- Formula (9) gives good results in a wide range of ν_f. In particular for $\nu_f \in [0;\ 0.4]$, the error are less than 10% in all the cases considered.
- The discrepancy becomes higher for larger values of E_f/E_s and t_f/t_s.
- The agreement is poorer for wide plates than for slender ones. Thanks to Saint-Venant's principle, the boundary conditions become negligible at distances which are large compared with the dimensions of the plate and notably W/L. Moreover, the anticlastic curvature effect becomes more important for wide plates [28, 29];
- For $\nu_f < 0$ the error is larger than for $\nu_f > 0$, probably because the anticlastic curvature effect is amplified in these cases.

4 Conclusion

By performing full 3D finite elements calculations we have shown that:

- For $t_f/t_s \ll 1$ and $E_f/E_s \ll 1$, the stress state in the film is biaxial and uniform with $\sigma_f \sim \frac{1-2\nu_f}{1-\nu_f}\sigma_0$. The deflection then verifies both formulas (1) and (10-11) written on σ_f and

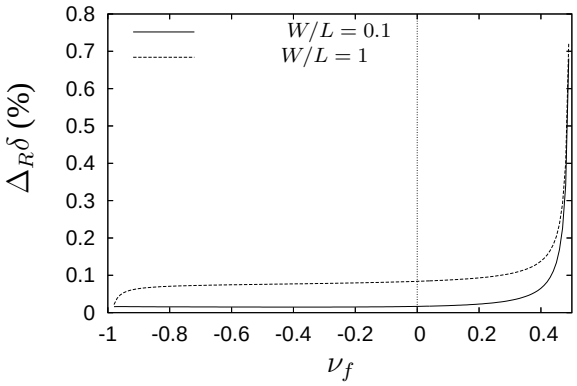

(a) $t_f/t_s = 0.1$, $E_f/E_s = 0.01$

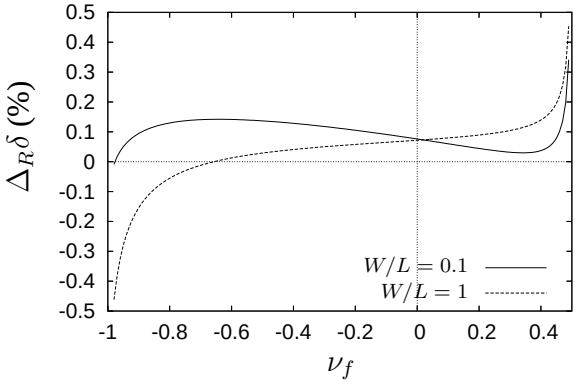

(b) $t_f/t_s = 1$, $E_f/E_s = 0.01$

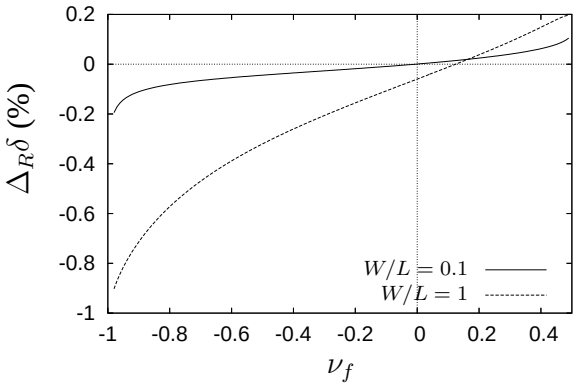

(c) $t_f/t_s = 10$, $E_f/E_s = 0.01$

Figure 7: Relative error between equation (9) and numerical results for $E_f/E_s = 0.01$.

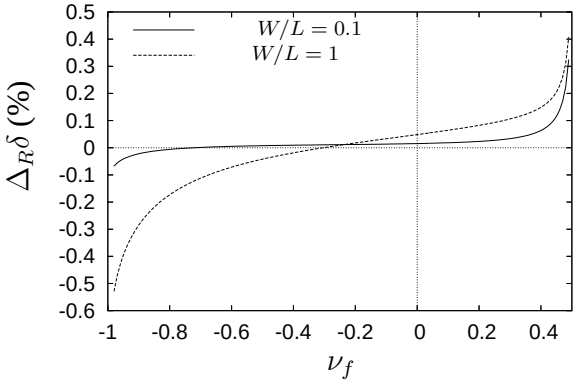

(a) $t_f/t_s = 0.1$, $E_f/E_s = 1$

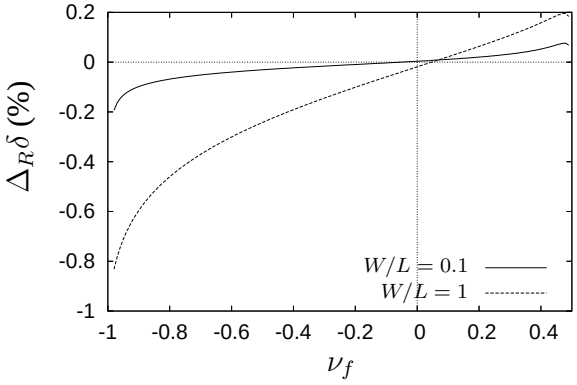

(b) $t_f/t_s = 1$, $E_f/E_s = 1$

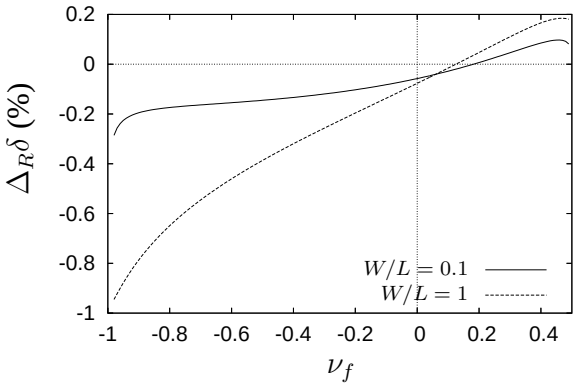

(c) $t_f/t_s = 10$, $E_f/E_s = 1$

Figure 8: Relative error between equation (9) and numerical results for $E_f/E_s = 1$.

σ_0 respectively. Their validity limit of (11) on t_f/t_s is given in figure 6 as a function of E_f/E_s.

- For arbitrary t_f/t_s in the limit $t_{s,f} \ll L$, only formula (9) accurately estimates the deflection since the stress state is no longer uniform. Any formula invoking a uniform stress state does not yield reasonable estimates. This formula is accurate to less than 10% error for $\nu_f \in [0;\, 0.4]$ ($\nu_s = 0.3$).

- The formulas are more accurate for slender plates than for square plates. This is due to the fact that for wider plates, the clamped boundary condition and anticlastic curvature have a greater influence on the stress state and the deflection.

In some film/substrate systems, the misfit strain may damage the film/substrate interface. For instance, delamination may appear [4]. Our analysis supposing perfect adhesion at the interface is then no more valid. Moreover, these formulas are valid only in the limit of the small perturbations hypothesis. For large perturbations, bifurcations may appear. Freund [14], by performing finite elements calculations based on plate models, gives the following upper bound for the small perturbations approach to be valid:

$$\frac{3(1-\nu_s)\sigma_f t_f L^2}{2E_s t_s^3} < 0.3 \tag{15}$$

His approach assumes that the plate boundary is traction free. Guyot *et al.* [24] have recently show that bifurcation arises later for slender plates. It may be interesting to verify whether the clamped boundary condition, which has a rigidifying effect, also results in a higher upper bound.

References

[1] Stoney, G. G., 1909, “The tension of metallic films deposited by electrolysis,” Proceedings of the Royal Society of London. Series A, Containing Papers of a Mathematical and Physical Character, **82**(553), pp. 172–175.

[2] Rosakis, A. J., Singh, R. P., Tsuji, Y., Kolawa, E., and Moore, N. R., 1998, “Full field measurements of curvature using coherent gradient sensing: application to thin film characterization,” Thin Solid Films, **325**(1-2), pp. 42– 54.

[3] Petersen, C., Heldmann, C., and Johannsmann, D., 1999, “Internal stresses during film formation of polymer latices,” Langmuir, **15**(22), pp. 7745–7751.

[4] Tirumkudulu, M. S. and Russel, W. B., 2005, “Cracking in drying latex films,” Langmuir, **21**(11), pp. 4938–4948.

[5] Guisbiers, G., Strehle, S., and Wautelet, M., 2005, “Modeling of residual stresses in thin films deposited by electron beam evaporation,” Microelectronic Engineering, **82**(3-4), pp. 665–669.

[6] Gravier, S., Coulombier, A., M.and Safi, Andre, N., Boe, A., Raskin, J.-P., and Pardoen, T., 2009, “New On-Chip Nanomechanical Testing Laboratory - Applications to Aluminum and Polysilicon Thin Films,” Journal of microelectromechanical systems, **18**(3), pp. 555–569.

[7] Flinn, P., Gardner, D., and Nix, W., 1987, “Measurement and interpretation of stress in aluminum-based metallization as a function of thermal history,” IEEE Transactions on electron devices, **34**(3), pp. 689–699.

[8] Freund, L. B. and Suresh, S., 2004, *Thin Film Materials; Stress, defect formation and surface evolution*, Cambridge University press, Cambridge, UK.

[9] Ngo, D., Feng, X., Huang, Y., Rosakis, A. J., and Brown, M. A., 2007, "Thin film/substrate systems featuring arbitrary film thickness and misfit strain distributions. Part I: Analysis for obtaining film stress from non-local curvature information," International Journal of Solids and Structures, **44**(6), pp. 1745–1754.

[10] Feng, X., Huang, Y., and Rosakis, A. J., 2007, "On the stoney formula for a thin film/substrate system with nonuniform substrate thickness," Journal of Applied Mechanics, **74**(6), pp. 1276–1281.

[11] Shen, Y. L., Suresh, S., and Blech, I. A., 1996, "Stresses, curvatures, and shape changes arising from patterned lines on silicon wafers," Journal of Applied Physics, **80**(3), pp. 1388–1398.

[12] Wikstrom, A., Gudmundson, P., and Suresh, S., 1999, "Thermoelastic analysis of periodic thin lines deposited on a substrate," Journal of the Mechanics and Physics of Solids, **47**(5), pp. 1113–1130.

[13] Salamon, N. J. and Masters, C. B., 1995, "Bifurcation in isotropic thin-film substrate plates," International Journal of Solids and Structures, **32**(3-4), pp. 473–481.

[14] Freund, L. B., 2000, "Substrate curvature due to thin film mismatch strain in the nonlinear deformation range," Journal of the Mechanics and Physics of Solids, **48**(6-7), pp. 1159–1174.

[15] Zhang, Y. and Zhao, Y. P., 2006, "Applicability range of Stoney's formula and modified formulas for a film/substrate bilayer," Journal of applied physics, **99**(5), p. 053513.

[16] Janssen, G., Abdalla, M., van Keulen, F., Pujada, B., and van Venrooy, B., 2009, "Celebrating the 100th anniversary of the stoney equation for film stress: Developments from polycrystalline steel strips to single crystal silicon wafers," Thin Solid Films, **517**(6), pp. 1858 – 1867.

[17] Huang, Y. and Rosakis, A. J., 2005, "Extension of Stoney's formula to non-uniform temperature distributions in thin film/substrate systems. The case of radial symmetry," Journal of the Mechanics and Physics of Solids, **53**(11), pp. 2483–2500.

[18] Ngo, D., Huang, Y., Rosakis, A. J., and Feng, X., 2006, "Spatially non-uniform, isotropic misfit strain in thin films bonded on plate substrates: The relation between non-uniform film stresses and system curvatures," Thin Solid Films, **515**(4), pp. 2220–229.

[19] Huang, Y. and Rosakis, A. J., 2007, "Extension of stoney's formula to arbitrary temperature distributions in thin film/substrate systems," Journal of Applied Mechanics, **74**(6), pp. 1225–1233.

[20] Feng, X., Huang, Y., and Rosakis, A. J., 2008, "Stresses in a multilayer thin film/substrate system subjected to nonuniform temperature," Journal of Applied Mechanics, **75**(2), 021022.

[21] Feng, X., Huang, Y., and Rosakis, A., 2008, "Multi-layer thin films/substrate system subjected to non-uniform misfit strains," International Journal of Solids and Structures, **45**(13), pp. 3688 – 3698.

[22] Freund, L. B., Floro, J. A., and Chason, E., 1999, "Extensions of the Stoney formula for substrate curvature to configurations with thin substrates or large deformations," Applied Physics Letters, **74**(14), pp. 1987–1989.

[23] Klein, C. A., 2000, “How accurate are Stoney’s equation and recent modifications,” Journal of Applied Physics, **88**(9), pp. 5487–5489.

[24] Guyot, N., Harmand, Y., and Mézin, A., 2004, “The role of the sample shape and size on the internal stress induced curvature of thin-film substrate systems,” International Journal of Solids and Structures, **41**(18-19), pp. 5143 – 5154.

[25] Lakes, R. S., 1987, “Foam structures with a negative poisson’s ratio,” Science, **235**, pp. 1038–1040.

[26] Evans, K. E., 1991, “Auxetic polymers - A new range of materials,” Endeavour, **15**(4), pp. 170–174.

[27] Yang, W., Li, Z. M., Shi, W., Xie, B. H., and Yang, M. B., 2004, “On auxetic materials,” Journal of materials science, **39**(10), pp. 3269–3279.

[28] P., T. S. and S., W.-K., 1959, *Theory of plates and shells*, McGraw-Hill, New-York.

[29] Pomeroy, R. J., 1970, “The effect of anticlastic bending on the curvature of beams,” International Journal of Solids and Structures, **6**(2), pp. 277 – 285.